

Fiscal Year 2020: Second Quarter

Progress Reports:
**Advanced Battery Materials Research
(BMR) Program
&
Battery500 Consortium**

**Released June 2020
for the period of January – March 2020**

Approved by

Tien Q. Duong, Program Manager
Advanced Battery Materials Research Program & Battery500 Consortium
Vehicle Technologies and Electrification Program
Energy Efficiency and Renewable Energy

TABLE OF CONTENTS

A Message from the Manager:

Advanced Battery Materials Research Program and Battery500 Consortium xx

Advanced Battery Materials Research Program

Task 1 – Liquid/Polymer Solid-State Electrolytes.....	1
Task 1.1 – Advanced Lithium-Ion Battery Technology: High-Voltage Electrolyte (Joe Sunstrom, Ron Hendershot, and Alec Falzone, Daikin)	4
Task 1.2 – Multi-Functional, Self-Healing Polyelectrolyte Gels for Long-Cycle-Life, High-Capacity Sulfur Cathodes in Lithium-Sulfur Batteries (Alex Jen and Jihui Yang, University of Washington)	7
Task 1.3 – Dual Function Solid-State Battery with Self-Forming, Self-Healing Electrolyte and Separator (Esther Takeuchi, Stony Brook University)	10
Task 1.4 – Characterization and Modeling of Li-Metal Batteries: Characterization of Li ⁺ Transport in Polyelectrolytes (Bryan D. McCloskey, University of California at Berkeley)	13
Task 1.5 – Advanced Polymer Materials for Batteries (Zhenan Bao and Yi Cui, Stanford University)	16
Task 1.6 – Improving the Stability of Lithium-Metal Anodes and Inorganic-Organic Solid Electrolytes (Nitash Balsara, Lawrence Berkeley National Laboratory)	20
Task 1.7 – Development of Thin, Robust, Lithium-Impenetrable, High-Conductivity, Electrochemically Stable, Scalable, and Low-Cost Glassy Solid Electrolytes for Solid-State Lithium Batteries (Steve Martin, Iowa State University of Science and Technology)	23
Task 1.8 – Composite Solid Ion Conductor with Engineered Lithium Interface (Kyler Carroll and Cam Peebles, Wildcat Discovery Technologies)	27
Task 1.9 – Physical and Mechano-Electrochemical Phenomena of Thin-Film Lithium-Ceramic Electrolyte Constructs (Jeff Sakamoto, University of Michigan).....	30
Task 1.10 – Lithium Dendrite-Free Li ₇ N ₂ I-LiOH Solid Electrolytes for High-Energy Lithium Batteries (Chunsheng Wang, University of Maryland).....	32
Task 1.11 – Hot Pressing of Reinforced Li-NMC All-Solid-State Batteries with Sulfide Glass Electrolyte (Thomas Yersak, General Motors)	39

Task 1.12 – Low Impedance Cathode/Electrolyte Interfaces for High-Energy-Density Solid-State Batteries (Eric Wachsman and Yifei Mo, University of Maryland).....	43
Task 1.13 – Developing an <i>In Situ</i> Formed Dynamic Protection Layer to Mitigate Lithium Interface Shifting: Preventing Dendrite Formation on Metallic Lithium Surface to Facilitate Long Cycle Life of Lithium Solid-State Batteries (Deyang Qu, University of Wisconsin Milwaukee)	45
Task 1.14 – Molecular Ionic Composites: A New Class of Polymer Electrolytes to Enable All-Solid-State and High-Voltage Lithium Batteries (Louis Madsen, Virginia 48Polytechnic Institute and State University)	48
Task 1.15 – All-Solid-State Batteries Enabled by Multifunctional Electrolyte Materials (Pu Zhang, Solid Power, Inc).....	52
Task 1.16 – Developing Materials for High-Energy-Density Solid-State Lithium-Sulfur Batteries (Donghai Wang, Pennsylvania State University).....	55
Task 2 – Diagnostics	59
Task 2.1 – Characterization and Modeling of Li-Metal Batteries: Model-System Synthesis and Advanced Characterization (Guoying Chen, Lawrence Berkeley National Laboratory)	60
Task 2.2 – Interfacial Processes – Diagnostics (Robert Kostecki, Lawrence Berkeley National Laboratory)	63
Task 2.3 – Advanced <i>In Situ</i> Diagnostic Techniques for Battery Materials (Xiao-Qing Yang and Seong-Min Bak, Brookhaven National Laboratory)	65
Task 2.4 – <i>In Situ</i> Diagnostics of Coupled Electrochemical-Mechanical Properties of Solid Electrolyte Interphases on Lithium-Metal Rechargeable Batteries (Xingcheng Xiao, General Motors; Brian W. Sheldon, Brown University; Yue Qi, Michigan State University; and Y. T. Cheng, University of Kentucky).....	68
Task 2.5 – Probing Interfacial Processes Controlled Electrode Stability in Rechargeable Batteries (Chongmin Wang, Pacific Northwest National Laboratory)	72
Task 2.6 – Integrated Atomic-, Meso-, and Micro-Scale Diagnostics of Solid-State Batteries (Yi Cui, William Chueh, and Michael Toney; Stanford University/SLAC National Accelerator Laboratory).....	75
Task 2.7 – Investigating the Stability of Solid/Solid Interface (Zonghai Chen, Argonne National Laboratory)	77
Task 2.8 – Fundamental Understanding of Interfacial Phenomena in Solid-State Batteries (Xingcheng Xiao, General Motors).....	80
Task 2.9 – Multidimensional Diagnostics of the Interface Evolutions in Solid-State Lithium Batteries (Yan Yao, University of Houston).....	83

Task 3 – Modeling	86
Task 3.1 – Characterization and Modeling of Li-Metal Batteries: First-Principles Modeling and Machine Learning (Kristin Persson, Lawrence Berkeley National Laboratory)	87
Task 3.2 – Understanding and Strategies for Controlled Interfacial Phenomena in Lithium-Ion Batteries and Beyond (Perla Balbuena and Jorge Seminario, Texas A&M University; Partha Mukherjee, Purdue University).....	90
Task 3.3 – Electrode Materials Design and Failure Prediction (Venkat Srinivasan, Argonne National Laboratory).....	93
Task 3.4 – Dendrite Growth Morphology Modeling in Liquid and Solid Electrolytes (Yue Qi, Michigan State University).....	96
Task 3.5 – Modeling of Amorphous Solid-State Conductors (Gerbrand Ceder, University of California Berkeley).....	99
Task 3.6 – Characterization and Modeling of Li-Metal Batteries: Force Field Theory and Lithium-Sulfur Battery Simulations (Lin-Wang Wang, Lawrence Berkeley National Laboratory)	102
Task 3.7 – <i>In Situ</i> and <i>Operando</i> Thermal Diagnostics of Buried Interfaces in Beyond Lithium-Ion Cells (Ravi Prasher, Lawrence Berkeley National Laboratory).....	105
Task 3.8 – Multi-Scale Modeling of Solid-State Electrolytes for Next-Generation Lithium Batteries (Anh Ngo, Larry A. Curtiss, and Venkat Srinivasan, Argonne National Laboratory).....	108
Task 3.9 – Integrated Multi-Scale Modeling for Design of Robust 3D Solid-State Lithium Batteries (Brandon Wood, Lawrence Livermore National Laboratory)	111
Task 3.10 – First-Principles Modeling of Cluster-Based Solid Electrolytes (Puru Jena, Virginia Commonwealth University)	115
Task 3.11 – Predictive Engineering of Interfaces and Cathodes for High-Performance All-Solid-State Lithium-Sulfur Batteries (Badri Narayanan, University of Louisville)	118
Task 3.12 – First-Principles Modeling and Design of Solid-State Interfaces for the Protection and Use of Lithium-Metal Anodes (Gerbrand Ceder, University of California Berkeley)	123
Task 4 – Metallic Lithium	126
Task 4.1 – Lithium Dendrite Prevention for Lithium Batteries (Wu Xu and Ji-Guang Zhang, Pacific Northwest National Laboratory)	128
Task 4.2 – Composite Electrolytes to Stabilize Metallic Lithium Anodes (Nancy Dudney and X. Chelsea Chen, Oak Ridge National Laboratory).....	131
Task 4.3 – Enabling Solid-State Batteries through Characterization and Modeling (Nenad M. Markovic and Larry A. Curtiss, Argonne National Laboratory)	136

Task 4.4 – 3D Printing of All-Solid-State Lithium Batteries (Jianchao Ye, Lawrence Livermore National Laboratory)	139
Task 4.5 – Interfacial Studies on Lithium Thiophosphate Based Solid Electrolytes and Cathodes (Jagjit Nanda, Oak Ridge National Laboratory)	142
Task 4.6 – Prelithiation of Silicon Anode for High-Energy Lithium-Ion Batteries (Yi Cui, Stanford University)	145
Task 5 – Sulfur Electrodes	147
Task 5.1 – Novel Chemistry: Lithium Selenium and Selenium Sulfur Couple (Khalil Amine, Argonne National Laboratory)	149
Task 5.2 – Development of High-Energy Lithium-Sulfur Batteries (Dongping Lu and Jun Liu, Pacific Northwest National Laboratory)	152
Task 5.3 – Nanostructured Design of Sulfur Cathodes for High-Energy Lithium-Sulfur Batteries (Yi Cui, Stanford University).....	155
Task 5.4 – Investigation of Sulfur Reaction Mechanisms (Enyuan Hu, Brookhaven National Laboratory; Deyang Qu, University of Wisconsin at Milwaukee).....	158
Task 5.5 – New Electrolytes for Lithium-Sulfur Battery (Gao Liu, Lawrence Berkeley National Laboratory)	161
Task 6 – Air Electrodes/Electrolytes.....	163
Task 6.1 – Rechargeable Lithium-Air Batteries (Ji-Guang Zhang and Wu Xu, Pacific Northwest National Laboratory).....	165
Task 6.2 – Lithium-Air Batteries (Khalil Amine, Larry A. Curtiss, and Jun Lu, Argonne National Laboratory)	168
Task 6.3 – Lithium Oxygen Battery Design and Predictions (Larry A. Curtiss/Anh Ngo, Argonne National Laboratory; Amin Salehi-Khojin, University of Illinois at Chicago).....	171
Task 7 – Sodium-Ion Batteries	174
Task 7.1 – Exploratory Studies of Novel Sodium-Ion Battery Systems (Xiao-Qing Yang and Enyuan Hu, Brookhaven National Laboratory).....	175
Task 7.2 – Development of a High-Energy Sodium-Ion Battery with Long Life (Chris Johnson and Khalil Amine, Argonne National Laboratory)	178
Task 7.3 – High-Capacity, Low-Voltage Titanate Anodes for Sodium-Ion Batteries (Marca Doeff, Lawrence Berkeley National Laboratory)	181
Task 7.4 – Electrolytes and Interfaces for Stable High-Energy Sodium-Ion Batteries (Ji-Guang Zhang, Pacific Northwest National Laboratory)	183
Battery500 Consortium Program	
Innovation Center for Battery500 (Jun Liu, Pacific Northwest National Laboratory; Yi Cui, Stanford University)	186

TABLE OF FIGURES

Figure 1. Representative 200-mAh pouch cell following calendar life test (left). Coated 200 mAh following calendar life test (right).....	5
Figure 2. Powder X-ray diffraction patterns of cycled NMC-532 cathodes as a function of time/voltage/electrolyte.....	5
Figure 3. (a) Cycling performances of cathodes with PENDI-350 / polyethylene oxide / polyvinylidene fluoride (PVDF), referred to as PPPVDF, and PVDF as binders at different C rates. Their sulfur loadings are 4.4 mgS/cm ² and 4.2 mgS/cm ² , respectively. (b) Cycling performances of cathodes with different S/electrolyte ratios. The sulfur loadings are 4.1 mgS/cm ² (5E), 4.6 mgS/cm ² (7E), and 4.2 mgS/cm ² (10E).....	8
Figure 4. Electrochemical impedance spectra as a function of temperature of (a) Control, (b) Process I, (c) Process II, and (d) Process III composites from 1 MHz to 10 Hz. Expanded figures of (e) Process II and (f) Process III are provided.....	11
Figure 5. Arrhenius plot of the Control, Process I, Process II, and Process III composites.....	12
Figure 6. Effective diffusion coefficients of LiPF ₆ in 3:7 EC:EMC in Celgard 2500 as measured by the restricted diffusion method. Different curves represent different data fitting methods. The team can observe that restricting the data fitting regime to the characteristic diffusion time (l^2/D) is essential to obtaining diffusion coefficients of the right order of magnitude. Literature values taken from Landesfield & Gasteiger, <i>Journal of the Electrochemical Society</i> 166 (2019): A3079–A3097.	14
Figure 7. Lithium transference number calculated using the Balsara Newman method (orange) for LiPF ₆ at various concentrations in 3:7 wt:wt EC:EMC. Using an ideal transference number of 0.35 from literature, the team obtains transference numbers similar to those reported in literature using the Hittorf method. Literature values from Landesfield & Gasteiger, <i>Journal of the Electrochemical Society</i> 166 (2019): A3079–A3097.	15
Figure 8. (a) Schematic showing the structure of ionic polymer coated on the Li-metal electrode. The ionic polymer comprises of x: PFPE-DMA backbone, y: PETMP crosslinker and z: STFSI-Li salts. (b) I-V curve obtained from cycling voltammetry measurements using microelectrode. The inset shows schematic of three-electrode configuration using a microelectrode working electrode, lithium as counter electrode, and Ag/AgCl as reference. The electrolyte used in the measurement is 1 M LiTFSI in EC/DEC. (c) Comparison of exchange current density measured by cyclic voltammetry measurements where the microelectrode is either bare or coated with polymer of different immobilized salt content. Inset shows results only for the polymer-coated microelectrodes.....	18

Figure 9. (top left) Comparison of Coulombic efficiency measurements in Li Cu configuration, where the copper is coated with or without different ionic polymers and the bulk electrolyte utilized is 1 M LiTFSI in DME as well as 2 M LiTFSI in DME. (top right) Comparison of lithium morphology on copper electrode after depositing and stripping 5 mAh/cm ² of lithium before re-depositing the same amount, using the electrolyte 1 M LiTFSI in DME. The scale bars represent 5 μm. (bottom) Long-term Coulombic efficiency measuring using a Li Cu electrode for the polymer coated and bare copper cases at two different current densities of 1 mA/cm ² and 3 mA/cm ² , with the plating time in both cases being 1 hour. The electrolyte utilized here is 1 M LiTFSI in DOL/DME with 1 wt% LiNO ₃ .	19
Figure 10. Electrochemical filtering treatment to reduce concentrations of impurity particles near the electrode/electrolyte interfaces in lithium symmetric cells. (a) Schematic of electrochemical filtering of lithium impurities. (b) Current density and voltage of the treatment. (c) Slice through a reconstructed volume of a symmetric cell. (d) Slices through a reconstructed volume of the symmetric cell in (c) after an electrochemical filtering treatment. (e) Slices through a different area of the cell after treatment showing impurity particles attached to the polymer electrolyte at both lithium/electrolyte interfaces. Adapted from Reference 1.	22
Figure 11. (a) Small LiPO ₃ preform in first-version grip. (b) Full LiPO ₃ preform. (c) Highly flexible drawn film ~ 200-μm thick.	24
Figure 12. (left) 100g sodium MOS preform. (right) Drawn, partially crystallized, MOS sodium film.	24
Figure 13. (a) Differential scanning calorimetry scan of a mixed-glass-former (MGF) mixed-oxy-sulfide-nitride (MOSN) glassy solid electrolyte (GSE) showing that this glass far exceeds the milestone. (b) Arrhenius plot of the Li ⁺ ion conductivity of a MGF MOSN GSE that shows it has conductivity of 1.3 x 10 ⁻⁴ (Ωcm) ⁻¹ at 25°C, below the milestone; GSEs with higher conductivities are being developed. (c) DC electronic ASR of a MGF MOSN GSE showing that this GSE far exceeds the milestone. (d) Cyclic voltammetry scan on a MGF MOSN GSE showing that this GSE has electrochemical stability up to 5 V versus Li ⁺ /Li and exceeds the milestone. (e) Thermal gravimetric analysis measurements of MOSN GSE in air showing that this glass meets the milestone.	25
Figure 14. (a) Electrochemical impedance spectroscopy results for Au//Au blocking electrode for this quarter's ceramic ion conductor designs. (b) X-ray diffraction results for Wildcat synthesized LATP and LLZO powders.	28
Figure 15. Scanning electron microscopy and ionic conductivity data for various LATP/Li ₃ BO ₃ ratios.	29
Figure 16. (a-b) Ionic conductivity of LATP/Li ₃ BO ₃ with varied processing condition. (c-d) Ionic conductivity of various M-site dopants on Li _{1.3} Ti _{1.7} M ₃ PO ₄ . (Note: triplicate cells were used for all data points).	29

Figure 17. Manufacturing of thin-film composite with desired microstructure and thickness. (a) Fracture surface of 70- μm -thick LLZO thin film, in comparison to the (b) fracture surface of a 1-mm-thick hot-pressed LLZO pellet.....	31
Figure 18. Electrochemical impedance spectra of 1-mm-thick hot-pressed LLZO using 10- μm -thick precision micro electrodes.	31
Figure 19. Synthesis and characterization of bi-layer $\text{Li}_7\text{N}_2\text{I-LiOH} \text{Li}_3\text{YCl}_6$ solid-state electrolyte. (a) Scheme of the synthesis process for the electrolyte pellet. Scanning electron microscopy images of (b) Li_3YCl_6 , (c) $\text{Li}_7\text{N}_2\text{I-LiOH}$, and (d) the cross section of the cold-pressed pellet.....	33
Figure 20. Electrochemical performance of the bi-layer $\text{Li}_7\text{N}_2\text{I-LiOH} \text{Li}_3\text{YCl}_6$ solid-state electrolyte. (a) Electrochemical potential window and (b) lithium plating/stripping curve at the current density of $10 \mu\text{A}/\text{cm}^2$	34
Figure 21. Lithium dendrite formation mechanism in solid-state electrolytes (SSEs). (a) Illustration of Butler-Volmer model for lithium plating in SSE. (b) Lithium dendrite formation and growth mechanism in SSE with different properties.	35
Figure 22. Density functional theory calculated interface energy for compounds against lithium metal.	36
Figure 23. The electrochemical performances of lithium plating and stripping in the $\text{Li}/\text{Li}_3\text{N-LiF/LPS}/\text{Li}_3\text{N-LiF}/\text{Li}$ cell at room temperature. (a) Voltage profiles in the symmetric cell at increased current densities with constant capacity of $0.3 \text{ mAh}/\text{cm}^2$. The details indicated by the red dashed lines are shown in (b) and (c).	37
Figure 24. Voltage profile of lithium plating/stripping for large current density. Voltage profiles of the symmetric cell at (a) current density of $1.0 \text{ mA}/\text{cm}^2$ and (b) step-increased current densities and capacity (fixed 1-hour time for lithium plating/stripping). (c) Scheme for activation process at the interface; the red dashed line indicates the new interface after activation process.	37
Figure 25. (a) High-resolution transmission electron microscopy image of NMC-85105@LiNbO_3 powder. The LiNbO_3 coating is amorphous and $\sim 10.1\text{-nm}$ thick on this particular NCM particle (parallel red lines). (b) In addition to scanning electron microscopy energy-dispersive X-ray spectroscopy, $\text{NMC-85105@Li}_3\text{PO}_4$ was characterized using X-ray photoelectron spectroscopy. P2p signal provides evidence for phosphate species.....	40
Figure 26. (a) Differential scanning calorimetry (DSC) results for composites composed of 70 wt% NCM-85105 and 30 wt% $\beta\text{-Li}_3\text{PS}_4$. Onset of exothermic signal is shifted to higher temperatures with the application of NCM coating (black arrow). (b) DSC results for composites composed of 70 wt% NCM-85105 and 30 wt% $\text{Li}_6\text{PS}_5\text{Cl}$. Onset of exothermic signal is unchanged, but peak response is reduced by nearly an order of magnitude, and completion of the reaction is shifted to higher temperature.....	41

Figure 27. Statistics of the interface stability for different compositions of NMC and layered oxides compositions.	44
Figure 28. Lithium with graphite lamination (right) in comparison with pristine lithium surface (left) after 0, 1 st , and 5 th cycles.	46
Figure 29. Comparison of coated and pristine lithium anode. (top right) Pristine lithium surface. (top left) Pristine lithium surface after five high-rate cycles. (lower left) Elastic surface coating. (lower right) Elastic surface coating after five high-rate cycles.....	46
Figure 30. (a) Chemical composition of baseline-optimized molecular ionic composite (MIC) film with relative percentages of each component. (b) Photograph of MIC film with improved uniformity and flexibility. (c) Temperature dependence of ionic conductivity of the MIC film. (d) Separate diffusion coefficients of ionic liquid (IL) cation and anion in the film compared to the diffusion coefficients of pure IL. (Li ⁺ diffusion coefficient measurements are under way.) This composition enables robust electrolyte films down to 60- μ m thickness that can reversibly thermally cycle from -50°C to +200°C.	49
Figure 31. Li Li symmetric cell cycling plot acquired at 100°C, with current ramping to show maximum current density for this film at <i>ca.</i> 0.8 mA/cm ² . The team is in the process of pushing Li Li cell testing over a wide temperature range, and extracting electrochemical information such as Li ⁺ transference number.	50
Figure 32. Tensile stress-strain curve for molecular ionic composite (MIC) electrolyte film at room temperature. The three curves represent tests on dogbone samples cut from various locations spanning the as-cast film. Tensile modulus averages 400 MPa. These MIC films exhibit approximately 2 \times higher strain at break relative to non-Li-loaded MICs and comparable tensile modulus (see first-quarter report on dynamic mechanical analysis curves). Note that assembly under compression into (Li Li symmetric) coin cells does not damage the film, as observed after disassembly.	50
Figure 33. Conductivity and critical current density (CCD) of the electrolyte materials. Baseline material has conductivity of 4.5 mS/cm and CCD of 3 mA/cm ² at 25°C.	53
Figure 34. The progress of development of NMC cathode: improved specific capacity (left) and electrochemical loading (right).	54
Figure 35. From left to right: separator film, cathode film, and cathode/separator bilayer film (scanning electron microscopy cross-section image). The separator is 40 μ m and the cathode is 120 μ m in this case.	54
Figure 36. (a) X-ray diffraction spectra and (b) Arrhenius plot of Li ₇ P ₂ S ₈ Br _{0.5} I _{0.5} glass ceramic solid electrolyte.	56
Figure 37. (a) X-ray diffraction and (b) Raman spectra of synthesized 75Li ₂ S-25P ₂ S ₅ -5Li ₃ N-xAl ₂ S ₃ (x = 0, 1, 2, 3 and 4) glass solid electrolytes.	57

Figure 38. (a) X-ray diffraction spectra and (b) Arrhenius plot of 75Li ₂ S-25P ₂ S ₅ -5Li ₃ N-4Al ₂ S ₃ glass-ceramic solid electrolytes.....	57
Figure 39. (a) Rate performance and (b) corresponding second-cycle charge/discharge voltage profile of sulfur cathode <i>without</i> additives. (c) Rate performance and (d) corresponding second-cycle charge/discharge voltage profile of sulfur cathode <i>with</i> additives.	58
Figure 40. Scanning electron microscopy images of Al-LLZO particles before and after ball milling (a-b) and sintered Al-LLZO pellets (c-d) prepared from (a) and (b), respectively.	61
Figure 41. (a) X-ray diffraction patterns of polished pellets sintered from Al-LLZO and Al-LLZO_b samples. (b) Arrhenius plots of total ionic conductivity measured on sintered pellets.	61
Figure 42. (a) Schematic illustration of fabrication of the modified cell with graphene window to study electrode/electrolyte interfaces. (b) Tomography image in a region where graphene window is in contact with the solid-state electrolyte (SSE: PEO + LiTFSI mixtures at EO/Li ratios of 10:1) in the cell. (c) Nano Fourier transform infrared (nano-FTIR) spectra collected with IR laser at locations of SSE and SSE with graphene window. (d) Nano-FTIR spectra collected with synchrotron IR light source at locations of SSE with graphene window.	64
Figure 43. (a) 2D X-ray fluorescence (XRF) elemental map of pristine and cycled (100 cycles, 2.8-4.4 and 4.8 V versus Li/Li ⁺) concentration-gradient NMC-622 (CG-NMC-622) cathode particles. (b) Cross-sectioned view from 3D XRF reconstructed image of 100 cycled CG-NMC-622 (2.8-4.4 V versus Li/Li ⁺) and its quantitative composition analysis.	66
Figure 44. (a) The creep depth-punching stress profiles of the mossy and bulk lithium. (b) The impression velocity-holding time profiles of the mossy and bulk lithium during the holding period between 400 and 600 s. (c) and (d) are the Gaussian distributions of the impression velocity of bulk and the mossy lithium during the holding period between 400 and 600 s, respectively. The steady-state impression velocity is determined as the expectation value (the average value) of Gaussian distribution. (e) The impression velocity-punching stress profile of the mossy and bulk lithium. The impression creep velocity of bulk lithium caused by diffusion is also plotted in (e). (f) Schematic of the diffusion paths in lithium dendrites.	69
Figure 45. (a) The creep depth (h _{creep}) of bulk lithium during the holding period increases remarkably with the punch stress ($\sigma_{ind}=F_{max}/A$, where A is the projected area of the flat punch). Surprisingly, h _{creep} of the mossy lithium is much smaller than that of bulk lithium and increases slightly with increasing σ_{ind}	70

Figure 46. (a, left) Number of Li-O bonds at Li/Li ₂ O interface. (a, right) Number of Li-F bonds at Li/LiF interface before and after <i>ab initio</i> molecular dynamics simulation. (b) Kinetic Monte Carlo (KMC) results of (left) case I, reducing $\Delta E_{\text{TL}_{2 \rightarrow 1}}$ and of (right) case II, increasing $\Delta E_{\text{TB}_{2 < 1}}$. (c) Illustration of KMC simulation incorporating lithium delithiation (purple) and lithium atom diffusion in the lithium anode (yellow). (d) KMC results with different current density upon Li/Li ₂ O (10^{-3} , 10^2 , and 10^6 A/cm ²) and Li/LiF (10^{-3} and 10^{-6} A/cm ²).....	70
Figure 47. Intentional poisoning of the baseline electrolyte to identify the role of EC in lithium whisker formation in coin-cells. (a) Scanning electron microscopy image of lithium particles deposited in the baseline electrolyte (1 M lithium bis(fluorosulfonyl)imide salt in dimethoxyethane). (b) Corresponding cryo-transmission electron microscopy (cryo-TEM) image of the lithium particle. (c-d) Poisoning of the baseline electrolyte by adding 0.2% EC leads to a co-existence of distinguished morphology of both monolith and whisker. (e-f) Increasing EC concentration to 2% in the baseline electrolyte induces almost a dominance of lithium whisker formation. Inset in (f) shows high-resolution cryo-TEM image of the lithium metal viewing from the [110] zone axis as shown by the ball model. Note that small ice crystals can also be seen in the cryo-TEM images due to water vapor condensation in sample preparation process.	73
Figure 48. Capacity retention of Li-ion cells using a liquid electrolyte, showing that the decorated Ta-LLZO is compatible with NMC-622.....	78
Figure 49. Thermal gravimetric analysis of aged Ta-LLZO and aged Al-LLZO shows similar behavior between Ta-LLZO and Al-LLZO.	78
Figure 50. Plane view scanning electron microscopy images of the LLZO thin film on Nb- STO (100) substrate.	81
Figure 51. (left) X-ray diffraction scan of LLZO/Pt/STO (100) substrate. (right) Rocking curve scan of LLZO (004) peak.....	81
Figure 52. (a) Schematic of sample preparation for curvature measurement of LLZO – Li-metal anode stress evolution. (b) Schematic of bending measurement with laser reflection on a prepared sample.....	82
Figure 53. Micro-cell based on thin-stack solid-state cells. (a) Scanning electron microscopy image of thin-stack NMC/SSE/Li cell. (b) Micro-cell setup consisting of a mounting stage, heating module, and pressure-sensing module.....	84
Figure 54. Validation of the heating module in the micro-cell setup. (a) Calibration curve for the heating power–temperature relationship. (b-c) Nyquist plots for symmetrical micro-cell tested at 25°C (b) and 45°C (c), respectively.	84

Figure 55. Validation of pressure sensing module in the micro-cell setup. (a) Pressure change of micro-cell during complete cycle. (b) Corresponding charge–discharge profile of cell. Inset: schematics of the cell configuration.	85
Figure 56. Estimated room temperature self-diffusion coefficients of Li ⁺ (a) and O ²⁻ (b) in Al ₂ O ₃ and ZnO with varying Li ⁺ concentration.	88
Figure 57. Lithium electrodeposition morphologies and corresponding stress contours (σ_{yy}) in the SEI layer at an operating temperature of (a) 300K and (b) 350K. An increase in temperature from 300K to 350K results in smoothening of the metal morphology and a reduction in the mechanical stress experienced by the SEI layer.	91
Figure 58. Molecular dynamics simulations of LiPF ₆ /DME solutions in contact with lithium metal. (a) Expansion of top layers of lithium metal (average density ~ 0.25 g/cc); bottom layers remain at lithium crystal density (~ 0.55 g/cc). (b) Initial configuration of lithium slab (purple, bottom) and electrolyte phase (top). (c) Expansion of lithium metal. (d) Nucleation and growth of LiF phase (F: light blue, C: grey and O: red) at the top of the expanded region.	91
Figure 59. Impact of exchange current density on interfacial delamination and subsequent capacity fade. (a) NMC/LLZO interface. (b) LCO/LLZO interface. Applied current density is 1 A/m ² . For both NMC and LLZO, extent of delamination is independent of exchange current. However, capacity fade decreases with increasing exchange current density.	94
Figure 60. Fitting curve of predicted $E_{g,GB}$ (eV) versus density functional theory calculated $E_{g,GB}$ (eV).	97
Figure 61. (a) The list of simulated phases, that is, amorphous structures with different anion ratio and representative crystalline phases. (b) The ionic conductivity extrapolated 300K for the materials in the list.	100
Figure 62. Schematic illustration of preparation of Li-S cathode with poly (2-vinyl, 1, 4-phenylene sulfide).	103
Figure 63. (a) Adsorption energy of lithium polysulfide on PDVF and block co-polymer. (b) Mechanical properties of co-polymer with different ethylene ratio.	103
Figure 64. (a) 3ω sensor for analysis of lithium symmetric cell based on thermal signal. (b) Sensitivity analysis of symmetric cells with 100- μ m Li-metal anode assuming $R_{b_{Li-LLZO}} = 3 \times 10^{-5} \text{ m}^2\text{K/W}$	106
Figure 65. 3ω sensor used for (a) anode of the lithium symmetric cell and (b) LLZO pellet. (c) 3ω curve-fit for LLZO.	107

Figure 66. (a) 4ω sensitivity and (b) 2ω sensitivity for heat generated at the Li-Electrolyte interface of a symmetric Li-LLZO cell. Both 4ω and 2ω signals are the most sensitive to the interface while operating at a frequency greater than 1 Hz.	107
Figure 67. A snapshot of the optimized interface between NMC and LBCO.	109
Figure 68. (a) Designability map of the critical temperature T_{crit} that determines the transition between bulk grain- and grain boundary-dominated ion conduction, based on engineering mesoscopic and atomistic microstructural features of polycrystalline LLZO. T_{crit} is shown as a function of varying atomistic grain boundary diffusive prefactor and activation energy (D_0^{GB} , E_a^{GB}), as well as mesoscale grain size and grain boundary width ($\langle d \rangle$, $\langle l_{\text{GB}} \rangle$). (b) Computed anisotropy factor ($D_x^{\text{eff}}/D_y^{\text{eff}}$) as a function of temperature for the two grain structures with different grain shapes.	112
Figure 69. (a) Interfacial structure (Region 1: Li-rich) of LCO (100) / LLZO (001) from <i>ab initio</i> molecular dynamics (AIMD) simulations. The green, blue, yellow, cyan, and red spheres represent lithium, cobalt, lanthanum, zirconium, and oxygen in the LCO/LLZO structures, respectively. (b-e) Plots showing variation in linear atomic densities (along the direction normal to the interface cross-section) of lithium, lanthanum, zirconium, and cobalt, respectively, for the AIMD runs.	113
Figure 70. Demonstration of an electro-chemical impedance spectroscopy of a model polycrystalline sample. Grain boundary width is proportional to the misorientation between the adjacent grains. A sinusoidally varying voltage, with a varying frequency (0 to 108 Hz), is applied on the top edge; the bottom edge remains electrically grounded. The grain boundaries perpendicular to the direction of the current show maximum electric field and contribute most to overall impedance at low frequencies, while the grains contribute most at high frequencies.	114
Figure 71. (a) The found unit cell of a cluster-based solid electrolyte material containing two types of cluster-ions with different compositions and shapes. (b) Calculated phonon spectrum of the material showing that the material is lattice-dynamically stable. (c) Calculated electronic band structure showing the bandgap and density of states showing the elemental contributions.	116
Figure 72. Energetics of sulfur-halogen site-disordering in lithium argyrodites [$\text{Li}_6\text{PS}_5\text{F}_k\text{X}_{1-k}$] doped with two halogen species evaluated using density functional theory calculations. Using $\text{Li}_6\text{PS}_5\text{F}_{0.5}\text{Cl}_{0.5}$ as a representative example, selected configurations with different extent/type of site disordering between sulfur in $4c$ sites, and halogens (F/Cl) in $4a$ sites are shown, including (a) pristine fully ordered structure, (b-c) one antisite formed by swapping locations of nearest sulfur and chlorine [1 S-Cl (b)] and fluorine [1 S-F (c)], (d-f) two S/X antisites, (g-h) 3 S/X antisites, and (i) 4 antisites. In all panels, the final relaxed configuration is shown along with its cohesive energy relative to the fully ordered pristine structure (as shown in panel a). Quasi-rigid PS_4 tetrahedra are highlighted in orange, while lithium, sulfur, phosphorus, and chlorine atoms are depicted as purple, yellow, orange, green, and blue spheres, respectively.	119

Figure 73. <i>Ab initio</i> molecular dynamics (AIMD) simulations to understand Li ⁺ ion transport in halogen-doped lithium argyrodites. (a) Mean-squared displacement of lithium atoms over 100 ps of AIMD simulations at 700 K in Li ₆ PS ₅ Cl, Li ₆ PS ₅ F, and Li ₆ PS ₅ F _{0.5} Cl _{0.5} electrolytes. The spatial density distribution of lithium ions in the AIMD trajectory is shown for (b) Li ₆ PS ₅ F _{0.5} Cl _{0.5} , (c) Li ₆ PS ₅ F, and (d) Li ₆ PS ₅ Cl. Dark maroon colors represent the highest density value, followed by red and yellow colors.....	120
Figure 74. Synthesis and characterization of halogen-doped argyrodites. X-ray diffraction patterns of (a) F-doped lithium argyrodites and (b) F-Cl/Br/I co-doped lithium argyrodites. Arrhenius plots of (c) F-doped lithium argyrodites and (d) F-Cl/Br/I co-doped lithium argyrodites.....	121
Figure 75. Fabrication of mesoporous composite cathodes with sulfur and sulfide electrolyte. Carbon, sulfur, and phosphorus elemental maps of large (20-100 nm) carbon nanocages impregnated with (a-c) sulfur, (d-f) LPS, and (g-i) sulfur followed by LPS.	122
Figure 76. Schematic of the mix ionic-electronic conductor model for a full solid-state battery cell during charging process material.	124
Figure 77. Potential distribution in the solid electrolyte in a symmetric cell.	124
Figure 78. (a-d) Low magnification transmission electron microscopy images of electrochemically deposited lithium (EDLi) under current density of (a) 0.1 mA cm ⁻² , (b) 2 mA cm ⁻² , (c) 5 mA cm ⁻² , and (d) 9 mA cm ⁻² . Insets: Digital photos of deposited lithium. (e) Composition information acquired from EDLi interface between lithium and SEI, and SEI and the surface of SEI areas at different current densities.	129
Figure 79. Scanning electron microscopy images of electrochemically deposited lithium under deposition capacity of 1, 2, and 4 mAh cm ⁻² at a current density of 0.1 mA cm ⁻²	129
Figure 80. Relaxation behavior for different layers of electrolyte in Li//Li cell configuration under 10-mV DC bias.	133
Figure 81. Simulated evolution of concentration of Li ⁺ due to migration and diffusion in Li/PEPE/Li cell.	133
Figure 82. Charge capacity as a function of cycle number for: Li (1/2) PE (5/8) LFP (1/2) (a), Li (1/2) PE (5/8) LFP (3/8) (b), Li (3/8) PE (5/8) LFP (1/2) (c), Li (1/2) PE (1/2) LFP (1/2) (d), and their consistent discharge capacities for 30 cycles (e).	134
Figure 83. Infrared spectroscopy of polymer electrolyte (PE) from different regions (edge versus center) from Li (3/8) PE (5/8) LFP (1/2) after cycle 4 and cell Li (1/2) PE (1/2) LFP (1/2) after cycle 30.....	134
Figure 84. Atomic force microscopy roughness measurement on bare LLTO films in (100) and (001) orientations.....	137

Figure 85. Neutron reflectometry of bare LLTO films with different crystal orientations and crystallinity.	138
Figure 86. X-ray diffraction of sintered projection microstereolithography (PuSL) printed LLZTO films. (a) Bottom-up: LLZTO film with ball-milled powders, treated in argon at 1000°C (black) and 1100°C (red); LLZTO film with raw powders, treated at 900°C (blue) and 1100°C (green). (b) bottom-up: LLZTO-5LBO-1Al film treated in argon at 800°C (black), 900°C (red), 1000°C (blue), and 1100°C (green).	140
Figure 87. Electrochemical impedance spectroscopy of Li LLZTO-5LBO-1Al Li symmetric cell at room temperature. The solid-state electrolyte separator was prepared by projection microstereolithography (PuSL) printing followed with 900°C argon pyrolysis and 700°C dry-air burning.	141
Figure 88. (a) Cryo – transmission electron microscopy image of a composite solid electrolyte containing amorphous Li ₃ PS ₄ + 1 wt% PEO. (b-c) Li ⁺ conductivity measurements of β-Li ₃ PS ₄ and Li ₃ PS ₄ + PEO composites showing (b) Li ₃ PS ₄ + 1 wt% PEO dried at 25°C and 140°C and (c) Li ₃ PS ₄ + PEO composites containing 0.2-56 wt% PEO dried at 140°C.	143
Figure 89. (a) Photographs of lithium masks reagent with varied porosity from 50% to 80%. (b) Initial Coulombic efficiency improvement after prelithiation with the series of lithium masks with different porosity and the corresponding capacity in lithium masks. (Silicon mass loading, ~ 1.5 mg)	146
Figure 90. Rate performance of SeS _x -C with 10 wt% selenium doping in HFE electrolytes with a 1.2 mg cm ⁻² Se-S loading.	150
Figure 91. Charge/discharge curves of SeS _x -C with 10 wt% selenium doping in (a) DME and (b) HFE electrolytes with a 2.5 mg cm ⁻² Se-S loading under different electrolytes/Se-S ratio (μL mg ⁻¹).	150
Figure 92. (a) Cycling performance and (b) charge/discharge curves of SeS _x -C with 10 wt% selenium doping in HFE electrolytes with a high Se-S loading of 4.5 mg cm ⁻² at 0.8 mA cm ⁻² and E/S ratio of 10 μL mg ⁻¹	151
Figure 93. First discharging profiles and <i>in situ</i> electrochemical impedance spectroscopy of electrodes with < 20-μm and > 70-μm particles (Electrode: 45% porosity, 4 mg S/cm ² , and E/S = 4 μL/mg S, I = 0.1C, room temperature, and electrolyte: 1 M LiTFSI/DOL/DME + 0.3 M LiNO ₃).	153

- Figure 94. *In situ* optical observation and electrochemical performance of the nickel foam and graphene-coated nickel (G/Ni) foam electrodes in lithium polysulfide electrolyte. Optical images of (A) nickel foam, (E) G/Ni foam. Optical images of nickel foam in lithium polysulfide electrolyte: (B) at initial state, (C) after charging to 3.0 V, and (D) discharging to 1.5 V. Optical images of G/Ni foam in lithium polysulfide electrolyte: (F) at initial state, (G) after charging to 3.0 V, and (H) discharging to 1.5 V. Snapshots of the constant voltage charging process for nickel foam electrode at: (I) 60s, (J) 90s, (K) 120s, and (L) 150s. Snapshots of the constant voltage charging process for G/Ni foam electrode at: (M) 60s, (N) 90s, (O) 120s, and (P) 150s. (Q) Rate performance of the nickel foam and G/Ni foam electrodes at different current densities. (R) Charge/discharge voltage profiles of the nickel foam (dash line) and G/Ni foam (solid line) electrodes at 0.2C, 1C, and 3C. (S) Cycling performance and Coulombic efficiency of the nickel foam and G/Ni foam electrodes at 0.2 C for 100 cycles. 157
- Figure 95. (left): Schematic representation of the synthesis process for the semi-graphitic ordered mesoporous carbons with metal and nitrogen anchor to lock sulfur within; sulfide anchoring mechanism on Me-N-GOMCs. (right): (a) optimized geometries of most stable Li_2S on Fe/Co/Ni/Cu and nickel double-doped carbon framework surfaces, (b) corresponding adsorption energies on different surfaces of framework and visual adsorption tests of Li_2S_6 in DME by the various powders (inset, left to right: control, Ni-N-GOMC, Cu-N-GOMC, Co-N-GOMC, and Fe-N-GOMC), and (c) S 2p X-ray photoelectron spectra of Fe-N-GOMC/ Li_2S_6 159
- Figure 96. (a) Voltage profiles of Li|Li symmetric cells cycling in different electrolytes at a current density of 1.0 mA cm^{-2} under a capacity limited protocol of 1.0 mAh cm^{-2} . (b) Cycle life of Li- O_2 battery using different electrolytes with repeated discharge and charge cycles at 0.2 mA cm^{-2} (200 mA g^{-1}) and capacity cutoff at 1.0 mAh cm^{-2} (1000 mA g^{-1}). (c) Cross-sectional scanning electron microscopy images of Li-metal anodes in cycled Li- O_2 battery cells with DCE, TFE-LHCE, TTE-LHCE, and OTE-LHCE after 10^{th} cycle at a current density of 0.2 mA cm^{-2} with a capacity limited protocol of 1.0 mAh cm^{-2} . (d) The radar chart for the properties of the electrolytes in this study. (e) Density functional theory calculation data about parasitic reaction energies of G4 solvent and three diluents with singlet oxygen. 166
- Figure 97. Schematic illustration of the charge and discharge processes with or without the LiI in Li- O_2 batteries using ACs electrodes. 169
- Figure 98. The initial discharge–charge voltage profiles of Li||1M LiTFSI/TEGDME||Cs- O_2 cell, Li||1 M LiTFSI/TEGDME||ACs- O_2 cell, and Li||1M LiTFSI/TEGDME+0.5 M LiI||ACs- O_2 cell at a current density of 0.02 mA/cm^2 (a), the CV curves of Li||1M LiTFSI/TEGDME||ACs- O_2 cell and Li||1M LiTFSI/TEGDME + 0.5 M LiI||ACs- O_2 cell within a voltage widow of 2.0~4.5 V at a scanning rate of 1 mv/s [inset: enlarged cyclic voltammetry curve of biomass-derived activated carbons] (b). 169

Figure 99. Discharge/Charge voltage profile. (a) 25mM InI ₃ and current density of 0.5Ag ⁻¹ . (b) 25mM InI ₃ and current density of 1Ag ⁻¹ . (c) 25mM InBr ₃ and current density of 1Ag ⁻¹ . (d) 25mM InBr ₃ and current densities of 1Ag ⁻¹ discharging and 2Ag ⁻¹ charging.....	172
Figure 100. (a) <i>Ex situ</i> X-ray diffraction data and (b) <i>ex situ</i> pair distribution function (PDF) data of pristine, charged, and discharged NaCrSSe. (c) PDF data of pristine sample and (d) PDF data of charged sample fitted using density functional theory calculated structural models. In both (c) and (d), contributions from major atomic pairs are also shown in the lower panels.....	176
Figure 101. X-ray diffraction patterns for the (a) Pb _{0.7} M _{0.3} -O-C and (b) Pb _{0.5} M _{0.5} -O-C nanocomposite materials prepared by high energy ball mill of PbO, carbon, and the additional elements, M (Sn, Sb, Fe, Mn, or Ni). The marked impurity phases are Sn (◆), Sb (♣), Fe ₂ O ₃ (*), Mn ₂ O ₃ (•), and NiO (Δ).....	179
Figure 102. The initial specific capacity of the Pb _{1-x} M _x -O-C nanocomposite anodes tested in (a) sodium and (b) lithium half-cells (voltage = 0.005 – 2.0 V versus sodium and 0.005 – 3.0 V versus lithium; current density = 100 mAh/g; electrolytes = 1 M NaPF ₆ in EC/DEC with 2% FEC for sodium cells, 1.2 M LiPF ₆ in EC/EMC with 10% FEC for lithium cells).....	180
Figure 103. Temperature-dependent powder X-ray diffraction data of Na _x Ti _{2-x/4} O ₄	182
Figure 104. Powder X-ray diffraction patterns of the products after the solid-state reactions of Cs _x Ti _{2-x/4} O ₄ with NaCl.	182
Figure 105. Electrolyte additive effect on cathode and hard carbon electrochemical performance. (a) Cycling stability and (b) Coulombic efficiency (CE) of Na NaCu _{1/9} Ni _{2/9} Fe _{1/3} Mn _{1/3} O ₂ cells in carbonate electrolyte with/without VC additive. (c) Cycling stability and (d) CE of Na NaCu _{1/9} Ni _{2/9} Fe _{1/3} Mn _{1/3} O ₂ cells in phosphate electrolyte with/without NaBF ₄ additive. (e) Cycling stability and (f) CE of Na hard carbon cells in phosphate electrolyte with/without NaBF ₄ additive.	184
Figure 106. (left) First-cycle of ECOPRO NMC-811 versus lithium with 1 hour charge at C/20 and then discharged to 2.8 V with different current rates: C/20, C/50, and C/200. (right) Comparison of NMC-811 with LCO charged to 120 mAh/g lithium removal.	187
Figure 107. Reduction of first loss of NMC-811 by a niobium treatment for three charge levels.....	187
Figure 108. Nyquist plots showing the electrode-level and whole-cell impedances for NMC-900505 cathodes cycled with Li-metal (left) and graphite (right) anodes as a function of cycle number.	188

Figure 109. Covalently attaching an ether to the hydrofluoroether allows for both high ionic conductivity and oxidative stability (the team’s approach). Synthesis of fluorinated ethers through deprotonation of fluorinated tetraethylene glycol (FTEG) and fluorinated triethylene glycol (FTriEG) and subsequent addition of varying alkoxy halides.	189
Figure 110. Ionic transport and conductivity. Ionic conductivity as a function of LiFSA salt content (closed symbol: 0.1 M; open symbol: 1 M) for (a) FTEG compounds and (b) FTriEG compounds with tetraglyme as the control in both. (c) Activation energy obtained from Arrhenius fits of conductivity versus temperature for 0.1 M LiFSA salt concentration. (d) ⁷ Li cation and FSA (¹⁹ F) anion diffusivities and lithium transference number obtained through pulsed field gradient nuclear magnetic resonance for 0.1 M LiFSA in FTriEG compounds. (e) Linear sweep voltammetry of Li stainless-steel cells with different electrolytes to measure their oxidation stability.	189
Figure 111. (a) Coulombic efficiency as a function of stacking pressure under various current densities. (b/d) Top view and cross-section view of deposited lithium morphology formed under no pressure. (c/e) Top view and cross-section view of deposited lithium morphology formed under critical pressure. The lithium in (b-e) was deposited at 2 mA/cm ² for 1 hour.....	190
Figure 112. Comparison of cycling performance of sulfur/polyacrylonitrile (SPAN) electrodes in different electrolytes. (a-c) Thick SPAN electrode with areal capacity loading of 6 mAh cm ⁻² , at 1.2 mA cm ⁻² (C/5). (b) Voltage profiles of thick SPAN electrode in conventional carbonate electrolyte. (c) Voltage profiles of thick SPAN electrode in novel ether electrolyte. The amount of electrolyte is 3g Ah ⁻¹	191
Figure 113. Voltage versus time for 10 cycles: (a) 2D model 1C rate, (b) 2D model C/3 rate, (c) 1D model 1C rate, and (d) 1D model C/3 rate.....	192
Figure 114. (a) Initial and (b) 50 th charge–discharge curves of pristine and LATP-coated Al-NMC-811 electrodes. (c) Cycling performance of pristine and LATP-coated Al-NMC-811 electrodes.	193
Figure 115. Proposed mechanism and corresponding data for initial nucleation and growth of Li-metal deposits in electrolyte that contains HF.	193
Figure 116. Incremental capacity analysis (dQ/dV) of Li NMC-811 performance and capacity fading with a LiFSI/DME-TFEO diluted high-concentration electrolyte-containing cell. Incremental capacity variations associated with phase transitions (H1-M-H2-H3) are identified and quantified.....	194

TABLE OF TABLES

Table 1. Properties of electrolytes used for lithium filtering study.	21
Table 2. Decomposition energy and phase equilibria of LLZ with lithiated and delithiated (prefix “d-”) LCO and NMC-111 from thermodynamic analyses based on first-principles data.	44
Table 3. Charge transfer resistance values at NMC/LLZO interfaces and LCO/LLZO interfaces with corresponding exchange current densities.	94
Table 4. Density functional theory calculated bandgaps for bulk, grain boundaries, and surfaces in LiF, Li ₂ O, and Li ₂ S.	97
Table 5. Room-temperature (25°C) ionic conductivity (σ) of 0.5 M LiTFSI electrolyte with various HFE amphiphilic additives (F ₄ EO ₂ and F ₈ EO ₄) and TTE dilution.	162

A MESSAGE FROM THE MANAGER: ADVANCED BATTERY MATERIALS RESEARCH PROGRAM AND BATTERY500 CONSORTIUM

The DOE Vehicle Technologies Office Annual Merit Review was held on June 1–4, 2020. During the meeting, the FY 2019 Advanced Battery Materials (BMR) and Battery500 Consortium efforts were reviewed at a high level for their value and contributions. Over 350 participants joined the virtual conference. In this document, we report in a more in-depth manner on the progress made from January 1, 2019, through March 30, 2019.

A few notable achievements from the BMR investigators this quarter are summarized below.

- The Pacific Northwest National Laboratory group (Wang) found that poor Li-conducting carbonate species in the initial SEI adjacent to lithium metal plays a critical role in formation of lithium whiskers, demonstrating that dendrite-free lithium deposition requires facile transport of lithium in the initial SEI.
- The Argonne National Laboratory group (Markovic, Curtis) confirmed the interface reaction of lithium and polyethylene oxide (PEO) using X-ray photoelectron analysis (XPA). New features in the O1s, C1s, and Li1s spectra revealed evidence for lithium dissolution in the PEO and reaction forming organolithium (LiCR) and lithium alkoxide (LiOR) species.
- The University of California – Berkeley group (Ceder) gained a better understanding of lithium phosphorus sulfide (LPS) solid electrolyte conductivity by investigating the role of anion building blocks (PS_4^{3-} , $\text{P}_2\text{S}_6^{4-}$, and $\text{P}_2\text{S}_7^{4-}$). Anion building blocks have been regarded as a key descriptor for ionic conductivity. The team generated amorphous structures with different ratios of building blocks, maintaining the chemical composition at $\text{Li}_3\text{PS}_{4-\delta}$, using the *ab initio* molecular dynamics (AIMD) simulated melt-quench method. While the simulations reproduced the experimental results, no correlation was found between the presence of certain anion blocks and calculated conductivities.
- The University of Michigan group (Sakamoto) developed a scalable approach to manufacturing thin ($\leq 100 \mu\text{m}$) $\text{Li}_7\text{La}_3\text{Zr}_2\text{O}_{12}$ (LLZO) films with comparable microstructures and conductivities to that of bulk-processed LLZO presently manufactured using hot-pressing methods.
- The Brookhaven National Laboratory group (Yang and Bak) used advanced hard X-ray fluorescence (XRF) imaging techniques to study the structural stability of concentration-gradient Ni-rich NMC cathode particles, which revealed a well-maintained compositional gradient even after 100 cycles. This work represents the first report on the use of a non-invasive technique to observe the concentration gradient structure, without the need of cross-sectioning samples.
- The Stanford University group (Cui) demonstrated improvements in electrochemical performance when using liquid sulfur in Li-S batteries. During this investigation, a nickel-foam current collector was observed to exhibit good polysulfide trapping and chemisorption confinement response, displaying a capacity of 360 mAh/g and 300 mAh/g at 2C and 3C current rates, respectively, with a stable capacity of 500 mAh/g at the end of 100 cycles. In contrast, a carbon-coated nickel exhibited a capacity of only 275 mAh/g and 110 mAh/g under similar current rates.
- The University of Wisconsin – Milwaukee group (Qu) collaborated with Brookhaven National Laboratory (Hu) to synthesize carbon structures containing metal-nitrogen anchors ($\text{M} = \text{Cu}, \text{Ni}, \text{Fe}, \text{Co}$) for sulfide and polysulfide species. Density functional theory (DFT) calculations showed that Fe-N containing ordered mesoporous structures exhibit the most favorable adsorption energies for Li_2S (-3.01 eV) compared to -0.3 eV for pure carbon and -0.54 eV for nitrogen-doped carbon, suggesting the ability of nickel and iron dopants in carbon to effectively suppress active sulfur loss and improve cycling stability.

Highlights from the Battery500 Consortium team include the following:

Keystone Project 1 (Materials and Interfaces)

- The different behavior of NMC-811 and LCO first-cycle loss was elaborated. Coating NMC-811 cathode with niobium oxide was shown to be effective in reducing the first-cycle loss (Binghamton University).
- Anode-to-cathode crossover was suggested as a contributor to the failure mechanism in ultra-high nickel ($\text{LiNi}_{0.9}\text{Mn}_{0.05}\text{Co}_{0.05}\text{O}_2$) Li-metal batteries (University of Texas – Austin).
- A series of fluorinated ether electrolytes was designed and synthesized to simultaneously obtain high ion conductivity, high transference number, and high voltage stability (Stanford University).

Keystone Project 2 (Electrode Architectures)

- Significant advancements were made in understanding the quantitative dependence of lithium nucleation, growth, dissolution, morphology, and cell performance on stack pressure when employing a sulfur/polyacrylonitrile (SPAN) cathode (University of California – San Diego).
- A 2D moving boundary model was developed to study the nature of transport in a liquid electrolyte and the resulting 2D deposition profile on the lithium anode. The model can be used to study how charging rate, anode length, separator length and thickness, and cycling influence the deposition profile on the anode (University of Washington).

Keystone Project 3 (Cell Fabrication and Testing, and Diagnosis)

- Incremental capacity analysis was found to aid in identifying the cycling implications from lithium loss (Idaho National Laboratory).
- A pressure aware model has been developed that can be used to study how charging rate and design parameters influence the deposition profile on the lithium anode (University of Washington / University of Texas – Austin).

We encourage you to follow our progress as we proceed. Our next report is expected to be available in September 2020.

Sincerely,

Tien Q. Duong

Tien Q. Duong
Manager, Advanced Battery Materials Research Program & Battery500 Consortium
Batteries & Electrification R&D
Energy Efficiency and Renewable Energy
U.S. Department of Energy

TASK 1 – Liquid/Polymer Solid-State Electrolytes

Summary and Highlights

The BMR Program goal is to develop long-life batteries superior to commercial Li-ion systems in terms of cost, vehicle range, and safety. The BMR Program addresses the fundamental problems of electrode chemical and mechanical instabilities that have slowed development of affordable, high-performance, automotive batteries. The aim is to identify electrode/electrolyte materials that yield enhanced battery performance and lead to greater acceptance of electric vehicles (EVs). Currently, the U. S. Department of Energy (DOE) Vehicle Technologies Office (VTO) supports 16 projects in the BMR Program under this Electrolytes Task. These projects can be categorized into four general topics:

- **Liquid.** The projects for liquid electrolyte aim to develop electrolyte formulations, based on fluoro-chemistries, to achieve significantly improved operating voltage, increased durability, and increased energy density of Li-ion batteries at a reasonable cost. Nonaqueous polyelectrolyte solutions with high Li^+ transference numbers will be developed to achieve high rate capabilities at room temperature. In addition, electrolytes with new polymer binders bearing a pentafluorophenyl group on the backbone will be designed, synthesized, and tested.
- **Polymer.** The targets of polymer electrolyte projects include inorganic/polymer and polymer/gel hybrid electrolytes that have flexibility, mechanical strength, thermal stability, high ionic conductivity, stable interfaces against lithium metal, and polysulfide-trapping capability enabling energy density Li-S batteries, with comparable cycle life.
- **Self-Forming & Self-Healing.** The self-forming, self-healing electrolyte projects are focused on developing and implementing Li-metal-based metal fluorite and metal iodide batteries, capable of energy densities > 400-500 Wh/kg and 1000 Wh/L.
- **Solid-State.** The solid-state projects are to develop high conductivities solid electrolytes / composite solid electrolytes that are scalable, are chemically and electrochemically stable, and will enable low-cost, high energy-density solid-state lithium batteries (SSLBs).

Highlights

At the Daikin group (Sunstrom, Hendershot, and Falzone), testing of the interim cells sent to Idaho National Laboratory (INL, *Go/No-Go* FY 2019 Milestone) has been completed, with data being compiled for delivery. Pouch cells with NMC-532 cell chemistry were delivered, with baseline hydrocarbon cells failing prior to reaching 300 cycles at 4.5 V and 4.6 V. The fluorinated electrolyte cells showed promising results at 4.5 V and 4.6 V and met the project performance targets. An improved method for quantifying evolved gas in pouch cells was developed in this quarter.

The University of Washington (UW) group (Jen and Yang) is waiting for data of test cells sent for performance evaluation at a designated DOE testing laboratory. They have designed and optimized the composites of PENDI-350 / polyethylene oxide (PEO) / polyvinylidene fluoride (PVDF), referred to as PPPVDF, as a binder for deliverable test cells that possesses the following advantages: (1) PENDI-350 impedes diffusion of long-chain lithium polysulfides (LiPS) via electrostatic trapping and redox mediation by the NDI units, (2) PVDF helps to improve the film forming mechanical property of the binder system, and (3) long-chain PEO improves electrolyte compatibility between PVDF and PENDI-350, both in wettability and mixability. In addition, the team has chosen the ratio of 7 μL electrolyte per mgS to fabricate the final cells.

At Stony Brook University (SBU, Takeuchi), significant gains in conductivity were achieved through process modification of the solid electrolyte. This was demonstrated through impedance testing over a series of temperatures.

The University of California (UC) at Berkeley team (McCloskey) continued their method development to fully characterize liquid electrolyte transport properties by investigating the origins of parameter sensitivity through rigorous data fitting and optimization, as well as COMSOL Multiphysics modeling. They found that the ideal solution transference number obtained by the Bruce Vincent method choice is largely responsible for the accuracy of transference number; therefore, they plan to test the feasibility of performing Bruce-Vincent measurements in Li-Al alloy cells, which should have improved interfacial stability over Li-metal cells.

The Stanford University group (Bao and Cui) is completing evaluation of polymer basic cycling performance: 0.5 and 1 mA/cm² conditions in Li|Li and Li|Cu cells using carbonate electrolyte.

The Lawrence Berkeley National Laboratory (LBNL) group (Balsara) has completed a milestone: electrochemical filtering treatment was used to reduce concentrations of impurity particles near the electrode/electrolyte interfaces in lithium symmetric cells. Cells filtered were imaged using hard X-ray microtomography. No inhomogeneities were observed at the top nor the bottom lithium electrode/electrolyte interfaces after 14 conditioning cycles. They found that for most cells, increased lifetime due to electrochemical filtering was not due to a reduction in the number of deposition defects per area, but rather due to differences in defect morphology (voids versus protrusions). Thus, this electrochemical filtering treatment will be used to reduce concentrations of impurities in hybrid organic-inorganic materials before cycling in future experiments.

The Iowa State University (ISU) group (Martin) moved onto using the low-cost, easily produced Li⁺ ion conducting glassy solid electrolyte (GSE) LiPO₃ glass. They have been successful in drawing over 5 meters of film while optimizing the use of the draw tower. To access all levels of the draw tower safely, a scaffold with access platforms was purchased and installed. The mixed-glass-former (MGF) mixed-oxy-sulfide-nitride (MOSN) GSEs they are developing have met all milestones for the project except Li⁺ ion conductivity.

The Wildcat group (Carroll/Peebles) first synthesized two types of ceramic ion conductors, Li_{6.55}La₃Zr_{1.5}Ta_{0.5}O₁₂ (LLZO) and Li_{1.3}Al_{0.3}Ti_{1.7}PO₄ (LATP) by solid-state methods. Phase pure materials were synthesized using Wildcat's high-throughput (HT) synthesis platform. They have synthesized LATP and films with 3% Li₃BO₃ with the appropriate conductivity, which will be used as the control ceramic ion conductor in the next several quarters in the trilayer testing.

The University of Michigan (UM) group (Sakamoto) used a scalable approach to manufacture thin ($\leq 100 \mu\text{m}$) LLZO films with comparable microstructures and conductivities to bulk-processed LLZO that is manufactured using hot-pressing methods. This approach will guide manufacturing of thin-film composites (TFCs) throughout subsequent milestones. In addition, using thermal vapor deposition (TVD), thin Li-metal microelectrodes can be manufactured with precise thicknesses below 100 μm . Precision microelectrodes can be deposited and tested successfully on thick LLZO membranes and will be incorporated into TFC constructs. These electrodes will be used throughout subsequent milestones.

The University of Maryland (UMD) group (Wang) demonstrated successful fabrication of the Li₇N₂I-LiOH|Li₃YCl₆ solid-state bilayer, which has the stability window of 0.0-5.0 V. They also worked on lithium dendrite suppression criterion for solid electrolytes, and identified Li₃N-LiF electrolyte as protective layer for LPS electrolyte. The long cycle stability of Li/Li₃N-LiF/LPS/Li₃N-LiF/Li cell at a high and fixed current of 1.0 mA/cm² and capacity of 1 mAh/cm² is demonstrated.

General Motors (GM, Yersak) applied LiNbO₃ and Li₃PO₄ coatings to NCM-85105 powders. In addition, they showed that the kinetics of the reaction between NCM and the Li₆PS₅Cl solid-state electrolyte (SSE) are slowed down by 80-90% by the presence of a passivating coating.

At UMD (Wachsman and Mo), Computational studies based on the thermodynamic analyses of first-principles calculations have been completed in evaluation of the thermodynamic interface stability between LLZ solid electrolytes and layered oxide cathode materials. They found that Ni-rich cathode materials such as NMC exhibit mutual chemical reactions, suggesting a limited interface stability between LLZ garnet and

NMC cathode materials. In addition, delithiated NMC shows poor interface stability with LLZ garnet, indicating potential interface degradation during cycling or the charged state of the solid-state battery (SSB). In addition, their data suggest that higher nickel content in cathodes generally leads to poor stability.

The team at University of Wisconsin Milwaukee (UWM, Qu) has started to develop engineering processes to create dynamic interfacial layers on metallic lithium anodes. Three approaches were applied: physical lamination, surface self-assembled interfacial layer, and surface fluorination. They showed that the *ex situ* formed artificial interface on lithium anode can become an effective interface between lithium anode and SSE.

The team at Virginia Polytechnic Institute and State University (Virginia Tech, Madsen) has searched the composition space of lithium salts, ionic liquids, and polymer (PBDT) molecular weight, as well as the relative concentrations of each component. In Li|Li symmetric cell testing, so far the Pyr₁₄TFSI ionic liquid and LiTFSI salt have the best chemical and electrochemical stability, evidenced by current cycling from +23°C to +100°C. The team has so far cycled a Li|Li cell for > 100 hours at 0.6 mA/cm² and 100°C. Mechanical testing of the molecular ionic composite films has also been conducted.

The team at Solid Power (Zhang) and UC San Diego (UCSD, Meng) found two electrolyte materials that outperformed the first-quarter baseline on both conductivity and critical current density (CCD). For the cathode, capacity was increased to 160 mAh/g (at electrode level) from 130 mAh/g by optimizing the cathode formulation. Electrochemical loading was also successfully increased to 3.5 mAh/cm². In addition, the separator was fabricated by using the same slurry-casting method as the cathode, which can be directly laminated to a cathode to form a cathode/separator bilayer film.

The Pennsylvania State University (PSU, Wang) group has successfully prepared two types of solid electrolytes; Li₆PS₅Cl and Li₇P₂S₈Br_{0.5}I_{0.5} use ball milling and post heat treatment process with high ionic conductivity similar to the literature report. In addition, a series of glass-ceramic solid electrolytes of 75Li₂S-25P₂S₅-5Li₃N-xAl₂S₃ (x = 0, 1, 2, 3 and 4) was synthesized using dry ball milling method. Due to existence of Li₂S impurities, the ionic conductivity at 25°C is merely 0.08 mS cm⁻¹ and activation energy is 0.27 eV. To solve the issue of low ionic conductivity, they plan to decrease Li₂S content in the designed solid electrolyte system. Furthermore, utilization of sulfur was greatly improved in the cathode they developed, fulfilling the proposed milestone of demonstrating sulfur cathode with high discharge capacity of > 1000 mAh g⁻¹ using new solid additives.

Task 1.1 – Advanced Lithium-Ion Battery Technology: High-Voltage Electrolyte (Joe Sunstrom, Ron Hendershot, and Alec Falzone, Daikin)

Project Objective. The project objective is to identify electrolyte formulations, based on fluoro-chemistries, that will allow significantly improved operating voltage, increased durability, and increased energy density of Li-ion batteries at a reasonable cost. The project seeks to understand the conditions under which the electrolyte degrades, the effect on battery performance, and solutions that can overcome current limitations of the electrolyte. Gassing in Li-ion batteries is one of the most common failure mechanisms and poses the greatest safety risk in consumer devices. This project aims to investigate gas composition as a function of cathode material, electrolyte formulation, and operating voltage, and proposes optimal cell compositions at decomposition voltages.

Project Impact. Developing an understanding of the operating conditions in which gasses form in Li-ion batteries enables the project to propose optimized cell compositions that operate at higher voltages for a longer period. Different fluorinated electrolyte components and additives may suppress and/or eliminate gas generation at or above hypothesized decomposition voltages. To investigate these topics, it is imperative that the project utilize multiple approaches, including, but not limited to, cathode material, electrolyte composition, operating voltage, and cycle number.

Approach. The evolving composition of the electrolyte in the battery will be examined by various analytical instruments to study volatiles [gas chromatography – mass spectrometry / thermal conductivity detection (GC-MS/TCD)], liquid [liquid chromatography MS (LC-MS)], and solid [time-of-flight secondary ion mass spectrometry (TOF-SIMS), thermogravimetric analysis MS (TGA-MS), X-ray photoelectron spectroscopy (XPS), and auger electron spectroscopy (AES)] electrolyte decomposition products during battery operation. In the first year, the team addressed gas composition and kinetics for both hydrocarbon and fluorocarbon as a function of several charge/discharge conditions. In the second year, the project will transition into analysis of the SSE decomposition components of its tested batteries to obtain valuable information about solid electrolyte interphase (SEI) layer formation and how it manifests change in both the anode (graphite) and cathode (LCO and NMC). The third year is focused on measuring changes in the solid-state structure of the cathode following high-voltage operation. The project aims to quantify any dissolved metal ions originating from the cathode and deposited on the anode using inductively coupled plasma – mass spectrometry (ICP-MS). It will also study changes in the cathode structure using powder X-ray diffraction (XRD).

Out-Year Goals. Work will progress toward understanding how electrolyte formulation and cell operation affect stability of transition metals (TMs) in the cathode structure. The project aims to quantify metal ions, if any, dissolved into solution as a function of operating parameters (that is, voltage, time, etc.) and electrolyte formulation. In addition, measurements will be made using powder XRD to detect changes in the crystal structure of the cathode (LCO and NMC). Understanding effects on the solid-state structure in Li-ion batteries will provide valuable information on the required cathode chemistry for increased performance at high voltage.

Collaborations. The project has initiated a collaboration with Dr. J. Chan (University of Texas, or UT, at Dallas) for powder XRD measurements to investigate changes in cathode structure as a function of operating conditions.

Milestones

1. *Go/No-Go Decision:* Interim cells achieve significant improvement at 4.6 V. (Q4, FY 2019; Complete)
2. Cathode structure versus time/voltage. (Q3, FY 2020; In progress)
3. Data compilation and selection of new electrolyte composition. (Q4, FY 2020; In progress)

Progress Report

As reported, preliminary results were obtained last quarter from the interim cell submission to INL (*Go/No-Go* FY 2019 Milestone). Testing of the cells is completed, and data are being compiled for delivery. Pouch cells with NMC-532 cell chemistry were delivered, with baseline hydrocarbon cells failing prior to reaching 300 cycles at 4.5 V and 4.6 V. The fluorinated electrolyte cells showed promising results at 4.5 V and 4.6 V and met the project performance targets.

An improved method for quantifying evolved gas in pouch cells was developed this quarter. A multilayer coating was applied to the outside of the pouch cells prior to gas injection. This modification allows for repeat injections along with minimizing the introduction of air during manual GC/MS injections. The first applied layer serves as an interfacial surface to promote adhesion to the external surface of the Mylar pouch. The top, rubberized layer adheres to the interfacial surface and is the functional layer that enables repeat injections and suppresses atmospheric dilution. Figure 1 (left) depicts a typical coated 200-mAh pouch cell following a calendar life test at 55°C. Figure 1 (right) depicts representative pouch cells with the applied coating. Quantitative results from the optimized method of GC/MS analysis are being compiled and will be reported next quarter.

Powder XRD data were obtained on tested full cells with NMC-532 as the cathode (200 cycles, 0.7C, CC/CC) and were analyzed at the respective upper cutoff voltage. Cells were deconstructed in a glovebox; the NMC-532 cathode was washed with dimethyl carbonate (DMC), dried *in vacuo*, and sealed with an air-tight material prior to analysis. The initial aim is to determine effects on cathode structure at the upper cutoff voltage as a function of electrolyte in NMC-532 cells (4.2 V versus 4.6 V).^[1-2] In addition, the team aims to investigate differences in cathode structure from portions taken from the edge and middle areas of the jelly roll to investigate potential variations in the regional structure. Figure 2a-b depicts NMC-532 cathodes at 4.2 V from each region of the cell. Figure 2c-d depicts NMC-532 cathodes at 4.6 V from each region of the cathode.



Figure 1. Representative 200-mAh pouch cell following calendar life test (left). Coated 200 mAh following calendar life test (right).

Diffraction patterns from the edge and middle portions of the NMC-532 cathodes at both 4.2 V and 4.6 V did not show much variance, and are consistent with what has been reported previously in the R $\bar{3}m$ layered structure.^[1-3] As expected, voltage has the largest effect on changes to the layered structure, with electrolyte composition having little to no effect. Previously reported dissolved metals analysis (FY 2019) of the anode suggests accelerated TM dissolution at 4.6 V. Identifying defect sites with TM deficient regions of the cathode will be performed in Q3 utilizing X-ray fluorescence (XRF).

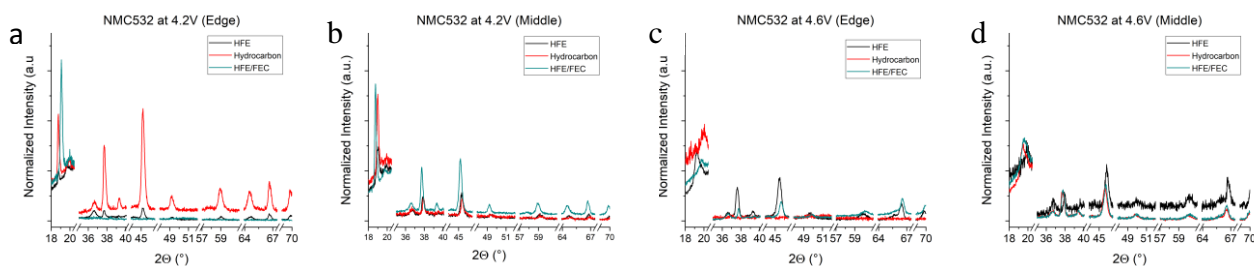


Figure 2. Powder X-ray diffraction patterns of cycled NMC-532 cathodes as a function of time/voltage/electrolyte.

References

- [1] Tian, C., D. Nordlund, et al. *Journal of the Electrochemical Society* 165 (2018): A696–A704.
- [2] Bak, S., E. Hu, et al. *ACS Applied Materials & Interfaces* 6 (2014): 22594–22601.
- [3] Yin, L., Z. Li, et al. *Chemistry of Materials* 32 (2020): 1002–1010.

Patents/Publications/Presentations

The project has no patents, publications, or presentations to report this quarter.

Task 1.2 – Multi-Functional, Self-Healing Polyelectrolyte Gels for Long-Cycle-Life, High-Capacity Sulfur Cathodes in Lithium-Sulfur Batteries (Alex Jen and Jihui Yang, University of Washington)

Project Objective. The project objective is to develop self-healing and polysulfide-trapping polyelectrolyte gels containing room-temperature ionic liquid (RTIL) for the Li-S battery system. The Li-S battery design will be able to achieve gravimetric and volumetric energy densities of ≥ 800 Wh/kg and ≥ 1000 Wh/L, respectively.

Project Impact. The Li-S battery system is hampered by poor capacity retention, primarily caused by dissolution of polysulfide reaction intermediates in typical organic electrolytes, as well as poor electrical contact between insulating sulfur and the conductive carbon matrix. This project aims to produce a high-capacity, long-cycle-life Li-S battery system by using rational molecular design strategies to address each capacity loss mechanism directly. A long-cycle-life Li-S battery system capable of doubling Li-ion energy density would enable production of lighter, longer range EVs at a cost that is affordable to the average U. S. household.

Approach. The team will develop Li-S coin cells that utilize self-healing, interpenetrated ionomer gel electrolytes in both the cathode and separator. The team will synthesize necessary starting materials and fabricate components of these gels while testing their relevant electrochemical and mechanical properties. All components are combined into interpenetrating structures, which are being tested both alone and in cell configurations. Device performance data were collected and used to further optimize designs of both material and cell, culminating in an optimized Li-S battery design capable of doubling the energy density of traditional Li-ion batteries. The team has focused on (1) design and synthesis of various precursors for gel electrolytes, (2) fabrication and testing of both reference materials and novel materials made from these precursors, and (3) iterative validation and improvement of design principles through both materials and device testing.

Out-Year Goals. Work will progress toward developing structure-property relationships for the self-healing, interpenetrated gel ionomer electrolyte and its individual components, as well as successful incorporation of such an electrolyte into a working Li-S cell. The team plans to demonstrate significant improvements in both capacity and retention when using the project's developed materials, as compared to state-of-the-art reference systems.

Collaborations. This project funds work at UW. Dr. A. Jen, principal investigator (PI), focuses on design, synthesis, and testing of novel materials, as well as device-based verification of design principles. Dr. J. Yang (co-PI) focuses on optimizing device fabrication and testing, as well as investigating failure mechanisms in devices using novel materials. Pacific Northwest National Laboratory (PNNL) facilities are used for detailed material characterization study.

Milestones

1. Provide test cells for performance evaluation at a designated DOE testing laboratory: 12 baseline cells or half cells with a minimum capacity of 10 mAh, and 12 improved cells or half cells with a minimum capacity of 10 mAh. (Q1, FY 2020; Completed)
2. Suggest test procedures for the cells/half-cells evaluation. This should include discharge/charge voltage and current limits, number of test sequences, recommended cycling temperature, or other relevant test conditions as appropriate. (Q1, FY 2020; Completed)
3. Analysis of deliverable test cell performance data collected by the designated DOE testing laboratory. (Q2, FY 2020; Expected)

Progress Report

Self-Healing Polymer Binders for S/C Composite Cathodes. As reported earlier, the team has designed and optimized composites of PPPVDF as a binder for deliverable test cells that possesses the following advantages: (1) PENDI-350 impedes diffusion of long-chain lithium polysulfides (LiPS) via electrostatic trapping and redox mediation by the NDI units, (2) PVDF helps to improve the film forming mechanical property of the binder system, and (3) long-chain PEO improves electrolyte compatibility between PVDF and PENDI-350, both in wettability and mixability. Moreover, the team has modified the surface of mesoporous carbon (MJ430) with -SH (thiol) functional groups. The polar, surface thiol groups improve wetting of the electrode surface by the electrolyte due to the dipole-dipole interaction of the thiol groups with lithium ion in the electrolyte, which improves utilization of active sulfur during cycling.

As shown in Figure 3a, a sulfur cathode using PPPVDF as binder with sulfur loading of 4.4 mgS/cm^2 was fabricated, and cycling performance of the cell was tested at different C rates. The initial specific discharge capacity at C/20 was 1197 mAh/g , corresponding to 10.5 mAh of discharge capacity and thus meeting the project goal. Specific discharge capacity reaches 947 mAh/g , even at C/2 rate at 11th cycle. It remains $\sim 870 \text{ mAh/g}$ at 80th cycle. In addition, the team has fabricated control sulfur cathode by using PVDF as binder with sulfur loading of 4.4 mgS/cm^2 to compare. The initial specific discharge capacity of the PVDF cathode was as high as 1347 mAh/g at C/20, followed by a sharp drop to 1176 mAh/g . However, the control cathode using PVDF as binder failed at 10th cycle. The team attributes this to the significant dissolution of sulfur into electrolyte, which leads to shuttle effect and side reaction on anode side.

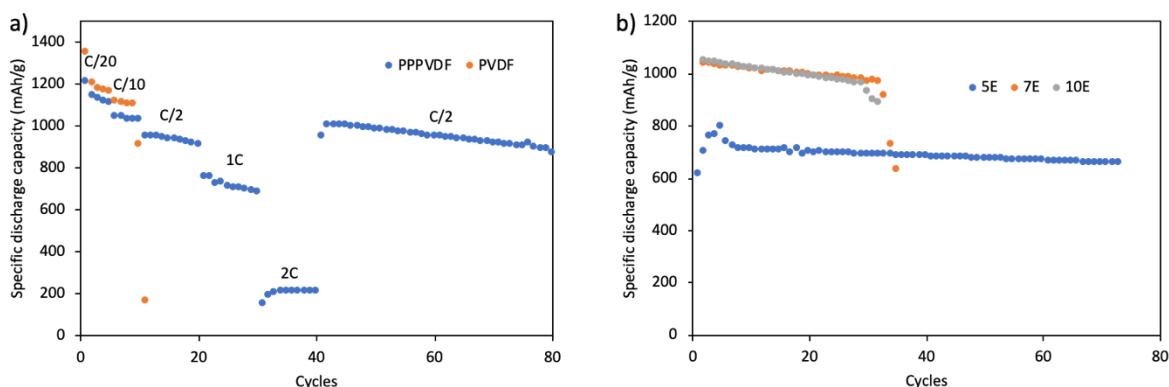


Figure 3. (a) Cycling performances of cathodes with PENDI-350 / polyethylene oxide / polyvinylidene fluoride (PVDF), referred to as PPPVDF, and PVDF as binders at different C rates. Their sulfur loadings are 4.4 mgS/cm^2 and 4.2 mgS/cm^2 , respectively. (b) Cycling performances of cathodes with different S/electrolyte ratios. The sulfur loadings are 4.1 mgS/cm^2 (5E), 4.6 mgS/cm^2 (7E), and 4.2 mgS/cm^2 (10E).

The shuttle effect and anode side reaction are strongly related to electrolyte, especially the ratio between electrolyte and sulfur loading. A low S/electrolyte ratio is known to limit the dissolution of sulfur into electrolyte, consequently improving stability of cycling performance. Additionally, a low S/electrolyte ratio improves the gravimetric energy density of the whole cell by decreasing inactive material contents. However, too low of S/electrolyte ratio could result in limited utilization of sulfur, resulting in a significant drop in specific discharge capacity. Therefore, the team has optimized the S/electrolyte ratio of sulfur cathode using PPPVDF binder and 3-dioxolane (DOL)/1,2-dimethoxythane (DME) electrolyte. Based on the team's previous study, optimization focuses on the ratios of 10, 7, and 5 μL of electrolyte per mgS , noted as 10E, 7E, and 5E. As shown in Figure 3b, cathodes with 7E and 10E ratios follow a similar trend. Their initial specific discharge capacities are around 1034 mgA/g (7E) and 1045 mAh/g (10E), followed by a slow and smooth decrease until around 30 cycles. On the contrary, the initial specific discharge capacity of 5E cathode is 614 mgA/g , implying

much lower utilization of active sulfur. The specific discharge capacity then increases to 712 mgA/g at 8th cycle. The team attributes this to the poor wetting issue of electrolyte in the cathode. On the other hand, this helps stabilize specific discharge capacity to much longer cycles. After consideration, they have chosen the ratio of 7 μ L electrolyte per mgS to fabricate the final cells, which gives high sulfur utilization by using relatively low S/electrolyte ratio. Further investigation to understand sudden failure mechanism after around 35 cycles in cells with lower S/electrolyte ratio is ongoing. Initially, the team has attributed this to failure on anode side. Electrolyte may be repeatedly consumed during the cycles, forming thick SEI that leads to rapid decrease in ion conductivity.

Patents/Publications/Presentations

The project has no patents, publications, or presentations to report this quarter.

Task 1.3 – Dual Function Solid-State Battery with Self-Forming, Self-Healing Electrolyte and Separator (Esther Takeuchi, Stony Brook University)

Project Objective. The project objective is to demonstrate a solid-state rechargeable battery based on a Li-metal anode and iodine cathode with a self-forming, self-healing electrolyte and separator with high gravimetric and volumetric energy density.

Project Impact. This program will enable demonstration of the proposed rechargeable battery with improved power capability, high energy density, and a self-forming, self-healing SSE/separator. Technical insight will be gained regarding improved conductivity of the solid LiI based electrolyte, power capability of the proposed system, the self-healing nature of the LiI layer, the nature of the electrode-electrolyte interfaces, and feasibility of the system to reach the DOE targets.

Approach. The proposed concept is a dual function rechargeable SSB utilizing LiI combined with silver iodide (AgI) as the electrolyte, with lithium metal (and small quantities of silver metal) as the anode and iodine as the cathode and with a self-forming, self-healing separator/electrolyte. The battery will be assembled in the discharged state, where the anode and cathode will be created during the first formation (charge) step. Initially, silver ion (Ag^+) will diffuse toward the negative electrode and be reduced to silver metal (Ag^0), and iodine ion (I^-) will be oxidized to elemental iodine (I_2) at the cathode side. As the formation of the battery continues, lithium ion (Li^+) will form a Li-metal layer at the anode, with generation of iodine at the cathode. LiI will remain and serve as both the separator and electrolyte.

Out-Year Goals. This is a multi-year program where the effort is divided into three major tasks.

- Year 1 involves electrolyte preparation and characterization including preparation of SSEs and conductivity measurements.
- Year 2 will focus on cell construction and testing including both *in situ* and *ex situ* analysis.
- Year 3 will focus on cell characterization. Under the program, cycle life, efficiency, energy density, and the functional capacity of cells will be determined.

Collaborations. This project collaborates with A. Marschilok and K. Takeuchi of SBU.

Milestones

1. Determine cycling performance at elevated temperature. (Q1, FY 2020; Completed)
2. Determine behavior of conductivity as a function of temperature to determine resistance as well as fundamental thermodynamic parameters of the SSEs. (Q2, FY 2020; Completed)
3. Conduct destructive analysis of tested cells. (Q3, FY 2020)
4. Perform extended cycle life testing. (Q4, FY 2020)

Progress Report

Effect of Solid Electrolyte (SE) Processing on Impedance

As reported previously, cell design A included the composite LiI solid electrolyte with LiI(3-hydroxypropionitrile)₂ additive. Last quarter involved significant effort in modifying the preparation process for the SSE. Consideration was made to homogeneity of the composite electrolyte as well as control and determination of the particle size of the LiI constituent in the electrolyte. It was anticipated that the resistance of the electrolyte and the resulting cells could be significantly impacted by the process. The results obtained this quarter demonstrate that supposition to be true.

Variations in processing progressed from the least processed (Process I), to the most processed (Process III). All types were compared to a Control, which received no additional processing beyond the original method used for preparation of the SSE. As the team anticipated impacting the resultant cell resistance, the cells were tested using electrochemical impedance spectroscopy (EIS) as a function of temperature. The data collected for the various cell types are shown in Figure 4. The results revealed that modifying the processing of the electrolyte indeed induced a decrease in impedance of the pristine cells. The pristine, uncharged Control and processed solid-state materials were tested from 33°C to 45°C in 3-degree increments with the series plotted in Figure 4. Clearly, increasing electrolyte processing from the Control (Figure 4a) to Process III (Figure 4d/f) significantly lowers the electrolyte impedance by almost two orders of magnitude. Overall, the shape of the impedance spectra remains similar for the various SSE-containing cells, with slightly flattened semicircles and diffusional tails, angled ~ 45° from the x-axis. The data were further analyzed to determine resistance values from each cell type at each temperature.

Arrhenius Plots

The observed impedance response is typical of solid electrolytes and can be represented with a simple circuit (Figure 5),^[1] with a depressed high-frequency semicircle mainly determined by the bulk electrolyte resistance (R1) in parallel with capacitor (C1) and a constant-phase-angle element (CPE1) attributed to ion movement across grain boundaries (GBs) in a polycrystalline sample. A tilted, low-frequency branch caused by a constant-phase-angle element (CPE2) accounts for the diffusion of ions to the stainless-steel current collectors.

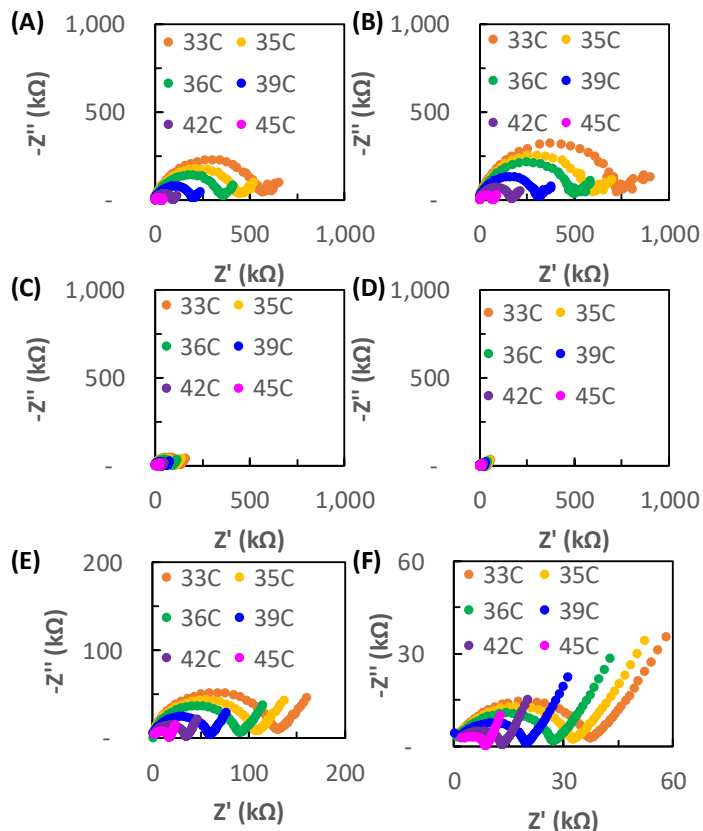


Figure 4. Electrochemical impedance spectra as a function of temperature of (a) Control, (b) Process I, (c) Process II, and (d) Process III composites from 1 MHz to 10 Hz. Expanded figures of (e) Process II and (f) Process III are provided.

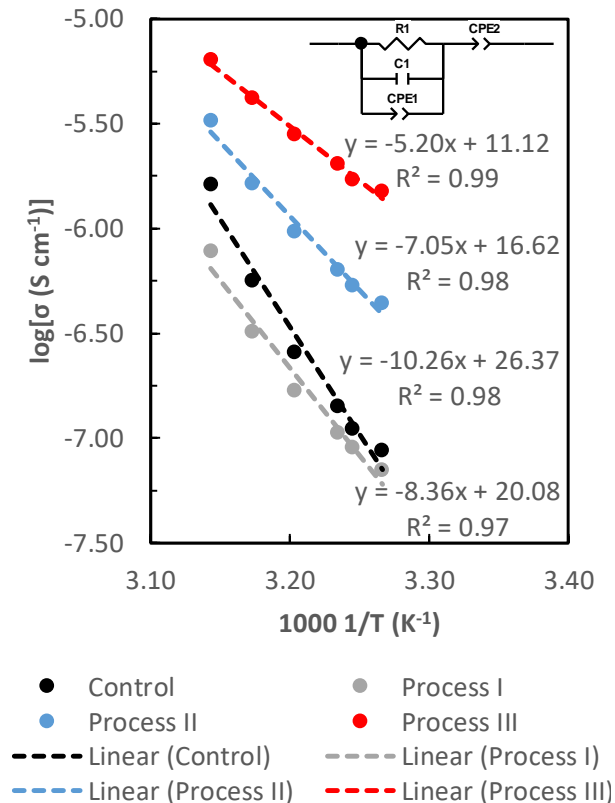


Figure 5. Arrhenius plot of the Control, Process I, Process II, and Process III composites.

References

- [1] Neudecker, B. J., and W. Weppner. "Li₉SiAlO₈: A Lithium Ion Electrolyte for Voltages above 5.4 V." *Journal of Electrochemical Society* 143, no. 7 (1996): 2198–2203.
- [2] Schlaikjer, C. R., and C. C. Liang. "Ionic Conduction in Calcium Doped Polycrystalline Lithium Iodide." *Journal of the Electrochemical Society* 118 (1971): 1147–1450.
- [3] Poulsen, F. W. "Ionic Conductivity of Solid Lithium Iodide and its Monohydrate." *Solid State Ionics* 2 (1981): 53–57.
- [4] Phipps, J. B., and D. H. Whitmore. "Interfacial Conduction in Lithium Iodide Containing Inert Oxides." *Journal of Power Sources* 9 (1983): 373–378.

Patents/Publications/Presentations

Presentation

- Ashton Cary Lecture, Georgia Institute of Technology, Atlanta, Georgia (March 3–4, 2020): "From Medical Applications to the Environment: The Important Role of Electrochemical Energy Storage." Invited named lectureship.

At 33°C, the team found this trend in conductivity: Process III > Process II > Control ~ Process I, with the Process III composite sample reaching a maximum conductivity of 1.5×10^{-6} . The Control sample exhibiting slightly higher ionic conductivity than Process I may be due to differences in sample packing. Previous reports of LiI have determined the conductivity of LiI alone typically to be between 10^{-7} and $10^{-8} \text{ S cm}^{-1}$,^[2-4] proving that the team's LiI solid electrolyte with LiI(3-hydroxypropionitrile)₂ heterostructure and materials processing significantly improves the electrolyte with regard to conductivity. Diffusion through LiI is largely achieved through defects in crystal structure and along GBs. Modifying particle size also results in a larger population of GBs, resulting in greater levels of diffusion along these paths consistent with observed results.

Summary

Significant gains in conductivity have been achieved through process modification of the solid electrolyte. This was demonstrated through testing over a series of temperatures revealing the relative conductivity and response to temperature.

Task 1.4 – Characterization and Modeling of Li-Metal Batteries: Characterization of Li⁺ Transport in Polyelectrolytes (Bryan D. McCloskey, University of California at Berkeley)

Project Objective. This task aims to understand lithium plating and stripping in non-traditional electrolyte systems (specifically, polyelectrolyte solutions and concentrated binary salt electrolytes) that have been proposed to reduce dendrite formation during lithium stripping and plating due to their high Li⁺ transference numbers (t_+). The team will develop capabilities that allow them to understand how ion dynamics in these electrolytes impact macroscale transport properties and Li-metal plating and stripping.

Impact. Ultimately, this task will develop an understanding of how electrolyte composition and molecular interactions can be manipulated to positively impact ion transport of potential electrolytes for Li-metal batteries. This will provide a set of general design rules for novel electrolytes that enable stable, efficient high capacity Li-metal stripping and plating.

Approach. To understand various aspects of lithium plating and ion transport in these systems, the team will develop novel diagnostic and computational modeling techniques. Model polyelectrolytes, with pendant triflimide anions, will be used as polyanions, as their properties can be easily tuned via changes in the polymerization chemistry. Solution parameters that can be varied for both polyelectrolyte solutions and concentrated electrolytes include solvent and salt composition, additive inclusion, and the aforementioned polymer properties, all of which can have a profound impact on electrostatic interactions between charged species in solution, as well as interfacial stability and reaction kinetics of the lithium electrode. The team will develop capabilities that allow them to understand how molecular-level ion dynamics in these electrolytes impact macroscale transport properties and Li-metal plating and stripping. These computational simulations will be validated and refined by comparing results to experimentally measured transport properties of these electrolytes. They will optimize electrochemical methods for these electrolytes to evaluate relevant transport properties under the Newman Concentrated Solution Theory framework, which has never been performed on these non-traditional electrolytes. ¹H and ¹⁹F nuclear magnetic resonance (NMR) diffusometry will also be used to measure single-ion self diffusion coefficients without an applied electric field; solution viscosity measurements using a state-of-the-art rotating sphere viscometer can be performed under entirely air/water-free conditions. The team will develop capabilities to quantitatively understand degradation mechanisms of various electrolytes during Li-metal stripping and plating. Specifically, differential electrochemical MS will be used to study outgassing that occurs from electrolyte degradation processes.

Out-Year Goals. The ultimate goal of this project is to understand the influence of electrolytes with novel transport characteristics on the performance of Li-metal electrodes. Work will continue to build toward a complete understanding of Li-ion and counterion transport in polyelectrolyte solutions and concentrated electrolytes, as well as the impact of electrolyte transport properties on Li-metal uniformity during electrochemical stripping and plating. Outgassing measurements using differential electrochemical MS will be developed to further probe the interfacial reactivity of lithium metal with electrolytes created in this project.

Collaborations. Collaborators on this project include K. Persson (atomistic and coarse-grained modeling) and N. Balsara (electrochemical characterization of polymer electrolytes), both at LBNL.

Milestones

1. Complete study of solvent influence of transport in polysulfone-based polyelectrolyte solutions. (Q1, FY 2020; Completed)
2. Complete development and validation (using known liquid electrolytes) of electrochemical transport methods. (Q2, FY 2020; Completed)

- Complete synthesis and transport characterization of model triflimide-based polyion (pTFSI) solutions in symmetric cells with Li-metal electrodes. (Q3, FY 2020)
- Complete development of coarse-grained polyelectrolyte model to study effect of polyelectrolyte composition on transport of model polyelectrolyte systems. Progress measure: publish article on scaling of transport properties of polyelectrolyte solutions as a function of polymer and solvent properties. (Q4, FY 2020)

Progress Report

Last quarter, the team reported sensitivity analysis of the Balsara-Newman method for electrochemically measuring transport properties in non-aqueous liquid electrolytes, with the goal of implementing this strategy for characterizing polyelectrolyte solutions. They identified significant deviation in transport properties of LiPF₆ in ethylene carbonate : ethyl methyl carbonate (EC:EMC; 3:7 w/w) measured using this method when compared to those in literature that are typically obtained by the Hittorf method. The team noted significant sensitivity of the analysis to fitting of concentration cell and diffusion data. This quarter, they continue method development to fully characterize liquid electrolyte transport properties by investigating origins of parameter sensitivity through rigorous data fitting and optimization, as well as COMSOL Multiphysics modeling.

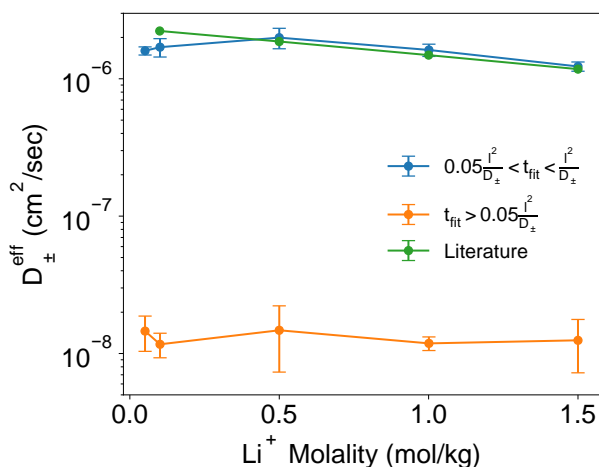


Figure 6. Effective diffusion coefficients of LiPF₆ in 3:7 EC:EMC in Celgard 2500 as measured by the restricted diffusion method. Different curves represent different data fitting methods. The team can observe that restricting the data fitting regime to the characteristic diffusion time (l^2/D) is essential to obtaining diffusion coefficients of the right order of magnitude. Literature values taken from Landesfield & Gasteiger, *Journal of the Electrochemical Society* 166 (2019): A3079–A3097.

gradients prior to measuring diffusion coefficients, effectively increasing the measurement signal-to-noise ratio. The team was further able to acquire more reliable concentration cell data fits (needed for calculating the thermodynamic factor, one of the four important parameters necessary to accurately define electrolytic transport) by acquiring more data points at logarithmic spacings. They found that cell-to-cell variability in concentration cell was significantly smaller than variability induced by the fitting methods. This indicates that testing more concentration conditions is more important than exhaustive replicates of each concentration condition. The team found that nine different logarithmically space concentration cell compositions were needed for fitting methods to converge on the same $\left(\frac{dU}{d\ln(m)}\right)$ behavior for electrolytes over the 0.05 – 1.5 mol/kg range. This knowledge is necessary for rigorous analysis of experimental data, but is not discussed in previous reports that characterize liquid electrolytes.

Last quarter, the team observed that diffusion coefficients found via the restricted diffusion method were particularly sensitive to the data fitting range, with fits over the entire experiment time resulting in diffusion coefficients 2 orders of magnitude smaller than those reported in the literature. This quarter, they found that through restricting the fit window to the characteristic diffusion time for each cell according to the relationship $0.05 \frac{l^2}{D} < t_{fit} < \frac{l^2}{D}$, where l is the separation distance between the planar electrodes, they can obtain more accurate salt diffusion coefficients (see Figure 6). The drastic effect of bounding the fit indicates that at longer relaxation times, they are not actually measuring diffusive phenomena and are instead likely measuring surface phenomena related to slow corrosion of Li-metal electrodes. Despite the new fitting procedure, at low lithium concentration in the electrolyte, the team still sees slight deviation from the diffusion coefficients reported for the LiPF₆/EC/EMC electrolyte system. They believe that this deviation can be further reduced by inducing larger concentration

Incorporating transport coefficients calculated with the expanded data set and new fitting regimes, the team recalculated the transference number, t_+^0 according to equation 1, where t_+^{id} is the ideal solution transference number obtained by the Bruce Vincent method.

$$t_+^0 = 1 - \left[\frac{FD_{\pm}c}{\kappa(v^+z^+)^{\frac{1}{2}} \left(\frac{dU}{d \ln(c)} \right)} \left(\frac{1}{t_+^{id}} - 1 \right) \right] \quad \text{Equation 1}$$

Using this approach, they obtained transference numbers that were negative and much lower than those published in the literature, particularly at higher Li^+ concentrations. Through additional sensitivity analysis of parameters, the team found that the t_+^{id} measurement is largely responsible for this deviation. Adjusting t_+^{id} to a fixed value of 0.35 (within the range expected from the literature), and recalculating t_+^0 , they obtain results in much better agreement with the literature (see Figure 7). They believe significant error from the Bruce-Vincent measurement of t_+^{id} is due to parasitic reactions of the electrolyte with the Li-metal electrodes. Further insight from COMSOL models indicates that the concentration gradients established during the Bruce-Vincent method may result in a potential difference (\sim mV) between electrodes that cannot be precisely resolved by the potentiostat. The team will test this hypothesis in the coming quarter using higher experimental polarization potentials and comparing data to newly developed COMSOL models. Additionally, they plan to explore non-electrochemical method to measure activity coefficients and diffusion coefficients, eliminating the need for the Bruce-Vincent measurement. They also plan to test the feasibility of performing Bruce-Vincent measurements in Li-Al alloy cells, which should have improved interfacial stability over Li-metal cells.

Working toward Milestone 4, the team has developed a coarse-grained polyelectrolyte model to study how transport changes when transitioning from monomeric to polymeric anions. The system is composed of a standard Kremer-Grest polymer model, with charged and neutral Lennard-Jones particles to represent counterions and explicit solvent molecules, respectively. Thus far, the team has used this model to run molecular dynamics (MD) simulations over 13 chain lengths ranging from $N = 1$ to $N = 25$ at five concentrations. The team is analyzing transport properties of these systems by computing the Onsager transport coefficients, which enables them to quantify ion correlations as well as directly compute conductivity, mobility, and transference number. In the coming months, completion of this analysis will give the team some predictive power as to the types of polyelectrolyte solutions that should have the most favorable transport properties.

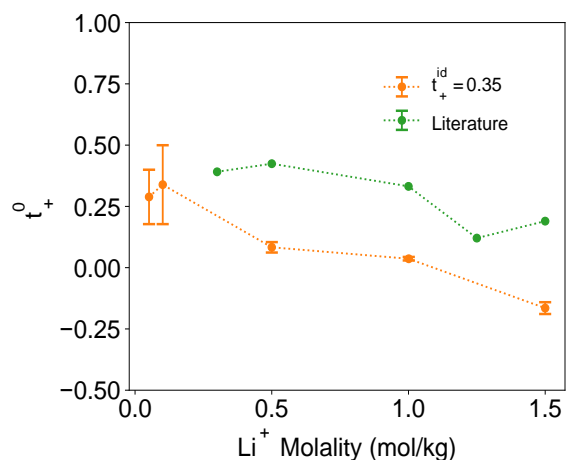


Figure 7. Lithium transference number calculated using the Balsara Newman method (orange) for LiPF_6 at various concentrations in 3:7 wt:wt EC:EMC. Using an ideal transference number of 0.35 from literature, the team obtains transference numbers similar to those reported in literature using the Hittorf method. Literature values from Landesfield & Gasteiger, *Journal of the Electrochemical Society* 166 (2019): A3079–A3097.

Patents/Publications/Presentations

Presentation

- Gordon Research Conference on Batteries, Ventura, California (February 16–21, 2020): “Li-Ion Transference Numbers in Nonaqueous Polyelectrolyte Solutions”; Kara Fong. Poster.

Task 1.5 – Advanced Polymer Materials for Batteries (Zhenan Bao and Yi Cui, Stanford University)

Project Objective. This project will develop new polymer materials for batteries. The team will develop polymer coatings with specific mechanical properties that can accommodate the volume expansion and contraction of the Li-metal anode associated with deposition and stripping (charging and discharging).

Project Impact. The cycling stability and CE of Li-metal electrodes will be increased by implementation of a polymer-based protective layer that functions as an artificial SEI with desired properties. The improved performance will enable further development toward practical utilization of Li-metal anodes with higher cycling efficiency and less susceptibility to dendrite-based failure.

Approach. The project uses soft polymer coatings with dynamic crosslinking to give the resulting polymers liquid-like rheological properties and stretchable and self-healing properties. In previous work, the project has shown that such coatings resulted in uniform deposition/stripping of lithium metal and improved cycling stability of Li-metal electrodes. To understand the design rules for effective polymer coatings, the team chose a few representative polymers to systematically understand structure property relationships. Here, the team investigates the correlation between surface energy of the polymer and exchange current for lithium deposition.

Out-Year Goals. Work will progress toward the correlation between dielectric constant and exchange current. These findings will enable further understanding and development of various polymer coatings for protecting Li-metal anodes.

Collaborations. This quarter, the team is collaborating with J. Qin at Stanford University.

Milestones

1. Analyze the solvation structure and lithium diffusivity of polymer/electrolyte using NMR, Fourier transform infrared (FTIR) spectroscopy, electrochemical tests, and molecular simulations. (Q1, FY 2020; Completed)
2. Evaluate the polymer basic cycling performance: 0.5 and 1 mA/cm² conditions in Li|Li and Li|Cu cells using carbonate electrolyte. (Q2, FY 2020; Completed)
3. Self-healing polymer coated Li||NMC battery: Stable cycling at C/3 rate for 150 cycles using 15 μ l/mAh electrolyte. (Q3, FY 2020)
4. Self-healing polymer coated Li||NMC battery: Stable cycling at C/3 rate for at least 50 cycles using 50- μ m lithium. (Q4, FY 2020)

Progress Report

Li-metal anode suffers from several instabilities during the electrodeposition process in battery charging. Specifically, lithium deposition leads to inhomogeneous coverage on the electrode substrate, resulting in concentration of electric field at the tip of these deposits, ultimately resulting in dendritic growth that shorts the battery. The high surface area metal deposition also causes faster parasitic reactions between the lithium metal and organic electrolyte that is responsible for the rapid fade of battery capacity. According to conventional understanding, the primary sources of instabilities in electrodeposition are diffusion limitations in ion transport processes both in the bulk electrolyte and at the electrode-electrolyte interfaces. Consequently, many theoretical efforts have been focused on modeling dendritic growth in a purely diffusion limited condition by varying the transport properties like ion conductivity and relative mobility of anions and cations (transference number) and on studying their effect on electrolyte modulus or electrode geometry. Likewise, several experimental efforts have reported improved electrodeposition stability with electrolytes with high transference number, conductivity, or modulus. While the ion transport and mechanics are important determinants of morphological evolution of the metal electrode, other coupled parameters like electrochemical kinetics and electrostatic potential landscape can play a critical role. For example, several experimental findings have reported observation of fractal structures during electrodeposition of metallic lithium, even at rates much below the diffusion limited current density. This further indicates that transport parameters in the electrolyte may not be the sole determinant of morphological stability. The relative effect of the electrochemical kinetics and ion transport is particularly important considering the metal electrode does not have a smooth surface, which is aggravated even at earlier stages of deposition. The physical perturbations on the metal surface result in abrupt enhancement of local electric field, causing the ions to be preferentially directed toward the dendritic tips and ultimately leading to unstable growth. In addition, a major challenge in understanding this phenomenon is the fact that the transport and kinetics essentially rely on the same physical factors such as ion concentration, viscosity, and temperature. Here, the team leverages ultrafast scanning voltammetry and pulse-field gradient NMR to decouple the effects of kinetics and transport, respectively. Based on these analyses, they design a polymer interface that stabilizes electrodeposition by maintaining a uniform ion flux to the electrode. Subsequently, they intend to utilize the polymer interface for improving Li-metal battery cycling both in Li||Cu and Li||NMC configurations.

Polymer Coating Design and Electrochemical Analysis

Previously, the team reported the design and synthesis of an ionic polymer network having perfluoropolyether-dimethacrylate (PFPE-DMA) as the polymer backbone, and pentaerythritol-tetrakis(3-mercaptopropionate) (PETMP) as the crosslinker with lithium-styrene-trifluoromethanesulfonyl-imide (Li-STFSI) utilized as salt linker in different ratios (shown in Figure 8a). They further analyzed the Li-ion diffusivity and interfacial resistance using NMR and impedance spectroscopy, respectively. In addition to the ion transport characteristics, the team is also interested in understanding the effect on electrochemical kinetics due to presence of the polymeric networks. Therefore, the team utilizes an in-house built three-electrode setup (shown in inset of Figure 8b) that is comprised of Ag/AgCl reference electrode, lithium metal as counter electrode, and for the working electrode the team uses titanium-based ultramicroelectrode (dia. = 25 μm). The electrolyte media is chosen to be 1 M LiTFSI EC/DEC to mimic the electrochemical environment of the battery. Here, the team uses an ultra-fast scan rate ($v = 30 \text{ V/s}$) for cyclic voltammetry (CV), so that electrodeposition is a reaction-limited process that can reveal important details about the kinetics of electrochemical reaction as well as solvation properties of lithium ions near the metal electrode. The I-V data from the CV experiments is plotted in Figure 8b for different cases of bare and polymer-coated ultramicroelectrodes. The dependence of current on the overpotential, at low values of polarization, can be assumed to be linear, given as, $i \approx i_o \frac{zF}{RT} \eta$. The team plots the corresponding exchange current densities (i_o) for the different samples in Figure 8c. They observe that for the bare electrode exchange current density, $i_o \approx 15 \text{ mA/cm}^2$, while that of crosslinked PFPE (no tethered salts) coated electrode is two orders of magnitudes lower, indicating that the deposition kinetics are significantly slowed down at the electrode. This observation implies that the polymer coating acts as a blocking interface to

inhibit the Li-ion reduction on the anode surface. The presence of grafted salt molecules (Li-SFTFSI) in the network, however, results in increased exchange current density (inset of Figure 8c). The progressive rise with increasing immobilized salt content signifies that the lithium ions experience a loosened solvation shell to undergo faster electrochemical reduction.

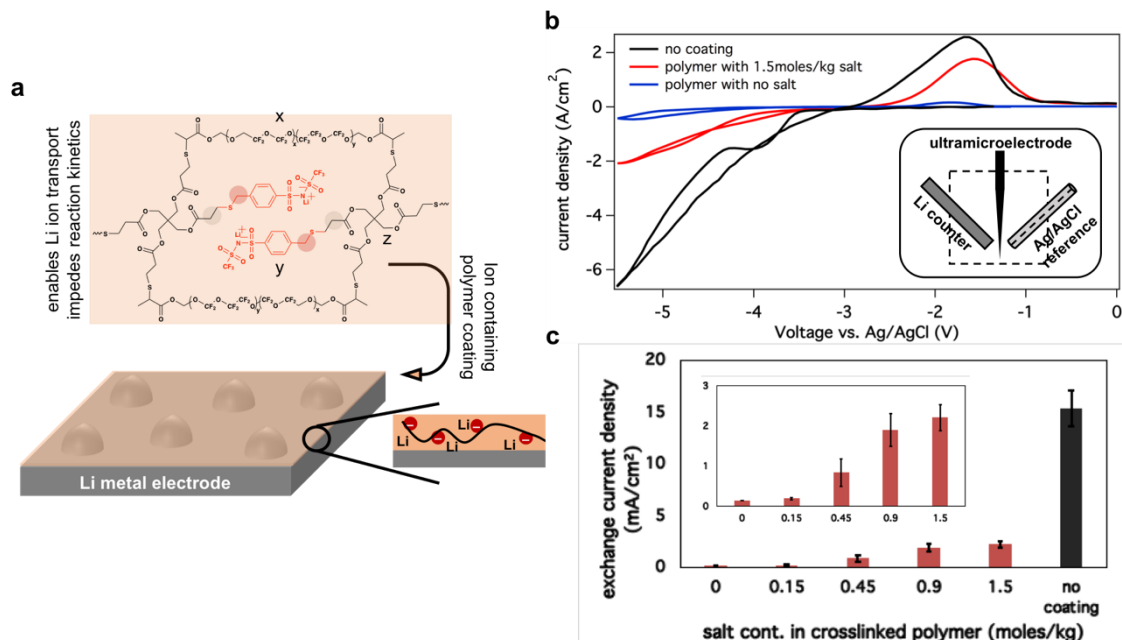


Figure 8. (a) Schematic showing the structure of ionic polymer coated on the Li-metal electrode. The ionic polymer comprises of x: PFPE-DMA backbone, y: PETMP crosslinker and z: STFSI-Li salts. (b) I-V curve obtained from cycling voltammetry measurements using microelectrode. The inset shows schematic of three-electrode configuration using a microelectrode working electrode, lithium as counter electrode, and Ag/AgCl as reference. The electrolyte used in the measurement is 1 M LiTFSI in EC/DEC. (c) Comparison of exchange current density measured by cyclic voltammetry measurements where the microelectrode is either bare or coated with polymer of different immobilized salt content. Inset shows results only for the polymer-coated microelectrodes.

Coulombic Efficiency (CE) Measurements and Morphological Studies

The team examines the effect of the synthesized polymer coatings on the electrode in a Li-metal battery. Figure 9a shows the comparison of the CE for the neat electrolyte with that of polymer-coated electrodes. It is seen with the electrolyte 1 M LiTFSI in DME that there is successive improvement in the CE of lithium metal plating-and-stripping as the grafted salt concentration is increased in the polymer coating, which indicates that the ionic polymers suppress dendritic growth and chemical side-reactions of the lithium metal. It is further seen in Figure 9a that the CE measured using 2 M LiTFSI/DME shows similar behavior such that the ionic polymer coating outperforms the bare electrode. The team analyzed the morphology of lithium deposits using scanning electron microscopy (SEM). In this experiment, they plated 25 μm (5mAh/cm²) of lithium onto a copper electrode with and without the polymer coating; thereafter, they stripped and re-plated the same amount, before disassembling the battery for the SEM analysis using the electrolyte 1 M LiTFSI in DME. As shown in Figure 9b, the electrodeposits without the polymer coating (bare) are fibrous and comprise heterogenous shapes. However, the electrodeposition morphology with 1.5 moles/kg grafted salts is significantly more stable. The long-term performance of the ionic polymer coatings in Li||Cu configuration was analyzed using the electrolyte 1 M LiTFSI in DOL/DME (1 wt% LiNO₃), and the CE was plotted at 1 mA/cm² and 3 mA/cm² current densities. The team observes that the 3M immobilized salt containing polymer coatings significantly outperform the control cells.

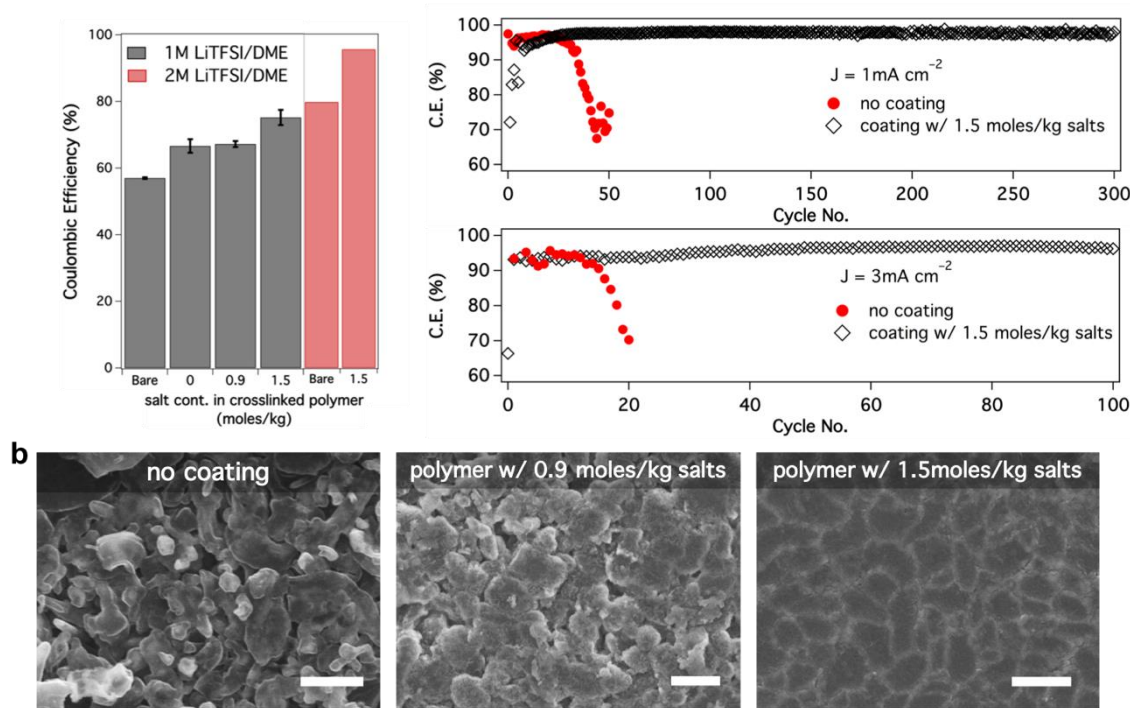


Figure 9. (top left) Comparison of Coulombic efficiency measurements in Li||Cu configuration, where the copper is coated with or without different ionic polymers and the bulk electrolyte utilized is 1 M LiTFSI in DME as well as 2 M LiTFSI in DME. (top right) Comparison of lithium morphology on copper electrode after depositing and stripping 5 mAh/cm² of lithium before re-depositing the same amount, using the electrolyte 1 M LiTFSI in DME. The scale bars represent 5 μ m. (bottom) Long-term Coulombic efficiency measuring using a Li||Cu electrode for the polymer coated and bare copper cases at two different current densities of 1 mA/cm² and 3 mA/cm², with the plating time in both cases being 1 hour. The electrolyte utilized here is 1 M LiTFSI in DOL/DME with 1 wt% LiNO₃.

Patents/Publications/Presentations

Publication

- Amanchukwu, C. V., Z. Yu, X. Kong, J. Qin, Y. Cui, and Z. Bao. "A New Class of Ionically Conducting Fluorinated Ether Electrolytes with High Electrochemical Stability." *Journal of American Chemical Society* 142, no. 16 (2020): 7393–7403. <https://doi.org/10.1021/jacs.9b11056>.

Presentation

- DOE BMR Battery500 Quarterly Review Meeting, Stanford, California (2020): "Stabilizing Lithium Metal Anode by Interfacial Layer"; A. Z. Bao.

Task 1.6 – Improving the Stability of Lithium-Metal Anodes and Inorganic-Organic Solid Electrolytes (Nitash Balsara, Lawrence Berkeley National Laboratory)

Project Objective. The project objective is to establish a new hybrid electrolyte that will be stable against cells with a Li-metal anode.

Project Impact. Polymer electrolytes offer increased stability in lithium batteries in comparison to more widely used liquid electrolytes. Nanostructured electrolytes containing both soft, ion-conducting domains and rigid, nonconducting domains offer the opportunity to tune both mechanical and electrical properties separately. Such electrolytes are conveniently made by block copolymer self-assembly. Most of the block copolymer electrolytes studied thus far comprise organic polymer chains for both the conducting and rigid domains. The team hopes to synthesize new electrolytes that simultaneously have high transport properties and have greater stability against lithium in comparison to organic diblock copolymers.

Approach. First, the team synthesizes hybrid diblock copolymers by incorporating monomers that contain an inorganic component. Then, electrolytes are prepared by mixing these diblock copolymers with salt. Electrochemical and mechanical characterization of these materials is performed before carrying out cycling X-ray tomography (XRT) experiments. The combination of these approaches enables rational design of materials that exhibit improved stability against lithium metal.

Out-Year Goals. The project will synthesize a new hybrid electrolyte that is designed to be stable against lithium metal. The material is a block copolymer wherein acryloisobutyl polyhedral oligomeric silsesquioxane (POSS) is covalently bonded to the chain. The second block is a conventional polymer electrolyte, PEO. Electrochemical characterization of this polymer will include measurement of all transport properties including conductivity, diffusion coefficient, and the transference number. The stability against lithium metal will be evaluated by CV, while its applications as an electrolyte will be evaluated and visualized using cycling XRT experiments on symmetric Li-hybrid-Li cells.

Collaborations. There are no active collaborations this quarter.

Milestones

1. Synthesize a series of POSS-containing block copolymer electrolytes for electrochemical studies. (Q1, FY 2020; Completed)
2. Create impurity-free lithium layers. (Q2, FY 2020; Completed)
3. Complete electrochemical characterization of POSS-containing block copolymer electrolytes. (Q3, FY 2020)
4. Provide cycling data for at least two POSS-containing block copolymer electrolytes. (Q4, FY 2020)

Progress Report

The following milestone was completed: electrochemical filtering treatment was used to reduce concentrations of impurity particles near the electrode/electrolyte interfaces in lithium symmetric cells.

Lithium symmetric cells are fabricated with all organic polystyrene-block-poly(ethylene oxide) (PS-PEO, or SEO) diblock copolymer/LiTFSI electrolytes using the method outlined in Reference 1. The electrolyte properties are summarized in Table 1.

In newly fabricated cells, impurity particles are found at the lithium/electrolyte interface. Figure 10a demonstrates a schematic of electrochemical filtering of lithium impurities. The blue blocks are lithium electrodes, white triangles are impurity particles, and brown strips are impurity-free lithium layers. First, lithium is deposited on the bottom electrode to create a layer free of impurity particles. By reversing the direction of current, lithium is plated from the bottom electrode onto the upper electrode, creating impurity-free layers on both electrodes. Figure 10b demonstrates the current density and voltage of the treatment described in Figure 10a during lithium deposition onto the bottom electrode, then lithium deposition onto the top electrode, as a function of time. Lithium was deposited on to the lower electrode at a low current density of 0.04 mA cm^{-2} for ~ 44 hours ($8.5 \text{ }\mu\text{m}$ deposited lithium thickness) and deposited back on to the upper electrode at the same current density for about 9 hours ($1.7 \text{ }\mu\text{m}$ deposited lithium thickness).

Table 1. Properties of electrolytes used for lithium filtering study.

SEO	M_{PS} (kg mol^{-1})	M_{PEO} (kg mol^{-1})	f_{EO} (kg mol^{-1})	PDI
(115-172)	115	172	0.59	1.10
(200-222)	200	222	0.51	1.08

Cells filtered using the above method were imaged using hard X-ray microtomography. Figure 10c shows a slice through a reconstructed volume of a symmetric cell after 14 conditioning cycles. No inhomogeneities were observed at the top nor the bottom lithium electrode/electrolyte interfaces. Figure 10d shows slices through a reconstructed volume of the symmetric cell in Figure 10c after an electrochemical filtering treatment. Yellow dashed lines differentiate deposited impurity-free lithium after the treatment from the original bulk lithium electrode. Impurity particles are visibly pushed away from the electrode–electrolyte interface, resulting in a void defect. Figure 10e shows slices through a different area of the cell shown in Figure 10c-d. Yellow dashed lines in this figure also indicate the calculated height of filtered lithium after the treatment. In this section, there are still impurity particles attached to the polymer electrolyte at both lithium/electrolyte interfaces.

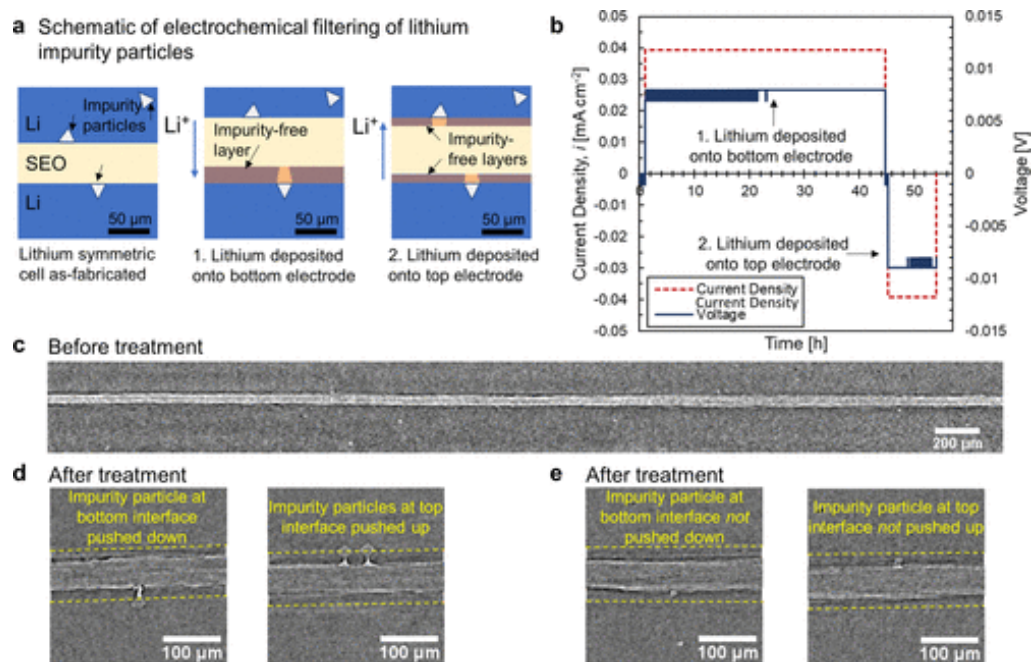


Figure 10. Electrochemical filtering treatment to reduce concentrations of impurity particles near the electrode/electrolyte interfaces in lithium symmetric cells. (a) Schematic of electrochemical filtering of lithium impurities. (b) Current density and voltage of the treatment. (c) Slice through a reconstructed volume of a symmetric cell. (d) Slices through a reconstructed volume of the symmetric cell in (c) after an electrochemical filtering treatment. (e) Slices through a different area of the cell after treatment showing impurity particles attached to the polymer electrolyte at both lithium/electrolyte interfaces. Adapted from Reference 1.

While this treatment resulted in a reduction in the concentration of impurity particles at the lithium/electrolyte interfaces, the cycled lithium layers contained void defects. In general, treated cells had a higher number of deposition defects per area, but most defects were confined within the lithium electrode. However, most of the deposition defects seen in the control cells were protrusions in the electrolyte. For most cells, increased lifetime due to electrochemical filtering was not due to a reduction in the number of deposition defects per area, but rather due to the differences in defect morphology (voids versus protrusions). Thus, this electrochemical filtering treatment will be used to reduce concentrations of impurities in hybrid organic-inorganic materials before cycling in future experiments.

Reference

- [1] Maslyn, J. A., L. Frenck, W. S. Loo, D. Y. Parkinson, and N. P. Balsara. “Extended Cycling through Rigid Block Copolymer Electrolytes Enabled by Reducing Impurities in Lithium Metal Electrodes.” *ACS Applied Energy Materials* 2, no. 11 (2019): 8197–8206.

Patents/Publications/Presentations

Publications

- Devaux, D., et al. “Lithium-Sulfur Batteries with a Block Copolymer Electrolyte Analyzed by X-Ray Microtomography.” *Journal of The Electrochemical Society* 167, no. 6 (2020): 060506.
- Galluzzo, M. D., et al. “Measurement of Three Transport Coefficients and the Thermodynamic Factor in Block Copolymer Electrolytes with Different Morphologies.” *The Journal of Physical Chemistry B* 124, no. 5 (2020): 921–935.

Task 1.7 – Development of Thin, Robust, Lithium-Impenetrable, High-Conductivity, Electrochemically Stable, Scalable, and Low-Cost Glassy Solid Electrolytes for Solid-State Lithium Batteries (Steve Martin, Iowa State University of Science and Technology)

Project Objective. The objective of this project is to develop new Li⁺-conducting MOSN GSEs that are impermeable to lithium dendrites, have high conductivities, are scalable through low-cost glass manufacturing, are chemically and electrochemically stable, and will enable low-cost, high-energy-density solid-state lithium batteries (SSLBs). The SSLBs constructed from these new GSEs will meet and exceed all program objectives: useable specific energy @ C/3 \geq 350 Wh/kg, calendar life 15 years, cycle life (C/3 deep discharge with < 20% energy fade) 1,000, and cost \leq \$100/kWh.

Project Impact. This project will enable the team to demonstrate that (1) thin MOSN GSE films yield superior performance in a much safer, lower-cost, and Li-dendrite impenetrable form and (2) high rate and long cycle life can be achieved in SSLBs using thin-film MOSN GSEs. The new GSEs in SSLBs are anticipated to increase the energy density (anode basis) from \sim 300 mAh/g to \sim 4,000 mAh/g, enabling replacement of internal combustion engines in both light and heavy duty vehicles. Each 20% reduction in the \sim 1.6 billion liters of gasoline used per day in the United States would reduce CO₂ emissions by \sim 4 billion kg or 2×10^{12} l of CO₂ per day. The team will also increase scientific and engineering knowledge of thin-film GSEs in SSLBs.

Approach. The MOSN MGF glasses used for the GSEs in this project have been developed in previous work to have the necessary thermal stability and high ionic conductivity for successful use as a drawn-film electrolyte. In this project, the glass chemistry will be tuned for even more desirable properties, by investigating structure-property relationships and testing variations in glass chemistry.

Out-Year Goals. Work will progress toward developing a glass capable of being drawn to 100-micron thickness, while having high conductivity and electrochemical stability and good cycling ability.

Collaborations. There are no active collaborations this quarter.

Milestones

1. Preform redraw capability to form 5-m ribbons verified. (Q1, FY 2020; Completed)
2. Accomplish: MOSN MGF GSEs are thermally stable between -20°C and 100°C, have a Li⁺ ion conductivity > 1 mS/cm at 25°C, have a Li⁺ ion area specific resistance (ASR) of ≤ 100 Ohm-cm², have an electronic ASR of > 0.1 M Ohm-cm², are electrochemically stable between 0 and 4.5 V versus Li/Li⁺, and have no more than 1 wt% weight change in 45% relative humidity (RH) air. (Q2, FY 2020; Completed except conductivity, March 31, 2020)
3. Accomplish: MOSN MGF GSE are stable against lithium through 100 cycles. (Q3, FY 2020)
4. *Go/No Go Decision:* MOSN MGF GSE is chemically stable and resistant to crystallization. Analysis indicates technical approach capable of achieving performance targets. (Q4, FY 2020)

Progress Report

The glass melting and casting scale-up of the compositional series of glasses being investigated is highly dependent on batch size and quality of starting materials. Continued efforts are being made to improve the processability and electrochemical properties of the glasses to improve their scale up.

The team is beginning the glass preform and film forming tests on more easily handled GSEs. They are thus working on a sodium-based GSE composition that is known for being a particularly good glass former and more easily melted, cast, annealed, and drawn into thin films. They have used this sodium mixed oxy-sulfide (MOS) GSE, and a preform ~ 0.5 cm x ~ 10 cm x ~ 20 cm was cast and annealed. Because the sodium-based glass is easier to scale up, it is being used to optimize the scale-up process that requires the team to increase melting and casting sizes from small 7-g batches to large 150-g to 200-g batches needed for a preform. This process includes scaling up raw material production, ball milling the materials to homogenize them before melting, and melting the large batch in a nitrogen atmosphere at < 5 ppm H_2O and O_2 . The team has found that the lower-cost sodium-based GSE and materials for testing and optimizing the process allowed them to make many more glass melting and casting trials more quickly and easily; this was effective in helping to optimize the process.

Using the sodium-based GSE as a way to optimize the glass melting system, the team has moved on to using the low-cost, easily produced Li^+ ion conducting GSE LiPO_3 glass. This quarter, they have been successful in drawing over 5 meters of film while optimizing the use of the draw tower. To access all levels of the draw tower safely, a scaffold with access platforms was purchased and installed. This optimization led from pulling fibers from narrow preforms to being able to use full-size preforms that produced 5-cm-wide, < 20 - μm -thick film. During this testing, it was found that better grips were needed for holding the larger, heavier full-size preforms. To this end, a trident-styled grip was designed and ordered. Additionally, it was found that an improved film cutting method was needed to prevent the film from splitting vertically. Because the films are so thin, it was found that a hot knife was sufficient to melt a thin line across the glass film to separate it.



Figure 11. (a) Small LiPO_3 preform in first-version grip. (b) Full LiPO_3 preform. (c) Highly flexible drawn film ~ 200 - μm thick.

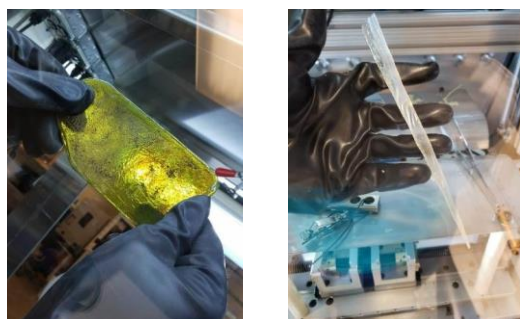


Figure 12. (left) 100g sodium MOS preform. (right) Drawn, partially crystallized, MOS sodium film.

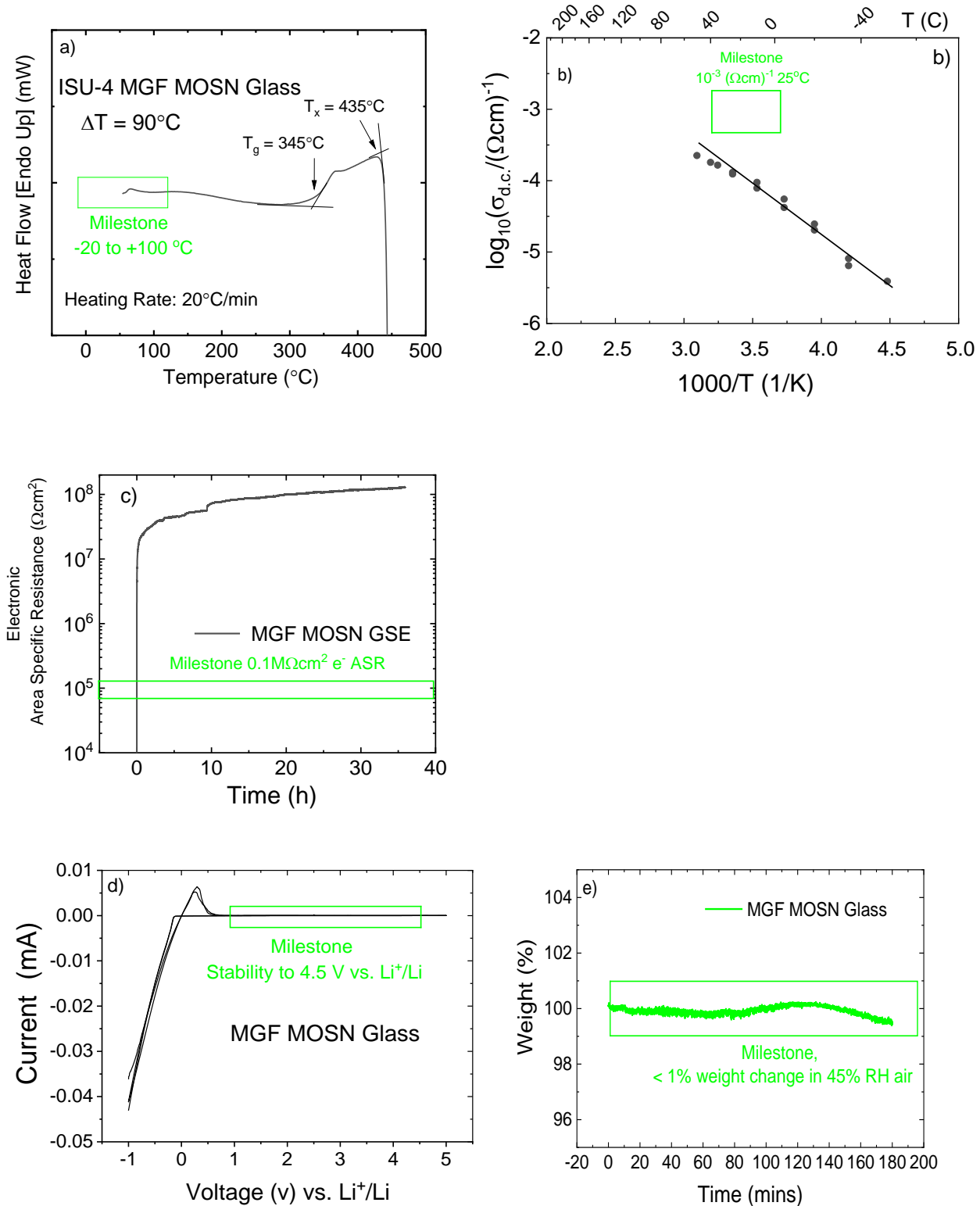


Figure 13. (a) Differential scanning calorimetry scan of a mixed-glass-former (MGF) mixed-oxy-sulfide-nitride (MOSN) glassy solid electrolyte (GSE) showing that this glass far exceeds the milestone. (b) Arrhenius plot of the Li^+ ion conductivity of a MGF MOSN GSE that shows it has conductivity of $1.3 \times 10^{-4} (\Omega\text{cm})^{-1}$ at 25°C , below the milestone; GSEs with higher conductivities are being developed. (c) DC electronic ASR of a MGF MOSN GSE showing that this GSE far exceeds the milestone. (d) Cyclic voltammogram scan on a MGF MOSN GSE showing that this GSE has electrochemical stability up to 5 V versus Li^+/Li and exceeds the milestone. (e) Thermal gravimetric analysis measurements of MOSN GSE in air showing that this glass meets the milestone.

As shown in Figure 13, the MGF MOSN GSEs being developed have met all of the project milestones except Li^+ ion conductivity. The team is working aggressively on this milestone and anticipates that new dopants and other compositional changes being made to the glass will create new GSEs that meet this requirement.

Patents/Publications/Presentations

Ph. D. Graduate Student Graduation

- Kmiec, S. “Development of Sodium Ion Conducting Mixed Anion Glasses for Solid State Electrolytes.” Ph. D., Department of Materials Science & Engineering, Iowa State University (May 2020).

Publications

- Zhao, R., G. Hu, S. Kmiec, R. Gebhardt, A. Whale, and S. W. Martin. “A New Amorphous Oxy-Sulfide Solid Electrolyte Material: Anion Exchange, Electrochemical Properties, and Lithium Dendrite Suppression via *In Situ* Interfacial Modification.” Pending submission next quarter.
- Lazar, M., S. Kmiec, A. Joyce, and S. W. Martin. “Investigations into Reaction between Sodium and Solid-State Sodium Electrolytes.” *ACS Applied Energy Materials*. Submitted April 21, 2020.
- Zhao, R., S. Kmiec, G. Hu, and S. W. Martin. “Lithium Thiosilicophosphate Glassy Solid Electrolytes Synthesized by High-Energy Ball-Milling and Melt-Quenching: Improved Suppression of Lithium Dendrite Growth by Si Doping.” *Applied Materials & Interfaces* 12, no. 2 (2020): 2327–2337. <http://dx.doi.org/10.1021/acsami.9b16792>.
- Kmiec, S., A. Joyce, D. Bayko, and S. W. Martin. “Glass Formation and Structure of Melt Quenched Oxy-Sulfide $\text{Na}_4\text{P}_2\text{S}_{7-x}\text{O}_x$ Glasses for $0 \leq x \leq 5$.” *Journal of Non-Crystalline Solids* 534 (2020): 119776.

Task 1.8 – Composite Solid Ion Conductor with Engineered Lithium Interface (Kyler Carroll and Cam Peebles, Wildcat Discovery Technologies)

Project Objective. In this project, Wildcat seeks to perform focused, fundamental research and development on composite polymer/ceramic electrolytes and for the protection of Li-metal anodes to develop an all-solid-state Li-metal battery that achieves DOE requirements for performance that enable potential commercialization of this technology. Wildcat will leverage its HT battery platform to explore a broad composite electrolyte compositional space. Additionally, the HT platform will allow the team to screen hundreds of inorganic and organic coatings for lithium metal protection and translate the best results to all solid cells.

Project Impact. Successful widespread commercialization of EVs is contingent on developing safe high-energy-density batteries capable of long cycle life. Lithium metal affords the highest theoretical capacity (3,860 mAh/g) and lowest electrochemical potential (-3.04 V versus SHE), which offers the highest specific energy density of anode materials today. However, significant progress toward the passivation of lithium metal must occur before the energy density benefit can be realized. The intrinsic high reactivity between lithium metal with conventional Li-ion electrolytes (organic carbonate-based solvents) makes it extremely difficult to overcome these problems. The proposed composite polymer/ceramic electrolyte and a protected Li-metal anode will enable an all-solid-state Li-metal battery. It is expected that the outcomes from this effort will deliver a safe all-solid-state Li-metal pouch cell with over 350 Wh/kg and over 1,000 cycles (C/3) with the cost estimate below \$100/kWh.

Approach. The project approach involves (1) identifying a suitable combination of solid ion conductor, polymer, and additive that minimizes overall interfacial impedance between the polymer electrolyte and solid ion conductor, and (2) identification of stable Li-metal protection agent or combination of agents that show enhanced cycling performance (relative to a non-protected system) using the down-selected cell architectures.

Out-Year Goals. The out-year goals involve screening hundreds of additive, polymer, and solid ion conductor combinations using a HT trilayer cell architecture developed during method development phase. Based on the best combinations, Wildcat will develop a composite polymer/ceramic electrolyte where the Li-ion conductivity is occurring at the ceramic phases of the composite. Additionally, the team will screen hundreds of Li-metal protection agents using the designed HT cell architecture with the goal of identifying those that offer highest stability.

Collaborations. All project tasks will be performed at Wildcat Discovery Technologies.

Milestones

1. Establish baseline performance. (Q1, FY 2020; Completed)
2. Complete synthesis of ceramic ion conductors. (Q2, FY 2020; In progress)
3. Perform down-selection of best ceramic ion conductors for further optimization. (Q3, FY 2020; In progress)
4. Perform down-selection of best composite solid electrolyte additives for further optimization. (Q4, FY 2020; In progress)
5. Perform down-selection of best high-voltage polymer formulations for further optimization. (Q4, FY 2020; In process)
6. Demonstrate composite ionic conductivity >> polymer ionic conductivity. (Q4, FY 2020)

Progress Report

Work this quarter focused on synthesis of ceramic ion conductor membranes. The choice of ceramic ion conductor was based on its air stability as well as its ionic conductivity and processability. The team has completed synthesis of ceramic ion conductors, and the ceramic ion conductor will be used for primary screening of additives and high voltage (HV) polymers using the trilayer testing vehicle developed last quarter.

Synthesis of Ceramic Ion Conductors

The Wildcat HT platform allows for the ability to synthesize many inorganic materials, in parallel, and measure their phase purity and ionic conductivity using XRD and EIS, respectively. Figure 14a shows an overview plot of ceramic ion conductors synthesized this quarter and their conductivity measured by EIS in a gold blocking electrode setup. The team first synthesized two types of ceramic ion conductors, LLZO and LAMP, by solid-state methods. To obtain phase purity, the annealing conditions for LLZO followed a two-step process in an air furnace at a 5°C/min ramp rate. To obtain phase pure LAMP, a two-step process in an inert furnace with flowing N₂ gas was utilized. The LLZO and LAMP XRD patterns are shown in Figure 14b. Based on diffraction patterns, the team can see that phase pure materials were synthesized using the Wildcat HT synthesis platform. Based on the FTIR data (not shown), a lithium carbonate layer is formed on the LLZO surface (~1465 cm⁻¹). Since the majority of the work to be performed in the next two quarters is to form covalent bonds between the additive and the polymer to lower the interfacial resistance, the native carbonate would not be ideal. The team has therefore chosen LAMP as the ceramic ion conductor for testing the interfacial impedance in the trilayer setup. To measure the ionic conductivity of the ceramics, dense pellets need to be formed. At Wildcat, the team developed a film-casting process to make sintered pellets, as opposed to conventional hydraulic cold pressing, which allows for more flexibility and scalability. They utilize a sintering aid, Li₃BO₃, to bind the ceramic particles and enable high ionic conductivity films. This process also allows the dimensions of the films to be easily varied depending on cell architecture. Sintered pellets are formed via a solution containing the ceramic ion conductor, sintering agent, and binder solution where the ceramic ion conductor and sintering agent ratio can vary; this results in changes in the density of the final pellet. The solutions were then cast onto a Teflon sheet, dried, punched to their desired dimensions, calendered, and annealed. The annealing followed a three-step process in air. Figure 15 shows the SEM micrograms of 3 pellets with 0%, 1%, and 3% Li₃BO₃ sintering agent mixed with the LAMP ceramic ion conductor. From the SEM, one can see that increasing the sintering agent results in more dense pellets. The resulting EIS shows that the increased density results in higher ionic conductivity. Each condition has three repeats, and the cell-to-cell reproducibility is good. Additionally, since the films are cast by a conventional film casting method, the casting height and calender heights can be adjusted to modify film density and improve ionic conductivity. Figure 16a-b shows the conductivity of three processing conditions. Based on the results, one can see that blade casting height has minimal effect on ionic conductivity, while increasing the calendering thickness results in higher ionic conductivity. Lastly, the team conducted a single-dopant screen on the

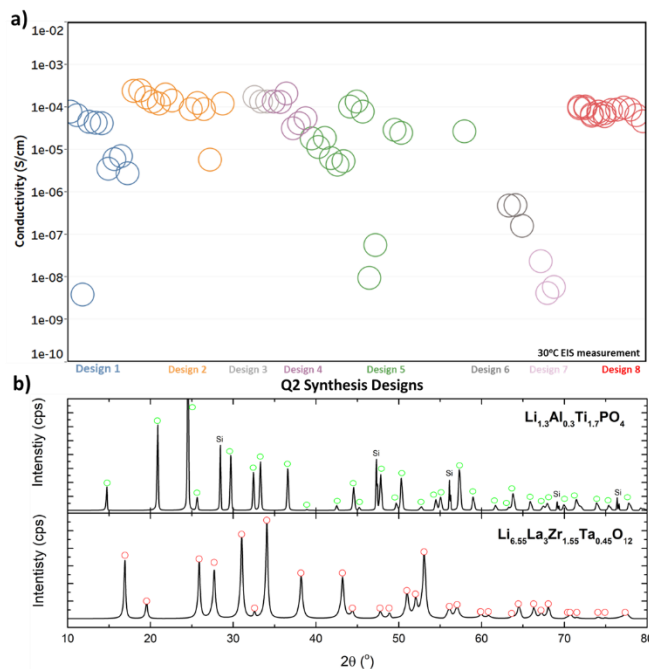


Figure 14. (a) Electrochemical impedance spectroscopy results for Au//Au blocking electrode for this quarter's ceramic ion conductor designs. (b) X-ray diffraction results for Wildcat synthesized LAMP and LLZO powders.

$\text{Li}_{1.3}\text{Ti}_{1.7}\text{M}_3\text{PO}_4$ material by varying the M-site metal. Figure 16c-d shows the ionic conductivity of the doped materials and shows that aluminum doping has the highest ionic conductivity. The Wildcat synthesized LATP and films with 3% Li_3BO_3 will be used as the control ceramic ion conductor in the next several quarters in the trilayer testing. The team will also continue to investigate other high ionically conductive ceramics and, after the conclusion of the HT additive, development screening will take several of the best hits and compare results with other ceramic ion conductors.

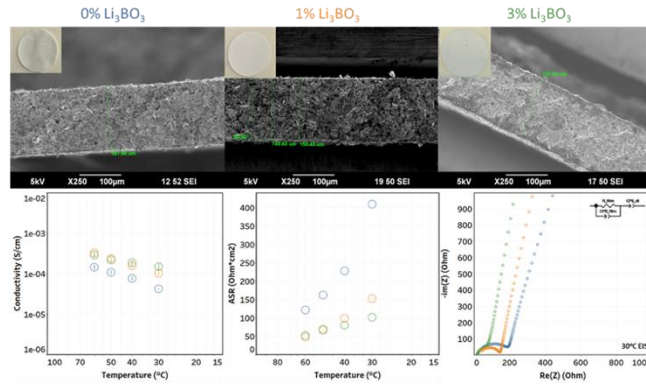


Figure 15. Scanning electron microscopy and ionic conductivity data for various LATP/ Li_3BO_3 ratios.

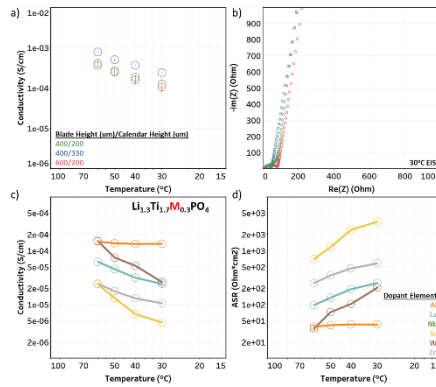


Figure 16. (a-b) Ionic conductivity of LATP/ Li_3BO_3 with varied processing condition. (c-d) Ionic conductivity of various M-site dopants on $\text{Li}_{1.3}\text{Ti}_{1.7}\text{M}_3\text{PO}_4$. (Note: triplicate cells were used for all data points).

Patents/Publications/Presentations

The project has no patents, publications, or presentations to report this quarter.

Task 1.9 – Physical and Mechano-Electrochemical Phenomena of Thin-Film Lithium-Ceramic Electrolyte Constructs (Jeff Sakamoto, University of Michigan)

Project Objective. While a small number of solid electrolytes exhibit high ionic conductivity ($\sim 1 \text{ mS cm}$ at 298K), few are stable against lithium metal. The garnet-type solid electrolyte, based on the nominal formula $\text{Li}_7\text{La}_3\text{Zr}_2\text{O}_{12}$ (LLZO), is unique in that it is a fast ion conductor and—as demonstrated in the team’s recent project (DE-EE-00006821)—is stable against lithium. Moreover, the team’s former project successfully demonstrated a decrease in Li-LLZO interface resistance from 12,000 to 2 Ohms cm^2 and stable cycling at 1 mA cm^2 for 100 cycles ($\pm 15 \text{ }\mu\text{m}$ lithium per cycle). Although the past project demonstrated that LLZO is a viable solid electrolyte for enabling batteries using metallic lithium, the studies used thick pellets (1 mm) and thick anodes ($\sim 500 \text{ }\mu\text{m}$). The goal of this project is to acquire a deep fundamental understanding of the physical and mechano-electrochemical phenomena that control the performance of cells consisting of thin LLZO ($\sim 10 \text{ }\mu\text{m}$), thin lithium anodes ($\sim 20 \text{ }\mu\text{m}$), and thin solid-state composite cathodes.

Project Impact. If successful, the project will gain knowledge to guide closely related commercialization efforts to scale the production of LLZO-based SSBs.

Approach. The team believes that to achieve a step increase in technology readiness level (TRL), the same performance characteristics previously shown should be demonstrated in technologically relevant cells, for example, thin LLZO and thin lithium.

Out-Year Goals. The out-year goals involve the following: custom thin-film construct development, preliminary cycling studies, Vis cell development, lithium cycling, and polymer gel electrolyte screening.

Collaborations. This project collaborates with Professors N. Dasgupta and D. Siegel of UM, Mechanical Engineering.

Milestones

1. Complete custom TFC design. (Q1, FY 2020; Completed)
2. Demonstrate manufacturing and preliminary cycling tests. (Q2, FY 2020; Completed)
3. Initial integration of precision micro reference electrodes with thin lithium TFC. (Q3, FY 2020; In progress)
4. Determine maximum cycling rates of TFC. (Q3, FY 2020; In progress)
5. Demonstrate manufacturing and preliminary cycling tests of TFC with reference electrodes. (Q4, FY 2020; In progress)

Progress Report

This quarter’s milestone, to demonstrate manufacturing and preliminary cycling tests of TFC was successfully completed. A scalable approach was used to manufacture thin ($\leq 100 \mu\text{m}$) LLZO films with comparable microstructures and conductivities to bulk-processed LLZO manufactured using hot-pressing methods. This approach will guide the manufacturing of TFCs throughout subsequent milestones.

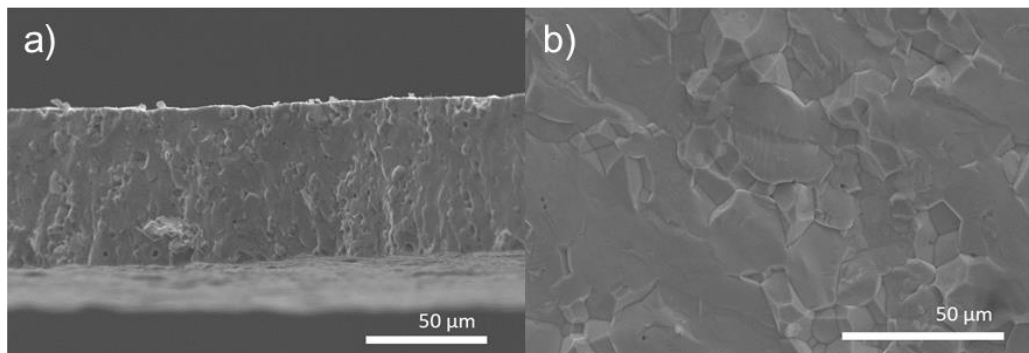


Figure 17. Manufacturing of thin-film composite with desired microstructure and thickness. (a) Fracture surface of 70- μm -thick LLZO thin film, in comparison to the (b) fracture surface of a 1-mm-thick hot-pressed LLZO pellet.

Work on next quarter’s milestone for initial integration of precision micro reference electrodes with thin lithium and thick LLZO is in progress. Using TVD, thin Li-metal microelectrodes can be manufactured with precise thicknesses below 100 μm . Precision microelectrodes can be deposited and tested successfully on thick LLZO membranes and will be incorporated into TFC constructs. These electrodes will be used throughout subsequent milestones.

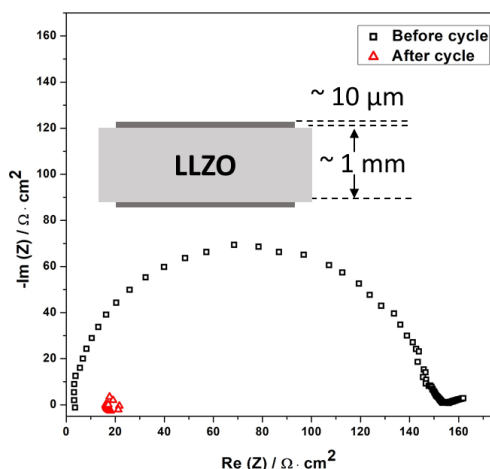


Figure 18. Electrochemical impedance spectra of 1-mm-thick hot-pressed LLZO using 10- μm -thick precision micro electrodes.

Patents/Publications/Presentations

Presentation

- GORDON Invited Presentation, Materials Research Society (MRS), Boston, Massachusetts (Fall 2019): “Stabilizing Solid Li and Na Metal Anodes using Ceramic Membrane Technology”; J. Sakamoto.

Task 1.10 – Lithium Dendrite-Free $\text{Li}_7\text{N}_2\text{I-LiOH}$ Solid Electrolytes for High-Energy Lithium Batteries (Chunsheng Wang, University of Maryland)

Project Objective. The objective of this project is to research, develop, and test Li-metal-based batteries that implement solid Li-ion conductors (LICs) equipped with $\text{Li}_7\text{N}_2\text{I-LiOH}$ solid electrolyte capable of achieving cell performance of 350 Wh/Kg energy density for 1000 cycle life with a cost of $\leq \$100/\text{kWh}$.

Project Impact. Lithium dendrite growth during charge/discharge cycles limits the use of all-solid-state batteries (ASSBs). A criterion for lithium dendrite suppression that is developed through systematical investigation on thermodynamics and kinetics of lithium dendrite growth will guide the electrolyte design. $\text{Li}_7\text{N}_2\text{I-LiOH}$ and Li_3YCl_6 solid electrolyte with high ionic conductivity and low electronic conductivity will be used to validate the criterion for lithium dendrite suppression, to achieve the project objective.

Approach. Electrochemical property of $\text{Li}_7\text{N}_2\text{I-LiOH}$ and $\text{Li}_7\text{N}_2\text{I-LiOH/Li}_3\text{YCl}_6$ bi-layer film will be tested. The dendrite suppression criterion will be developed based on Butler-Volmer model and total energy analysis. The dendrite suppression criterion will be validated by using $\text{Li}_3\text{N-LiF}$ SSE, which is stable against lithium metal and has high ionic conductivity and high interface energy against lithium.

Out-Year Goals. In year one, the project will synthesize, modify, and optimize the $\text{Li}_7\text{N}_2\text{I-LiOH}$ and Li_3YCl_6 electrolytes, and $\text{Li}_7\text{N}_2\text{I-LiOH/Li}_3\text{YCl}_6$ bi-layered electrolytes to achieve a high ionic conductivity to $> 5 \times 10^{-4} \text{ S/cm}$ and to suppress lithium dendrite even at a high current of $> 3.0 \text{ mA/cm}^2$ and capacity of $> 3.0 \text{ mAh/cm}^2$. The team will focus on enhancing the CE for lithium anode to $> 99\%$. The CE of the solid electrolyte is a sensitive indicator of stability of the electrolyte against lithium and lithium dendrite, but it has been ignored by the SSB community due to very low CE ($< 90\%$) of the solid electrolytes such as LPS.

Collaborations. There are no reported collaborations this quarter.

Milestones

1. Synthesis of $\text{Li}_7\text{N}_2\text{I-LiOH}$ and Li_3YCl_6 electrolytes with high ionic conductivity. (Q1, FY 2020; Completed, December 31, 2019)
2. Electrochemical property of $\text{Li}_7\text{N}_2\text{I-LiOH}$ and $\text{Li}_7\text{N}_2\text{I-LiOH/Li}_3\text{YCl}_6$ bi-layer film. (Q2, FY 2020; Completed)
3. Lithium dendrite suppression capability. (Q3, FY 2020; Initiated)
4. High CE for lithium plating/stripping. (Q4, FY 2020)

Progress Report

Electrochemical Characterization of $\text{Li}_7\text{N}_2\text{I-LiOH}|\text{Li}_3\text{YCl}_6$ Electrolyte Pellets

The $\text{Li}_7\text{N}_2\text{I-LiOH}$ and Li_3YCl_6 solid-state powders were successfully synthesized and used to fabricate the $\text{Li}_7\text{N}_2\text{I-LiOH}|\text{Li}_3\text{YCl}_6$ solid-state bi-layer electrolyte pellet by cold-press. As shown in Figure 19a, the yellow $\text{Li}_7\text{N}_2\text{I-LiOH}$ powders were mixed in toluene and ball-milled under argon atmosphere for 4 hours to achieve $\text{Li}_7\text{N}_2\text{I-LiOH}$ suspension. The white Li_3YCl_6 powder was also ball-milled in toluene for 4 hours to achieve Li_3YCl_6 suspension. A small amount of $\text{Li}_7\text{N}_2\text{I-LiOH}$ suspension was dropped into the PTFE die and pressed at room temperature for 10 minutes. The Li_3YCl_6 suspension was then casted onto the $\text{Li}_7\text{N}_2\text{I-LiOH}$. The die was heated to 80°C overnight under argon atmosphere. Finally, the bi-layer electrolyte was pressed at 360 MPa to form the bi-layer $\text{Li}_7\text{N}_2\text{I-LiOH}|\text{Li}_3\text{YCl}_6$ SSE pellet. As shown by the SEM images in Figure 19b-c, the cold-pressed Li_3YCl_6 and $\text{Li}_7\text{N}_2\text{I-LiOH}$ are rather dense. The cross section of the bi-layer SSE is shown in Figure 19d. Li_3YCl_6 and $\text{Li}_7\text{N}_2\text{I-LiOH}$ were in close contact.

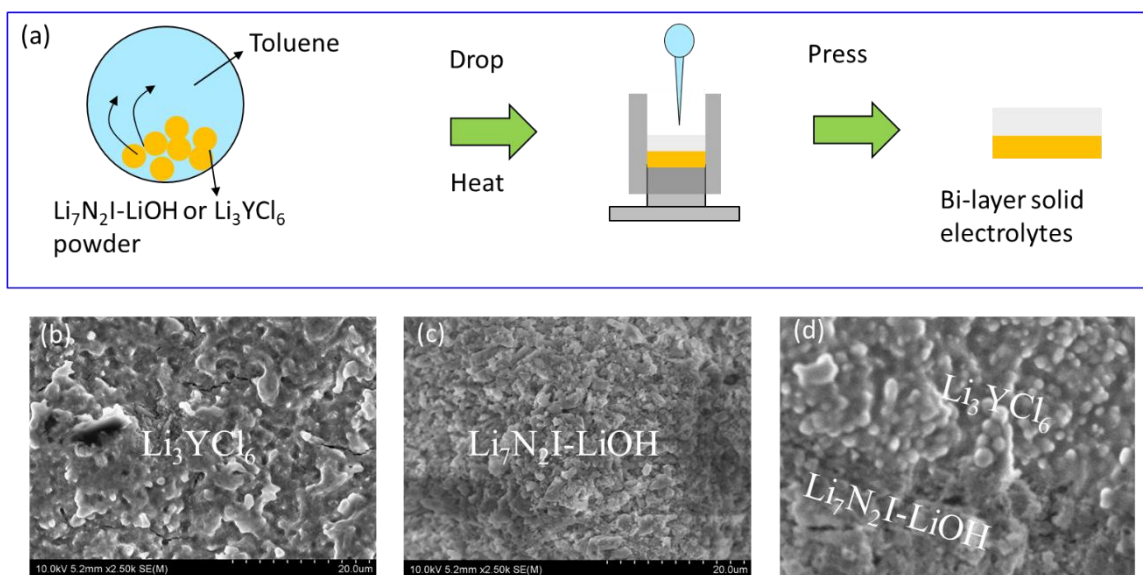


Figure 19. Synthesis and characterization of bi-layer $\text{Li}_7\text{N}_2\text{I-LiOH}|\text{Li}_3\text{YCl}_6$ solid-state electrolyte. (a) Scheme of the synthesis process for the electrolyte pellet. Scanning electron microscopy images of (b) Li_3YCl_6 , (c) $\text{Li}_7\text{N}_2\text{I-LiOH}$, and (d) the cross section of the cold-pressed pellet.

The electrochemical stability window of the bi-layer $\text{Li}_7\text{N}_2\text{I-LiOH}|\text{Li}_3\text{YCl}_6$ SSE pellet was measured using CV at the scan rate of 1 mV/s from -0.5 V to 5 V (Figure 20a). The stability window of bi-layer $\text{Li}_7\text{N}_2\text{I-LiOH}|\text{Li}_3\text{YCl}_6$ solid-state bilayer electrolyte is 0.0-5.0 V. The lithium plating and stripping process seems reversible with high efficiency. The $\text{Li}|\text{Li}_7\text{N}_2\text{I-LiOH}|\text{Li}_3\text{YCl}_6|\text{Li}$ cell was assembled by sandwiching the $\text{Li}_7\text{N}_2\text{I-LiOH}|\text{Li}_3\text{YCl}_6$ pellet with two lithium foils. The cell was then heated to 90°C for 10 hours to reduce contact resistance. The lithium plating/stripping curve at current density of $10 \mu\text{A}/\text{cm}^2$ and capacity of $10 \mu\text{Ah}/\text{cm}^2$ is shown in Figure 20b. No sharp voltage drop was observed during the 25 cycles.

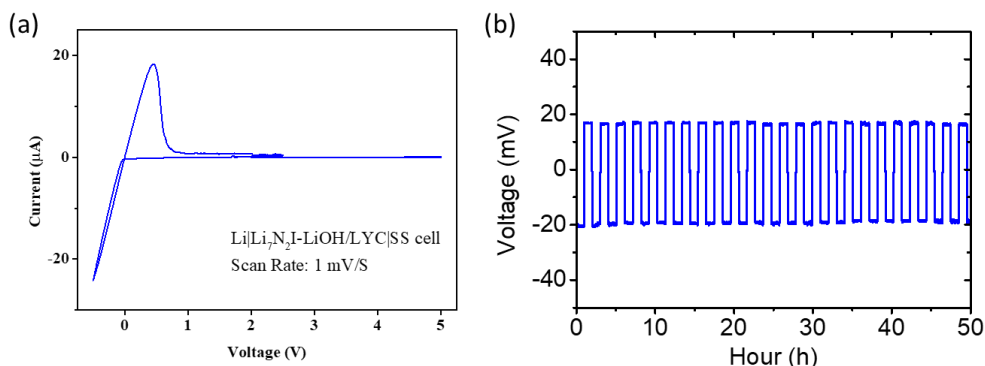


Figure 20. Electrochemical performance of the bi-layer $\text{Li}_7\text{N}_2\text{I-LiOH|Li}_3\text{YCl}_6$ solid-state electrolyte. (a) Electrochemical potential window and (b) lithium plating/stripping curve at the current density of $10 \mu\text{A}/\text{cm}^2$.

Development of Lithium Dendrite Suppression Criterion for Solid Electrolytes

Lithium Dendrite Suppression Principles in SSEs

Lithium dendrite nucleation and growth in SSEs depend on the energy landscape for lithium deposition and stripping inside the SSEs, which is represented by Butler-Volmer kinetics (Figure 21a). The parabolas on the left designate reaction coordinate of lithium deposition ($\text{Li}^+ + e^- \rightarrow \text{Li}$); the parabolas on the right designate that of lithium stripping ($\text{Li} \rightarrow \text{Li}^+ + e^-$). At an open-circuit after the SSE contacts lithium metal, the activation energy and reaction rate for lithium plating in SSEs are much larger than lithium stripping in SSEs (Figure 21a, blue dashes). The difference in activation energy between lithium plating and stripping increases with the increasing of interface energy and decreasing of electronic conductivity of the SSEs. Once lithium plating starts, electrolyte potential up-shifts by η and lithium plating driving energy inside SSE moves up by $F\eta$, which reduces the energy barrier for lithium plating inside electrolyte ($\Delta G'_{\text{Li}^+ + e^- \rightarrow \text{Li}}$) while increasing energy barrier for lithium stripping ($\Delta G'_{\text{Li} \rightarrow \text{Li}^+ + e^-}$). When lithium plating reaches a critical current, in which the potential shift (overpotential) reaches a critical value η^* (critical overpotential), the activation energy of lithium plating is the same as that of lithium stripping in SSEs (Figure 21a, red dashes). Lithium dendrite will be formed in SSE when the overpotential is larger than critical overpotential η^* where the current is larger than the critical current ($I^* = \eta^*/\text{ASR}$). The critical current is high when the activation energy difference between lithium plating and stripping at open-circuit is large and ASR is low. Therefore, the critical current of SSEs increases with the increasing of interface energy against lithium, the increasing of ionic conductivity (reducing ASR), and the decreasing of electronic conductivity. Since the high interface energy of SSE can provide large interface tension to prevent lithium dendrite nucleation and growth in SSE, especially at void, defect, and GB, highly dense SSE is not required. However, if SSEs are lithiophilic with a much lower interface energy against lithium, SSEs should have a high density with fewer GB defects since the large interface tension forces lithium to penetrate into the GB, especially at GB and defects.

The impact of thermodynamic stability, interface energy, and electronic conductivity of SSEs on lithium dendrite formation is summarized in Figure 21b. When the SSEs are stable with lithium, electronically insulated, and have low interface energy, lithium dendrites grow from lithium anode into GBs or hole of SSEs through mechanical lithium infiltration due to high interface tension and lithium plating pressure. The mechanical lithium dendrite growth mainly contributes to intergranular growth, such as propagation in GBs, pores, and cracks induced by lithium growth (Figure 21b, first row). However, if local electronic conductivity of SSEs is high, the lithium chemical potential in SSEs will drop to a negative potential similar to the lithium plating anode, so lithium can even directly nucleate and grow inside SSE (Figure 21b, second row). When the SSEs are stable with lithium, have high interface energy against lithium, and have insulated electronic conductivity, lithium dendrite will not nucleate and grow inside SSEs and will not penetrate into SSEs because

the high interface energy significantly increases the energy barrier of homogeneous nucleation, and the high interface tension between SSEs and lithium also suppresses lithium propagation and penetration into SSEs (Figure 21b, third row). If the SSEs are unstable with lithium and the formed interphases have a high electronic conductivity, the electrochemical reaction between lithium and SSE accelerates lithium dendrite nucleation and growth in SSEs. The lithium dendrite growth in SSEs changes from a mechanical pattern to an electrochemical-mechanical pattern (Figure 21b, fourth row).

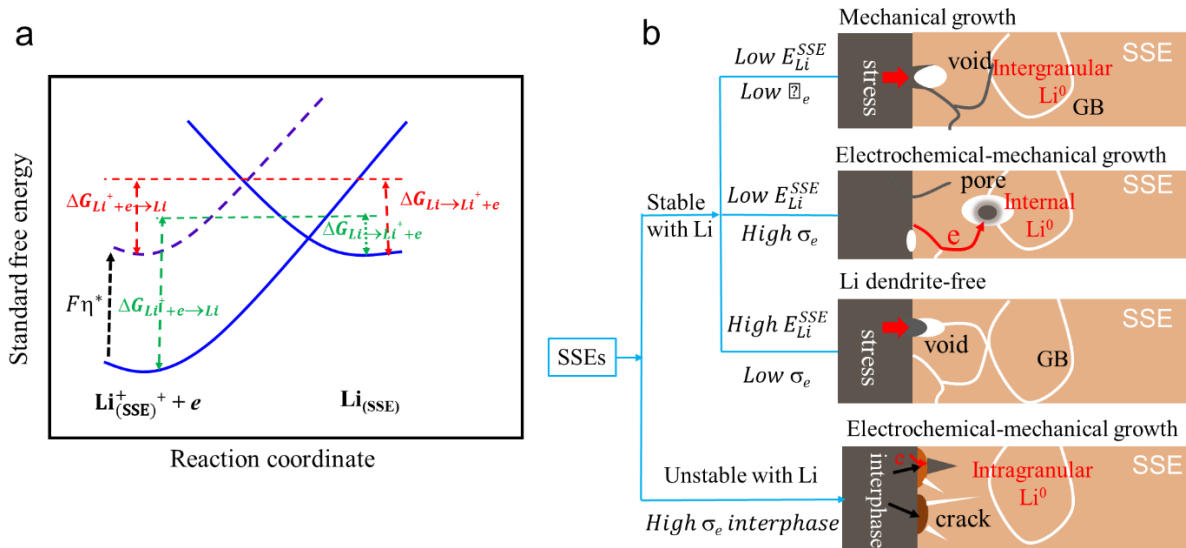


Figure 21. Lithium dendrite formation mechanism in solid-state electrolytes (SSEs). (a) Illustration of Butler-Volmer model for lithium plating in SSE. (b) Lithium dendrite formation and growth mechanism in SSE with different properties.

The interface energy of SSE against lithium is the most critical property for SSEs in addition to the high ionic conductivity and low electronic conductivity. The high interface energy of SSE can prevent lithium nucleation inside SSE and lithium penetration into SSEs, even if SSEs have a high porosity. Since the most highly ionic conductivity electrolytes are not stable with lithium, interphases will generate because of the chemical reaction. If the formed interphases have a high interface energy with lithium, the SEI can still suppress lithium dendrite nucleation and growth. However, if the SEI has a low interface energy and high electronic conductivity, the SEI will accelerate lithium dendrite growth. Based on the aforementioned dendrite suppression principles, the interface energy for LPS was calculated using first-principles calculation based on density functional theory (DFT). The results shown in Figure 22 demonstrate that the interface energy for $\text{Li}|\text{LPS}$ is $-88.92 \text{ meV}/\text{\AA}^2$. The negative interface energy indicates that the LPS is not thermodynamically stable against lithium metal. Once the LPS makes contact with lithium metal, the LPS will be reduced. For the interfaces between lithium and Li_2S , Li_3N , Li_3P , and LiF , the interface energies are positive. The $\text{Li}|\text{LiF}$ demonstrates the highest interface energy among these compounds, which indicates that LiF is a good choice for dendrite suppression. However, the low ionic conductivity of the LiF limits its direct use as SSE. To validate the dendrite suppression principles, Li_3N with high ionic conductivity was chosen as primary electrolyte with LiF added to enhance the interface energy of the electrolyte to form $\text{Li}_3\text{N-LiF}$ SSE.

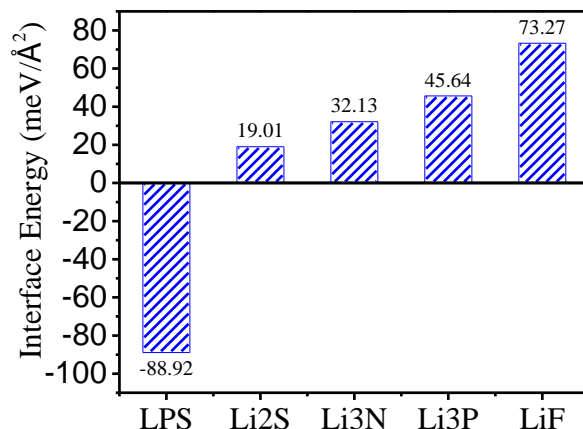


Figure 22. Density functional theory calculated interface energy for compounds against lithium metal.

Since Li₃N will be oxidized above 0.45 V, Li₃N-LiF electrolyte is used as protective layer for LPS electrolyte. The lithium dendrite suppression capability of Li₃N-LiF electrolyte to LPS was evaluated by sandwiching Li₃N-LiF on both sides of LPS to form a Li₃N-LiF/LPS/Li₃N-LiF three-layer composite electrolyte. Figure 23 shows the voltage profiles of a Li/Li₃N-LiF/LPS/Li₃N-LiF/Li symmetric cell during lithium plating and stripping with an increasing current density from 0.3 mA/cm² to 3.0 mA/cm² at a fixed capacity of 0.3 mAh/cm². An activation process is observed from the voltage profiles at a current of 0.3 mA/cm², where the voltage gradually decreases in the first 20 cycles from ~ 300 mV to 50 mV and then stays stable (Figure 23b). This activation phenomenon is commonly observed in the solid-state symmetric cell if interface energy is high. The gradual decrease in the voltage of Li/Li₃N-LiF/LPS/Li₃N-LiF/Li cells can be attributed to increase of specific contact area of the interface and decrease of real electrolyte thickness resulting from lithium penetration into the voids of the Li₃N-LiF layer. The steady voltage profiles reached after 20 cycles suggest that lithium will not further grow and penetrate the SSE under current density of 0.3 mA/cm² due to high interface energy of LiF. As the current density increases, the lithium plating and stripping voltage increase follows Ohm's law. Even at a current density of 3.0 mA/cm², which is more than three times higher than the reported CCD of LPS SSE (0.5 to 1.0 mA/cm²), no abrupt drop of voltage can be observed during cycling, indicating that no lithium dendrites penetrate through the SSE at such a high current density (Figure 23c).

The long cycle stability of Li/Li₃N-LiF/LPS/Li₃N-LiF/Li cell at a high and fixed current of 1.0 mA/cm² and capacity of 1 mAh/cm² is shown in Figure 24a. The voltage profile is stable, and no sudden voltage drop of short circuit is observed even after 220 hours of lithium plating/stripping cycles. The impedance is slightly smaller than that cycled at 0.3 mAh/cm², indicating that the increased stress at a high lithium plating/stripping capacity pushes more lithium metal into the Li₃N-LiF layer, increasing the interfacial contact at Li/Li₃N-LiF. A more aggressive protocol of step-increasing the current densities with a fixed plating and stripping time of 1 hour was conducted for the Li/Li₃N-LiF/LPS/Li₃N-LiF/Li symmetric cell. As shown in Figure 24b, no short circuit during cycling is observed, even at a high current of over 6 mA/cm² and capacity of 6 mAh/cm². The lower increase in voltage with current density than with Ohm's law after 12 hours of cycling is mainly attributed to increased lithium penetration into the Li₃N-LiF layer at a high capacity. The gradually increased lithium plating capacity in each cycle increases the force to drive more plated lithium into the pores of Li₃N-LiF layer, as illustrated in Figure 24c. However, the high interface energy of Li₃N-LiF generates a large opposite force to balance the increased pressure from lithium plating and prevent lithium dendrite amplification. The intergranular pores serve as a three-dimensional (3D) lithium reservoir, releasing stress for lithium plating on the anode rather than SSEs. The results clearly demonstrate that the Li₃N-LiF layer between lithium and LPS SSE can significantly suppress lithium dendrite propagation through the SSE, increasing CCD by 15 times. The results indicate that introducing LiF into Li₃N enhances the capability in suppressing lithium dendrite penetration, especially for high-energy capacity cells.

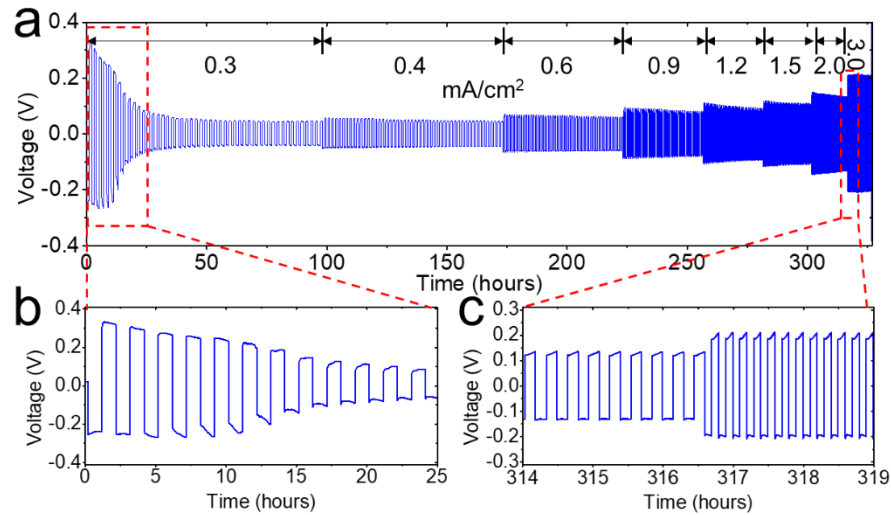


Figure 23. The electrochemical performances of lithium plating and stripping in the Li/Li₃N-LiF/LPS/Li₃N-LiF/Li cell at room temperature. (a) Voltage profiles in the symmetric cell at increased current densities with constant capacity of 0.3 mAh/cm². The details indicated by the red dashed lines are shown in (b) and (c).

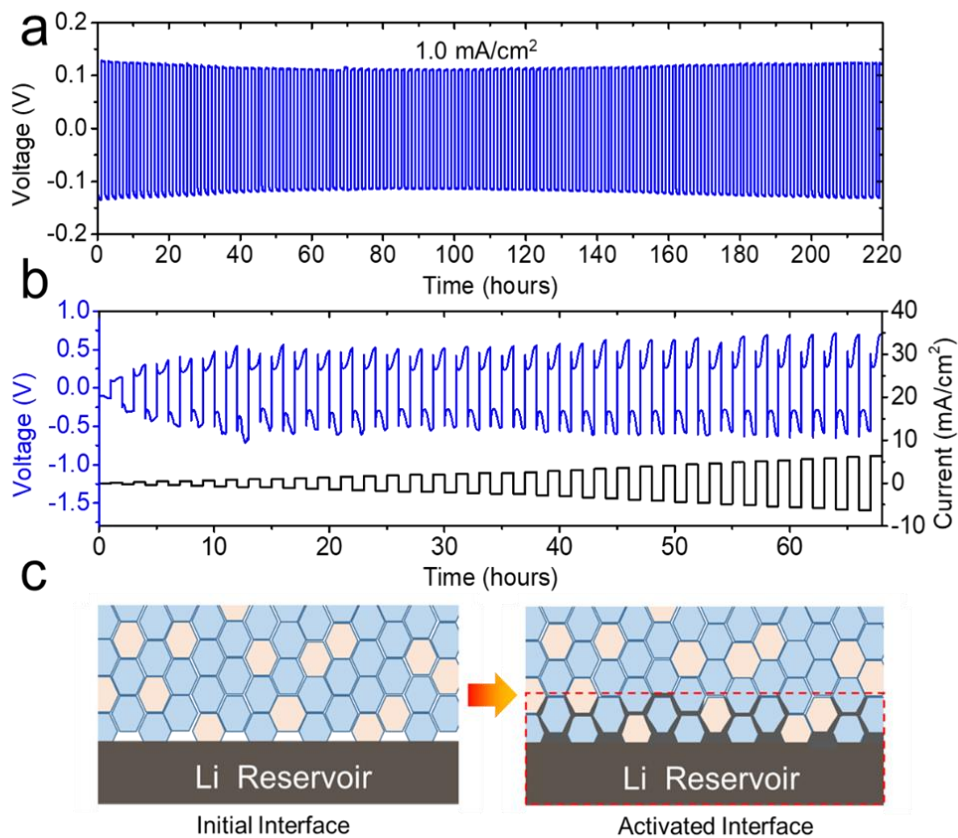


Figure 24. Voltage profile of lithium plating/stripping for large current density. Voltage profiles of the symmetric cell at (a) current density of 1.0 mA/cm² and (b) step-increased current densities and capacity (fixed 1-hour time for lithium plating/stripping). (c) Scheme for activation process at the interface; the red dashed line indicates the new interface after activation process.

Patents/Publications/Presentations

The project has no patents, publications, or presentations to report this quarter.

Task 1.11 – Hot Pressing of Reinforced Lithium-NMC All-Solid-State Batteries with Sulfide Glass Electrolyte (Thomas Yersak, General Motors)

Project Objective. The objective of this project is to research, develop, and test Li-NMC ASSBs capable of achieving program performance metrics by implementing sulfide glass SSEs and hot press processing in a dry room environment. The performance of ASSBs with sulfide SSEs is limited because they are essentially green tapes with up to 20% porosity. In composite cathodes, the porosity limits energy density and power, while porosity in the separator acts as a conduit for Li-metal deposits if cycling conditions (that is, C-rate, operating temperature, and pressure) are not strictly controlled. The goal of the project is to demonstrate that the hot pressing method and appropriately formulated sulfide glass SSEs can eliminate porosity to enable Li-NMC ASSBs with energy density of ≥ 350 Wh/kg.

Project Impact. The hot press processing method and appropriately formulated sulfide glass SSEs may enable Li-NMC ASSBs with improved energy density > 350 Wh/kg. The GM processing technology depends on heating a sulfide glass SSE above its glass transition temperature, T_g , at which point it can consolidate via viscoplastic flow. In the composite cathode, hot pressing provides liquid-like contact between the NMC cathode and SSE to increase energy density and power by enabling thick composite cathodes with high active material loading. Furthermore, cathode-supported sulfide glass separators can be made dense and thin by hot pressing. A dense separator enables the robust use of a Li-metal anode because lithium deposits may be more effectively blocked, preventing cell shorting.

Approach. The sulfide SSE used in the composite cathode, otherwise known as the catholyte, will dictate the processing specifications for ASSB hot pressing. Thermal stability can be achieved by NMC passivation and proper catholyte formulation. This project will systematically evaluate different NMC coatings, catholyte formulations, and hot-press processing specifications (that is, temperature, time, and pressure). The performance of hot-pressed ASSBs will be compared to green baseline ASSBs and hot-pressed control ASSBs consisting of the β -Li₃PS₄ and Li₆PS₅Cl model SSEs. Electron microscopy will be employed to understand interfacial phenomena and track composite cathode microstructure before and after hot pressing.

Out-Year Goals. In the second year of this project, a sulfide glass SSE will be formulated specifically for use as the separator. The separator glass SSE formulation will be designed to achieve full densification under the hot-press processing specifications determined for the catholyte. Separator glass formulation design will also consider cathodic stability, moisture stability, and ionic conductivity. Once a system of separator glass SSE and catholyte has been determined, the third year of the project will demonstrate hot-pressed full cells at the coin-cell and single-layer pouch cell levels, which meet program target performance metrics.

Collaborations. GM will lead this project with no subrecipients.

Milestones

1. Establish protective coating on cathode: select best coating method and coating chemistry. Confirm conformality of coating using microscopy. (Q2, FY 2020; Completed)
2. Develop suitable baseline system with reversible capacity of ~ 120 mAh/g. (Q3, FY 2020; In progress)
3. Determine parameters required to prepare cathode samples via focused ion beam (FIB)/SEM lift-out and to analyze samples via high-resolution transmission electron microscopy (HRTEM). (Q4, FY 2020; In progress)
4. Demonstrate hot-pressed cathode with reversible capacity of 120 mAh/g. Analysis indicates technical approach capable of achieving performance targets. (Q1 FY 2021; In progress)

Progress Report

The stability of the NCM/SSE interface during hot pressing is a function of catholyte SSE formulation, processing protocol (time, temperature, and pressure), and NCM protective coating. It is well established that sulfide SSEs are not thermodynamically stable at potentials greater than 3.0 V versus Li⁺/Li.^[1] Fortunately, kinetic stability may be achieved between sulfide SSEs and high-voltage layered oxide cathode materials by applying an appropriate passivating coating. However, hot pressing will exacerbate the chemical instability between NCM and sulfide SSE, and it is not well understood how coating characteristics (that is, composition and thickness) influence thermal stability. Therefore, the first project goal was to apply state-of-the-art coatings to NCM, confirm coating adequacy, and establish a HT experimental method to quantify the thermal stability of cathode composites. This progress report details those efforts.

High-Ni-content NCM cathode materials obtained from commercial vendors often have proprietary surface coatings such as TiO₂, SiO_x, or amorphous carbon. These coatings are optimized for conventional Li-ion batteries with liquid electrolyte and not for application in ASSB. For this reason, GM acquired bare LiNi_{0.85}Co_{0.1}Mn_{0.05}O₂ (NCM-85105) from BASF. To properly study interfacial phenomena in hot-pressed ASSB, it is crucial for GM to control coating composition and thickness. Three NMC coatings are targeted for study, namely, LiNbO₃,^[2] Li₂O-ZrO₂ (LZO),^[3] and Li₃PO₄.^[4] The thermal stability of Li₂O-ZrO₂ coatings will be reported next quarter.

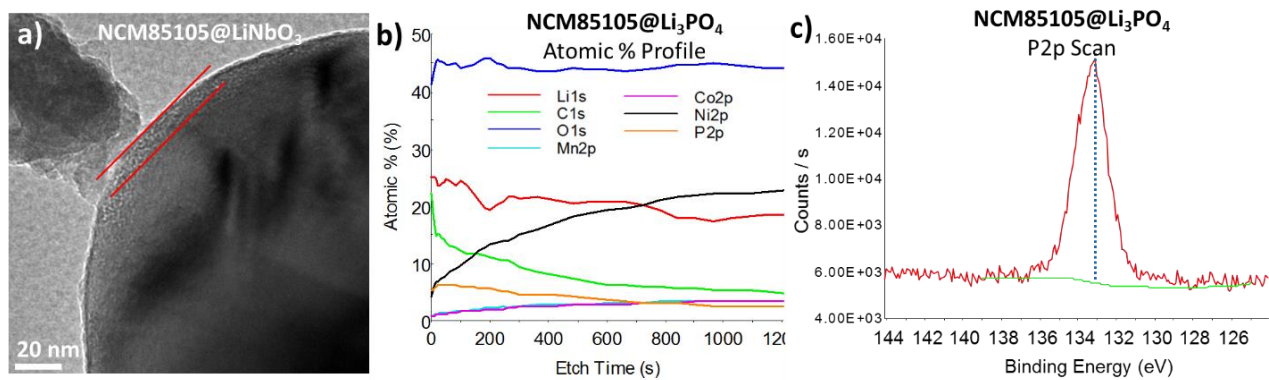


Figure 25. (a) High-resolution transmission electron microscopy image of NCM-85105@LiNbO₃ powder. The LiNbO₃ coating is amorphous and ~ 10.1-nm thick on this particular NCM particle (parallel red lines). (b) In addition to scanning electron microscopy energy-dispersive X-ray spectroscopy, NCM-85105@Li₃PO₄ was characterized using X-ray photoelectron spectroscopy. P2p signal provides evidence for phosphate species.

LiNbO₃ coatings were applied by treating NCM-85105 powders in an ethanol solution of lithium and niobium alkoxides using either a small batchwise process,^[5] or a spray coating process.^[2] The coated samples were then annealed under oxygen flow at 400°C for 1 hour. HRTEM was employed to characterize the NCM@LiNbO₃ sample prepared by the batchwise process (Figure 25a). The expected coating thickness was 5 nm based on a LiNbO₃ precursor loading of 0.6 wt%; however, the coating thickness was observed here to be ~ 10 nm. The NCM@LiNbO₃ sample prepared by spray coating is expected to have a much more uniform coating thickness; however, this sample was unavailable before the closing of GM's facilities. Nonetheless, the batchwise NCM@LiNbO₃ sample was sufficient for preliminary testing.

NCM-85105 was also coated with Li₃PO₄ via treatment in an aqueous phosphoric acid solution. In this process, NCM's native LiOH and Li₂CO₃ surface species are reacted with phosphoric acid (H₃PO₄) to produce Li₃PO₄. The Li₃PO₄ coating was characterized using SEM energy-dispersive X-ray spectroscopy (EDS) and XPS (Figure 25b-c). EDS data (not shown) indicate a widespread distribution of phosphorus signal across the sample, suggesting a conformal coating. Furthermore, XPS depth profiling data (Figure 25b) indicate that the atomic concentrations of phosphorus and nickel are inversely related, suggesting a discriminate surface coating composed of phosphorus. The P2p scan (Figure 25c) also matches well with a metal phosphate and confirms the presence of Li₃PO₄.

Having established proper NCM coatings, GM then proceeded to develop an experimental method based on differential scanning calorimetry (DSC) to quickly screen the thermal characteristics of NCM and SSE composites. Previous work by Tsukasaki et al. conducted similar experiments with charged cathode composites of $\text{LiNi}_{0.33}\text{Co}_{0.33}\text{Mn}_{0.33}\text{O}_2$ and $(\text{Li}_2\text{S})_{75}(\text{P}_2\text{S}_5)_{25}$ SSE.^[6] However, charged NCM is more reactive^[7] and does not properly reflect GM's hot pressing process wherein the cells are processed in the discharged state. To determine whether discharged cathode composites provide a measurable DSC signal, GM prepared composites of NCM@ LiNbO_3 and NCM@ Li_3PO_4 with BMR model SSEs $\beta\text{-Li}_3\text{PS}_4$ and $\text{Li}_6\text{PS}_5\text{Cl}$. The $\beta\text{-Li}_3\text{PS}_4$ SSE was prepared in-house, while the $\text{Li}_6\text{PS}_5\text{Cl}$ SSE was acquired from NEI Corporation. The composites contain 70 wt% NMC, 30 wt% SSE, and no carbon additive since its presence may promote side reactions. Future work will determine whether the presence of carbon additive confounds the thermal response of composite cathodes.

All discharged cathode composites have a measurable exothermic response as shown in Figure 26, and the response is observed to be influenced by both the NCM coating and the SSE composition. For the $\beta\text{-Li}_3\text{PS}_4$ SSE composites (Figure 26a), the use of NCM coating increases the onset of the exothermic event from 300°C to 342°C, regardless of the coating composition or thickness. However, peak response remains approximately the same for all samples at 1.2 $\mu\text{V}/\text{mg}$. For the $\text{Li}_6\text{PS}_5\text{Cl}$ SSE composites (Figure 26b), the onset of the exothermic event remains unchanged, though the peak exothermic response is decreased by nearly an order of magnitude from 22 $\mu\text{V}/\text{mg}$ to 2.5 $\mu\text{V}/\text{mg}$ with the use of NCM coating. The extent of the reaction remains equivalent for each sample, and completion of the reaction is shifted from 400°C to 460°C. This result suggests that the kinetics of the reaction between NCM and the $\text{Li}_6\text{PS}_5\text{Cl}$ SSE are slowed by 80-90% by the presence of a passivating coating.

With verification of the experimental method, the project's future work entails systematically exploring other parameters such as coating thickness, catholyte composition, and the addition of carbon black. The aim is twofold. First, the thermal response of composites will aid in the design of hot-pressing protocols and identify promising cathode composite systems. Second, the thermal response will be correlated to cell performance (that is, cyclability and impedance) and electron microscopy of the NCM/SSE interface.

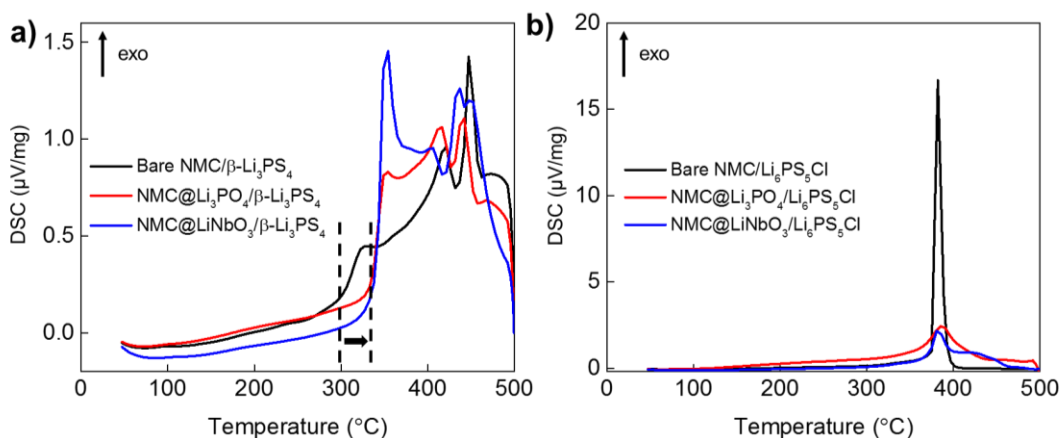


Figure 26. (a) Differential scanning calorimetry (DSC) results for composites composed of 70 wt% NCM-85105 and 30 wt% $\beta\text{-Li}_3\text{PS}_4$. Onset of exothermic signal is shifted to higher temperatures with the application of NCM coating (black arrow). (b) DSC results for composites composed of 70 wt% NCM-85105 and 30 wt% $\text{Li}_6\text{PS}_5\text{Cl}$. Onset of exothermic signal is unchanged, but peak response is reduced by nearly an order of magnitude, and completion of the reaction is shifted to higher temperature.

References

- [1] Zhu, Y., et al. *ACS Applied Materials & Interfaces* 7 (2015): 23685–23693.
- [2] Ohta, N., et al. *Electrochemistry Communications* 9 (2007): 1486–1490.
- [3] Lee, Y-G., et al. *Nature Energy*. doi: 10.1038/s41560-020-0575-z.

- [4] Deng, S., et al. *Energy Storage Materials* 27 (2020): 117–123.
- [5] Li, X., et al. *Energy Storage Materials* 18 (2019): 100–106.
- [6] Tsukasaki, H., et al. *Journal of Power Sources* 367 (2017): 42–48.
- [7] Bak, S-M., et al. *ACS Applied Materials & Interfaces* 6, no. 24 (2014): 22594–22601.

Patents/Publications/Presentations

The project has no patents, publications, or presentations to report this quarter.

Task 1.12 – Low Impedance Cathode/Electrolyte Interfaces for High-Energy-Density Solid-State Batteries (Eric Wachsman and Yifei Mo, University of Maryland)

Project Objective. The objective of this project is to research, develop, and test Li-metal-based batteries that implement solid LICs equipped with NMC cathodes integrated into the Li-metal/LLZ ($\text{Li}_7\text{La}_3\text{Zr}_2\text{O}_{12}$) tri-layer architecture. Specifically, the team will achieve the following: (1) identify and demonstrate interfacial layers to achieve low-impedance and stable NMC/LLZ interfaces; (2) develop novel processing techniques to fabricate NMC/LLZ composite cathodes with low interfacial resistance; and (3) enable high-performance ASSBs with an energy density of 450 Wh/kg and 1400 Wh/L and negligible degradation for 500 cycles.

Project Impact. Instability or high resistance at the interface of high-energy cathode materials with lithium-garnet solid electrolytes limits the high-energy-density all-solid-state lithium battery. This project will lead to a fundamental understanding of solid-electrolyte/solid-cathode interfaces and a unique and transformative LLZ framework to enable high-energy density, safe Li-metal batteries approaching ~ 400 Wh/kg.

Approach. In this new EERE project, the team will build on their demonstrated expertise with garnet electrolytes and ASSB cells to accomplish the following: (1) engineer interfaces to overcome high NMC/LLZ interfacial impedance and interfacial degradation; (2) develop processing and fabrication techniques to achieve high-loading NMC/LLZ composite cathodes with low resistance and high cyclability; and (3) integrate the NMC/LLZ cathodes into all-solid-state Li-metal/LLZ cells to achieve high-energy-density batteries.

Out-Year Goals. The project will solve the current challenges of integrating garnet solid electrolyte with a cathode to achieve a high-performance ASSB using a high-energy-density Li-metal anode. The resultant high energy density and stability using both high-energy-density Li-metal anodes and NMC cathodes will open new applications in portable electronics, EVs, and beyond.

Collaborations. This project funds work at UMD. Dr. E. Wachsman (PI) will have management responsibility and will lead experimental efforts including garnet synthesis, interface processing, cell fabrication, and testing. Dr. Y. Mo (Co-PI) will lead the computational efforts on understanding the stability between garnet and cathode and on identifying promising coating materials. No collaborations are reported this quarter.

Milestones

1. Computationally determine interfacial stability between LLZ solid electrolytes and NMC cathode. (Q2, FY 2020; Completed)
2. Determine thermochemical stability between LLZ and infiltrated NMC. (Q3, FY 2020; In progress)
3. Computationally determine the mechanism of interfacial stabilization between LLZ and NMC through coating layers. (Q3, FY 2020; In progress)
4. *Go/No-Go Decision*: Computationally determine appropriate compositions to stabilize the LLZ-NMC interface. Achieve design capable of meeting performance requirements. (Q4, FY 2020)

Progress Report

Computational studies based on the thermodynamic analyses of first-principles calculations have been completed in the evaluation of the thermodynamic interface stability between LLZ solid electrolytes and layered oxide cathode materials. The computational analyses based on the same method have been completed to identify the interface stability of LLZ solid electrolytes with NMC cathode (Table 2). The computation study found that Ni-rich cathode materials such as NMC exhibit mutual chemical reactions, suggesting a limited interface stability between LLZ garnet and NMC cathode materials. In addition, the delithiated NMC shows poor interface stability with LLZ garnet, indicating potential interface degradation during cycling or the charged state of the SSB. The team further analyzed the thermodynamic phase equilibria of the reaction products. The behavior of different TMs in the NMC cathodes was identified. The computation results will be compared with experimental results, which are being performed in parallel; the experimental feedback will help to improve the computation models.

Table 2. Decomposition energy and phase equilibria of LLZ with lithiated and delithiated (prefix “d-”) LCO and NMC-111 from thermodynamic analyses based on first-principles data.

	E_d (eV/atom)	Phase Equilibria
LCO	-0.0013	Li_5CoO_4 , La_2O_3 , $\text{Li}_6\text{Zr}_2\text{O}_7$
d-LCO	-0.039	La_2O_3 , O_2 , $\text{Li}_7\text{Co}_5\text{O}_{12}$, $\text{La}_2\text{Zr}_2\text{O}_7$
NMC-111	-0.012	La_2O_3 , Li_2MnO_3 , $\text{Li}_4\text{CoNi}_3\text{O}_8$, NiO , $\text{La}_2\text{Zr}_2\text{O}_7$, $\text{Li}_7\text{Co}_5\text{O}_{12}$
d-NMC-111	-0.050	O_2 , Li_2MnO_3 , $\text{Li}_7\text{Co}_5\text{O}_{12}$, Li_2NiO_3 , $\text{La}_2\text{Zr}_2\text{O}_7$, La_2O_3

In addition, the team compared the interface stability of LLZ garnet with a range of different layered oxide cathodes, such as LiCoO_2 , LiNiO_2 , NMC-111, and NMC in other compositions. The variation of materials stability was identified among these cathodes (Figure 27). It was found that higher nickel content in cathodes generally leads to poor stability. These results will be used for further detailed analyses to identify promising coating for LLZ-NMC interfaces.

In parallel to the computation results, experimental efforts have been initiated to study the interface stability of LLZ garnet and cathode. DSC experiments were performed on powdered samples to study the interface stability. Preliminary results indicate good agreement with computation results for the interface stability of LLZ and NMC.

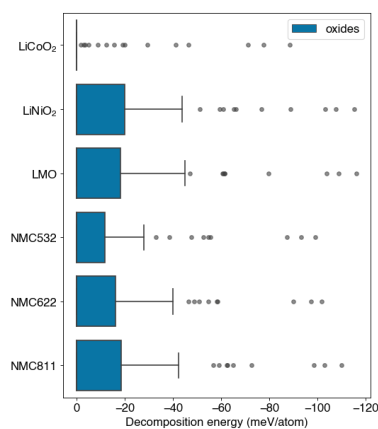


Figure 27. Statistics of the interface stability for different compositions of NMC and layered oxides compositions.

Patents/Publications/Presentations

Publication

- Nolan, A. M., Y. Liu, and Y. Mo.* “Solid-State Chemistries Stable with High-Energy Cathodes for Lithium-Ion Batteries.” *ACS Energy Letters* 4 (2019): 2444–2451.

Task 1.13 – Developing an *In Situ* Formed Dynamic Protection Layer to Mitigate Lithium Interface Shifting: Preventing Dendrite Formation on Metallic Lithium Surface to Facilitate Long Cycle Life of Lithium Solid-State Batteries
(DeYang Qu, University of Wisconsin Milwaukee)

Project Objective. The objective of this project is to research, develop, and test Li-metal-based batteries that implement solid LICs equipped with a formed dynamic protection layer. The proposed project aims to enable safe, long-cycle lithium anodes to achieve cell performance targets of 400 Wh/Kg, over 100 cycles, with 15-year shelf life and < \$100/KWh cost.

Project Impact. Project efforts are to contribute an in-depth understanding of the lithium interface and dendrite growth prevention to the field of Li-metal batteries, which will pave the way for eventual development of high-energy-density, low-cost, and long-lasting lithium batteries. This advancement could be a crucial selling point for the greater adoption of EVs. This project will make possible the translation of fundamental research into practical implementation of high-energy lithium anodes, enabling eventual achievement of cell performance targets.

Approach. The novelty of this approach is that the team intends to mitigate the dendrite problem by creating a dynamic protection layer during the interface shift to prevent dendrite formation throughout battery operation.

Out-Year Goals. The project has three out-year goals: (1) *in situ* diagnostic tools are fully functional; (2) potential candidates for Li-anode modifications are identified; and (3) synthesis routes are designed.

Collaborations. The PI is the Johnson Control Endowed Chair Professor, who has close and frequent collaboration with Johnson Controls' scientists and engineers. The collaboration enables the team to validate the outcomes of fundamental research in pilot-scale cells. The PI also has been working closely with top scientists at Argonne National Laboratory (ANL), Brookhaven National Laboratory (BNL), LBNL, and PNNL and with U. S. industrial collaborators, for example, GM, Millipore Sigma, and Clarios. In addition, the team works with international collaborators in China, Japan, and South Korea. These collaborations will be strengthened and expanded to give this project a vision with both today's state-of-the-art technology and tomorrow's technology in development, while incorporating feed-back from the material designers and synthesizers upstream, as well as from the industrial end users downstream.

Milestones

1. *Baseline.* Conduct literature review and establish baseline for proposed technologies. (Q1, FY 2020; Completed)
2. *Fully functional fixtures and setups.* *In situ* electrochemical-optical and *in situ* electrochemical-MS cells capable of observing dendrite growth and detecting gas generation in real time. (Q1, FY 2020; Completed)
3. *Coating methods.* Physical requirements of each coating technique and adaption of different coating methods for various coating materials based on their properties are identified. (Q2, FY 2020; Completed)
4. *N-type polymer compounds.* N-doped polymer compounds are synthesized. (Q3, FY 2020; In progress)
5. *In situ* diagnostic tools capable of investigating a coated lithium electrode / projected cell performance. Various selected materials can be coated on a lithium surface forming an artificial layer before cell assembly. The dendrite growth and gassing of the coated electrode can be investigated in real-time during cell operation with *in situ* diagnostic tools. Analysis indicates technical approach capable of achieving performance targets. (Q4, FY 2020; In progress)

Progress Report

This quarter's milestone was completed, with progress made on other milestones as well. Based on last quarter's results, the team is developing engineering processes to create dynamic interfacial layers on metallic lithium anodes. Three approaches were applied:

- *Physical lamination.* The active materials (for example, graphite, red-phosphorus, and tin) were mechanically applied to the surface of lithium. The coating layers are thin, uniform, and dense, which allows both lithium migration and electron exchange at the interface. The thickness can be adjusted in the sub-micron range.
- *Surface self-assembled interfacial layer.* Unlike in the previous approach, the dynamic interfacial layer is elastic, and liquid electrolyte can be trapped in the layer through strong bonding. The size of the layer can self-adjust to compensate the volume change of the lithium anode during cycling to maintain a stable electrochemical interface.
- *Surface fluorination.*

Figures 28 and 29 show the comparison of pristine lithium and surface-modified lithium created by first and second approaches described above. The electrodes were cycled at 2 mA cm^{-2} rate in a liquid electrolyte. The surface morphologies of pristine and modified anode surface are shown. Clearly, the dendrite growth and “dead lithium formation” during cycling were substantially depressed on the modified lithium surface. One hypothesis is that an artificial layer is not only formed *ex situ*, but also can chemically react *in situ* with lithium dendrite. Therefore, regardless of the degree of interfacial shift, as soon as the dendrite growth is high enough to reach the layer, lithium reacts with the layer. The height of dendrites is limited to the height of the gap between lithium and the artificial layer. The second hypothesis is that with the artificial interface, the surface energy of lithium anode can become more homogeneous, resulting in the lithium deposition being more uniform. The preliminary results support these hypotheses. The important hypothesis is that the *ex situ* formed artificial interface on lithium anode can become an effective interface between lithium anode and SSE.

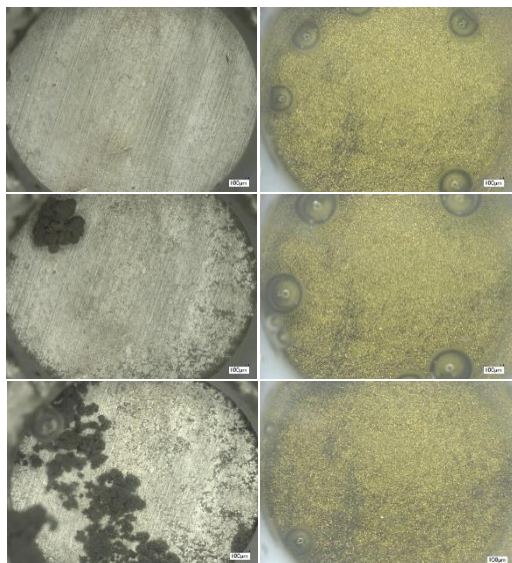


Figure 28. Lithium with graphite lamination (right) in comparison with pristine lithium surface (left) after 0, 1st, and 5th cycles.

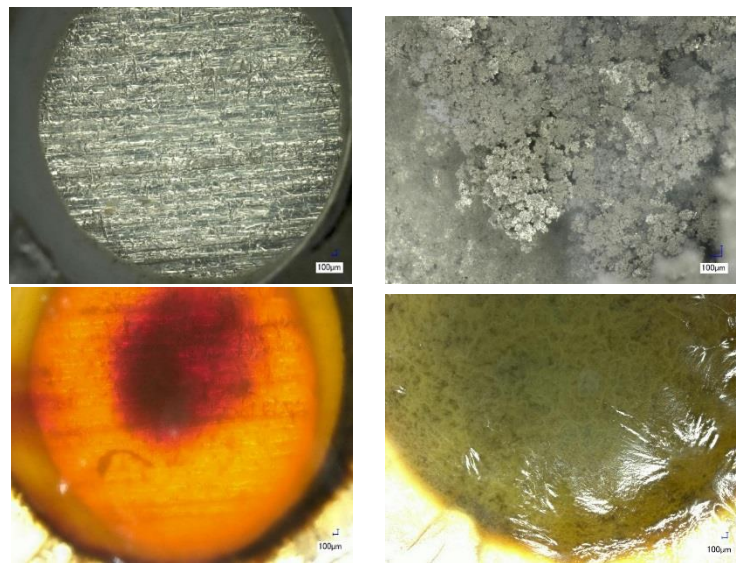


Figure 29. Comparison of coated and pristine lithium anode. (top right) Pristine lithium surface. (top left) Pristine lithium surface after five high-rate cycles. (lower left) Elastic surface coating. (lower right) Elastic surface coating after five high-rate cycles.

Patents/Publications/Presentations

The project has no patents, publications, or presentations to report this quarter.

Task 1.14 – Molecular Ionic Composites: A New Class of Polymer Electrolytes to Enable All-Solid-State and High-Voltage Lithium Batteries (Louis Madsen, Virginia Polytechnic Institute and State University)

Project Objective. Based on a newly discovered class of solid polymer electrolyte materials, that is, molecular ionic composites (MICs), the overall objective is to develop solid-state lithium conductors targeted for use in transportation applications. MICs form a mechanically stiff, electrochemically stable, and thermally stable matrix. Specific objectives include the following: (1) development of robust MIC electrolyte thin films (~ 20 μm) to serve as simultaneous nonflammable separators and dendrite-blocking Li^+ conductors, (2) electrochemical quantification of key performance metrics including electrolyte stability, interfacial reactions, and suitability/compatibility with a range of electrode materials, and (3) comprehensive investigation of ion transport mechanisms and electrode-electrolyte interfacial reactivity under practical operating conditions using NMR and synchrotron X-ray analyses.

Project Impact. Commercialization of Li-metal SSBs is hampered by lack of a functional nonflammable solid electrolyte that can provide high ionic conductivity, wide electrochemical window, favorable mechanical properties to inhibit lithium dendritic growth, and low interfacial resistance. The tunable MIC materials platform has potential to fulfill these requirements with relatively simple fabrication techniques, and thus shows promise for enabling SSBs that can be optimized for low cost and high energy density and are nonflammable.

Approach. MICs rely on a unique polymer that is similar to Kevlar® in its strength, stiffness, and thermal stability, but with densely spaced ionic groups that serve to form an electrostatic network that permeates mobile ions in the MIC. The team can tailor the ion concentrations and types to yield MIC electrolyte films that are electrochemically compatible with Li-metal anode as well as a range of high-voltage layered cathodes. They are searching the composition space of lithium salts, electrochemically compatible ionic liquids, and polymer (PBBDT) molecular weight to determine best composition windows for MIC electrolytes. The team is also investigating best methods for casting thin films in terms of temperature, solvent/evaporation conditions, and control over the initial liquid crystalline gel formation point. Concurrently, they are testing MIC films in various electrochemical cells, quantifying transport and structural/morphology parameters with NMR and X-ray techniques, and measuring key mechanical (dynamic mechanical thermal analysis, stress-strain) and thermal (DSC, TGA) properties.

Out-Year Goals. This year, the team is focused on understanding evolution of structure and morphology during the film casting process to optimize this process and obtain thin MIC electrolyte films. As part of the team's electrolyte optimization, they are determining the composition windows that yield fast Li^+ conduction, mechanical stability, and electrochemical compatibility with lithium metal and selected cathode materials. They will develop robust electrolyte films and an array of testing schemes (that is, electrochemical, thermal, mechanical, NMR, and X-ray) to sensibly feedback on film composition and fabrication.

Collaborations. The team is beginning a collaboration with T. J. Dingemans' group at University of North Carolina (UNC) Chapel Hill in which they are forming composites based on the PBBDT polymer and carbon materials such as graphene oxide, and are beginning to develop various charged rigid-rod polymers. The team is exploring a shear rheology and broadband dielectric spectroscopy collaboration with Prof. R. H. Colby at PSU. The team is also starting a collaboration with D. Nordlund at SLAC National Accelerator Laboratory (SLAC) to conduct synchrotron X-ray studies on MIC films.

Milestones

1. Determine synthetic conditions for 100- μm thick electrolyte. (Q1, FY 2020; Completed)

- Development of the baseline Li-ion loading and chemical composition. (Q2, FY 2020; Completed)
- Establish basic electrochemical, thermal, and mechanical testing protocols for solid electrolytes and battery cells. (Q3, FY 2020; In progress)

Progress Report

This quarter, the team has searched the composition space of lithium salts, ionic liquids, and polymer (PBDT) molecular weight, as well as the relative concentrations of each component. They have developed the baseline MIC electrolyte composition through variation of the component types and ratios, and then verified that they can obtain robust films with maximal conductivity and chemical/electrochemical stability in the presence of lithium metal and during Li|Li cell cycling. They have now achieved uniform flexible films of 60- μm thickness and are continuing to push this attainable thickness downward. Figure 30 shows the chemical structures and relative amounts of the solid electrolyte components, a photograph of a more uniform and flexible MIC film, ionic conductivity versus temperature, and separate ion diffusion coefficients versus temperature.

An exciting new frontier in this work is the ability to reversibly measure properties for these MIC electrolytes over a wide temperature range, at least from -50°C to $+200^\circ\text{C}$. This opens possibilities for a range of Li-based batteries where a monolithic solid lithium conductor electrolyte film can be employed with no thermal or mechanical degradation upon fast charging/discharging and/or when operating in extreme temperature environments. The team has explored such temperatures with ionic conductivity and NMR diffusometry experiments (Figure 30c-d), and will expand this work further.

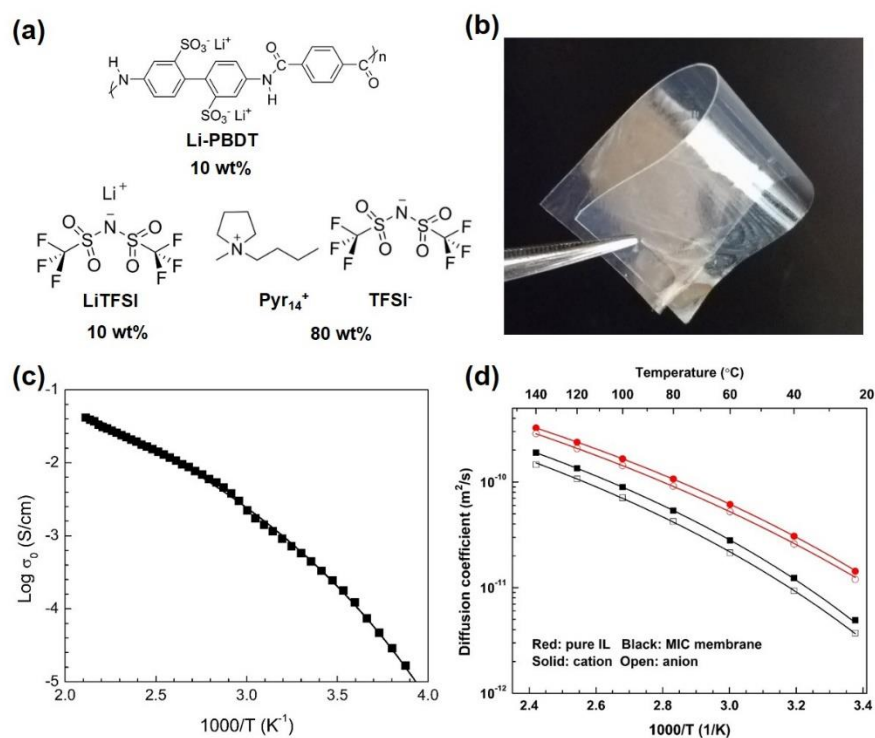


Figure 30. (a) Chemical composition of baseline-optimized molecular ionic composite (MIC) film with relative percentages of each component. (b) Photograph of MIC film with improved uniformity and flexibility. (c) Temperature dependence of ionic conductivity of the MIC film. (d) Separate diffusion coefficients of ionic liquid (IL) cation and anion in the film compared to the diffusion coefficients of pure IL. (Li^+ diffusion coefficient measurements are under way.) This composition enables robust electrolyte films down to 60- μm thickness that can reversibly thermally cycle from -50°C to $+200^\circ\text{C}$.

Regarding comparison of ionic conductivity and NMR diffusometry results in Figure 30c-d, the team is working toward a model for prediction of conductivity from diffusion coefficients. Initial observations suggest that something about the interface (between electrolyte and electrode, be it stainless steel for conductivity or lithium for cell cycling) is unduly influencing overall conductivity and Li|Li cell performance. The team is investigating the possibility of a surface layer that develops during casting that is more dense in PBDT polymer, thus reducing cell performance. They expect to use this fundamental knowledge to be able to tune the now relatively simple tape/solvent casting procedure (time, solvent removal, solvent composition) to alleviate this effect.

In Li|Li symmetric cell testing, so far the Pyr₁₄TFSI ionic liquid and LiTFSI salt have the best chemical and electrochemical stability, evidenced by current cycling from +23°C to +100°C. Figure 31 shows an example cycling plot at 100°C (with current ramping), demonstrating cycling up to ~0.8 mA/cm² for the present electrolyte. The team is using these Li|Li cells to establish and implement protocols for electrochemical testing such as Li⁺ transference number and long-term cycling stability at fixed current density. These tests will be followed by post-mortem failure analysis aided by electron and force microscopy, NMR spectroscopy and diffusometry, synchrotron X-ray, and other techniques. The team has so far cycled a Li|Li cell for > 100 hours at 0.6 mA/cm² and 100°C. They are also implementing CV and examining cell charge/discharge profiles, with results expected for the next report.

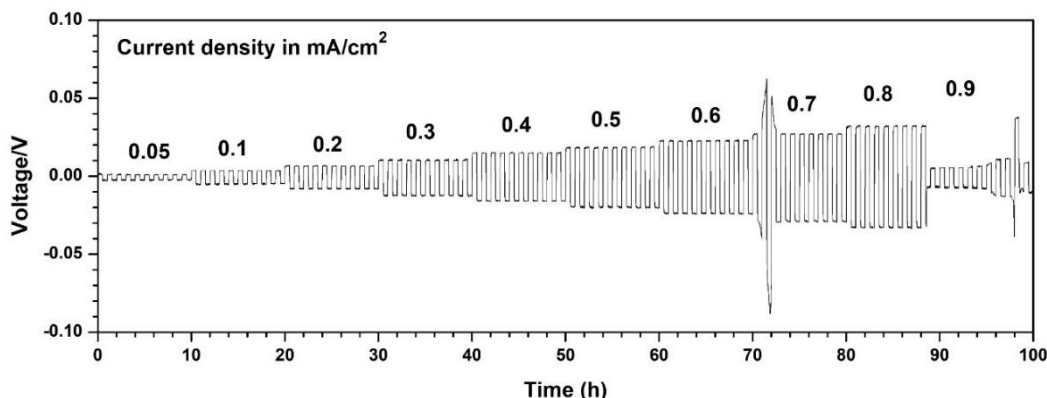


Figure 31. Li|Li symmetric cell cycling plot acquired at 100°C, with current ramping to show maximum current density for this film at *ca.* 0.8 mA/cm². The team is in the process of pushing Li|Li cell testing over a wide temperature range, and extracting electrochemical information such as Li⁺ transference number.

The team is additionally pursuing mechanical testing on these MIC films, including the beginning of variable-temperature shear rheology and dynamic mechanical tensile measurements. Figure 32 shows a tensile stress-strain curve for the present MIC film at room temperature, with mechanical results described.

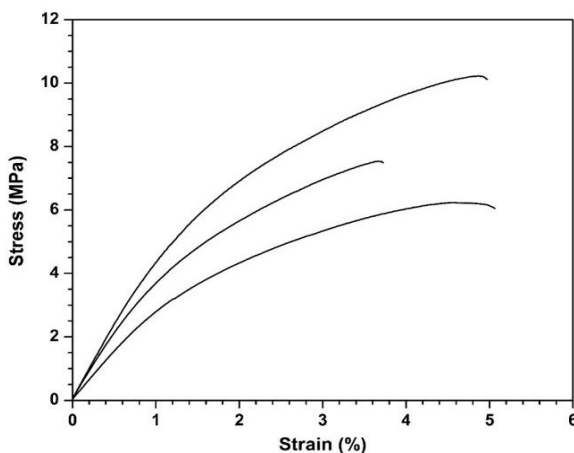


Figure 32. Tensile stress-strain curve for molecular ionic composite (MIC) electrolyte film at room temperature. The three curves represent tests on dogbone samples cut from various locations spanning the as-cast film. Tensile modulus averages 400 MPa. These MIC films exhibit approximately 2× higher strain at break relative to non-Li-loaded MICs and comparable tensile modulus (see first-quarter report on dynamic mechanical analysis curves). Note that assembly under compression into (Li|Li symmetric) coin cells does not damage the film, as observed after disassembly.

Patents/Publications/Presentations

Publication

- Bostwick, J. E., C. J. Zanelotti, C. Iacob, A. Korovich, L. A. Madsen, and R. H. Colby. “Ion Transport and Mechanical Properties of Non-Crystallizable Molecular Ionic Composite Electrolytes.” *Macromolecules* 53, no. 4 (2020): 1405–1414. doi: 10.1021/acs.macromol.9b02125.

Task 1.15 – All-Solid-State Batteries Enabled by Multifunctional Electrolyte Materials (Pu Zhang, Solid Power Inc)

Project Objective. The project objective is to develop Li-metal SSBs enabled by multifunctional SSEs for EV application. The ultimate goal is scalable production of large-format ASSBs able to deliver ≥ 350 Wh/kg specific energy, ≥ 1000 cycle life, and $\leq \$100/\text{kWh}$ cost.

Project Impact. The project impact is enabling scalable production of large format all-solid batteries required by the vehicle market and building domestic battery manufacturers as leaders in the global vehicle ASSB production. The proposed technology will address key limitations of state-of-the-art lithium batteries to meet DOE EV battery targets and accelerate their adoption as large-format EV batteries for sustainable transportation technology.

Approach. The project will develop a high-performance Li-metal solid-state cell enabled by a multifunctional SSE. The new SSE will: (1) have high conductivity (up to 10 mS/cm), (2) be stable against lithium metal and high-voltage cathode (0-4.5 V), (3) promote uniform lithium plating (enabling $> 2\text{C}$ charge rate), and (4) be compatible with large-scale manufacturing processes. The specific cell chemistry to be demonstrated will be the SSE with Li-metal anode and high-nickel-content Li-metal oxide cathode. The solid-state cell will be assembled by scalable roll-to-roll processes developed by Solid Power.

Out-Year Goals. In Year 1, multifunctional SSE will be developed with lithium ionic conductivity of $\geq 3 \times 10^{-3}$ S/cm. CCD of ≥ 6 mA/cm² will be achieved in a symmetric lithium cell. The SSE design concept will be proven by demonstrating cycle life of ≥ 200 in a full cell. In Year 2, SSE material will be optimized with lithium ionic conductivity of $\geq 5 \times 10^{-3}$ S/cm. Scalable cell assembly processes will be developed. Cycle life of ≥ 500 will be demonstrated in a full cell. In Year 3, large-format solid-state cells ($> 2\text{Ah}$) will be assembled/tested to meet the final goal: ≥ 350 Wh/kg, ≥ 1000 cycles, and $\leq \$100/\text{kWh}$ cost.

Collaborations. The proposed team consists of Solid Power and subcontractor UCSD. Solid Power (PI: Dr. P. Zhang) will develop the multifunctional SSE and other cell components, assemble cells, and conduct cell tests. UCSD (PI: Prof. S. Meng) will carry out material characterization by using advanced techniques such as XPS, Cryo-STEM imaging, Cryo-STEM EDX, electron energy loss spectroscopy (EELS), and cryo-FIB milling. The UCSD team seeks to quantify the kinetics and evolution of each contributing factor and its impact on battery performance.

Milestones

1. Secure precursors and equipment. (Q1, FY 2020; Completed, December 31, 2019)
2. Down-select cathode materials. (Q2, FY 2020; Completed, December 31, 2019)
3. Cathode loading ≥ 3.5 mAh/cm². (Q3, FY 2020; Completed, March 31, 2010)
4. SSE ionic conductivity ≥ 3 mS/cm; cell cycle life ≥ 200 . (Q4, FY 2020; Completed, March 31, 2010)
5. Cell cycle life ≥ 200 . (Q4, FY 2020; In progress)

Progress Report

SSE Development

The Solid Power halogenated LPS material was used as a starting point. Li_2S , P_2S_5 , a halogen, and other selected dopants were ball-milled to form glassy sulfide electrolytes by using a mechanical ball mill. A subsequent heat-treatment was conducted to obtain glass-ceramic solid electrolytes. A promising multifunctional SSE was demonstrated with a conductivity of $4.5 \times 10^{-3} \text{ S/cm}$ at 25°C in the first quarter. Based on this material, the “Design of Experiments” (DOE) method was applied this quarter to investigate the composition and process of the electrolyte materials. An L18 orthogonal matrix was created for the experiments, by controlling the critical factors including dopant parameters, milling parameters, and heat treatment parameters. Li-ion conductivity and CCD with lithium of the electrolyte were used as the key criteria to screen the electrolyte materials.

The “DOE” resulted in two electrolyte materials that outperformed the first-quarter baseline on both conductivity and CCD. They showed 50% higher conductivity and 90% higher CCD than the baseline (Figure 33). The electrolyte materials will be further evaluated for long-term cycling stability next quarter.

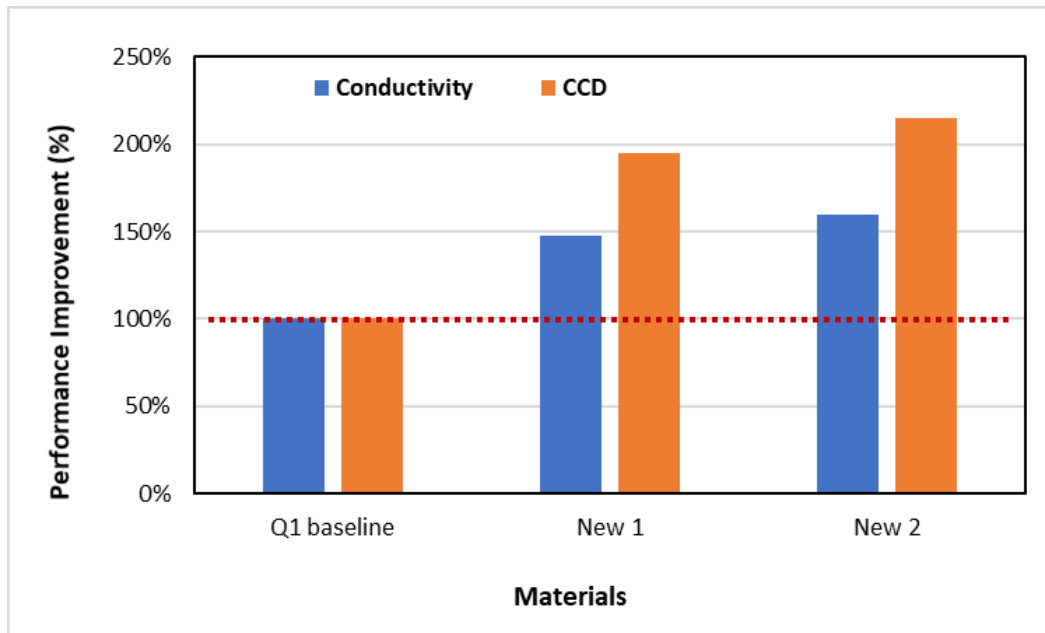


Figure 33. Conductivity and critical current density (CCD) of the electrolyte materials. Baseline material has conductivity of 4.5 mS/cm and CCD of 3 mA/cm² at 25°C.

Cathode Development

NMC-622 material has been selected for the concept-proven demonstration in Year 1, based on its combined advantages of both high capacity and long-term stability. All the cathodes were fabricated by using a slurry-casting method. This quarter, cathode capacity was increased to 160 mAh/g (at electrode level) from 130 mAh/g by optimizing the cathode formulation. The electrochemical loading was also increased to 3.5 mAh/cm² successfully. Figure 34 shows the progress in Q2.

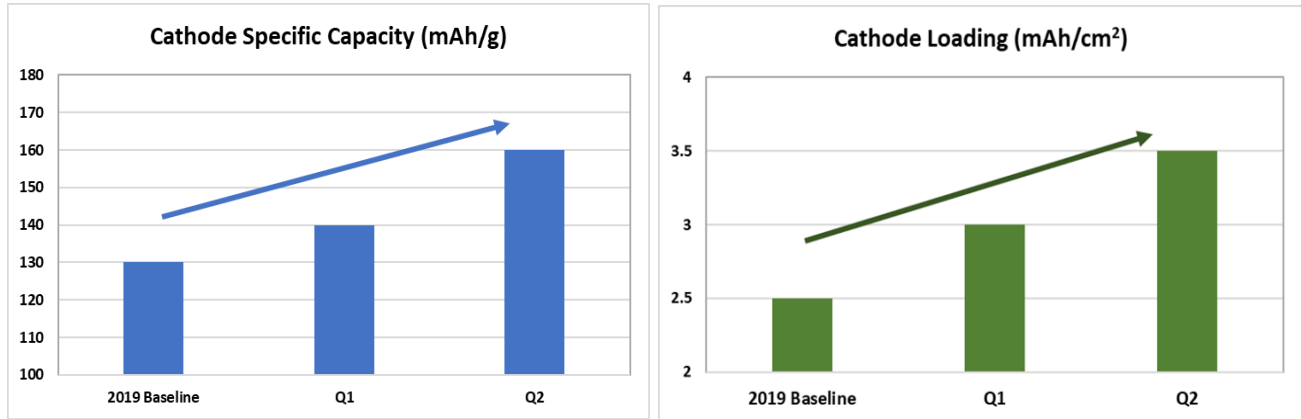


Figure 34. The progress of development of NMC cathode: improved specific capacity (left) and electrochemical loading (right).

Cell Development

A solid-state cell includes a cathode, a separator (electrolyte), and a Li-metal anode. A thin lithium foil was selected for the cell last quarter. Both the cathode and separator were developed for cell assembly this quarter.

The cathode progress is described in the section above. The separator was fabricated by using the same slurry-casting method as the cathode. First, the electrolyte powder, a binder, and a solvent were mixed to form a separator slurry. The slurry was then coated on a substrate by either hand-cast in lab scale or slot-die coating in pilot scale to form a separator film. The separator can be used as a stand-alone film after a calendaring process. The separator also can be directly laminated to a cathode to form a cathode/separator bilayer film. Figure 35 shows the separator film, the cathode, and the cathode/separator bilayer film, respectively.

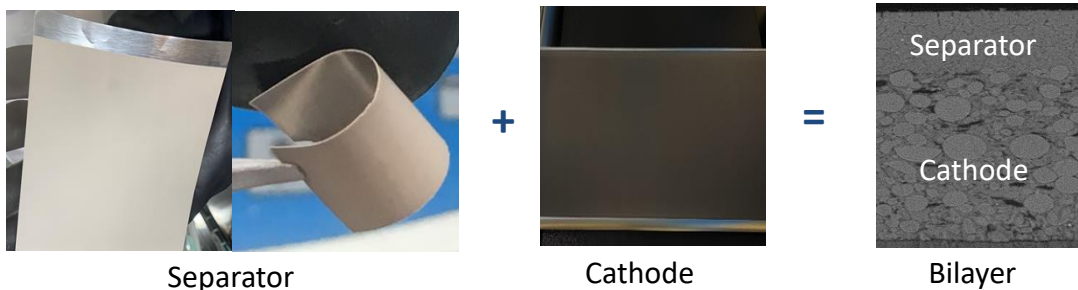


Figure 35. From left to right: separator film, cathode film, and cathode/separator bilayer film (scanning electron microscopy cross-section image). The separator is 40 μm and the cathode is 120 μm in this case.

A single piece of the bilayer film or multiple pieces of the bilayer film will match lithium anode to form a single-layer or multilayer cell stack. After welding tab to the stack and sealing the tabbed stack into a pouch, a pouch cell will be formed. The pouch cell assembly and testing will be conducted next quarter.

Patents/Publications/Presentations

The project has no patents, publications, or presentations to report this quarter.

Task 1.16 – Developing Materials for High-Energy-Density Solid-State Lithium-Sulfur Batteries (Donghai Wang, Pennsylvania State University)

Project Objective. The project objectives are to develop materials involving advanced S-C composite materials, solid additives, and sulfide-based SSEs, and to acquire knowledge for Li-S ASSBs. Li-S ASSBs with large areal sulfur loading ($\geq 5 \text{ mg cm}^{-2}$) and high sulfur content ($\geq 50 \text{ wt\%}$ in cathode), pairing with lithium or lithium alloy anode, shall deliver a high initial specific capacity of over 1200 mAh g^{-1} at high charge/discharge rate ($> 0.3 \text{ C}$) for 500 cycles with over 80% capacity retention.

Project Impact. This project aims to develop new materials to enable Li-S ASSBs with high energy density, excellent cycling stability, and good rate performance, and thus to build knowledge for fabrication of prototype Li-S ASSBs batteries. Specifically, the developed new materials will greatly increase the specific capacity of sulfur and sulfur utilization at high areal sulfur loading, alleviate the interfacial problem between S-C composite and SSE within sulfur cathode, boost Li-ion conductivity, and improve moisture stability of glass and glass-ceramic sulfide-based SSE. Meeting the technical targets will potentially promote development of high-energy-density Li-S ASSBs and their practical application in EVs and plug-in hybrid EVs (PHEVs), and reduce petroleum consumption in the transportation sector by helping battery-powered vehicles become more accepted by consumers as a reliable source of transportation.

Approach. The project goal will be accomplished through developing new materials, together with in-depth characterization of sulfur cathode. Specifically, approaches to realize the project objectives include: (1) development of new carbon material with unique structure, high surface area, and large pore volume; (2) development of new S-C materials to facilitate electron/ion transport; (3) development of novel additives to tune interfacial behavior among components in the cathode; (4) development and optimization of new SSE through cation and anion doping with superior properties such as high ionic conductivity, good moisture, and stability; and (5) diagnostics, characterization, and cell tests on the developed new material or advanced sulfur cathode.

Out-Year Goals. The out-year goals are as follows: (1) develop new S-C materials, new cathode additives, and cation-doped solid electrolytes (ionic conductivity above 2 mS cm^{-1} at room temperature), (2) conduct characterization and performance tests on both material and electrode levels. The *Go/No-Go Decision* will be demonstration of all-solid-state sulfur cathode with over 1000 mAh g^{-1} discharge capacity at 0.3 C discharge rate and 50 wt\% sulfur content for 50 cycles at 60°C .

Collaborations. There are no active collaborations.

Milestones

1. Demonstrate sulfur cathode with above 800 mAh g^{-1} capacity at 0.1 C at 60°C . (Q1, FY 2020; Completed, December 31, 2019)
2. Demonstrate sulfur cathode $> 1000 \text{ mAh g}^{-1}$ using new solid additives or developed new electrolyte ($> 1 \text{ mS cm}^{-1}$, at 25°C). (Q2, FY 2020; Completed March 31, 2019)
3. Demonstrate sulfur cathode with $> 1000 \text{ mAh g}^{-1}$ using optimized carbon materials. (Q3, FY 2020; In progress)
4. Demonstrate sulfur cathode with $> 1000 \text{ mAh g}^{-1}$ at 0.3 C for 50 cycles at 60°C . (Q4, FY 2020)

Progress Report

This quarter, the team continued work to meet milestones and gain more knowledge of all-solid-state Li-S battery systems. As solid electrolyte is one of the most significant components affecting battery performance, the team synthesized more electrolytes with higher ionic conductivity ($> 1 \text{ mS cm}^{-1}$ at room temperature) that meet requirements for practical battery application. Following the literature, two types of solid electrolytes, $\text{Li}_6\text{PS}_5\text{Cl}$ and $\text{Li}_7\text{P}_2\text{S}_8\text{Br}_{0.5}\text{I}_{0.5}$, were successfully prepared using ball milling and post heat treatment process with high ionic conductivity similar to the literature report. Using $\text{Li}_7\text{P}_2\text{S}_8\text{Br}_{0.5}\text{I}_{0.5}$ as an example, Li_2S , P_2S_5 , LiBr , and LiI were mixed together with heptane and ball milled for 48 hours. Afterward, the samples were collected and vacuum dried under 120°C for 1 hour to remove the solvents. The obtained glass-type solid electrolyte was further annealed at 160°C for 60 hours to get glass-ceramic solid electrolytes. XRD spectra of the glass-ceramic $\text{Li}_7\text{P}_2\text{S}_8\text{Br}_{0.5}\text{I}_{0.5}$ is shown in Figure 36a. The obtained electrolyte showed a high ionic conductivity of 6.2 mS cm^{-1} at 25°C . The measured ionic conductivity at various temperatures is shown in Figure 36b. The calculated activation energy is 0.182 eV . The knowledge acquired in synthesizing these highly ionic conductive solid electrolytes will not only contribute to the design of new solid electrolyte, but also help the team make all-solid-state Li-S batteries with superior performance.

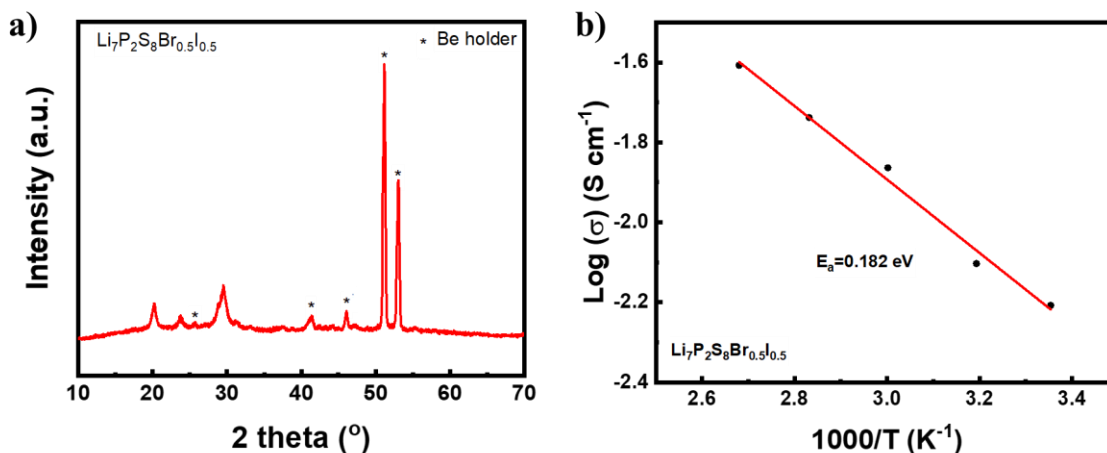


Figure 36. (a) X-ray diffraction spectra and (b) Arrhenius plot of $\text{Li}_7\text{P}_2\text{S}_8\text{Br}_{0.5}\text{I}_{0.5}$ glass ceramic solid electrolyte.

Besides synthesizing solid electrolytes that have already been reported in previous literature, the team also started to develop new solid electrolytes. For real application, solid electrolytes should possess high ionic conductivity at room temperature ($>1 \text{ mS cm}^{-1}$), superior stability against lithium, and chemical stability against moisture. To fulfill all of these requirements, the team incorporates nitrogen and aluminum into the solid electrolyte framework to investigate their influence on properties of solid electrolytes and develop new solid electrolytes. Therefore, a series of glass-ceramic solid electrolytes $75\text{Li}_2\text{S}-25\text{P}_2\text{S}_5-5\text{Li}_3\text{N}-x\text{Al}_2\text{S}_3$ ($x = 0, 1, 2, 3,$ and 4) was synthesized using dry ball milling method. In detail, precursors Li_2S , P_2S_5 , Li_3N , and Al_2S_3 were mixed and ball milled for 20 hours to obtain solid electrolyte glass. The XRD patterns of the acquired samples were shown in Figure 37a. Several peaks representing Li_2S could be observed on the XRD spectra for all samples, while peaks standing for P_2S_5 , Li_3N , and Al_2S_3 were not observed. Raman was further used to characterize the samples, and the results are depicted in Figure 37b. A peak at 421 cm^{-1} was observed for all samples, which represents PS_4^{3-} . To get glass-ceramic solid electrolyte, these samples were further heated at 300°C for 1 hour. As shown in the XRD pattern for $75\text{Li}_2\text{S}-25\text{P}_2\text{S}_5-5\text{Li}_3\text{N}-4\text{Al}_2\text{S}_3$ in Figure 38a, the thio-LISICON III analog phase is precipitated in the solid electrolyte while peaks representing Li_2S impurity could still be observed. The ionic conductivity of $75\text{Li}_2\text{S}-25\text{P}_2\text{S}_5-5\text{Li}_3\text{N}-4\text{Al}_2\text{S}_3$ glass-ceramic solid electrolytes was measured at different temperatures, and was plotted in Figure 38b. However, due to the existence of

Li_2S impurities, the ionic conductivity at 25°C is merely 0.08 mS cm^{-1} and activation energy is 0.27 eV . To solve the issue of low ionic conductivity, the team plans to decrease Li_2S content in the designed solid electrolyte system to eliminate Li_2S impurities and form $\text{Li}_7\text{P}_3\text{S}_{11}$ highly conductive phase in future study.

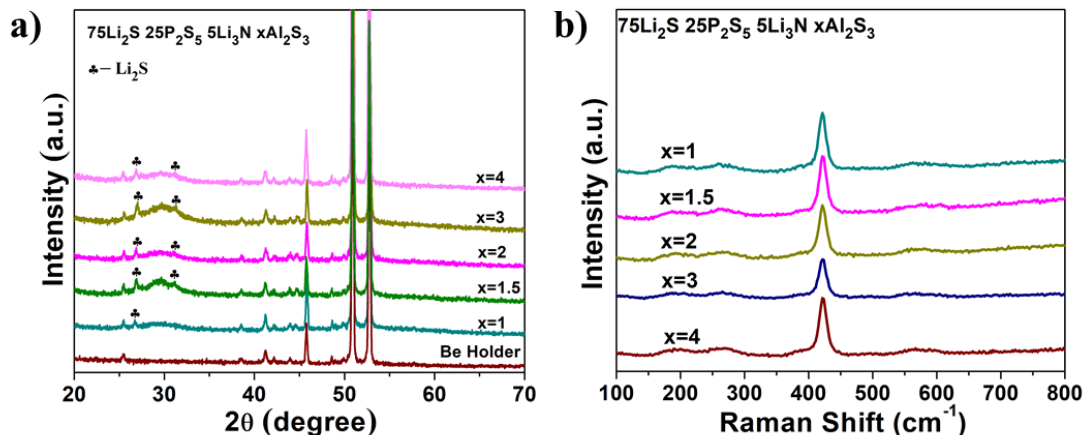


Figure 37. (a) X-ray diffraction and (b) Raman spectra of synthesized $75\text{Li}_2\text{S} \cdot 25\text{P}_2\text{S}_5 \cdot 5\text{Li}_3\text{N} \cdot x\text{Al}_2\text{S}_3$ ($x = 0, 1, 2, 3$ and 4) glass solid electrolytes.

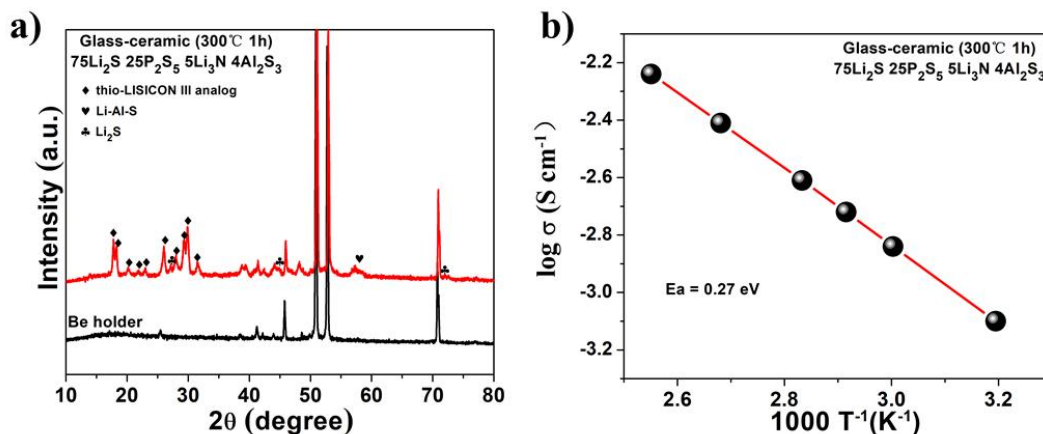


Figure 38. (a) X-ray diffraction spectra and (b) Arrhenius plot of $75\text{Li}_2\text{S} \cdot 25\text{P}_2\text{S}_5 \cdot 5\text{Li}_3\text{N} \cdot 4\text{Al}_2\text{S}_3$ glass-ceramic solid electrolytes.

In addition to synthesizing new solid electrolytes, the team also tried to increase sulfur content in the cathode composite to 50 wt%. The cathode composite is made of sulfur, solid electrolyte ($75\text{Li}_2\text{S} \cdot 25\text{P}_2\text{S}_5$ glass) and conductive carbon (Ketjenblack). The weight ratio of sulfur is 50 wt%, and the weight ratio of solid electrolyte is 20 wt%. The cathode composite was prepared by two-step ball milling process as described in last quarter's report. The cycling performance at 0.1 C discharge/charge rate of the as-fabricated sulfur cathode was tested using $75\text{Li}_2\text{S} \cdot 25\text{P}_2\text{S}_5$ glass (LPS) as solid electrolyte membrane and Li-In alloy as anode at 60°C . The results and corresponding second-cycle voltage profile are shown in Figure 39a-b. At 0.1 C , the sulfur cathode could only deliver a fairly low specific capacity of $\sim 550 \text{ mAh g}^{-1}$. To improve cathode performance, the team investigated the effect of using bis(phenylacetyl) disulfide (BPDS) as cathode additives. Following a similar preparation procedure, they fabricated sulfur composite cathode in which the weight ratio of sulfur, conductive carbon, BPDS, and solid electrolyte is 50:20:1:30. The cycling performance at 0.1 C charge/discharge rate of the obtained cathode is illustrated in Figure 39c. The voltage profile at the second cycle is shown in Figure 39d. Compared with the sulfur cathode without additive addition, the discharge capacity was significantly improved to above 1000 mAh g^{-1} . The utilization of sulfur was greatly improved. To be noted, the specific capacity was

calculated based on the weight of sulfur. Such a result fulfilled the proposed milestone of demonstrating sulfur cathode with high discharge capacity of $> 1000 \text{ mAh g}^{-1}$ using new solid additives. Next quarter, the team plans to further investigate the impact of new additives and optimize sulfur composite cathode preparation.

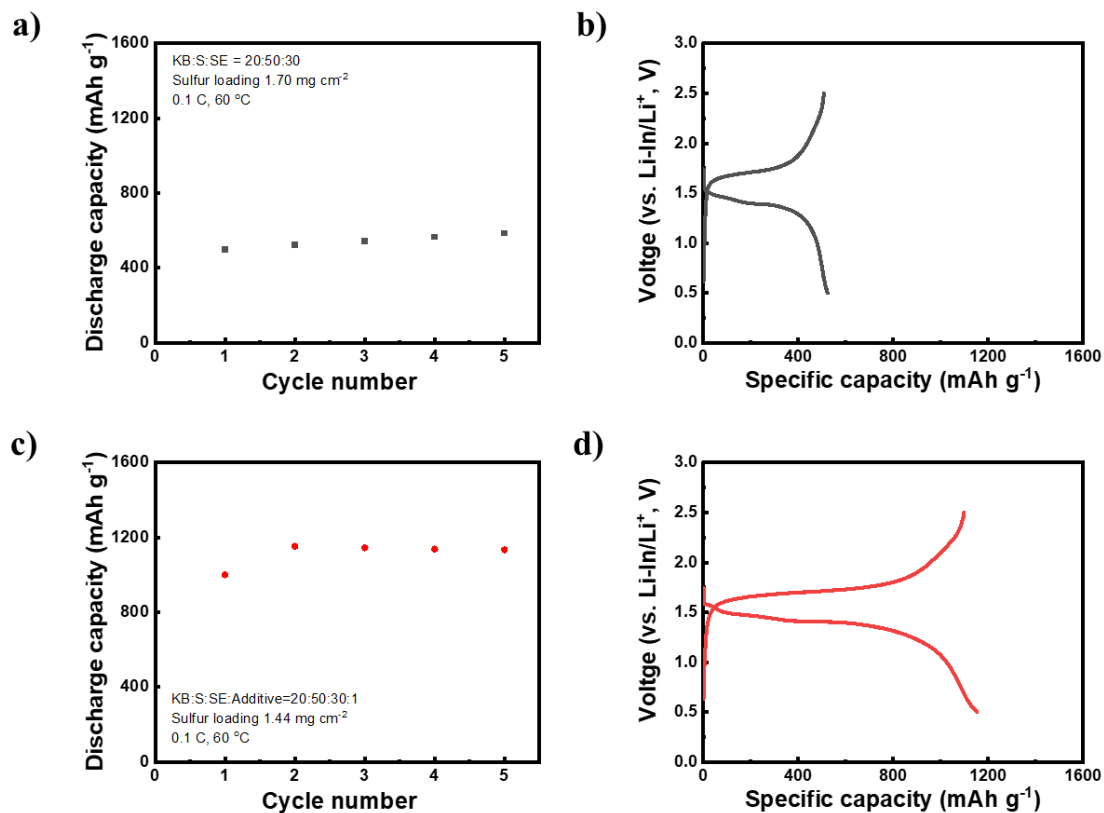


Figure 39. (a) Rate performance and (b) corresponding second-cycle charge/discharge voltage profile of sulfur cathode *without* additives. (c) Rate performance and (d) corresponding second-cycle charge/discharge voltage profile of sulfur cathode *with* additives.

Patents/Publications/Presentations

The project has no patents, publications, or presentations to report this quarter.

TASK 2 – DIAGNOSTICS

Summary and Highlights

To meet the goals of the VTO programs on next-generation EVs, low-cost and abuse-tolerant batteries with higher energy density, higher power density, better safety, and longer lifetimes are needed. In pursuit of these goals, high cell operating voltages and demanding cycling conditions are used, which leads to unprecedented chemical and mechanical instabilities in cell components. Successful implementation of promising electrode materials (such as silicon anode and high-voltage cathodes) and new cell chemistry (such as high-energy Li-metal cells combined with SSEs) requires better understanding of fundamental processes, especially those at the interface/interphase of both anode and cathode. Identifying and understanding structure-property-electrochemical performance relationships in materials and various failure modes in cell chemistry are therefore more pressing than ever, not only in guiding battery development activities but also the scale-up efforts needed for commercialization.

Task 2 takes on these challenges by combining model systems, *ex situ*, *in situ*, and *operando* approaches, with an array of state-of-the-art analytical and computational tools. Numerous subtasks are tackling the chemical processes and reactions at the electrode/electrolyte interfaces in Li-metal batteries. Researchers at LBNL use surface- and bulk-sensitive techniques, including FTIR, attenuated total reflectance (ATR)-FTIR, near-field infrared (IR) and Raman spectroscopy/microscopy, and scanning probe microscopy (SPM) to characterize changes in materials and the physio-chemical phenomena occurring at the interface of Li-metal electrode. GM is developing *in situ* diagnostic techniques, including atomic force microscopy (AFM), nano-indentor, dilatometer, and stress-sensor, to be combined with atomic/continuum modeling schemes to investigate the coupled mechanical/chemical degradation of the SEI layer as well as the microstructural evolution at the interface/interphase of Li-metal anode. ANL aims to develop high-conductivity ceramic electrolytes through cation doping and identify mechanistic barriers that limit the chemical/mechanical/electrochemical durability of the solid/solid interfaces. University of Houston (UH) is developing multidimensional diagnostic tools, including FIB-SEM, TOF-SIMS, and in-SEM nanoindentation, to probe structural, chemical, and mechanical evolution at the interfaces of SSLBs. At LBNL, model systems of electrode, SSE, and their interfaces with well-defined physical attributes are being developed and used for advanced diagnostic and mechanistic studies at both bulk and single-particle levels. These controlled studies remove the ambiguity in correlating a material's physical properties and reaction mechanisms to its performance and stability, which is critical for further optimization. Subtasks at BNL and PNNL focus on the understanding of fading mechanisms in electrode materials, with the help of synchrotron-based X-ray techniques (diffraction and hard/soft X-ray absorption) at BNL and HRTEM / scanning transmission electron microscopy (STEM) and related spectroscopy techniques at PNNL. The final subtask at Stanford/SLAC develops and utilizes an integrated X-ray characterization toolkit to investigate and generate insights on SSBs, by tracking the evolution of nanoscale chemistry as well as structure, microstructure, and transport properties. The diagnostics team not only produces a wealth of knowledge that is key to development of next-generation batteries, it also advances analytical techniques and instrumentation that have a far-reaching effect on material and device development in various fields.

Highlights. The highlights for this quarter are as follows:

- The BNL team (Yang and Bak) used advanced hard XRF imaging techniques to study the structural stability of concentration-gradient Ni-rich NMC cathode particles, which revealed well-maintained compositional gradient even after 100 cycles. Their work represents the first report on use of a noninvasive technique to observe the concentration gradient structure, without the need of cross-sectioning samples.
- The PNNL group (Wang) reports that poor Li-conducting carbonate species in the initial SEI adjacent to lithium metal plays a critical role in formation of lithium whiskers, demonstrating that dendrite-free lithium deposition requires facile transport of lithium in the initial SEI.

Task 2.1 – Characterization and Modeling of Li-Metal Batteries: Model-System Synthesis and Advanced Characterization (Guoying Chen, Lawrence Berkeley National Laboratory)

Project Objective. This project will use a rational, non-empirical approach to design and develop SSE materials and interfaces for next-generation Li-metal batteries. Combining a suite of advanced diagnostic techniques with carefully prepared model-system samples, the project will perform systematic studies to achieve the following goals: (1) obtain understanding on the role of SSE grain and GBs on ion conduction and dendrite formation, (2) obtain fundamental knowledge on rate- and stability-limiting properties and processes in SSEs when used in Li-metal batteries, (3) investigate the reactivities between SSE and electrodes and gain insights on the dynamic evolution of the interfaces, and (4) design and synthesize improved SSE materials and interfaces for safer and more stable high-energy Li-metal batteries.

Impact. The project will focus on fundamental understanding of SSE and relevant interfaces to enable its use in Li-metal batteries. Knowledge gathered from model-system based studies will guide the design and engineering of advanced materials and interfaces. The use of the non-empirical, rational-design approach will develop high-energy battery systems with improved commercial viability.

Approach. The project will combine model-system synthesis and advanced diagnostic studies to investigate ion conduction and interfacial chemistry of SSE in Li-metal batteries. Single crystalline, polycrystalline, and amorphous model SSE samples with various grain and GB properties will be synthesized. Model interfaces between the SSE and electrodes with controlled properties will also be developed. Both bulk-level and single-grain level characterization will be performed. Global properties and performance of the samples will be established from the bulk analyses, while the single-grain-based studies will utilize time- and spatially-resolved analytical techniques to probe the intrinsic redox transformation processes and failure mechanisms under battery operating conditions.

Out-Year Goals. In the out-years, the project will deliver fundamental knowledge on the role of SSE microstructure in Li⁺ conduction and lithium dendrite formation/propagation. Insights on performance-limiting physical properties and phase transition mechanisms as well as dynamic evolution of SSE/electrode interfaces will be obtained. Mitigating approaches, such as use of surface coating or “buffer layer” in stabilizing SSE/electrode interfaces, will be evaluated. Further, advanced SSE materials and interfaces for improved high-energy Li-metal batteries will be designed and synthesized.

Collaborations. This project collaborates with the following PIs: G. Ceder, K. Persson, M. Doeff, B. McCloskey, R. Kostecki, and R. Prasher (LBNL); W. Yang (Advanced Light Source, ALS); D. Nordlund and Y. Liu (Stanford Synchrotron Radiation Lightsource, SSRL); C. Wang (PNNL); and J. Nanda (Oak Ridge National Laboratory, ORNL).

Milestones

1. Develop model systems suitable for studying the impact of SSE grain and GBs in Li-metal based batteries. (Q1, FY 2020; Completed)
2. Synthesize model SSE samples with various grain and GB characteristics. (Q2, FY 2020; Completed)
3. Advanced diagnostic studies of SSE model samples at both particle-level and bulk-sample level. (Q3, FY 2020; On schedule)
4. Obtain understanding on SSE grain and GB chemistry, properties, and their effect on ion conduction and dendrite formation. (Q4, FY 2020; On schedule)

Progress Report

In the previous study, model samples of Al-substituted LLZO ($\text{Li}_{6.75}\text{Al}_{0.25}\text{La}_3\text{Zr}_2\text{O}_{12}$, Al-LLZO) primary particles with various sizes and morphologies were synthesized. This quarter, the team evaluated processing approaches to vary grain and GB characteristics in densified SSEs. Al-LLZO primary particles with an average grain size of 3-4 μm were further ball milled to reduce their size, with nearly 10x size reduction achieved after milling at 300 rpm for 6 hours. Samples before and after ball milling (Al-LLZO_a and Al-LLZO_b, Figure 40a-b) were then sintered in air at 1100°C for 12 hours. Figure 40c-d shows the densified pellets prepared from the Al-LLZO_a and Al-LLZO_b particles, respectively. While large grains with defined GBs were clearly observed in the former, denser pellets without obvious presence of GBs were obtained in the latter. Reduction in particle size promotes grain growth during sintering and enables more effective densification of the garnet electrolyte. The process of particle size/morphology control followed by sintering can be adapted to tune grain and GB properties of SSEs other than the garnets.

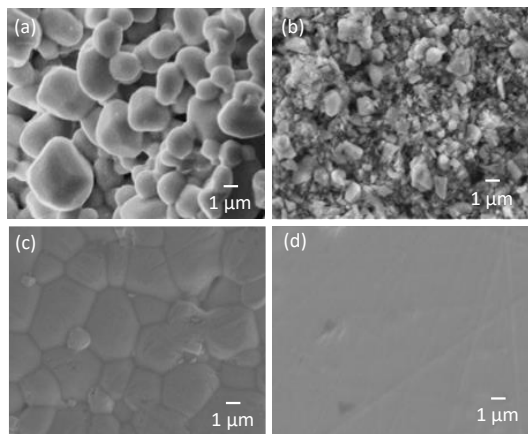


Figure 40. Scanning electron microscopy images of Al-LLZO particles before and after ball milling (a-b) and sintered Al-LLZO pellets (c-d) prepared from (a) and (b), respectively.

Changes in crystal structure after sintering were investigated.

While phase pure cubic structure maintained in the as-prepared pellet from Al-LLZO_a, a small amount of $\text{La}_2\text{Zr}_2\text{O}_7$ impurity was detected on the sintered Al-LLZO_b sample. This is likely a result of increased surface area in the latter, which results in more lithium loss at high temperatures. Gentle surface polishing with 4000 grit SiC paper was able to effectively remove the impurity. Figure 41a

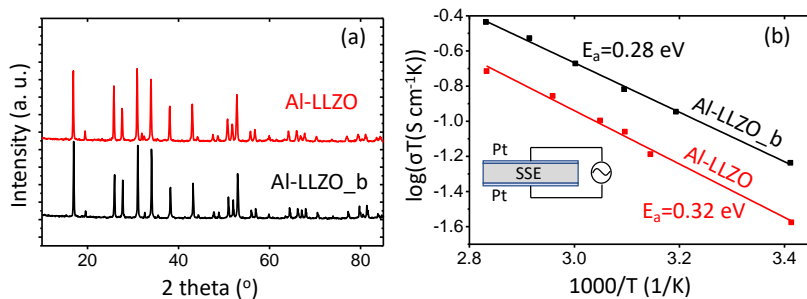


Figure 41. (a) X-ray diffraction patterns of polished pellets sintered from Al-LLZO_a and Al-LLZO_b samples. (b) Arrhenius plots of total ionic conductivity measured on sintered pellets.

were collected in the temperature window of room temperature to 80°C, at an increment of 10°C per measurement. Total ionic conductivity, including contributions from grains and GBs, was determined based on the real component of impedance at the frequency when AC ion conduction migrates through the pellet. Figure 41b shows the resulting Arrhenius plots from the EIS measurements. For the pellet made from large grain Al-LLZO_a, the activation energy was 0.32 eV, corresponding to a total ionic conductivity of $1.0 \times 10^{-4} \text{ S cm}^{-1}$ at room temperature. On the other hand, the denser pellet of Al-LLZO_b was found to have a lower activation energy of 0.28 eV, corresponding to a total ionic conductivity of $2.1 \times 10^{-4} \text{ S cm}^{-1}$, which is two times higher than the former. The results suggest that the presence of defined GBs negatively impacts SSE conductivity. Although the origin is unclear, as it may relate to the resistance between the grains or the changes in chemistry/conductivities due to impurities at the GBs, it is expected that performing controlled studies by varying grain and GB characteristics will provide further insights on the role of various physical properties in ion conduction as well as lithium dendrite propagation.

Patents/Publications/Presentations

Publications

- Chen, D., J. Wu, J. K. Papp, B. D. McCloskey, W. Yang, and G. Chen. “Role of Redox-Inactive Transition-Metals in the Behavior of Cation-Disordered Rocksalt Cathodes.” *Small*. Accepted (2020).
- Zou, L., W. Zhao, H. Jia, J. Zheng, L. Li, D. P. Abraham, G. Chen, J. R. Croy, J-G. Zhang, and C. Wang. “The Role of Secondary Particle Structures in Surface Phase Transitions of Ni-Rich Cathodes.” *Chemistry of Materials* (2020). doi: 10.1021/acs.chemmater.9b04938.
- Yi, E., H. Shen, S. Heywood, J. Alvarado, D. Y. Parkinson, G. Chen, S. W. Sofie, and M. M. Doeff. “All-Solid-State Batteries Using Rationally Designed Garnet Electrolyte Frameworks.” *ACS Applied Energy Materials* 3, no. 1 (2020): 170. doi: 10.1021/acsaem.9b02101.

Task 2.2 – Interfacial Processes – Diagnostics (Robert Kostecki, Lawrence Berkeley National Laboratory)

Project Objective. The objective of the proposed research is to establish specific design rules toward the next generation of low impedance Li-metal rechargeable batteries that are capable of performing 1000 deep discharge cycles at CE > 99.9% and suppress lithium dendrites formation at high current densities (> 2 mA/cm²). This project aims at the following: (1) establishing general rules between Li⁺ transport properties in novel liquid/solid electrolytes, and (2) determining the mechanism of the SEI layer (re)formation. The other goal is development and application of far- and near-field optical probes and synchrotron-based advanced X-ray techniques to obtain insight into the mechanism of Li⁺ transport and interfacial reactions in lithium/liquid model systems. Through an integrated synthesis, characterization, and electrochemistry effort, this project aims to develop a better understanding of Li/liquid electrolyte interface so that rational decisions can be made as to their further development into commercially viable Li-metal cells.

Project Impact. Chemical instability and high impedance at the interface of Li-metal electrodes limits electrochemical performance of high-energy-density batteries. A better understanding of the underlying principles that govern these phenomena is inextricably linked with successful implementation of high-energy-density materials in Li-metal-based cells for PHEVs and EVs. New state-of-the-art techniques to identify, characterize, and monitor changes in materials structure and composition that take place during battery operation and/or storage will be developed and made available to the Program participants. The proposed work constitutes an integral part of the concerted effort within the BMR Program, and it supports development of new electrode materials for high-energy, Li-metal-based rechargeable cells.

Approach. The pristine and cycled composite electrode and model thin-film electrodes will be probed using various surface- and bulk-sensitive techniques, including FTIR, ATR-FTIR, near-field IR and Raman spectroscopy/microscopy, and SPM to identify and characterize changes in materials structure and composition. Novel *in situ* / *ex situ* far- and near-field optical multi-functional probes in combination with standard electrochemical and analytical techniques are developed to unveil the structure and reactivity at interfaces and interphases that determine materials electrochemical performance and failure modes.

Out-Year Goals. In the out-years, the project aims to achieve the following: (1) understand factors that control performance and degradation processes, (2) unveil structure and reactivity at hidden or buried interfaces and interphases that determine electrochemical performance and failure modes, and (3) propose effective remedies to address inadequate Li-metal-based battery calendar/cycle lifetimes for PHEV and EV applications.

Collaborations. The diagnostic studies will be carried out in sync with other diagnosticians (G. Chen, B. McCloskey, R. Prasher, and L-W. Wang) and theory and computational scientists (G. Ceder and K. Persson).

Milestones

1. Develop novel experimental approach(es) suitable for studying Li/electrolyte interfaces. (Q1, FY 2020; Completed)
2. Manufacture model thin-film lithium model electrodes for *ex situ* and *in situ* fundamental studies of Li/electrolyte interfaces. (Q2, FY 2020; In progress)
3. Characterize chemistry of Li/electrolyte with *ex situ* near-field IR, X-ray absorption spectroscopy (XAS), and XPS. (Q3, FY 2020; In progress)
4. Gain preliminary insights into SEI composition and reaction pathways for baseline electrolytes. Propose first approximative reaction scheme. (Q4, FY 2020; In progress)

Progress Report

This quarter, the team further optimized the experimental setup to obtain high-quality IR signal from a model graphene-SSE interface at nano-scale spatial resolution. The measurements were performed with a unique combination of SPM and nano-FTIR. The single-layer graphene (SLG) on copper mesh was replaced with a freestanding SLG to perform as an optical window and simultaneously as the current collector for lithium deposition during electrochemical polarization. The counter electrode consists of a copper foil on a flat silicon wafer, which provides good electronic conductivity and stable mechanical support for the SSE layer. Two electrodes were separated by a plastic spacer, and the gap was filled with the solid electrolyte.

The near-field IR local probing of the electrode/SSE interface was accomplished by the SPM tip through the SLG window. This novel and unique experimental setup enables direct IR probing of the interface of electrode/electrolyte at nanometer resolution, which enables *in situ* characterization of the active species adjacent to the electrode.

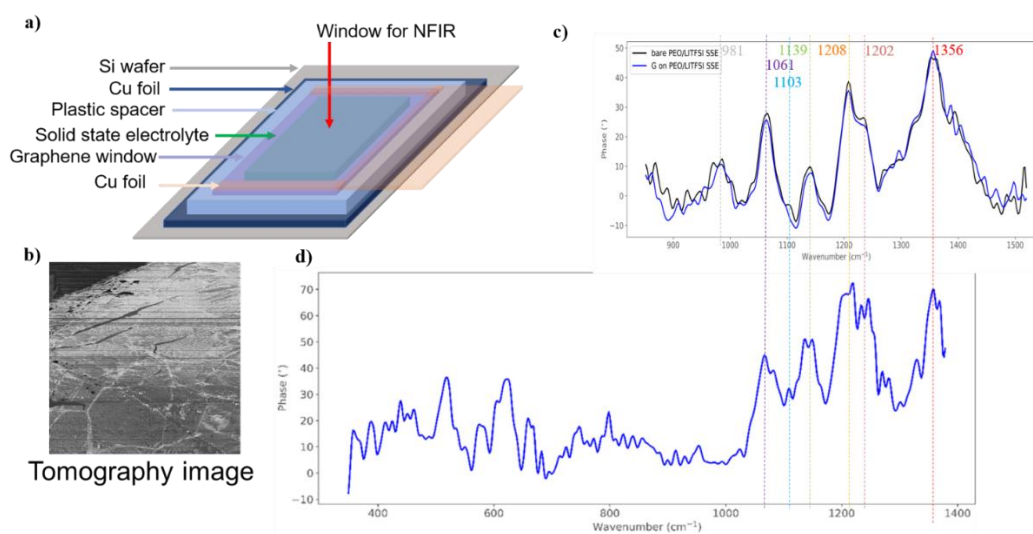


Figure 42. (a) Schematic illustration of fabrication of the modified cell with graphene window to study electrode/electrolyte interfaces. (b) Tomography image in a region where graphene window is in contact with the solid-state electrolyte (SSE: PEO + LiTFSI mixtures at EO/Li ratios of 10:1) in the cell. (c) Nano Fourier transform infrared (nano-FTIR) spectra collected with IR laser at locations of SSE and SSE with graphene window. (d) Nano-FTIR spectra collected with synchrotron IR light source at locations of SSE with graphene window.

Figure 42a shows the experimental cell set-up for *in situ* nano-FTIR measurements. The mixture of PEO and LiTFSI fills the space between two copper and SLG electrodes. The representative tomography image (Figure 42b) shows that the SSE is uniformly covered by the SLG sheet without any defects or folding. The SSE under SLG and SSE sample were characterized by nano-FTIR measurement. The team was able to observe IR bands characteristic for SSE through SLG, which fully match the spectrum of SSE recorded in direct contact with the nano-FTIR probe. The quality of spectra has been significantly improved when compared with previous results (through copper mesh). In addition, a similar spectrum could be observed from the data collected from synchrotron IR light source. The detected wave range is much wider, including the signal of lithium and its relevant compounds. These preliminary results constitute the proof of concept and foundation for future *in situ* studies of Li/SSE interfaces. This concludes efforts toward Milestone 2.

Patents/Publications/Presentations

The project has no patents, publications, or presentations to report this quarter.

Task 2.3 – Advanced *In Situ* Diagnostic Techniques for Battery Materials (Xiao-Qing Yang and Seong-Min Bak, Brookhaven National Laboratory)

Project Objective. The primary objective of this project is to develop new advanced *in situ* material characterization techniques and to apply these techniques to support development of new cathode and anode materials with high energy and power density, low cost, good abuse tolerance, and long calendar and cycle life for beyond Li-ion battery systems to power PHEVs and battery electric vehicles (BEVs). The diagnostic studies will focus on issues relating to capacity retention, thermal stability, cycle life, and rate capability of beyond Li-ion battery systems.

Project Impact. The VTO Multi-Year Program Plan describes the goals for battery: “Specifically, lower-cost, abuse-tolerant batteries with higher energy density, higher power, better low-temperature operation, and longer lifetimes are needed for development of the next-generation of HEVs, PHEVs, and EVs.” The knowledge gained from diagnostic studies through this project will help U. S. industries develop new materials and processes for next-generation Li-ion batteries in the effort to reach these VTO goals.

Approach. This project will use the combined synchrotron-based *in situ* X-ray techniques (XRD; and hard and soft XAS) with other imaging and spectroscopic tools such as HRTEM and MS to study the mechanisms governing performance of electrode materials.

Out-Year Goals. In the out years, the project will complete development of diagnostic techniques using X-ray pair distribution function (*x*-PDF), XRD, and XAS combined with neutron diffraction and neutron PDF (*n*-PDF), as well as STEM imaging and transmission X-ray microscopy (TXM) for cathode materials studies. It will then apply these techniques to study the structural changes of various new cathode and anode materials.

Collaborations. The BNL team will work closely with material synthesis groups at ANL (Drs. Shin and Amine) for the high-energy composite, at PNNL for the S-based cathode and Li-metal anode materials, and with ORNL on neutron scatterings. This project will also collaborate with industrial partners at GM and Johnson Controls, as well as with international collaborators.

Milestones

1. Complete the first-stage development of diagnostic techniques to study and improve performance of high-energy-density Li-ion batteries and Li/S batteries. (Q1, FY 2020; Completed)
2. Complete hard XRF imaging on the concentration gradient Ni-rich NCM cathode particles in a noninvasive manner with 3D reconstructed images through tomography scans to study the 3D nickel, cobalt, and manganese elemental distribution from surface to the bulk. (Q2, FY 2020; Completed)
3. Complete hard X-ray absorption spectroscopy (hXAS) and soft XAS (sXAS) on the concentration gradient Ni-rich NCM cathode particles to study the valence state changes of nickel, cobalt, and manganese at the surface and bulk. (Q3, FY 2020; In progress)
4. Complete spatially resolved XAS at sulfur K-edge and imaging of sulfur-based chemical species using XRF on the Li-metal anode in a cycled high-energy Li/S pouch cell. (Q4, FY 2020; In progress)

Progress Report

This quarter, the second milestone was completed, and progress on other milestones was made. BNL has focused on development of new diagnostic techniques to study and provide valuable information for improving performance of high-energy-density LIBs and Li/S batteries. The BNL team has applied advanced hard XRF imaging techniques with a high spatial resolution (down to 30 nm) and high probing sensitivity (under ppm level). This advanced imaging technique was used to study the structural stability of concentration-gradient Ni-rich NMC (CG-NMC) cathode particle in a noninvasive manner with 3D reconstructed images through tomography scans to study the 3D nickel, cobalt, and manganese elemental distribution.

The *ex situ* 2D XRF element mapping results are shown in Figure 43a for pristine and cycled CG-NMC-622. The line-scan from the 2D image revealed that the pristine CG-NMC-622 has NMC-701515 composition in the core and NMC-442 at the shell with about 800 nm of concentration gradient layer from the surface. This compositional gradient structure was well maintained even after 100 cycles with 2.8-4.4 V (versus Li/Li⁺) voltage range and high voltage cycling (2.8-4.8 V versus Li/Li⁺). This result is the first observation of the concentration gradient structure in a noninvasive manner without cross-sectioning the sample using FIB. The clear feature of the Mn-rich shell structure shown in Figure 43a was not observed from the project's previous studies using TXM. This demonstrated the power of high spatial resolution and high elemental selectivity of this nano-XRF imaging technique. Furthermore, the *ex situ* 3D reconstructed XRF image (Figure 43b) revealed that the secondary particle of CG-NMC-622 did not show a micro-crack generation at the particle core, which is typically shown in similar composition Ni-rich NMC (Ni > 70%) system. The quantitative composition analysis from the 3D XRF image shows clear evidence that the unique compositional gradient of this material is well kept even after 100 cycles. The results revealed that the compositional gradient structure is stable over the long- and high-voltage cycling, and that the Mn-rich surface of CG structure enhanced the structural stability at the secondary particle level. To further study the surface chemistry of the CG-NMC system, a combination of soft and hard XAS study will be conducted next quarter.

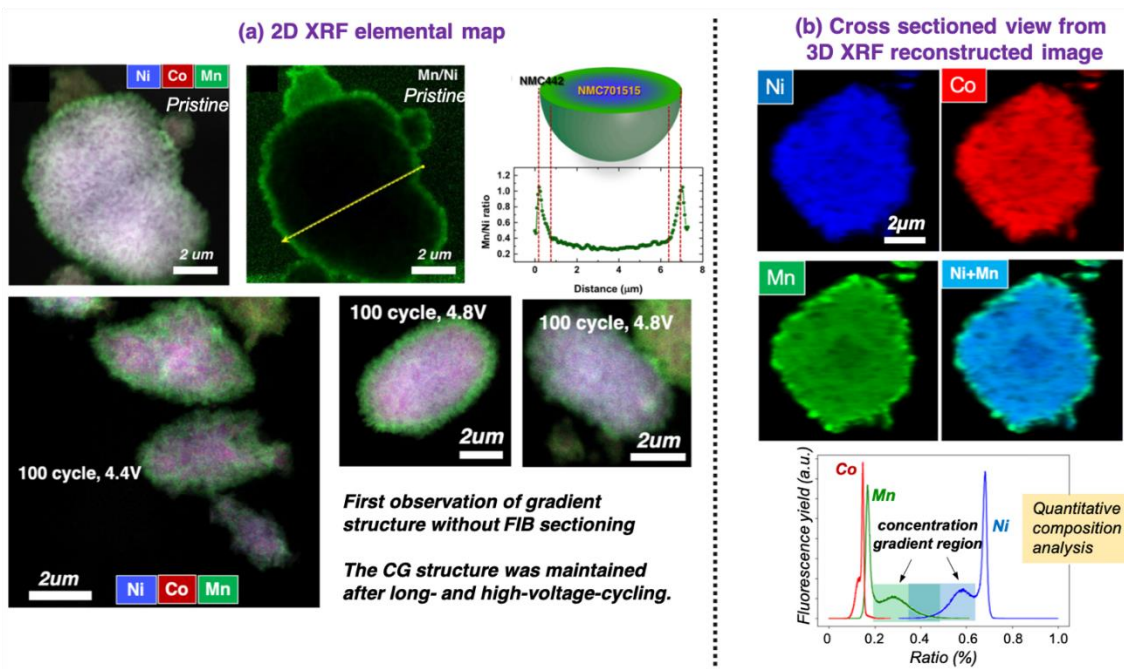


Figure 43. (a) 2D X-ray fluorescence (XRF) elemental map of pristine and cycled (100 cycles, 2.8-4.4 and 4.8 V versus Li/Li⁺) concentration-gradient NMC-622 (CG-NMC-622) cathode particles. (b) Cross-sectioned view from 3D XRF reconstructed image of 100 cycled CG-NMC-622 (2.8-4.4 V versus Li/Li⁺) and its quantitative composition analysis.

Patents/Publications/Presentations

Publication

- Jiang, Q., P. Xiong, J. Liu, Z. Xie, Q. Wang, X-Q. Yang, E. Hu, Y. Cao, J. Sun, Y. Xu, L. Chen. “A Redox-Active 2D Metal-Organic Framework for Efficient Lithium Storage with Extraordinary High Capacity.” *Angewandte Chemie* 132 (2020): 5311–5315. Publication date (Web): March 23, 2020.

Presentation

- The Minerals, Metals, and Materials Society (TMS) Annual Meeting, San Diego, California (February 24, 2020): “Multi-Modal and Multi-Length-Scale Characterization of Composition Graded Ni-Rich Layered Oxide Cathode Materials”; S-M. Bak, Y. Shin, and X-Q. Yang. Invited.

Task 2.4 – *In Situ* Diagnostics of Coupled Electrochemical-Mechanical Properties of Solid Electrolyte Interphases on Lithium-Metal Rechargeable Batteries
(Xingcheng Xiao, General Motors; Brian W. Sheldon, Brown University; Yue Qi, Michigan State University; and Y. T. Cheng, University of Kentucky)

Project Objective. The project objective is to develop a comprehensive set of *in situ* diagnostic techniques combined with atomic/continuum modeling schemes to investigate and understand the coupled mechanical/chemical degradation of the SEI layer / lithium system during lithium cycling. The goal of this understanding is to develop a new coating design strategy to achieve dendrite-free, high-cycle efficiency and extend the cycle life of high-energy-density batteries with lithium as the anode for EV application.

Project Impact. The fundamental understanding of the coupled mechanical/chemical degradation of the SEI layer during lithium cycling will enable the project to identify the desirable mechanical properties on SEI/lithium as a system and also the specific transport properties that enable the homogenous lithium stripping/plating while avoiding the mossy structure. Furthermore, it will allow the project to develop a highly impactful strategy to protect lithium metal and achieve dendrite-free high cycle efficiency, which can dramatically increase the energy density of lithium batteries for EV applications.

Approach. Different *in situ* techniques, including AFM, nano-indentor, dilatometer, and stress-sensor, will be developed to investigate the mechanical compatibility between SEI and soft lithium and the relationship between surface morphology and CCD that results in an inhomogeneous lithium plating/stripping process. Multiple strategies will be developed to tailor the mechanical and transport properties of SEI and to properly engineer the protective coating / lithium interface.

Out-Year Goals. The out-year goals involve using *in situ* electrochemical tools to reveal failure mechanisms of SEI/lithium as a whole electrode system, including correlating mechanical failure mechanisms of SEI/lithium, morphology evolution, cycle efficiency, and transport properties of SEI. Then, the project will develop continuum framework to establish the failure modes of SEI layer on lithium metal and provide the governing mechanical/material properties of SEI responsible for the critical failure mode based on experimental results and atomic-scale simulation.

Collaborations. Prof. H. Gao (Brown University) and Dr. Q. Zhang (GM) will be the key researchers involved in continuum simulation and postmortem analysis. Dr. C. Wang (PNNL), Dr. W. Yang (LBNL), and Dr. J. Xiao (PNNL) will be collaborators on advanced *in situ* analysis and electrolyte additives.

Milestones

1. Determine coating design window required to achieve mechanically stable coating on lithium metal. (Q1, FY 2019; Completed)
2. Determine impact of stress on morphological evolution of coated Li-metal surface, and identify failure modes of protective coatings on lithium. (Q2, FY 2019; Completed)
3. Vary coating modulus and investigate its impact on interfacial strength and cycle efficiency, and develop coating with desirable mechanical and transport properties. (Q3, FY 2019; Completed)
4. Establish a design strategy of protective coatings as artificial SEI on Li-metal electrode to achieve high cycle efficiency (> 99.8%). (Q4, FY 2019; Completed)
5. Last quarterly report for no-cost extension period. No milestone.

Progress Report

Investigated the Mechanical Behavior of Plated Lithium Electrode. From flat-punch indentation measurements, the Young's modulus (E) of bulk lithium is determined to be ~ 7.8 GPa, which is consistent with reported values by macroscopic tensile and nanoindentation measurements. The Young's modulus, E , of the mossy lithium slightly increases from 1.6 to 2.6 GPa with increasing the maximum indentation load. The measured much smaller E of the mossy lithium than bulk lithium can be attributed to the highly compliant porous structure of the mossy lithium, even though the SEI layer has a much higher modulus than lithium. Figure 44a shows that the creep depth (h_{creep}) of bulk lithium during the holding period increases remarkably with the punch stress ($\sigma_{ind} = F_{max}/A$, where A is the projected area of the flat punch). Surprisingly, h_{creep} of the mossy lithium is much smaller than that of bulk lithium and increases slightly with increasing σ_{ind} .

The impression velocity, v_c , during the holding period of flat punch indentation is shown in Figure 44b. The steady-state creep velocity, v_{ind} , is determined as the expectation value of v_c during the steady-state creep period using Gaussian distribution (Figure 44c-d). As shown in Figure 44e, v_{ind} of the mossy lithium increases slightly as σ_{ind} increases from 5.04 MPa and 14.41 MPa. The average v_{ind} (in the range between 0.25 ± 0.03 and 0.74 ± 0.23 nm/s) of the mossy lithium is larger than the thermal drift rate limit of 0.05 nm/s. Under the same punching stress range between 4.93 and 5.76 MPa, v_{ind} of the mossy lithium is only one-thirtieth of that of bulk lithium. Thus, mossy lithium is more creep resistant than bulk lithium, which can have significant effects on the design and operation of Li-metal electrodes, including the effects of the liquid electrolyte and current density, as shown in Figure 45.

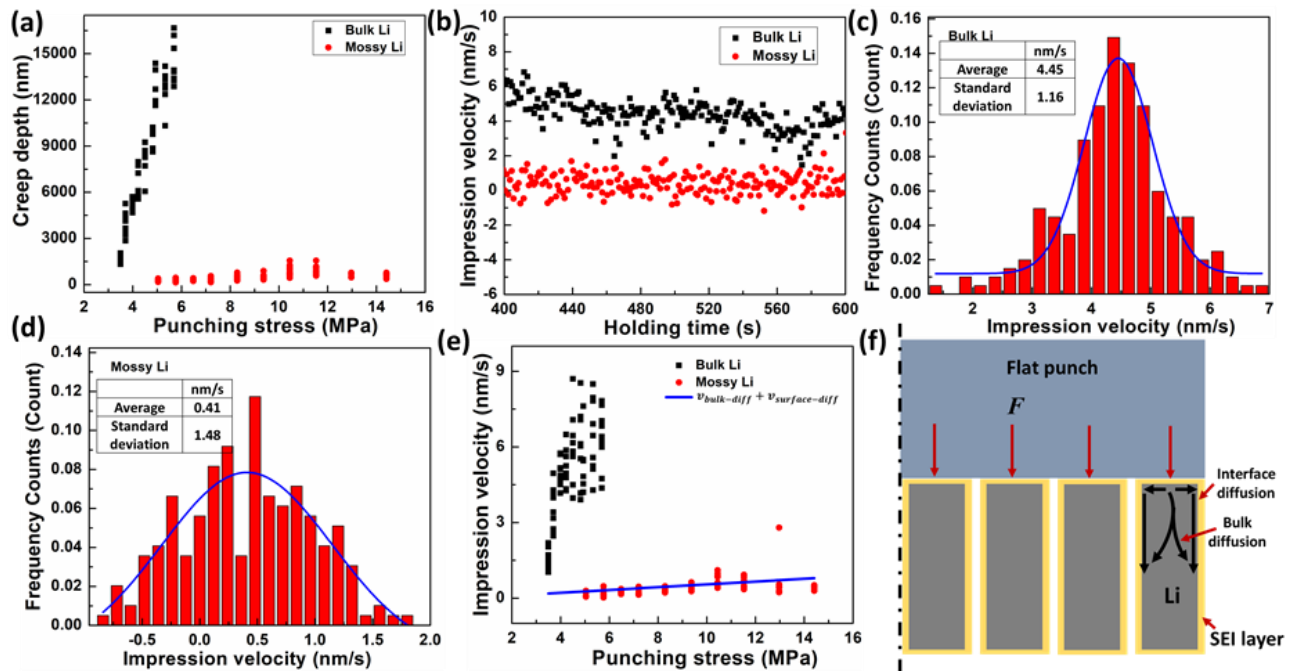


Figure 44. (a) The creep depth-punching stress profiles of the mossy and bulk lithium. (b) The impression velocity-holding time profiles of the mossy and bulk lithium during the holding period between 400 and 600 s. (c) and (d) are the Gaussian distributions of the impression velocity of bulk and the mossy lithium during the holding period between 400 and 600 s, respectively. The steady-state impression velocity is determined as the expectation value (the average value) of Gaussian distribution. (e) The impression velocity-punching stress profile of the mossy and bulk lithium. The impression creep velocity of bulk lithium caused by diffusion is also plotted in (e). (f) Schematic of the diffusion paths in lithium dendrites.

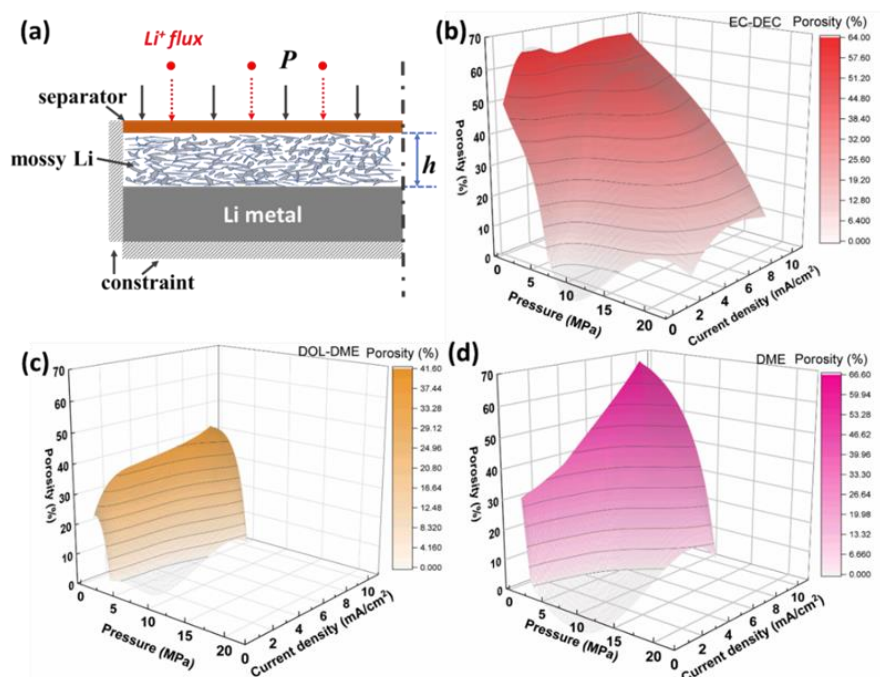


Figure 45. (a) The creep depth (h_{creep}) of bulk lithium during the holding period increases remarkably with the punch stress ($\sigma_{\text{ind}}=F_{\text{max}}/A$, where A is the projected area of the flat punch). Surprisingly, h_{creep} of the mossy lithium is much smaller than that of bulk lithium and increases slightly with increasing σ_{ind} .

A Stripping Mechanism was Incorporated in the Kinetic Monte Carlo (KMC) Simulation. The lithium atoms in the SEI layers are removed in the initial KMC structure to represent the lithium sink for lithium delithiation, as shown in Figure 46c. k_s is the probability (per unit time) with which a lithium atom leaves the interface. As shown in Figure 46d, KMC results show that at the typical current density of 10^{-3} A/cm², the interface of Li/Li₂O has no vacancy. When the current density is at 10^2 A/cm², though some vacancies generated due to stripping submerged into the bulk, vacancies at the interface can be seen (3 vacancies at L1 out of 7 delithiated lithium). When the current density is at 10^6 A/cm², the team can clearly see vacancies occurring at the interfaces (101 vacancies at L1 out of 327 delithiated lithium). On the other hand, even at the typical range of the current density (10^{-3} - 10^6 A/cm²), the presence of vacancies can be seen at the interface, 41 vacancies at L1 out of 42 delithiated lithium for the former current density. In sum, the tendency of lithium diffusion toward the interface determines vacancy-free surface and is one atomistic mechanism behind lithiophilic surface.

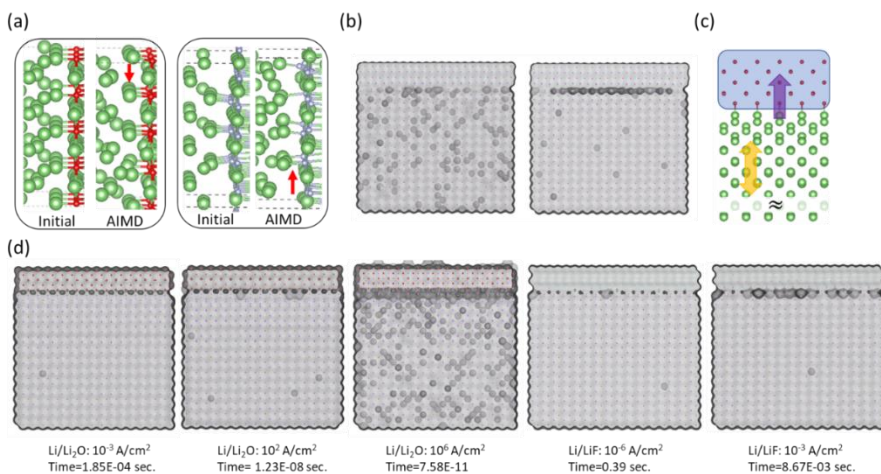


Figure 46. (a, left) Number of Li-O bonds at Li/Li₂O interface. (a, right) Number of Li-F bonds at Li/LiF interface before and after *ab initio* molecular dynamics simulation. (b) Kinetic Monte Carlo (KMC) results of (left) case I, reducing $\Delta E_{\text{TL},2 \rightarrow 1}$ and of (right) case II, increasing $\Delta E_{\text{TB},2 \leftarrow 1}$. (c) Illustration of KMC simulation incorporating lithium delithiation (purple) and lithium atom diffusion in the lithium anode (yellow). (d) KMC results with different current density upon Li/Li₂O (10^{-3} , 10^2 , and 10^6 A/cm²) and Li/LiF (10^{-3} and 10^{-6} A/cm²).

Patents/Publications/Presentations

Publications

- Guo, K., R. Kumar, X. Xiao, B. W. Sheldon, and H. Gao. “Failure Progression in the Solid Electrolyte Interphase (SEI) on Silicon Electrodes.” *Nano Energy* 68 (2020): 104257.
- Cho, J. H., X. Xiao, K. Guo, Y. Liu, H. Gao, and B. W. Sheldon. “Stress Evolution in Lithium Metal Electrodes.” *Energy Storage Materials* 24 (2020): 281–290.

Task 2.5 – Probing Interfacial Processes Controlled Electrode Stability in Rechargeable Batteries (Chongmin Wang, Pacific Northwest National Laboratory)

Project Objective. The main objective of the proposed research is to explore interfacial phenomena in rechargeable Li-ion batteries of both solid state and liquid electrolyte configuration, to identify the critical parameters that control the stability of interface and electrodes as well as solid electrolyte. The outcome will be establishing correlations between structural-chemical evolution of active components of batteries and their properties. These correlations will provide insight and guidance to battery materials development groups for developing high-performance battery materials.

Project Impact. The proposed characterization work focuses on atomic-level structural and chemical analysis and direct correlation with battery fading properties. The work can be directly used to guide design of electrode materials with tailored microstructure and chemistry for enhanced properties of increasing the energy density of Li-ion batteries and to accelerate market acceptance of EVs, especially for PHEVs as required by the EV Everywhere Grand Challenge.

Approach. The project will use integrated advanced microscopic and spectroscopic techniques, including *in situ* S/TEM and *ex situ* S/TEM, environmental S/TEM, cryo-electron microscopy, and *in situ* liquid secondary-ion mass spectrometry (SIMS) to directly probe the structural and chemical information during lithium deposition and stripping. Cryo-S/TEM with analytical tools, such as EDS and EELS, will be used to gain chemical and electronic structural information at the interface between lithium metal and electrolyte of both solid state and liquid, which will allow direct correlation between the morphology and chemistry. STEM – high-angle annular dark-field (HAADF) atomic-level imaging and EDS/EELS will be used to probe the interface and bulk lattice stability. The work will be in close collaboration with the battery development group within the BMR and U. S.–Germany Collaboration on Energy Storage.

Out-Year-Goals. This project has the following out-year goals:

- Atomic-level multi-scale *ex situ* / *in situ* and *operando* TEM and cryo-TEM investigation of failure mechanisms of energy-storage materials and devices; develop fundamental understanding of electrochemical energy-storage processes and kinetics of electrodes.
- Develop new *in situ* TEM capability for probing challenging questions related to energy storage technology.

Collaborations. This project collaborates with G. Chen (LBNL); J. Nanda (ORNL); K. Amine (ANL); D. Wang (PSU); A. Manthiram (UT Austin); W. Tong (LBNL); Y. Cui (Stanford University); J. Zhang (PNNL); J. Liu (PNNL); W. Xu (PNNL); X. Jie (PNNL); D. Lu (PNNL); X. Xiao (GM); S. Meng (UCSD); and M. S. Whittingham (State University of New York at Binghamton).

Milestones

1. Integration of AFM cantilever into TEM column to *in situ* measure lithium dendrite growth force. (Q1, FY 2020; Completed)
2. Identify correlation of SEI structure and chemistry with electrolyte composition and electrochemical operating condition. (Q2, FY 2020; Completed)
3. Establish molecular signature of SEI formation process. (Q3, FY 2020)
4. Establish cathode stability in solid-state configuration. (Q4, FY 2020)

Progress Report

Understanding the intrinsic formation mechanisms of the lithium whiskers is essential for solving the lithium dendrite problem. Here, the team uses *in situ* environmental TEM to control the growth environment of lithium dendrite. Therefore, they can control the SEI layer formed on the lithium dendrite and directly visualize the correlation between the growth behavior of lithium dendrite and SEI layer chemistry. They discovered that carbonate species in the initial SEI layer that is very adjacent to the developing lithium metal plays a decisive role in the subsequent formation of lithium with a whisker morphology.

During the *in situ* TEM deposition of lithium metal, the team found that under CO₂ gas environment, lithium will grow as a whisker. However, when they change to N₂ gas, lithium deposits as large particles. Apparently, the SEI formed in CO₂ is dominated by carbonate species, which has a sluggish Li-ion transport; for the case of N₂ gas, the SEI is dominated by Li₃N, a much better Li⁺-conductor than Li₂CO₃ and Li₂O. These observations indicate that the localized lithium deposition observed in CO₂ environment is tremendously attenuated in the case of N₂ environment, implying that dendrite-free lithium deposition is closely associated with facile transport of lithium in the initial SEI.

To validate the findings from the *in situ* environmental TEM experiments above in practical coin cells, the team designed “electrolyte-poison” experiments and characterized the deposited lithium by using SEM and Cryo-TEM. 1 M lithium bis(fluorosulfonyl)imide (LiFSI) salt in DME solvent is used as the baseline electrolyte, which is well-documented to induce primarily the formation of large lithium particles during deposition. Then, the team intentionally added EC into the baseline electrolyte to reduce the ionic conductivity of the SEI. Due to higher polarity of EC molecules compared to DME molecules, the EC molecules preferentially solvate the Li⁺ ions. As the solvated Li⁺ ions are driven by the electric field to the deposition site, the EC released there is expected to critically influence the deposited lithium by reacting with the freshly deposited lithium, generating dilithium ethylene dicarbonate (Li₂EDC) as the initial SEI. Since Li₂EDC has low Li⁺-conductivity, it is expected that the EC addition will considerably

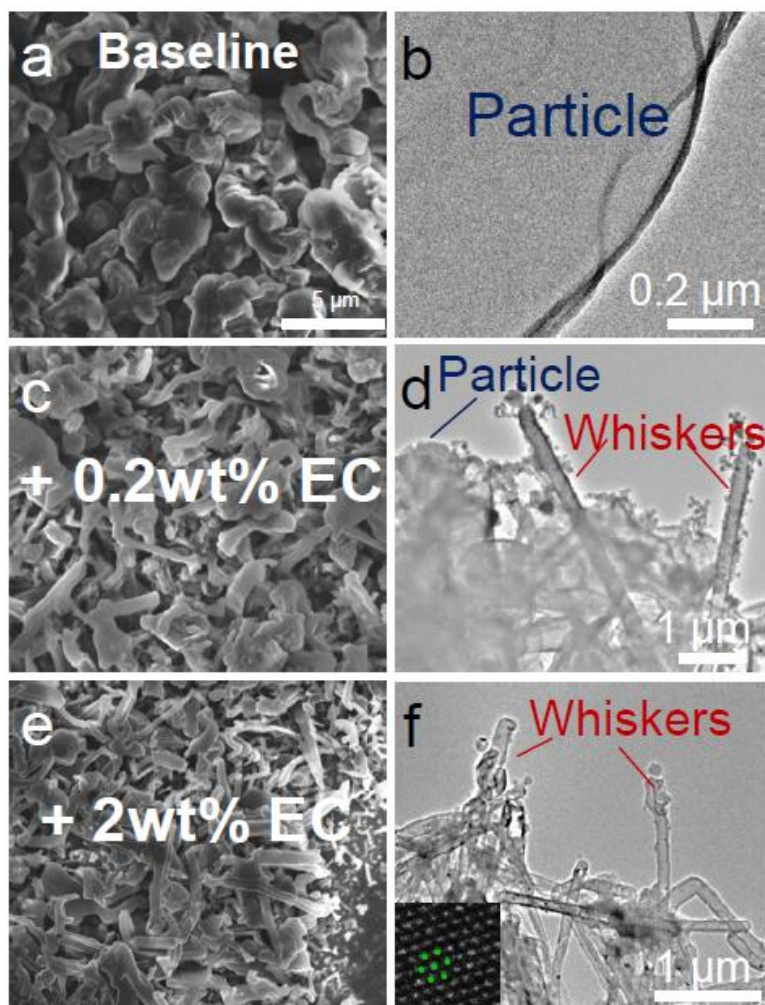


Figure 47. Intentional poisoning of the baseline electrolyte to identify the role of EC in lithium whisker formation in coin-cells. (a) Scanning electron microscopy image of lithium particles deposited in the baseline electrolyte (1 M lithium bis(fluorosulfonyl)imide salt in dimethoxyethane). (b) Corresponding cryo-transmission electron microscopy (cryo-TEM) image of the lithium particle. (c-d) Poisoning of the baseline electrolyte by adding 0.2% EC leads to a co-existence of distinguished morphology of both monolith and whisker. (e-f) Increasing EC concentration to 2% in the baseline electrolyte induces almost a dominance of lithium whisker formation. Inset in (f) shows high-resolution cryo-TEM image of the lithium metal viewing from the [110] zone axis as shown by the ball model. Note that small ice crystals can also be seen in the cryo-TEM images due to water vapor condensation in sample preparation process.

reduce the lithium deposition on the side surfaces, prompting whisker formation. Indeed, the team observes that lithium deposited in the baseline electrolyte is composed of pure monolithic morphology (Figure 47a-b), while lithium metal deposited in 0.2 wt% of EC-poisoned electrolyte shows mixed morphologies of monolith and whisker (Figure 47c-d). Increasing EC concentration to 2 wt% leads to almost pure lithium whiskers (Figure 47e-f). A similar effect is also observed by poisoning the baseline electrolyte with EMC, the reduction of which on lithium produces lithium alkyl carbonate.

These findings reveal the intrinsic cause and give a clear process on the formation and behavior of dendritic lithium under stress, providing much-needed insights for solving the lithium whisker formation from the root cause rather than the current approach of containing it, and therefore potentially leading to safe operation of Li-metal anode in batteries.

Patents/Publications/Presentations

Publications

- Xu, Y., H. Wu, Y. He, Q. Chen, J-G. Zhang, W. Xu, and C. Wang. “Atomic to Nanoscale Origin of Vinylene Carbonate Enhanced Cycling Stability of Lithium Metal Anode Revealed by Cryo-Transmission Electron Microscopy.” *Nano Letters* 20 (2020): 418–425.
- Jia, H., X. Li, J. Song, X. Zhang, L. Luo, Y. He, B. Li, Y. Cai, S. Hu, X. Xiao, C. Wang, K. M. Rosso, R. Yi, R. Patel, and J. G. Zhang. “Hierarchical Porous Silicon Structures with Extraordinary Mechanical Strength as High Performance, Lithium-Ion Battery Anodes.” *Nature Communications* 11 (2020): 1474.

Task 2.6 – Integrated Atomic-, Meso-, and Micro-Scale Diagnostics of Solid-State Batteries (Yi Cui, William Chueh, and Michael Toney; Stanford University / SLAC National Accelerator Laboratory)

Project Objective. By developing a characterization toolkit that tackles length scales (Å to mm), cell pressure (1-100 bars), and dynamics (during synthesis, fabrication, and cycling), the project aims to generate insights to engineer SSBs for deployment in EVs. This interdisciplinary team aims to achieve this objective by merging a broad range of characterization approaches as well as modeling to track the evolution of nanoscale chemistry and structure, microstructure, and transport.

Project Impact. The project will have an impact in several areas: (1) accelerate rational design of coatings and artificial SEIs in SSBs; (2) inhibit the root causes leading to cell shorting, and enable high current cycling; (3) accelerate design of cathode coating and composite electrode architectures; and (4) reduce degradation and variability during SSB manufacturing via composition and surface engineering.

Approach. The project has a multi-fold approach that will encompass the following: (1) resolve nanoscale structure and chemistry of SEIs via cryo-TEM; (2) track solid electrolyte and lithium microstructure evolution in 3D via X-ray micro and diffraction tomography; (3) visualize nanoscale ionic and electronic transport at GBs via conducting AFM; (4) map current distribution in cathodes via scanning transmission X-ray microscopy (STXM); and (5) monitor nanoscale solid electrolyte evolution with gas impurity via *in situ* environmental TEM (E-TEM).

Out-Year Goals. The project will develop an integrated characterization toolkit to characterize SSBs within a single cycle and over hundreds of cycles, spanning a wide range of relevant length scales.

Collaborations. Project collaborations include work with SSRL, ALS, and Advanced Photon Source (APS) synchrotron light sources.

Milestones

1. Design, build, and test *operando* SSB cell for depth-resolved XAS. (Q1, FY 2020; Completed)
2. Record micro-tomograms of Li / solid electrolyte / Li (Li/SE/Li) half cells for 10 cycling conditions. (Q2, FY 2020; Completed)
3. Record DC conducting AFM map of pristine solid electrolytes. (Q3, FY 2020)
4. Prepare X-ray transparent cathode / solid electrolyte by cryo-sectioning. (Q4, FY 2020)

Progress Report

This quarter, the team continued to develop an *operando* XRT platform for characterizing SSBs based on sulfide and oxide solid electrolytes. Building off the success achieved last quarter, the team has been able to reproducibly fabricate 2-mm-diameter cells, which allows X-rays to penetrate in the direction parallel to the electrode/electrolyte interface with high efficiency. Electrochemical evaluation of the Li/SE/Li cells via cycling, EIS, and CCD measurements confirmed that the *operando* cells performed similarly as standard cells. The team attributes part of the success to the ability to pressurize the cell during lithium plating and stripping, especially on sulfide solid electrolytes. In all cells, the team paid special attention to the density of the solid electrolytes, since it is known that porosity can lead to preferential plating. In all project solid electrolytes, no porosity can be detected via XRT or SEM. Specifically, for the cold-pressured sulfide solid electrolytes, based on operating pressure (as high as 1 GPa), the team expects negligible porosity. As for the oxides, density is greater than 98% of theoretical. This is an important distinction relative to literature work, since many published results show substantial porosity, which is likely not representative of well-functioning cells.

In the LPS-based Li/SE/Li cells, *operando* experiments recorded before and after shorting revealed surprisingly little fracture of the cells, in contrast to reports in literature based on lower density solid electrolytes. For the project's high-density cells, the cracks were slightly above the resolution limit for XRT, with a diameter on the order of a few to ~ 10 microns. Interestingly, analysis of resistance after short gave similar estimates for diameter of the “wire” responsible for the short, assuming electrical conductivity of lithium metal. The results suggest that high-density Li/SE/Li cells short via a very fine growth of lithium metal that connects the two electrodes. Some of these cracks propagate laterally at the electrode undergoing deposition within the cells and do not contribute to shorting. Instead, such cracks could lead to increased impedance at the solid electrolyte / lithium interface due to delamination.

In the LLZO-based Li/SE/Li cells, XRT recorded before and after shorting yielded no detectable microstructural differences within resolution limits, in contrast to LPS-based cells. Similar to LPS cells, on the other hand, electrical measurement after shorting implies a very narrow wire ($< 1 \mu$) that connects the two electrodes.

Patents/Publications/Presentations

Presentations

- Department of Physics & Atmospheric Sciences, Dalhousie University, Halifax, Canada (January 27, 2020): W. C. Chueh.
- Energy Seminar, Stanford University, Palo Alto, California (January 6, 2020): “Stanford’s StorageX Initiative”; W. C. Chueh.

Task 2.7 – Investigating the Stability of Solid/Solid Interface (Zonghai Chen, Argonne National Laboratory)

Project Objective. The project objective is to characterize the physical/chemical properties of species at the solid/solid interfaces and to fundamentally understand the critical issues that limit the mechanical, chemical, and electrochemical stability of solid/solid interfaces at the cathode and the anode.

Project Impact. The project will lead to several areas of impact: (1) to generate knowledge that supports the rational design of materials and process development; (2) to establish structure-properties relationship of the interface; and (3) to understand the formation mechanism of lithium dendrite and to predict potential solutions.

Approach. The project approach is multi-fold: (1) understanding the physics behind the transformation between the low conductivity phase and the high conductivity phase; (2) investigating the bonding strength of the cathode/electrolyte interface using model systems; and (3) developing electrolytes with high ionic conductivity and good bonding to cathodes through cation doping.

Out-Year Goals. The project has the following out-year goals:

- Developing synchrotron-based diagnosis tools to investigate physical/chemical properties of solid/solid interface.
- Identifying mechanistic barriers that limit the chemical/mechanical/electrochemical durability of solid/solid interface.
- Developing model systems to validate the failure mechanism of solid/solid interface.

Collaborations. The project collaborates with Dr. A. Ngo (ANL), Dr. L. A. Curtiss (ANL), Dr. V. Srinivasan (ANL), Dr. Y. Ren (ANL), Dr. J. Libera (ANL), Dr. T. Li (Northern Illinois University), Dr. F. Wang (BNL), Dr. X. H. Xiao (BNL), and Dr. D. Chen (University of Houston).

Milestones

1. Forming model Ta-LLZO/NMC-622 interface for physical diagnosis. (Q1, FY 2020; Completed)
2. Investigating the interaction between Ta-LLZO and NMC-622 at the interface on cycling. (Q2, FY 2020; In progress)
3. Investigating the chemical reactions of Ta-LLZO at the reducing environment. (Q3, FY 2020; In progress)
4. Investigating the chemical/mechanical stability of Li/Ta-LLZO interface. (Q4, FY 2020; In progress)

Progress Report

The team reported last quarter that a solid-solid interface between $\text{LiNi}_{0.6}\text{Mn}_{0.2}\text{Co}_{0.2}\text{O}_2$ (NMC-622) and $\text{Li}_{6.6}\text{La}_3\text{Zr}_{1.6}\text{Ta}_{0.4}\text{O}_{12}$ (Ta-LLZO) was successfully formed through a co-sintering between two oxides. The attempt to assemble an all-solid-state cell using the co-sintered sample was proven unsuccessful; the cell was not able to be charged, possibly due to lack of electrochemically functional interface without the presence of a liquid electrolyte. Hence, the co-sintered sample was tested in a liquid cell environment for confirmation. The model cell can be charged/discharged like a normal Li-ion cell with a slightly lower specific capacity (Ta-LLZO was decorated on the surface of the NMC-622 without reversible capacity). It was also observed that Ta-LLZO decorated NMC-622 has a slightly better capacity retention than the pristine NMC-622 cathode (see Figure 48). The electrochemical evidence indirectly demonstrated that a physical bonding between Ta-LLZO and NMC-622 was able to be achieved through the co-sintering process, and that this physical bonding was strong enough to survive the lattice expansion/contraction of NMC-622 during charging/discharging process. However, the difficulty in transporting lithium ions across the solid-solid interface remains a challenge.

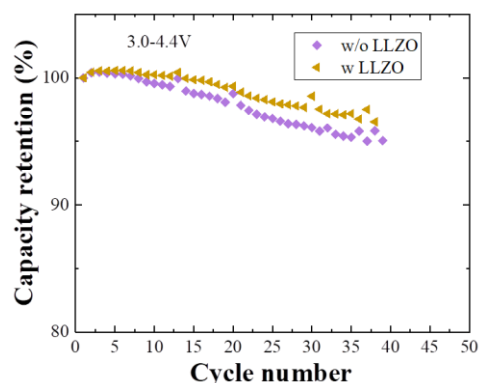


Figure 48. Capacity retention of Li-ion cells using a liquid electrolyte, showing that the decorated Ta-LLZO is compatible with NMC-622.

It was also previously reported that Ta-LLZO showed a huge lattice hysteresis between room temperature during the initial thermal processing; this was believed to be associated with the recovery of high-conductivity cubic phase from the aged low-temperature cubic phase (proton inserted form). Hence, the investigation was expanded to other doped LLZO (Al-LLZO and Ga-LLZO). The *in situ* high-energy X-ray diffraction (HEXRD) results indicated that both Al-LLZO and Ga-LLZO experienced the same lattice hysteresis as Ta-LLZO does. TGA shows 12-16% weight loss for all three samples during thermal treatment up to 800°C, with about half of the weight loss below 400°C (possibly due to the loss of $\text{LiOH}\cdot\text{H}_2\text{O}$) and about half of it between 400°C and 700°C (possibly due to the loss of Li_2CO_3) (see Figure 49). This suggests that the difficulty in charging/discharging all-solid-state cells is not a unique phenomenon for Ta-LLZO, but a generic problem for all LLZO electrolytes, possibly associated with their complicated phase diagram.

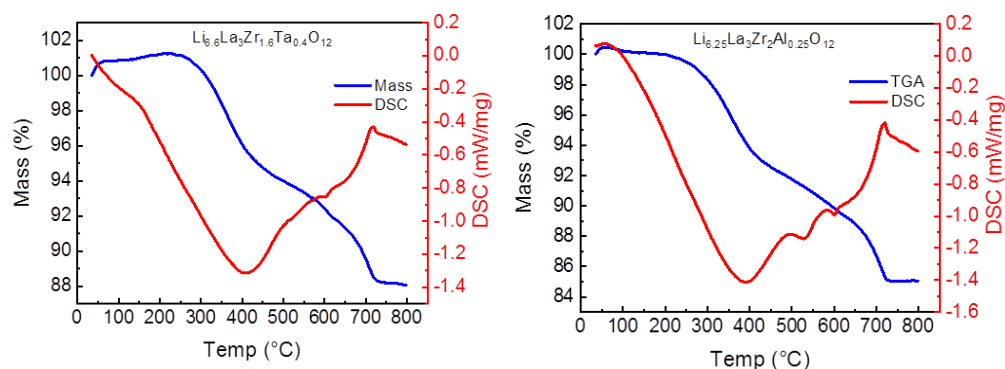


Figure 49. Thermal gravimetric analysis of aged Ta-LLZO and aged Al-LLZO shows similar behavior between Ta-LLZO and Al-LLZO.

Patents/Publications/Presentations

Publication

- Gim, J., H. Nguyen, T. Li, F. Wang, L. Wang, X. He, Y. Ren, and Z. Chen. “Phase Transformation of $\text{Li}_7\text{La}_3\text{Zr}_2\text{O}_{12}$: A Perspective from Thermodynamics and Kinetics.” *Journal of Physical Chemistry C* (2020). In revision.

Task 2.8 – Fundamental Understanding of Interfacial Phenomena in Solid-State Batteries (Xingcheng Xiao, General Motors)

Project Objective. The project objective is to develop a comprehensive set of *in situ* diagnostic techniques combined with atomic/continuum modeling schemes to investigate and understand the coupled mechanical/chemical degradation associated with dynamic interfacial phenomena in SSBs. Specifically, *in situ* observations and characterizations of lithium plating-stripping processes, lithium dendrite formation, interphase formation, and the induced interfacial stresses, as well as the mechanical and electrochemical properties of interfaces and interphases, are paramount. The study will provide useful guidelines for optimizing cell structure design and engineering interfaces and interphases to enable SSBs.

Project Impact. The project will provide fundamental understanding of the dynamic interfacial phenomena and the coupled mechanical and chemical degradation. In addition, it will establish a critical guideline to design safe and durable SSBs with energy density > 500 wh/kg for EV applications.

Approach. The multiscale *in situ* diagnostic tools, including AFM, nanoindentation, dilatometer, stress sensors, and pressure cells, will be used to investigate mechanical behavior and microstructure evolution at interface/interphase during lithium plating and stripping. The information (along with Li-ion transport properties and microstructure evolution obtained using the advanced spectroscopic ellipsometry, and *in situ* TEM) will be correlated with electrochemical performance toward high cycle efficiency and dendrite-free SSBs. The goal of this understanding is to develop strategies for surface and interface engineering, apply them to commercially available solid electrolytes (including powder, pellets, and foils), and assemble SSBs for further validation and optimization, eventually extending cycle life for EV application.

Out-Year Goals. The project seeks to develop SSB model systems to capture critical mechanical properties and probe the coupled mechanical-chemical degradation by further developing comprehensive *in situ* diagnostic tools. All results obtained from these *in situ* studies, combined with advanced postmortem analysis and modeling, will be correlated with the cycling stability of SSBs. The *in situ* tools developed will be applied to the following two periods to deeply understand the coupled mechanical and chemical degradation of interface/interphase.

Collaborations. The co-PIs involved in experiments and simulation will be as follows: Profs. B. W. Sheldon (Brown University), Y-T. Cheng and Ambrose Seo (University of Kentucky), Yue Qi (Michigan State), and Dr. Q. Zhang (GM).

Milestones

1. Thin-film electrode system for different *in situ* electrochemical tests developed. (Q1, FY 2020; Ongoing)
2. Thin-film solid electrolyte system established with the comparable ionic conductivity reported in the literature. (Q2, FY 2020)
3. *In situ* electrochemical-mechanical tools established. (Q3, FY 2020)
4. A rank of the interfacial adhesion between solid electrolyte and electrodes determined. (Q4, FY 2020)

Progress Report

Synthesized Epitaxial Thin Films of LLZO Electrolyte by Pulsed Laser Deposition (PLD). For the first time, the team has grown LLZO epitaxial thin-films on substrates such as platinum on SrTiO₃ (001) (Pt/ STO) and platinum on Yttrium Stabilized Zirconia (111) (Pt/YSZ). The successful epitaxial growth of LLZO and NMC thin films as electrolyte and electrodes, respectively, opens a way to understand the interfacial properties of these SSB materials, giving the team insight into the next-generation of Li-ion batteries. Figure 50a-b presents the plane view SEM images of the LLZO thin film on Nb- STO (100) substrate. Figure 51 (left) shows the θ - 2θ XRD scan with the (001) peaks of a LLZO thin film on Pt/STO (001) using a Bruker D8 Advance with Cu-K α radiation. The rocking curve scan of (004) shows good crystallinity of the film (Figure 51, right). As shown in Figure 50a-b using FIB SEM, the team has also measured the thickness of the LLZO thin films, which is ca. 100 nm.

Established Experimental Setup for Stress Evolution Measurement in LLZO Solid Electrolyte. As shown in the schematics in Figure 52, the direct bending measurement from the sample will be directly proportional to the overall stresses experienced in both the LLZO pallet and the plated lithium metal. By using various cycling techniques and appropriate finite element method (FEM) analysis aided by further post-mortem imaging, the team plans on decoupling the stress measurements to extrapolate the effect of interfacial and bulk stresses of the LLZO solid electrolyte. Considering that the plasticity of lithium metal will come into play significantly when modeling the curvature evolution, the team expects this particular property to affect the direct translation of stresses from the solid electrolyte to the bending quartz.

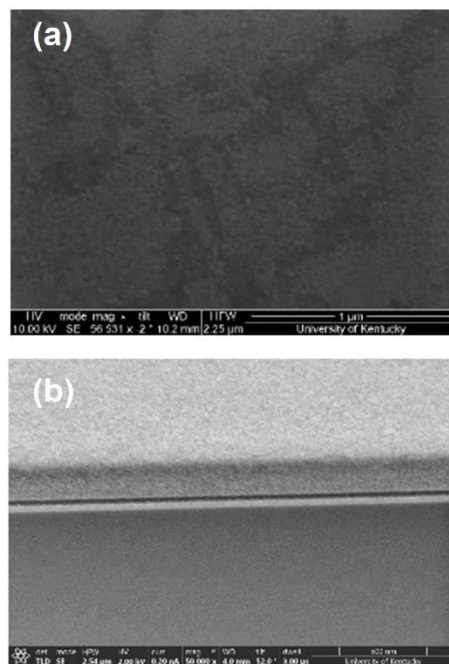


Figure 50. Plane view scanning electron microscopy images of the LLZO thin film on Nb- STO (100) substrate.

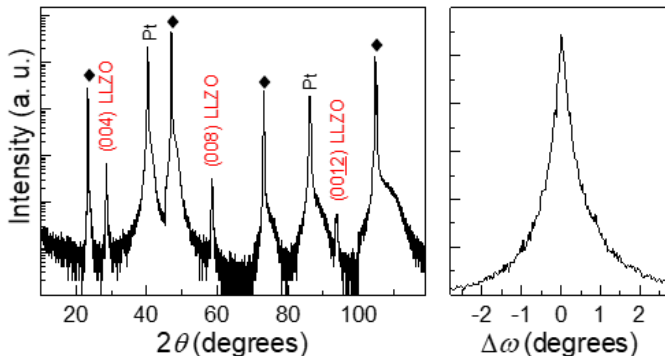


Figure 51. (left) X-ray diffraction scan of LLZO/Pt/STO (100) substrate. (right) Rocking curve scan of LLZO (004) peak.

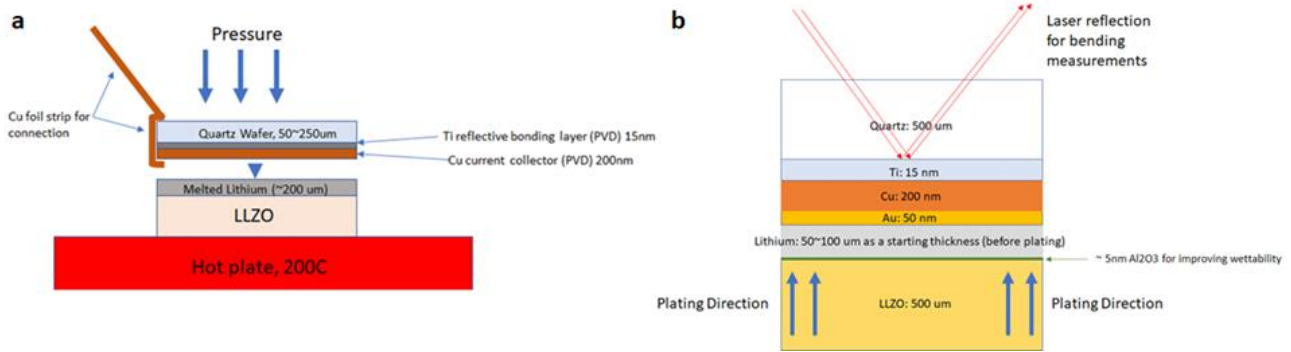


Figure 52. (a) Schematic of sample preparation for curvature measurement of LLZO – Li-metal anode stress evolution. (b) Schematic of bending measurement with laser reflection on a prepared sample.

Patents/Publications/Presentations

The project is new and has no patents, publications, or presentations to report this quarter.

Task 2.9 – Multidimensional Diagnostics of the Interface Evolutions in Solid-State Lithium Batteries (Yan Yao, University of Houston)

Project Objective. The project objective is to develop a platform combining FIB-SEM tomography, TOF-SIMS, and in-SEM nanoindentation-based stiffness mapping for structural, chemical, and mechanical characterizations in SSLBs. Assessment of the influence of cell design and testing conditions (external pressure, current density, temperature) on the evolutions of interfaces will be performed.

Project Impact. The consolidated *in situ* structural–chemical–mechanical diagnostic platform established in this project will provide unprecedented insights into the failure mechanisms of SSLBs.

Approach. Space- and time-resolved structural, chemical, and mechanical characterizations of the cathode–electrolyte and anode–electrolyte interfaces will be performed on all-solid-state lithium batteries using FIB-SEM, TOF-SIMS, and in-SEM nanoindentation. Tasks include (1) development of solid-state cell thin stacks and test-cell configurations that are suitable for *in situ* characterizations; (2) quantitative characterization and *in situ* tracking of interfacial voids formation within composite cathode and electrolyte layer; (3) identification and *in situ* tracking of the chemical composition, spatial distribution, and mechanical properties of electrolyte decomposition products at the lithium- and cathode-electrolyte interfaces; and (4) visualization, chemo-mechanical properties detection, and *in situ* tracking of lithium dendrites grown within the solid electrolyte layer.

Out-Year Goals. In the out years, the project will develop thin-stack solid-state cells, micro-cells, in-SEM nanoindentation, and testing protocols. The correlation between structural evolution, electrolyte decomposition, and interfacial resistance increase will be investigated.

Collaborations. The UH team (Drs. Yao, Fan, and Liang) works closely with the Rice University team (Drs. Lou and Guo).

Milestones

1. Thin-cell stack development. (Q2, FY 2020; In progress)
2. Micro-cell for TOF-SIMS development. (Q3, FY 2020)
3. In-SEM nanoindentation. (Q3, FY 2020)
4. Cell optimization and electrochemical benchmarking. (Q4, FY 2020)

Progress Report

Micro-cell setups with the desired dimension for the proposed structural-chemical-mechanical microscopic and spectroscopic measurements have been explored based on thin-stack solid-state cells. The cells consist of a solid-state composite cathode / SSE / Li-metal anode trilayer structure with a typical combined thickness of $< 100 \mu\text{m}$. Figure 53a shows the cross-section of such a thin-stack cell with a thickness of $90 \mu\text{m}$. A custom-made mounting stage has been designed for electrochemical measurements of the thin cells while providing an open window for microscopic and spectroscopic characterizations from the top (Figure 53b). The cell area is defined by the size of the mounting wedge, which is variable according to test needs. The stage is equipped with a heating plate that can vary testing temperature. A pressure-sensing module is also integrated into the system for *in situ* pressure sensing.

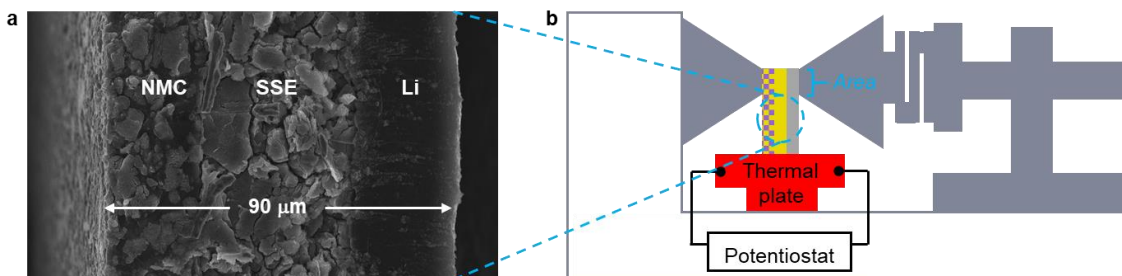


Figure 53. Micro-cell based on thin-stack solid-state cells. (a) Scanning electron microscopy image of thin-stack NMC/SSE/Li cell. (b) Micro-cell setup consisting of a mounting stage, heating module, and pressure-sensing module.

Both the heating and pressure-sensing modules were preliminarily established. A temperature-sensing module was built into the system during initial setup and validation stages so that calibration of temperature was achieved. The heating power–cell temperature relationship was determined after optimization of placement of the heating module, rate of heating, and monitoring of the delay between heating and the cell reaching stabilized temperatures. Figure 54a shows test temperatures ranging from room temperature to 63°C that can be precisely controlled by adjusting the heating power from 0 to 0.90 W; the degree of control is consistent in both heat-up and cool-down processes. The effectiveness of the applied elevated temperature was confirmed in electrochemical tests. Electrochemical impedance of a Li/SSE/Li symmetrical micro-cell saw a decrease by almost an order of magnitude when the test temperature

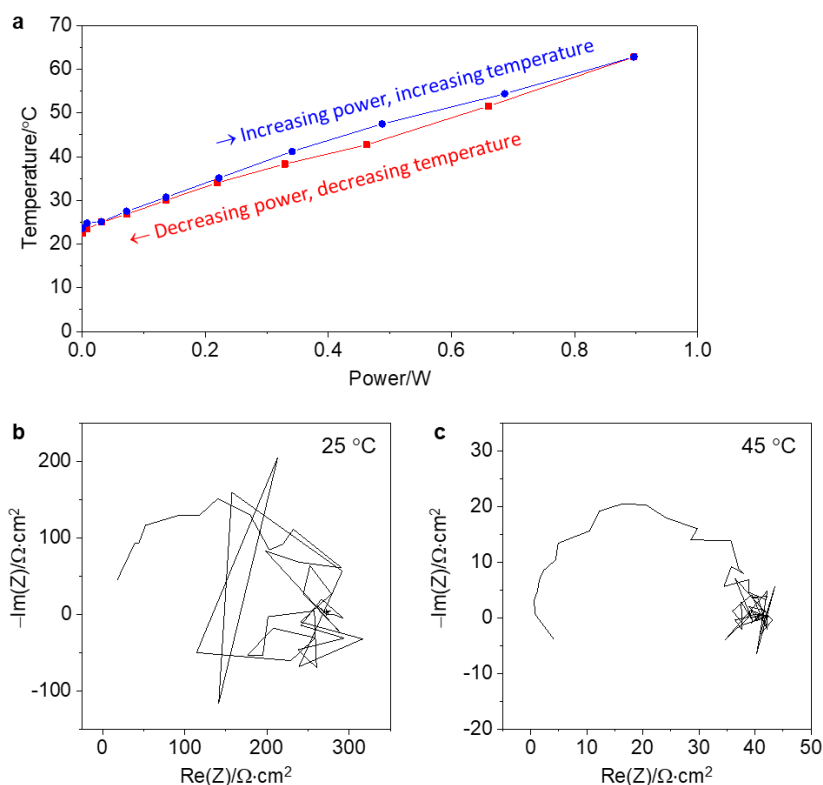


Figure 54. Validation of the heating module in the micro-cell setup. (a) Calibration curve for the heating power–temperature relationship. (b-c) Nyquist plots for symmetrical micro-cell tested at 25°C (b) and 45°C (c), respectively.

was raised from 25°C to 45°C, along with much less noisy spectra (Figure 54b-c). One possible interpretation of the result is softening of the lithium electrodes as a result of the elevated temperature, which improves overall contact in the cell. The result does show a need for improvement of the micro-cell fabrication.

The pressure-sensing module has demonstrated its capability in an *in situ* micro-cell test. Figure 55 shows that the pressure of an NMC/SSE/In micro-cell monotonously increased during charging, then monotonously decreased during discharging. Similar pressure changes have been reported in bulk-type solid-state lithium cells and are attributed to the volume change of the anode, which is the dominant volume change event in such cells. Here, the volume change of the indium anode is supposedly 50-100%, compared with the 2-6% for the NMC cathode. The pressure change is therefore dominated by the anode reaction. Reasonable pressure results aside, the cell is showing unsatisfactory electrochemical performance as seen from the low CE and relatively large polarization. This issue echoes the observation of symmetrical micro-cells that fabrication of the micro-cells overall needs time for more optimization, a focus of the team's ongoing efforts.

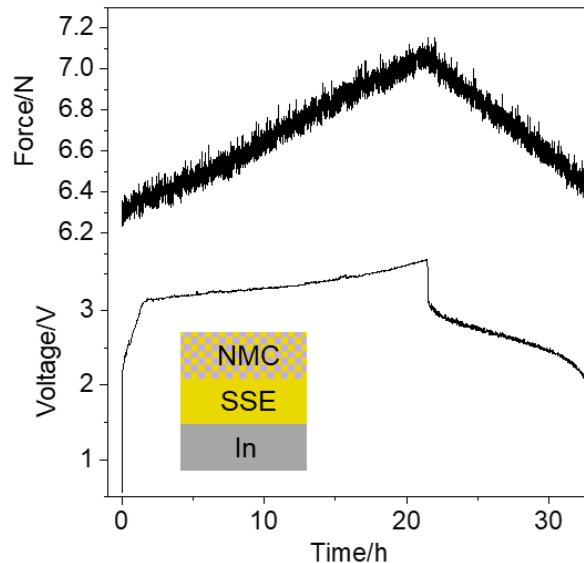


Figure 55. Validation of pressure sensing module in the micro-cell setup. (a) Pressure change of micro-cell during complete cycle. (b) Corresponding charge-discharge profile of cell. Inset: schematics of the cell configuration.

Patents/Publications/Presentations

The project has no patents, publications, or presentations to report this quarter.

TASK 3 – MODELING

Summary and Highlights

Achieving the performance, life, and cost targets outlined by VTO will require moving to next-generation chemistries, such as higher capacity Li-ion intercalation cathodes, silicon and other alloy-based anodes, Li-metal anode, and sulfur cathodes. However, numerous problems plague development of these systems, from material-level challenges in ensuring reversibility to electrode-level issues in accommodating volume changes, to cell-level challenges in preventing cross talk between the electrodes. In this task, a mathematical perspective is applied to these challenges to provide an understanding of the underlying phenomenon and to suggest solutions that can be implemented by the material synthesis and electrode architecture groups.

The effort spans multiple length scales, from *ab initio* methods to continuum-scale techniques. Models are combined with experiments, and extensive collaborations are established with experimental groups to ensure that the predictions match reality. Efforts also focus on obtaining parameters needed for the models, either from lower-length scale methods or from experiments. Projects also emphasize pushing the boundaries of the modeling techniques used to ensure that the task stays at the cutting edge.

In the area of intercalation cathodes, effort is focused on understanding working principles of high nickel layered materials with an aim of understanding structural changes and associated changes in transport properties. Coatings, an effective strategy for high-voltage operation, are being explored with the aim of providing a rational design approach for new coating materials. In parallel, design of liquid electrolytes and gaining understanding of their behavior are used to determine their usability at high voltages. In addition, focus is paid to assembling of porous electrodes with particles to predict conduction behavior and impact of heterogeneities on electrode behavior.

In the area of Li-metal anodes, the focus is on understanding how materials can be designed to prevent dendrite growth using continuum modeling approaches, combined with calculations on mobility in solid conductors. The results are used to guide materials development by providing the properties needed to prevent dendrites while also achieving energy and power goals. Models are also starting to examine the role of the SEI on morphology of the dendrite and to describe mechanical-electrochemical coupled effects that are critical for dendrite formation. Finally, models are being developed to examine the solid-cathode interface in Li-metal-based systems, where interface debonding issues are known to limit cycling.

Models are also being developed for solid electrolytes against intercalation cathodes and for developing methods to predict delamination at the interface during cycling in different cathode materials. These models are being used to understand how to prevent chemo-mechanical failure at the interface.

Highlight. While LPS solid electrolytes have demonstrated high conductivity, there are still gaps in understanding the underlying cause. It has been argued that the anion building blocks serve as a key descriptor for ionic conductivity in amorphous LPS solid electrolytes. These materials contain PS_4^{3-} , $\text{P}_2\text{S}_6^{4-}$, $\text{P}_2\text{S}_7^{4-}$, and polysulfides as building blocks, with their ratio being determined by the composition and synthesis method. To examine the connection between the anion building blocks and conductivity, the Ceder group (UC Berkeley) generated amorphous structures with different ratios of building blocks, maintaining the chemical composition at $\text{Li}_3\text{PS}_{4-\delta}$, using the AIMD simulated melt-quench method. While the simulations reproduce the experimental results, no correlation was found between the presence of certain anion blocks and calculated conductivities. For example, the “ $\text{1P}_2\text{S}_6$ ” structure exhibits conductivity $> 10^{-2} \text{ S}\cdot\text{cm}^{-1}$, whereas the “ $\text{2P}_2\text{S}_6\text{4S}$ ” shows a 1-order magnitude lower value. These results suggest that there are likely other structural factors affecting ionic conductivity, rather than the existence of a certain polyanion.

Task 3.1 – Characterization and Modeling of Li-Metal Batteries: First-Principles Modeling and Machine Learning (Kristin Persson, Lawrence Berkeley National Laboratory)

Project Objective. This project supports VTO programmatic goals by developing next-generation, high-energy cathode materials and enabling stable cathode operation at high voltages through target particle morphology design, functional coatings, and rational design of electrolytes. The end-of-project goals include the following: (1) understanding of the factors that govern charge transport in nonaqueous, superconcentrated liquid electrolytes, (2) critical surface and coating design and optimization strategies that will improve cycling of Li-ion battery cathodes by reducing cathode degradation from oxygen loss, and (3) simulation and machine learning of the early formation of the SEI on Li-metal electrodes.

Project Impact. This project is aimed to provide fundamental insights into the atomistic mechanisms underlying surface reactivity and performance of Li-ion cathode materials and electrolytes with the ultimate goal to suggest improvement strategies, such as coatings, surface protection, novel electrolyte formulations, and particle morphology design. Transport modes as a function of solvent and salt concentrations will be clarified, and a data-driven reaction network framework will be designed and implemented to predict early SEI formation on lithium metal.

Approach. First-principles calculations, both static and dynamic approaches, are used to model SSE material thermodynamics and kinetics. Liquid electrolytes are modeled through coupled classical MD and first-principles methods to accurately capture solvation structure as well as reactivity of the liquid system. The reaction network is built on large-scale first-principles data, using graph theory and machine learning models.

Out-Year Goals. Electrolyte work will be aimed toward understanding the atomistic interactions underlying performance of lithium electrolytes, specifically elucidating conductivity (as a function of salt concentration) and impact on the charge transport mechanisms at play. Amorphous coatings will be evaluated based on ionic transport metrics and thermodynamic stability. The reaction network will be tested against known interfacial species forming on lithium metal in LiPF₆/EC electrolytes.

Collaborations. This project is highly collaborative between BMR PIs G. Chen (LBNL), G. Ceder (UC Berkeley), and R. Kostecki (ANL). Improved coating formulations will be examined by Chen and Ceder, and interfacial reactivity insights corroborated by Kostecki.

Milestones

1. Obtain desirable chemical and structural traits of amorphous cathode coatings. (Q1, FY 2020; Completed, December 2019)
2. Identify the lithium diffusion bottlenecks in two known coating materials. (Q2, FY 2020; Completed)
3. Quantify the conduction mechanisms in superconcentrated LiPF₆/PC. (Q3, FY 2020; Completed)
4. Preliminary insights into the SEI composition and reaction pathways for baseline electrolytes. First approximative reaction scheme proposed. (Q4, FY 2020; In progress)

Progress Report

This project is aimed toward identifying the lithium diffusion bottlenecks in two known amorphous coating materials: Al_2O_3 and ZnO . The team considers two different scenarios of lithium diffusion in conformal coatings: (1) electron conducting model, that is, insert extra Li^0 into amorphous Al_2O_3 and ZnO to generate $\text{Li}_x\text{Al}_2\text{O}_3$ and Li_xZnO , respectively; (2) electrolyte model, that is, insert Li_2O as the coordination shells of Li^+ cations into amorphous Al_2O_3 and ZnO to generate $\text{Li}_{2x}\text{Al}_2\text{O}_{3+x}$ and $\text{Li}_{2x}\text{ZnO}_{1+x}$, respectively. Using *ab initio* molecular dynamics (AIMD) simulations to model Li^+ and O^{2-} diffusions in amorphous Al_2O_3 and ZnO , the room-temperature self-diffusion coefficients (D_{rt}) were obtained via Arrhenius relation.

In Figure 56, the extrapolated D_{rt}^{Li} and D_{rt}^{O} are plotted as function of Li^+ concentration. Several observations can be made. (1) In general, D_{rt}^{Li} and D_{rt}^{O} increase with a higher Li^+ content. Also, Li^+ and O^{2-} diffuse much faster in ZnO than in Al_2O_3 . Ion diffusion in the amorphous structure is accompanied by a bond breaking/making process; thus, Li^+ diffusion in ZnO is facilitated by the lower oxygen coordination. The slower O^{2-} diffusion in Al_2O_3 is rationalized by the stronger Al-O bond as compared to the Zn-O one, which can be demonstrated by crystal orbital Hamiltonian populations analysis. (2) In Al_2O_3 , the electrolyte model exhibits faster Li^+ transport than the electron conducting model. This suggests that the significantly impeded electron hopping in amorphous Al_2O_3 would impose a bottleneck for Li^+ diffusion. On the other hand, there is no major difference in D_{rt}^{Li} between the electron conducting and the electrolyte models in ZnO , which implies that the electron mobility in semiconducting ZnO is fast enough to support Li^+ diffusion. Indeed, the room-temperature electrical conductivity of ZnO is orders of magnitude higher than that of Al_2O_3 . Furthermore, the electron conducting model promotes O^{2-} transport in Al_2O_3 , which suggests that the reduced aluminum cations exhibit a weaker bond to oxygen, while aluminum cations remain 3^+ state in electrolyte model. (3) Based on the obtained Li^+ and O^{2-} diffusivities, the team finds that Al_2O_3 provides a better conformal coating for high-voltage cathodes than ZnO . A very thin Al_2O_3 coating layer would support sufficient Li^+ diffusion and also impede O^{2-} transport. The team emphasizes the need to monitor the coating thickness, as to avoid the coating layer from reducing Li-ion conductivity and, hence, the rate capability of the electrode. (4) While the lithiated counterparts of Al_2O_3 and ZnO can achieve a higher Li^+ transport, they are not stable against delithiation and subsequent decomposition to Al_2O_3 and ZnO at a high charge state cathode.

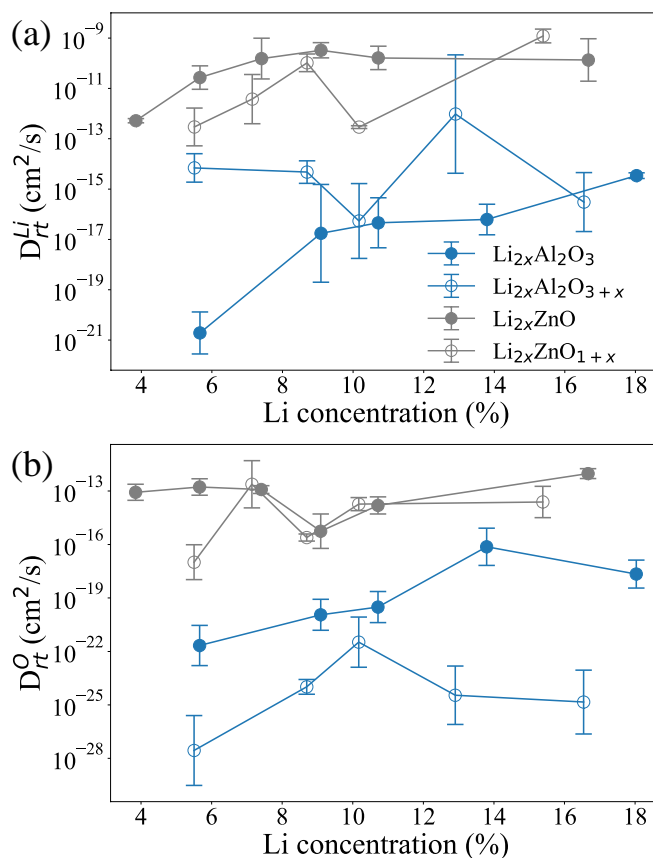


Figure 56. Estimated room temperature self-diffusion coefficients of Li^+ (a) and O^{2-} (b) in Al_2O_3 and ZnO with varying Li^+ concentration.

Patents/Publications/Presentations

Publication

- Cheng, J., E. Sivonxay, and K. A. Persson. “Evaluation of Amorphous Oxide Coatings for High-Voltage Li-ion Battery Applications using a First-Principles Framework.” *ACS Applied Materials & Interfaces*. In revision.

Task 3.2 – Understanding and Strategies for Controlled Interfacial Phenomena in Lithium-Ion Batteries and Beyond (Perla Balbuena and Jorge Seminario, Texas A&M University; Partha Mukherjee, Purdue University)

Project Objective. The project objective is to evaluate and characterize interfacial phenomena in lithiated silicon and Li-metal anodes and to develop guidelines for potential solutions leading to controlled reactivity at electrode/electrolyte interfaces of rechargeable batteries using advanced modeling techniques based on first principles.

Project Impact. Understanding SEI growth on constantly evolving silicon surfaces and on highly reactive Li-metal surfaces is expected to allow definition of the electrolyte properties required in high-performance cells. Strategies to control the silicon anode instability and pulverization issues and the well-known safety and short effective lifetimes of Li-metal anodes will be developed by tuning the electrolyte composition, structure, dynamic, and stability, as well as that of the electrode morphology and interactions with the electrolyte, based on multiple characterizations of interfacial phenomena.

Approach. A comprehensive multi-scale modeling approach, including first-principles *ab initio* static and dynamics, classical MD, and coarse-grained mesoscopic models, will focus on the roles of the electrolyte's chemical, structural, and dynamical properties and of the electrode micro- and nano- structure on the formation and evolution of the SEI layer and the associated electrochemical performance on silicon and on Li-metal anodes.

Out-Year Goals. Work will progress toward characterizing lithiation and SEI formation at silicon surfaces as well as the subsequent cracking and reforming events under the most realistic modeling conditions. Similarly, the project will investigate electrolyte effects on reactivity and dendrite formation in Li-metal surfaces. The project aims to capture how the chemistry of the various electrolyte components (mainly liquids, but also solid polymers and gels) affects the main issues that influence the electrode performance.

Collaborations. This project funds work at Texas A&M University (TAMU) and Purdue University. The team has collaborated with Prof. G. Somorjai (UC Berkeley), Prof. S. Yassar (University of Illinois at Chicago, or UIC), and Dr. V. Murugesan (PNNL).

Milestones

1. Complete thermal and chemical/electrochemical analysis of dendrite growth. (Q1, FY 2020; Completed)
2. Complete analysis regarding SEI formation and electrodeposition processes. (Q2, FY 2020; Completed)
3. Complete studies on cationic additive effect on electrodeposition. (Q3, FY 2020)
4. Complete mesoscale investigation on external field effects on electrodeposition. (Q4, FY 2020)

Progress Report

Thermal Stabilization of Chemo-Mechanical Metal-SEI Interactions. The electrodeposition phenomenon at the vicinity of the metal-SEI interface is fundamentally influenced by three mechanisms: desolvation of lithium ions from the electrolyte to the upper layer of the SEI; transport of lithium ions within the SEI layer; and electrochemical reaction of the metal ions at the metal-SEI interface. Among these mechanisms, sluggish transport of the Li-metal ions within the SEI can substantially impede formation of a smooth growth of the metal. In addition, an increase in the electrochemical reaction rate (relevant to higher applied current densities) can exacerbate the roughness of the metal morphology. However, an increase in the operating temperature of the battery can significantly enhance the diffusion of lithium ions within the SEI layer, via the Arrhenius equation. A coarse-grained mesoscale model was used to determine the range of temperatures required to maintain the mechanical integrity of the SEI layer. The model captures the dynamic evolution of the metal-SEI interface based on the three fundamental mechanisms described above.

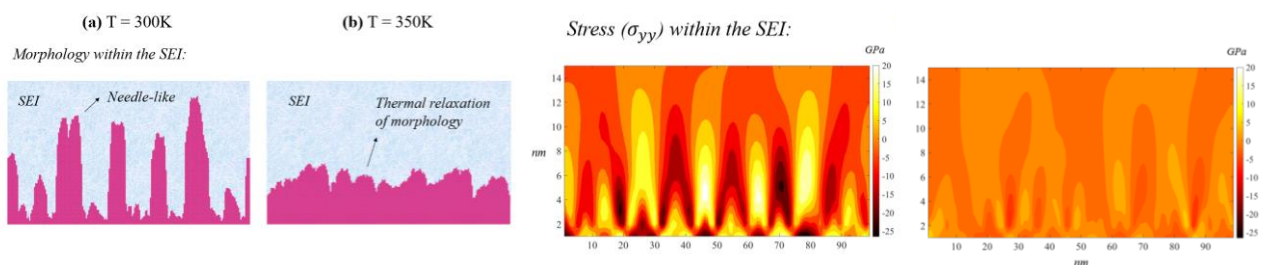


Figure 57. Lithium electrodeposition morphologies and corresponding stress contours (σ_{yy}) in the SEI layer at an operating temperature of (a) 300K and (b) 350K. An increase in temperature from 300K to 350K results in smoothening of the metal morphology and a reduction in the mechanical stress experienced by the SEI layer.

SEI Nucleation and Growth for Lithium Metal in Contact with a Liquid Electrolyte. Extended classical MD simulations of 20 nanoseconds each were conducted in eight electrolytes to evaluate the nucleation and growth of SEI phases when the electrolyte is in contact with a liquid electrolyte. The simulations clearly show the expansion of the top layers of the metal and the gradual oxidation of the metal atoms on contact with the electrolyte solution. The nucleation and growth of specific phases such as LiF are also evident from the MD trajectories.

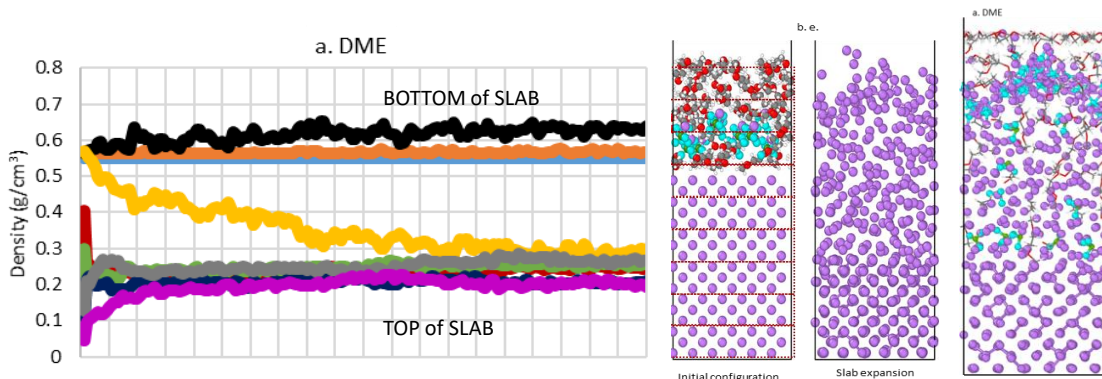


Figure 58. Molecular dynamics simulations of LiPF_6/DME solutions in contact with lithium metal. (a) Expansion of top layers of lithium metal (average density $\sim 0.25 \text{ g/cc}$); bottom layers remain at lithium crystal density ($\sim 0.55 \text{ g/cc}$). (b) Initial configuration of lithium slab (purple, bottom) and electrolyte phase (top). (c) Expansion of lithium metal. (d) Nucleation and growth of LiF phase (F: light blue, C: grey and O: red) at the top of the expanded region.

Patents/Publications/Presentations

Publications

- Tewari, D., S. P. Rangarajan, P. B. Balbuena, Y. Barsukov, and P. P. Mukherjee. “Mesoscale Anatomy of Dead Lithium Formation.” *Journal of Physical Chemistry C* 124, no. 12 (2020): 6502–6511. doi: 10.1021/acs.jpcc.9b11563.
- Kamphaus, E. P., K. Hight, M. Dermott, and P. B. Balbuena. “Model Systems for Screening and Investigation of Lithium Metal Electrode Chemistry and Dendrite Formation.” *Physical Chemistry Chemical Physics* 22 (2020): 575–588. Selected as 2019 Hot PCCP Article.
- Galvez-Aranda, D. E., and J. M. Seminario. “Solid Electrolyte Interphase Formation between the $\text{Li}_{0.29}\text{La}_{0.57}\text{TiO}_3$ Solid-State Electrolyte and a Li-Metal Anode: An *Ab Initio* Molecular Dynamics Study.” *RSC Advances* 10 (2020): 9000–9015. doi: 10.1039/c9ra10984f.

Presentation

- Seminar, University of Oklahoma, Norman, Oklahoma (February 11, 2020): “Interfacial Phenomena in Li Metal Batteries”; P. B. Balbuena. Invited.

Task 3.3 – Electrode Materials Design and Failure Prediction (Venkat Srinivasan, Argonne National Laboratory)

Project Objective. The main project objective is to develop computational models for understanding the various degradation mechanisms for next-generation Li-ion batteries. This year's goal is to use the continuum-based mathematical model to (1) investigate interfacial stability between electrodes and ceramic-based SSEs, and (2) experimentally measure and understand the impedance observed at the cathode/SSE interface. Ceramic-based SSEs are expected to enable high-energy-density and liquid-free, safe, next-generation Li-ion batteries. Li-metal anodes should be incorporated due to their substantially larger specific capacity, as compared to present day graphite-based anodes. During deposition, lithium dendrite growth through the SSEs, and subsequent short circuit, has been a major issue, limiting successful implementation of SSEs. Similarly, on the cathode side, diffusion of TMs into the SSEs, along with delamination between cathode and SSE, leads to increased interfacial resistance. The developed computational model will be used to investigate the impact of microstructural (grain size), physical (mechanical stiffness), and transport (conductivity) properties of the SSE on the overall interfacial degradation observed at both the cathode and anode sides. Due to the state of charge (SOC)-dependent electrochemical and mechanical properties of the cathode, an attempt will be made to experimentally measure the SOC-dependent impedance at the cathode/SSE interface. The main focus will be to elucidate interfacial issues, observed at both anode and cathode sides, and to devise strategies to enable successful implementation of SSE in next-generation Li-ion batteries.

Project Impact. Findings from this research will give a better understanding of the factors, at the cathode/SSE interface, limiting the cycle life of solid-electrolyte-based Li-ion batteries. These results will help to enable incorporation of cathode particles within SSEs.

Project Approach. The approach used here is to develop mesoscale models, based on continuum modeling, to describe the critical processes in the materials, and combining them with electrochemical, microscopic, and spectroscopic data to ensure parameter estimation and model validation. The model is then used to provide insights on impact of material properties on performance and life and as guidance for design of new materials.

Out-Year Goals. At the end of this project, a computational framework will be presented that is capable of estimating delamination and impedance at cathode/SSE interface.

Collaborations. This project collaborates with L. A. Curtiss, A. T. Ngo, and C. M. Phatak at ANL.

Milestones

1. Elucidate the difference in delamination mechanisms for NMC/LLZO- and LCO/LLZO- type cathode/SEIs. (Q1, FY 2019; Completed)
2. *Go/No-Go Decision:* Investigate impact of exchange current density on delamination-induced capacity fade. If effect is minor, use experimentally observed exchange current values. Otherwise, use value obtained from DFT calculations. (Q2, FY 2020; Completed)
3. Develop continuum model for charge transport and mechanical degradation incorporating an interphase layer between LLZO electrolyte and NMC cathode. (Q3, FY 2020; In progress)
4. Gain understanding of growth rate of electrodepositing lithium nuclei. (Q4, FY 2020; In progress)

Progress Report

Investigate Impact of Exchange Current Density on Delamination-Induced Capacity Fade

Last quarter, the team reported the difference in interfacial delamination experienced by NMC and LCO type cathodes at the cathode/solid-electrolyte interface due to their difference in partial molar volumes with respect to lithium. This quarter, the team investigated the impact of exchange current density on interfacial capacity fade experienced by NMC and LCO type cathodes while operating with solid electrolytes. The exact magnitude of exchange current density at NMC/LLZO interface as well as LCO/LLZO interface is difficult to determine using experimental procedures. In the present context, the exchange current density between cathode and LLZO has been estimated from the interfacial charge transfer resistances (R_{ct}). A correlation between exchange current density (i_0) and the charge transfer resistance can be estimated from the linearization of the Butler-Volmer equation: $i_0 = RT/(FR_{ct})$, where, R stands for universal gas constant, T indicates temperature, and F denotes Faraday's constant. Table 3 provides a list of charge transfer resistance values at NMC/LLZO and LCO/LLZO interfaces, reported by experimental researchers, and corresponding exchange current densities.

Table 3. Charge transfer resistance values at NMC/LLZO interfaces and LCO/LLZO interfaces with corresponding exchange current densities.

Type of cathode electrolyte interface	Interfacial charge transfer resistance ($\Omega \cdot cm^2$)	Exchange current density (A/m^2)	Reference
NMC/LLZO	2000	0.1284	ACS AMI (2019) 4954
LCO/LLZO	600	0.428	Chem. Mater. (2018) 6259
LCO/LLZO-Nb	170	1.51	JPS (2012) 332
LCO/LiPON	720	0.3566	JPS (2016) 342
LCO/LLZO	101	2.56	Joule (2018) 497

Please note that these exchange current densities are always affected by the presence of surface impurities, or other kinds of SEI layers. Following these experimental observations, the exchange current density at the NMC/LLZO interface has varied between 0.1 A/m^2 and 5.5 A/m^2 ; the exchange current density of LCO/LLZO interface has been altered between 0.2 A/m^2 and 2.0 A/m^2 . DFT calculations reveal that the exchange current density at NMC/LLZO interface should be around 5.5 A/m^2 . The extent of interfacial delamination, and subsequent capacity fade, at the NMC/LLZO interface and LCO/LLZO interface has been demonstrated in Figure 59a-b, respectively. Since exchange current density does not influence the magnitude of stress generation, the amount of delamination is independent of i_0 for both NMC/LLZO and LCO/LLZO interfaces. However, increasing i_0 helps to minimize the interfacial potential drop, which leads to suppression in capacity fade. Since the change in capacity fade with i_0 is substantial, the team will use the exchange current density obtained from DFT calculations, which is around 5.5 A/m^2 for NMC/LLZO interface.

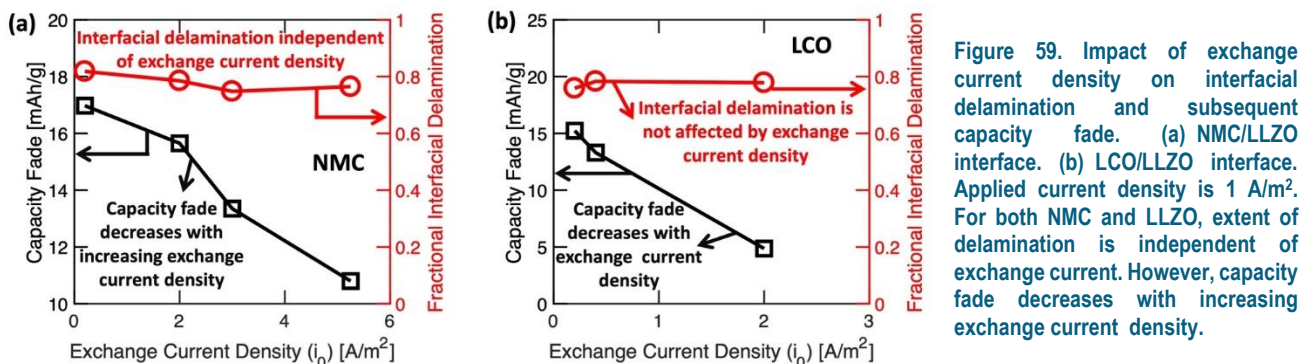


Figure 59. Impact of exchange current density on interfacial delamination and subsequent capacity fade. (a) NMC/LLZO interface. (b) LCO/LLZO interface. Applied current density is 1 A/m^2 . For both NMC and LLZO, extent of delamination is independent of exchange current. However, capacity fade decreases with increasing exchange current density.

Patents/Publications/Presentations

The project has no patents, publications, or presentations to report this quarter.

Task 3.4 – Dendrite Growth Morphology Modeling in Liquid and Solid Electrolytes (Yue Qi, Michigan State University)

Project Objective. The project goal is to develop a validated model to predict lithium dendrite morphology evolution in both liquid and solid electrolytes during electrodeposition and stripping to accelerate the adoption of Li-metal electrodes in current and emerging battery technologies. To achieve this goal, the project has four objectives: (1) formulate a general framework that captures the electrochemical-mechanical driving forces for lithium morphology evolution; (2) consider the role of the nm-thin SEI in liquid electrolytes as well as the microstructures of μm -thick solid electrolytes for lithium morphology evolution; (3) connect micron-scale phase-field models and atomic-scale DFT-based simulations via parameter- and relationship-passing to predict lithium dendrite nucleation and growth kinetics and morphology; and (4) validate the key input parameters and main conclusions of the multi-scale model as new capabilities are being developed step-by-step.

Project Impact. This atomically informed, fully coupled, electrochemical-mechanical dendrite morphology evolution model will allow the project to design the desired properties of artificial SEI coatings, the microstructure of solid electrolyte materials, and the corresponding battery operating conditions, so as to avoid dendrite growth during cycling. It will accelerate design of durable and safe lithium anodes for Li-S, Li-air, and all-solid Li-ion batteries. Thus, it directly impacts such emerging technologies that aim to meet the DOE target of the high-energy-density battery cells ($> 350 \text{ Wh/kg}$) for EV applications and to push the cost below $\$100/\text{kWh}_{\text{use}}$.

Approach. A multi-scale model approach is taken to connect micron-scale phase-field models and atomic-scale DFT-based simulations via parameter- and relationship-passing.

Out-Year Goals. The second-year goal is to establish the model to simulate metallic lithium precipitation in solid electrolytes while further developing understanding of lithium dendrite growth in liquid electrolytes. To reach this goal, mechanical and electrochemical driving forces for lithium dendrite growth in solid electrolytes will be coupled in phase-field model, while DFT is used to address the lithium plating tendency in various solid electrolyte and coating materials. Validation of the model will come from experiments to correlate the distinctive transport properties of artificial SEI layers with their impact on lithium dendrite morphology.

Collaborations. This project collaborates with UMD, Sandia National Laboratories (SNL), PNNL, University of Arkansas, and University of Houston.

Milestones

1. Determine the effect of multi-component SEI layer on dendrite morphology in a liquid electrolyte. (Q4, FY 2019; In progress)

Progress Report

DFT Prediction of Space Charges in Inhomogeneous SEI

One key inhomogeneity in the SEI is the GB. A systematic study of the electronic properties of GBs was conducted via DFT calculations. All the GBs reduced the bandgaps, and the tilt GBs reduced the bandgaps to a larger extent than the twist GBs. More detailed electronic structure and bond coordination numbers analysis was performed to understand what determines bandgap drop at GBs.

The team's previous work on the simulation of GBs in LiF and Li₂O, the main components in SEI, showed that with the same Σ values, tilt GBs decrease the corresponding bulk bandgaps to a larger extent than the twist ones. This quarter, they investigated GBs in Li₂S, which formed in SEI due to use of S-based electrolytes. Table 4 shows that the Li₂S Twist $\Sigma 3$ (111)/[111] GB led to a drop of 0.17 eV from the Li₂S bulk bandgap (3.54 eV), while the bandgap of the Li₂S Tilt $\Sigma 3$ ($\bar{1}\bar{2}\bar{1}$)/[111] GB is 2.50 eV (a 1.04 eV drop). This is consistent with the trend observed for GBs in LiF and Li₂O: the more GB atoms are less coordinated, the larger the band gap drop at the GBs. Furthermore, less coordinated GB traps more electrons.

Table 4. Density functional theory calculated bandgaps for bulk, grain boundaries, and surfaces in LiF, Li₂O, and Li₂S.

Bulk	E_g (bulk) (eV)	GB	GBE (mJ/m ²)	E_g (GB) (eV)	Surface	Υ (mJ/m ²)	E_g (surf.) (eV)
LiF	8.83	Twist $\Sigma 3$ (111)/[111]	460.62	8.58	(111)	1008.4	9.00
		Tilt $\Sigma 3$ ($\bar{1}\bar{2}\bar{1}$)/[111]	692.15	7.38	(121)	1027.0	5.13
		Twist $\Sigma 5$ (001)/[001]	571.78	7.61	(001)	299.33	6.84
		Tilt $\Sigma 5$ (310)/[001]	428.73	7.40	(310)	436.48	6.73
Li ₂ O	5.24	Twist $\Sigma 3$ (111)/[111]	632.12	4.94	(111)	513.44	2.99
		Tilt $\Sigma 3$ ($\bar{1}\bar{2}\bar{1}$)/[111]	1175.7	3.48	(121)	1175.4	2.40
Li ₂ S	3.54	Twist $\Sigma 3$ (111)/[111]	311.69	3.37	(111)	332.27	3.62
		Tilt $\Sigma 3$ ($\bar{1}\bar{2}\bar{1}$)/[111]	680.15	2.50	(121)	831.34	2.47

Due to the complexity and number of atoms involved in GB structures in some solid electrolytes, calculating the band structure of GBs was beyond the current DFT. In previous LLZO simulations, a simple linear extrapolation from the DFT-computed surface values was adopted. With the DFT-computed band gap data for both twist and tilt GBs in LiF, Li₂O, and Li₂S (Table 4), the team proposes a more accurate method to predict the GB bandgap, $E_{g,GB}$, in ionic materials from the surface and bulk bandgaps, $E_{g,bulk}$ and $E_{g,surface}$, according to

$$E_{g,GB} = \frac{d_{hkl}}{W_{GB}} [E_{g,bulk} - E_{g,surface}] + E_{g,surface} \quad (1)$$

where d_{hkl} is the distance between (hkl) planes in the bulk structure, and W_{GB} is the width of the GB structure. The W_{GB} was defined as the distance between the two planes parallel to the GB bound to the undercoordinated atoms in the GB region. The surface (hkl) has the same orientation as the planes that are parallel to the GB plane. Figure 60 shows good agreement between the predicted values and the DFT-computed values. This method allows quickly evaluating GB bandgaps, as the surface energy and bandgaps are much easier to compute with DFT.

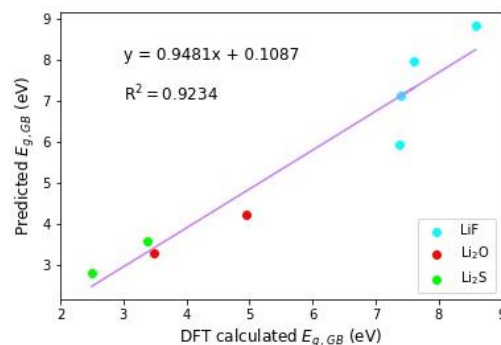


Figure 60. Fitting curve of predicted $E_{g,GB}$ (eV) versus density functional theory calculated $E_{g,GB}$ (eV).

Patents/Publications/Presentations

Presentation

- 47th Conference on the Physics & Chemistry of Surfaces & Interfaces (PCSI), Boulder, Colorado (January 19–23, 2020): “Modeling Interfaces in All-Solid-State Batteries”; Y. Qi, M. Swift, and H. K. Tian.

Task 3.5 – Modeling of Amorphous Solid-State Conductors (Gerbrand Ceder, University of California Berkeley)

Project Objective. SSBs are promising to achieve high energy density. The project objective is to determine the design principles needed to create SSEs with high Li-ion conductivity while also achieving stability against common Li-ion cathodes and Li-metal anodes.

Project Impact. The project will lead to understanding the factors that control Li-ion motion in crystalline and amorphous solids and will develop strategies to create stable interfaces against lithium metal and high-voltage cathode materials. The understanding of such processes is necessary to determine design principles to develop reliable ASSBs.

Approach. HT computation method is used to screen suitable solid electrolyte with high electrochemical stability and high ionic conductivity, by incorporating Nudged Elastic Band (NEB) and an AIMD method. Meanwhile, DFT is used to calculate bulk elastic constants of materials, surface energies, and interface decohesion energies of GBs. Thermodynamic interface stability is assessed from *ab initio* computed grand potential phase diagrams in which the lithium voltage can be controlled. Kinetic limits for solid electrolyte decomposition are assessed by topotactic lithium insertion and removal from the solid electrolyte.

Out-Year Goals. Future goals include the following: (1) gain insight into what creates high Li-ion conduction in sulfide and oxide solids, and (2) develop stable, processable solid-state conductors that can be applied in ASSBs.

Collaborations. There are no collaborative activities this quarter.

Milestones

1. Modeling of the $\text{Li}_2\text{S-P}_2\text{S}_5$ ground state phase diagram for SSEs: solid phases correctly modeled. (Q1, FY 2020; Completed)
2. Modeling of LPS lithium mobility in amorphous state with variations of PS_4 structural units. (Q2, FY 2020; Completed)
3. Develop model for the lithium conductivity in amorphous sulfide solids. (Q3, FY 2020)
4. Modeling of the full finite temperature L-S-P phase diagram to understand metastability of the highly conducting solids. (Q4, FY 2020)

Progress Report

Modeling of LPS Lithium Mobility in Amorphous State with Variations of PS₄ Structural Units

The nature of the anion building blocks of amorphous Li-P-S phase is regarded as a key descriptor for ionic conductivity in amorphous LPS solid electrolytes. These materials contain PS₄³⁻, P₂S₆⁴⁻, P₂S₇⁴⁻, and polysulfides as building blocks,^[1-2] with their ratio being determined by the composition and synthesis method. One objective has been to understand how these building blocks influence conductivity.

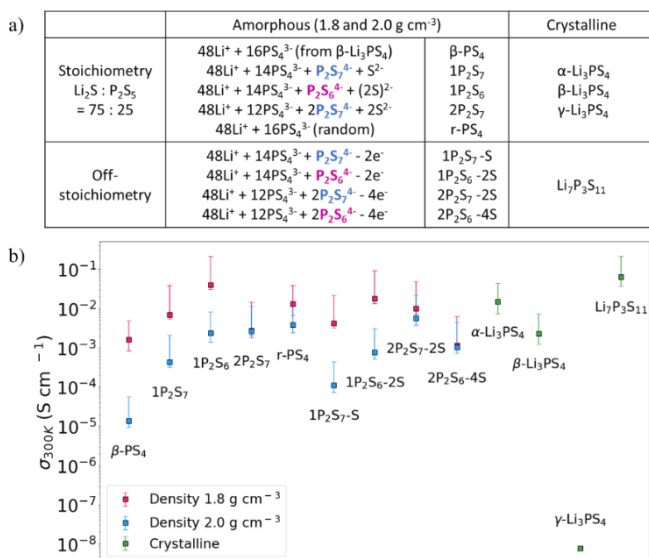


Figure 61. (a) The list of simulated phases, that is, amorphous structures with different anion ratio and representative crystalline phases. (b) The ionic conductivity extrapolated 300K for the materials in the list.

To solve this problem, the team generated amorphous structures with different ratio of building blocks, maintaining the chemical composition at Li₃PS_{4-δ}, using the AIMD-simulated melt-quench method. Figure 61a shows that two types of structures only consist of PS₄³⁻ anions, but with different position and orientation of the tetrahedra. From this structure, P₂S₆⁴⁻ or P₂S₇⁴⁻ are generated by removing two PS₄³⁻ polyanions, the stoichiometries being maintained by compensating S₂²⁻ or S²⁻ ions. To investigate the effect of free sulfur or polysulfide ions on the conductivity, the team also generates the structure without S₂²⁻ or S²⁻ ion, for which charges are compensated with additional holes. Through AIMD simulations (< 250 ps) at 5 to 7 temperatures, the conductivities at 300K are calculated for each structure in the list (Figure 61b). The conductivities of the amorphous structures with density 1.8 g·cm⁻³ are in the range of 10⁻⁴ to 10⁻² S·cm⁻¹, in good agreement with the experimental results.^[4] The conductivities of the crystalline phases also match those in the literature.^[4-5] While the simulations reproduce the experimental results, the team finds no correlation between the presence of certain anion blocks and calculated conductivities. For example, the “1P₂S₆” structure exhibits conductivity > 10⁻² S·cm⁻¹, whereas the “2P₂S₆-4S” shows a 1-order magnitude lower value. Similarly, the “2P₂S₇-2S” structure exhibits 1-order higher conductivity compared to the “2P₂S₇”. Furthermore, there is also an order of magnitude difference in conductivity between the structures only consisting of PS₄³⁻ anions, the “β-PS₄” and “r-PS₄”, with their only difference being position and orientation of tetrahedra. These results imply that there are likely other structural factors affecting ionic conductivity, rather than the existence of a certain polyanion.

References

- [1] Ohara, K., et al. *Scientific Reports* 6 (2016): 21302.
- [2] Dietrich, C., et al. *Journal of Materials Chemistry A*, 5 (2017): 18111–18119.
- [3] Klerk, N., et al. *ACS Applied Energy Materials* 1 (2018): 3230–3242.
- [4] Kudu, O., et al. *Journal of Power Sources* 407 (2018): 31–43.
- [5] Hori, S., et al. *Journal of the American Ceramic Society* 98 (2015): 3352–3360.

Patents/Publications/Presentations

The project has no patents, publications, or presentations to report this quarter.

Task 3.6 – Characterization and Modeling of Li-Metal Batteries: Force Field Theory and Lithium-Sulfur Battery Simulations (Lin-Wang Wang, Lawrence Berkeley National Laboratory)

Project Objective. The project objective is to develop force field based on *ab initio* calculations to study Li-S cathode and lithium liquid electrolyte. It also includes designs for Li-S cathode systems for high gravimetric and volumetric capacities. Lithium diffusion in both liquid electrolyte in a confined space, and in Li-S cathode systems, is a main focus of this subtask. To enable calculation of large systems, machine learning force field (ML-FF) trained on *ab initio* calculation data will also be developed. The success of this new approach will greatly expand the capability of theoretical simulation for battery systems. ML-FF can also be used in combination with traditional classical force field to deal with the nonreactive parts of the system.

Project Impact. Making the Li-S battery a commercial reality will have a major impact on society and also help to realize the VTO goal of 500 km per charge for EV. However, the nature of chemical reaction makes it different from the traditional intercalation-based Li-ion battery. The molecular nature of Li_2S_n also allows solvation in the electrolyte. To address these problems, it is essential to have fundamental studies and understandings of the underlying mechanisms. Theoretical simulations can play an important role in discovering and designing new cathode materials. However, traditional *ab initio* calculations are limited by their computational size, while the classical force field simulations are limited by their accuracy and the lack of adequate force field. The development of ML-FF can overcome these problems by bridging the size gap between the *ab initio* simulation and the real systems that need to be studied.

Approach. ML-FF will be developed by first running *ab initio* simulations, which can generate hundreds of thousands of data sets. The project has a unique capability of decomposing the total energy of a DFT calculation into the energy of each atom. Compared to conventional DFT calculations, this increases the number of data by hundreds of times, an important requirement for ML model training. The dependence of the atomic energy to the local atomic bonding environment will be captured using ML methods. Three ML approaches will be: linear fitting, neural network model, and Gaussian process regression (GPR) model. The team will compare the efficacies of these models. Meanwhile, they will also deal with the long-range Coulomb interactions existing in the electrolyte system and the ionic species in liquid electrolyte. The idea is to first fit the charge density of the system, and remove the long-range electrostatic energy before the fitting of the local energy on each atom. The team will also design new Li-S and Na-S cathode materials. In particular, they will design an amorphous Li-S mixture, with other materials such as carbon nanotube (CNT), black carbon, or electric conductive 2D materials).

Out-Year Goals. In outgoing years, the project will further develop computational methods for more accurate entropy and interaction energy calculations for the electrolyte, as well as for Li-S cathode systems.

Collaborations. The project will collaborate with G. Liu and Y. Cui for cathode design. It has also collaborated with Prof. F. Pan of Beijing University for lithium battery research in general.

Milestones

1. New Li-S design, mixing Li-S with CNT for an ultrafine mixture. (Q1, FY 2020; Partly completed)
2. Lithium charge density fitting in electrolyte, to fit the long-range Coulomb interaction. (Q2, FY 2020; Initiated)
3. Incorporation of Coulomb interaction in the local energy calculation; ML-FF fitting. (Q3, FY 2020)
4. Further study of Li-S cathode with polymer, to study electric conductivity in such a system. (Q4, FY 2020)

Progress Report

The team has proposed a practical approach to utilize the conduction materials, poly (2-vinyl, 1, 4-phenylene sulfide), via vulcanization as a Li-S cathode. Such an approach is to address the issue of conductivity, low sulfur content, and short cycling performance in conventional polymer as cathode. This theoretical investigation aims to answer fundamental questions in such designs, including the limit of gravimetric and specific capacities, the structure stability, and electronic conductivity in such systems. They have made several observations, as described here. (1) The unsaturated C=C bonds in the edge are the most active sites for vulcanization via crosslinking. (2) Substituting one hydrogen of poly (1, 4-phenylene sulfide) with the vinyl group, the simplest sulfur vulcanization sites with edge C=C bond, has almost no influence on the conductivity of the backbone. (3) The most stable sulfur chains for vulcanization on the polymer are S₆*. (4) The sulfur content obtained in this approach is extremely high: if a third of the vinyl groups are vulcanization, the sulfur content is 49% in weight. The value can reach to 69% while all vinyl groups are vulcanization. (5) During the lithiation process, the lithium atoms break down all the S-S bonds to gradually form Li_xS_τ clusters. However, the Li_xS_τ clusters are restricted by the polymers via the strong covalent C-S bonds, which suppress polysulfides shuttling phenomena effectively. (6) These polymer cathodes exhibit a unique redox process with only one discharge voltage plateau, which corresponds to the single discharge product Li₂S. (7) The maximum specific capacity and gravimetric energy densities for crosslinking polymers are 672 mAh/g and 1018 Wh/kg, respectively, more than twice the state-of-the-art Li-S value obtained by OXIS Energy Ltd (450 Wh/kg). (8) Dissolution energies in the crosslinking polymer case are positive throughout the discharge process, indicating that the crosslinking polymer can restrict the shuttling effect efficiently during the entire discharge process. This means, overall, that such conductive polymer substituted via vinyl group for vulcanization can be effective as Li-S cathode.

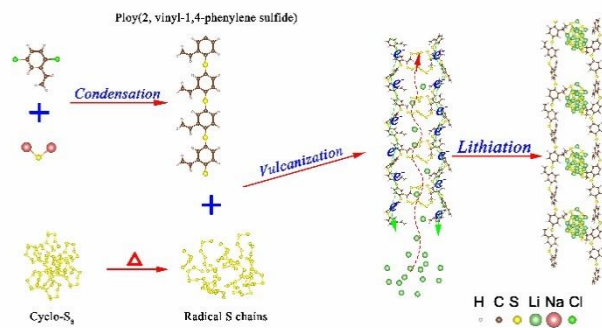


Figure 62. Schematic illustration of preparation of Li-S cathode with poly (2-vinyl, 1, 4-phenylene sulfide).

The team has also collaborated with R. Kostecki's group to understand the function of the partly swellable block-copolymer as a binder for Li-S batteries. They synthesized block-copolymers consisting of both ethylene oxide unit and styrene unit, and it is utilized as binder for Li-S batteries. The improved electrochemical performance is attributed to the synergistic effects contributed by different units of block-copolymer. Based on DFT calculation, the team finds that the ethylene oxide unit is able to trap polysulfides that strongly bond with the intermediate lithium polysulfide, and enhance the transport of lithium ions to reach high capacity. The adsorption energy of lithium polysulfide is much stronger than that on PVDF by 2.2 to 3.2 times. Meanwhile, the styrene unit plays the role of maintaining cathode integrity by promoting the mechanical properties and elasticity of the constructed block copolymer needed to accommodate the large volume changes. The optimized ethylene and styrene ratio is 2:1 for the best mechanical properties.

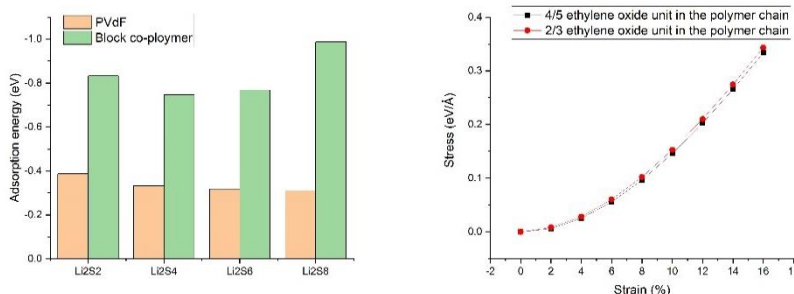


Figure 63. (a) Adsorption energy of lithium polysulfide on PVDF and block co-polymer. (b) Mechanical properties of co-polymer with different ethylene ratio.

Patents/Publications/Presentations

Publications

- Zhou, G., A. Yang, G. Gao, X. Yu, J. Xu, C. Liu, Y. Ye, A. Pei, Y. Wu, Y. Peng, Y. Li, Z. Yang, K. Liu, L. W. Wang, and Y. Cui. “Super-Cooled Liquid Sulfur Maintained in Three-Dimensional Current Collector for High-Performance Li-S Batteries.” *Science Advances* 6, no. 21 (2020). eaay5098.
- Gao, G., F. Zheng, and L. Wang. “Design via Stacking 2D Conductive Microporous Coordination Polymers and Amorphous Li-S Layers.” *Chemistry of Materials* 32, no. 5 (2020): 1974–1982.

Task 3.7 – *In Situ* and *Operando* Thermal Diagnostics of Buried Interfaces in Beyond Lithium-Ion Cells (Ravi Prasher, Lawrence Berkeley National Laboratory)

Project Objective. Transport at various interfaces in *beyond lithium ion* cells will play a major role in electrochemical performance and reliability. It has not yet been possible to thermally profile a Li-metal cell during operation to provide a spatially resolved map of thermal transport properties throughout the cell. The objective of this research is to create a metrology capable of spatially resolved *in operando* thermal property profiling, and then relate thermal property to the quality of electrodes and interfaces, and use the developed thermal metrology to understand electrochemical processes in Li-metal batteries such as dendrite growth, interface kinetics, and ionic transport.

Project Impact. Characterizing electrochemical processes in Li-metal cells such as lithium deposition and dendrite growth at interfaces is of great significance for understanding and enhancing their electrochemical performance and reliability. *In situ* and *operando* 3-omega micro thermal sensors can provide significant information regarding the impact of buried interfaces as a function of time, material, voltage, current, and temperature, etc. Therefore, it is important to develop *operando* 3-omega micro thermal sensors and develop models relating those signals to electrochemical performance for *beyond lithium ion* cells. The physics-based model relating thermal and electrochemical properties based on these measurements can facilitate future design of Li-metal batteries.

Approach. To accomplish project goals, the team will utilize an in-house adapted 3-omega technique to probe thermal properties of a Li-metal cell while it is in operation, without affecting the operation of the cell. The 3-omega sensors will be deposited and fabricated on Li-metal cells based on previous learning on 3-omega sensor fabrication. The characteristic depth of the thermally probed region is defined by the wave's "thermal penetration depth," $\delta_p = \sqrt{D/2\omega}$, where D is the sample's thermal diffusivity, and 2ω is the heating frequency of the thermal wave. By depositing the project's 3ω sensors on the battery's outer surface and adjusting ω , the team controls δ_p to span the full range from the top to the bottom layer, thereby noninvasively probing the thermal transport in subsurface layers and interfaces within the bulk of the battery. Thermal transport can be related to quality of the interface. By doing concurrent thermal transport and electrochemical performance measurements, the team plans to relate thermal transport to electrochemical performance. As frequency based thermal measurement techniques provide excellent spatial resolution within the cell, the team also plans to study heat generation at the electrolyte – Li-metal interface and relate the thermal signals to the interface kinetics and ionic transport. The frequency dependence of heat generated due to transport resistance is different from that due to kinetic resistance. The team plans to utilize this difference to separate the contributions of kinetic and transport resistance at the interface, which will enable understanding of interface kinetics and transport at the Li-metal – SSE interface.

Out-Year Goals. In outgoing years, the project will design, build, and implement the adapted 3-omega metrology to examine thermal properties and a general frequency dependent thermal metrology to examine heat generation. This will involve developing and testing the metrology itself along with accompanying theory, designing compatible battery samples, and applying the technique to live cells. The team will measure thermal transport properties of battery materials provided by collaborators. Combined with the electrochemical performance measurement, this will provide significant information relating the thermal signal to the electrochemical process.

Collaborations. This project collaborates with two LBNL groups: V. Battaglia's for cell assembly for 3-omega studies, and R. Kostecki's for pristine battery active material growths for studies of thermal signals related to electrochemical process.

Milestones

1. Design pristine samples to be compatible with 3-omega and ambient environments. (Q1, FY 2020; Completed)
2. Perform sensitivity analysis and pristine sample design optimization to maximize measurement sensitivity to thermal interfaces. (Q2, FY 2020; In progress)
3. Fabrication of bi-layer pristine samples to experimentally isolate different kinds of interfaces. (Q3, FY 2020)
4. Thermal measurements of battery composites made from various materials. (Q4, FY 2020)

Progress Report

The Prasher group is building *operando* 3ω micro thermal sensors and developing models relating thermal signals to electrochemical performance for *beyond lithium ion* cells. The anode-side 3ω sensor will be used to probe thermal properties of Li-metal anode and related interfaces. The group is also developing a general frequency-based thermal metrology to probe interface kinetics and transport.

Last quarter, the team performed sensitivity analyses for the anode-side 3ω measurement of thermal properties of Li-metal anode and interfaces and proposed use of the thermal interface resistance as a measure of morphology of lithium at the interface. For lithium symmetric cells using solid electrolyte LLZO, Figure 64b shows that the 3ω signal is sensitive to the thermal boundary resistance between lithium metal and LLZO, and the peak sensitivity around 1-10 Hz is ~ 0.1 . This quarter, the team has developed the 3ω sensors for the symmetric cells (Figure 65a) and has performed a symmetric cell assembly with the 3ω sensors. Further, they obtained the thermal properties of the electrolyte (LLZO) using 3ω . From the curve fit with the theoretical model for 3ω (Figure 65c), the specific heat and thermal conductivity of LLZO were obtained to be 500 J/kgK and 1.33 W/mK, respectively.

In combination with *ex situ* thermal measurement of lithium anode, it is possible to measure the thermal boundary resistance and characterize the contact between lithium metal and LLZO by thermal measurements. Further, this can be potentially applied to understand how the contact varies with temperature and pressure, which are two factors broadly used to modulate lithium dendrite growth in Li-metal batteries.

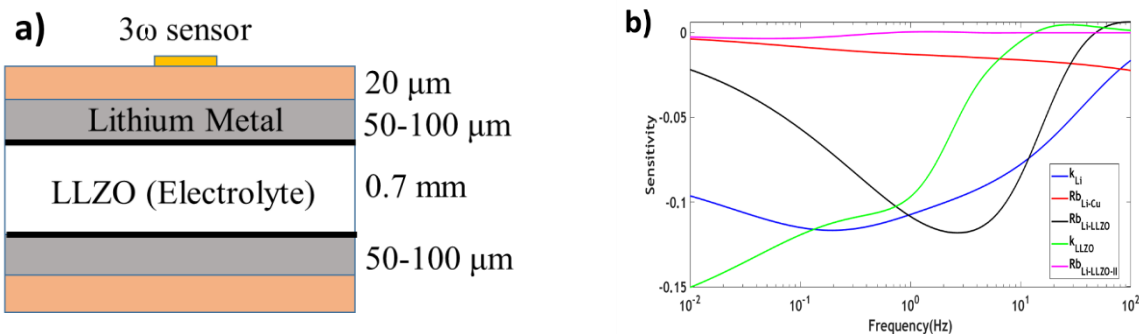


Figure 64. (a) 3ω sensor for analysis of lithium symmetric cell based on thermal signal. (b) Sensitivity analysis of symmetric cells with 100- μm Li-metal anode assuming $R_{b\text{Li-LLZO}} = 3 \times 10^{-5} \text{ m}^2\text{K/W}$.



Figure 65. 3ω sensor used for (a) anode of the lithium symmetric cell and (b) LLZO pellet. (c) 3ω curve-fit for LLZO.

Additionally, frequency-based thermal metrology can be used to study heat generation and accompanying electrochemical processes. One possible application of such a technique is separating the contributions of kinetic resistance and ionic transport resistance at the electrolyte-electrode interface. Conventional electrochemical methods that show a voltage drop at the interface cannot tell whether it is caused by the kinetic resistance or the transport resistance. However, as the heat generation in these processes are of a different nature, specifically dictated by Tafel Kinetics and Ohmic loss, the frequency dependence of heat generation is different for the two processes. For a current driven at a frequency ω , Ohmic loss produces heat at 2ω , whereas kinetic loss produces heat at 4ω and 2ω . Therefore, by looking at the 4ω and 2ω thermal signals, the team can exclusively separate kinetic and transport overpotential. They have completed the theoretical formulation and sensitivity analysis for this frequency-dependent heat generation method, and will develop thermal sensors and instrumentation next quarter. Figure 66a-b shows the sensitivity for 4ω and 2ω signals, respectively. It can be seen that by operating at a frequency greater than 1 Hz, the thermal signal can be sensitive to heat generated from the interface, which allows understanding the kinetic and transport overpotential at the interface.

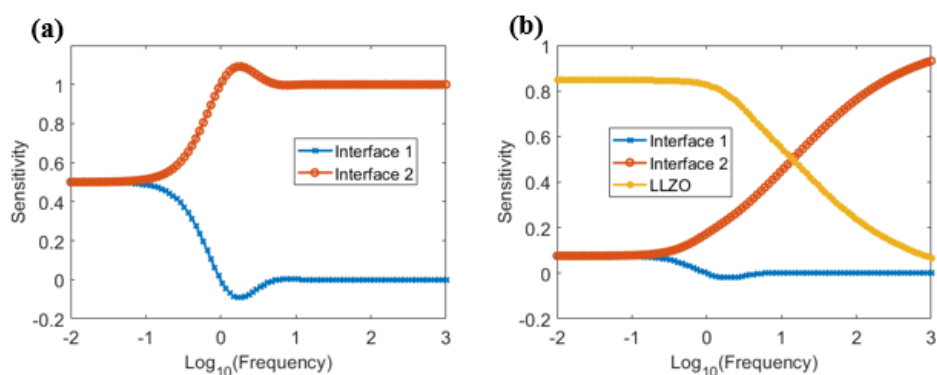


Figure 66. (a) 4ω sensitivity and (b) 2ω sensitivity for heat generated at the Li-Electrolyte interface of a symmetric Li-LLZO cell. Both 4ω and 2ω signals are the most sensitive to the interface while operating at a frequency greater than 1 Hz.

Patents/Publications/Presentations

Publication

- Lubner, S. D., S. Kaur, Y. Fu, V. Battaglia, and R. S. Prasher. “Identification and Characterization of the Dominant Thermal Resistance in Lithium-Ion Batteries using *Operando* 3-Omega Sensors.” *Journal of Applied Physics* 127, no. 10 (2020): 105104.

Task 3.8 – Multi-Scale Modeling of Solid-State Electrolytes for Next-Generation Lithium Batteries (Anh Ngo, Larry A. Curtiss, and Venkat Srinivasan, Argonne National Laboratory)

Project Objective. This project is part of a multi-scale modeling effort to obtain an in-depth understanding of the interaction of the electrode and the solid electrolyte aimed at developing highly efficient SSE batteries for vehicle applications. Input parameters needed for mesoscale (continuum) level calculations are being obtained from atomistic calculations including DFT and classical MD simulations. This atomistic input will enable a multi-scale computational procedure for SSEs that is capable of successfully capturing the physicochemical aspects during charge and discharge process including lithium transport mechanisms, interfacial phenomena during the insertion and extraction of lithium ions, and mechanical deformation of SSE.

Project Impact. A major safety concern experienced with commercially available Li-ion batteries under some scenarios is leakage of the liquid electrolyte, which can potentially catch fire. Replacement of the liquid electrolyte is necessary to decrease the fire hazard and improve safety associated with present-day Li-ion batteries. In addition, use of solid electrolytes provides a path to prevent dendrites in Li-metal anodes, thereby leading to batteries with significantly higher energy density. The impact of this project will be to help in development of good SSEs as a replacement for the commercially used organic liquid electrolytes to improve safety and energy density in Li-ion batteries.

Approach. Parameters needed for mesoscale modeling of grain interior (GI), GB, and electrode-electrolyte interface will be calculated by DFT-based calculations along with Monte Carlo (MC) and MD simulations. The calculations will be used to determine properties of the electrode with the solid electrolyte as well as in GB regions of the solid electrolyte. This will include calculations of structure, stability, ionic conductivity, Young's modulus, fracture toughness, exchange current density, and other properties.

Out-Year Goals. The out-year goals of this work are to calculate other properties such as fracture toughness and include other SSEs and coatings in the multi-scale modeling.

Collaborations. This project collaborates with Y. Cui at Stanford.

Milestones

1. Determine the most stable interface between LLZO solid electrolyte and lithium borate carbonate (LBCO) coating material. Calculate the activation energy barrier between LLZO and LBCO coating materials. (Q1, FY 2020; Completed)
2. Determine the most stable interface between NMC cathode and LBCO coating material, and calculate the activation energy barrier. (Q2, FY 2020; Completed)
3. Evaluate the exchange current density associated with charge transfer from LBCO coating to NMC cathode and LLZO solid electrolyte. (Q3, FY 2020; Initiated)
4. Incorporate the information obtained from the atomistic calculations into the mesoscale model, and predict the impact of coating on performance. (Q4, FY 2020; Initiated)

Progress Report

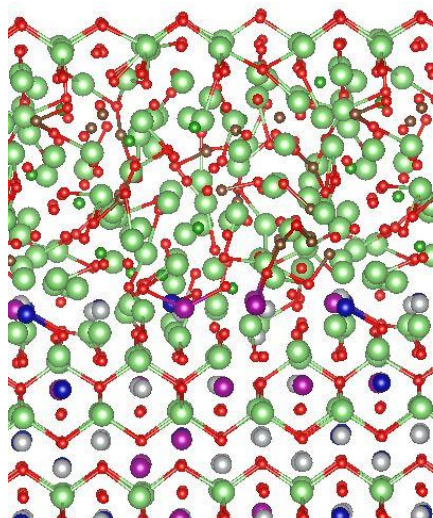


Figure 67. A snapshot of the optimized interface between NMC and LBCO.

The use of ceramic solid electrolytes to create ASSBs can enable the use of lithium metal by preventing propagation of lithium dendrites, therefore enhancing safety and decreasing capacity fade. The interfaces between the cathode and solid electrolyte must be stable to enable use of these materials in batteries. Multi-scale modeling can provide insight into the mechanism for dendrite growth and other instabilities for guidance into how to prevent them. Mesoscale (continuum) modeling requires atomistic level input from theory or experiment to accurately capture physicochemical aspects during charge and discharge processes. LBCO is an interesting compound that can be used as a coating material for stabilizing the cathode / solid electrolyte interface. The chemical composition of LBCO is given as $\text{Li}_{2.3}\text{B}_{0.3}\text{C}_{0.7}\text{O}_3$, and it is manufactured either by a solid-state reaction between Li_3BO_3 and Li_2CO_3 , or by atomic layer deposition (ALD) techniques that lead to formation of amorphous LBCO. In general, LBCO demonstrates decent ionic conductivity, around 10^{-5} S/cm, single-ion-conducting behavior, high electrochemical stability with lithium (~ 0.1 V to 6 V), and extremely low interfacial impedance against lithium,

around $5 \Omega\text{-cm}^2$. All these properties indicate that incorporation of a thin layer of LBCO between the cathode and LLZO solid electrolyte may not hamper the electrochemical performance substantially. LBCO is a better choice as a cathode coating material than LBO, because LBCO demonstrates higher ionic conductivity than LBO. Lithium carbonate can form on top of LLZO and cathode particles due to reaction with moisture and carbon dioxide from air. It is well known that Li_2CO_3 demonstrates extremely high resistance to transport of lithium. LBCO can easily form a solid solution with Li_2CO_3 due to the iso-structural lattice configuration, and can remove the resistive Li-carbonate layer from the surface of the cathode and electrolyte particles and effectively reduce interfacial impedance. However, the lithium ion transport mechanism between LLZO/LBCO and LBCO/cathode is not well understood. Delamination between the cathode and solid electrolyte, and subsequent capacity fade, have been reported with LBCO as the coating material. Hence, further study is required to better understand the interfacial properties of LBCO with the cathode and solid electrolyte materials.

To understand the transport mechanism at the interface of NMC electrode and LBCO, it is important to determine the various physical and chemical properties and reaction kinetics at the interface. The team has conducted *ab initio* density functional calculations on the amorphous LBCO and interfaces with NMC cathode. They investigated the surfaces of NMC-622 (10-14), which are known to be the most stable surfaces and in previous literature reported to provide apparent Li-ion conduction paths. The interfacial supercell between NMC-622 cathode and amorphous LBCO was constructed. The lattice mismatch between two materials is $\sim 11.19\%$ mean absolute strain.

Stability of the interface between amorphous LBCO and the lowest energy NMC-622 (10-14) was investigated with AIMD simulations. All production runs of AIMD trajectories were obtained after 5 ps of thermal equilibration. The team then carried out calculations for the barrier of lithium cation migration from the LBCO layer into the NMC-622 (10-14) to determine the Li-ion transport using DFT. The energy barrier obtained from DFT is around 0.6 eV.

The team is working on calculating the interfacial formation binding energy of the interfaces between NMC and LBCO as well as calculating the current density. The results will be used as input for continuum mechanism calculations.

Patents/Publications/Presentations

Publications

- Barai, P., K. Higa, A. T. Ngo, L. A. Curtiss, and V. Srinivasan. “Mechanical Stress Induced Current Focusing and Fracture in Grain Boundaries.” *Journal of The Electrochemical Society* 166, no. 10 (2019): A1752–A1762.
- Barai, P., A. T. Ngo, B. Narayanan, K. Higa, L. A. Curtiss, and V. Srinivasan. “Multiscale Modeling of Current Focusing and Dendrite Growth at Lithium/LLZO Interface.” Submitted.
- Barai, P., T. Rojas, A. T. Ngo, L. A. Curtiss, and V. Srinivasan. “Investigation of Delamination Induced Performance Decay at the Cathode/LLZO Interface.” Pending submission.

Task 3.9 – Integrated Multi-Scale Modeling for Design of Robust 3D Solid-State Lithium Batteries (Brandon Wood, Lawrence Livermore National Laboratory)

Project Objective. This project will develop a multi-scale, multi-physics modeling framework for probing the effects of materials microstructure and device architecture on ion transport within 3D ceramic SSB materials, with the goal of enhancing performance and reliability. The project has three primary objectives: (1) integrate multi-physics and multi-scale model components; (2) understand interface- and microstructure-derived limitations on ion transport; and (3) derive key structure-performance relations for enabling future optimization.

Project Impact. This project will lead to understanding interfacial losses and instabilities that impede performance and promote failure of SSBs. The multi-scale and multi-physics modeling framework developed in this work will address shortcomings of existing modeling strategies that either lack coupling of the multi-physics nature of various processes active in 3D batteries or fail to incorporate processes at different length scales to understand function. Ultimately, the tools and understanding generated by this project can be utilized to realize optimization of interface-dominated 3D batteries.

Approach. The project approach integrates simulations at three scales to predict ion transport limitations within the ceramic SSE LLZO, as well as across the interface between LLZO and LiCoO_2 (LCO) cathodes. A particular focus is on understanding the effects of microstructures and architectures resulting from processing of 3D SSBs as well as their mechanical and chemical evolution at different stages of cycling. First-principles and classical MD simulations are used to compute fundamental Li-ion diffusion within bulk solid electrolyte and cathode materials, along/across GBs of the electrolyte, and along/across electrolyte/cathode interfaces. Next, phase-field simulations are used to generate digital representation of realistic microstructures of the materials, which are combined with the atomistic simulation results to parameterize mesoscale effective property calculations and to establish microstructure-property relationships for ion transport. Finally, these relationships inform a cell-level macroscopic electro-chemo-mechanical modeling framework, which can be used to optimize performance of ceramic 3D SSLBs based on LLZO solid electrolytes.

Out-Year Goals. Future activities will focus on refining the project's atomistic interface models for improved fidelity of ion transport simulations through crystalline and amorphous LLZO and across interfaces. The team will also work with collaboration partners to reconstruct microstructures of 3D-printed materials and apply them to determine effective stresses and ion transport through the polycrystalline materials.

Collaborations. This project collaborates with Dr. N. Adelstein from San Francisco State University (SFSU, atomistic diffusion modeling) and Dr. Ye from LLNL (3D printing of SSB materials). They also partner with Drs. T. Danner and A. Latz from Deutsches Zentrum für Luft- und Raumfahrt (DLR), Dr. E. Ivers-Tiffée from Karlsruhe Institute of Technology (KIT, impedance spectroscopy of SSEs), Dr. P. Zapol from ANL (modeling of solute segregation in LLZO), and Prof. D. Fattakhova-Rohlfing from Forschungszentrum Jülich (FZJ, controlled synthesis of LLZO with varying densities and microstructures) as part of the U. S.–Germany partnership on SSB research.

Milestones

1. Construct models of solid-solid LCO/LLZO interface. (Q1, FY 2020; Completed)
2. Perform phase-field simulation to reproduce 3D-printed microstructure of LLZO and LCO. (Q2, FY 2020; Completed)
3. Perform AIMD of LCO/LLZO interface model to determine interdiffusion. (Q3, FY 2020; In progress)
4. Quantify threshold grain/pore size that eliminates Griffith-criterion hotspots based on computed internal stress in polycrystalline LLZO. (Q4, FY 2020; On schedule)

Progress Report

Mesoscale Modeling of Lithium Transport through Complex Microstructures. Last quarter, the team demonstrated that the project’s parameterized mesoscale model for computing effective ionic conductivity of a polycrystalline LLZO microstructure could effectively predict the key transition temperature between bulk grain- and GB-dominated ion conduction. The model incorporates microstructural parameters both at the atomistic scale—via GB properties—and at the mesoscale—via grain structure and morphology. This quarter, they used the model to complete analysis of microstructural effects on ionic conductivity by creating a “designability map,” which was incorporated into a manuscript as a way of connecting the predictions to actual 3D microstructures and processing conditions. This map, shown in Figure 68, illustrates the quantitative impact of the atomistic and mesoscale microstructural parameters on critical temperature, which is one way of quantifying the ionic conduction mechanism. The team is discussing how to integrate these results with those of their German collaborators at DLR, who have been developing an analogous methodology based on a finite-element approach.

The team notes that the wide range of the parameter space for grain size and GB width (Figure 68a) may cover the large potential variability of 3D-printed microstructural features. In addition to those two topological features, they also explored the impact of grain shape to account for possible morphological control by the printing and thermal processing conditions. Figure 68b compares the anisotropy in computed diffusion properties for two limiting cases of grain morphology that the team generated (see inset images in the figure) using phase-field simulations. The equiaxed grain structure exhibits isotropic effective diffusion (that is, $D_x^{eff}/D_y^{eff} \sim 1$) over the entire temperature range, whereas effective diffusion through the columnar grain structure is anisotropic. The team’s calculations also captured temperature-dependent anisotropy of the effective diffusivity in the columnar grain structure.

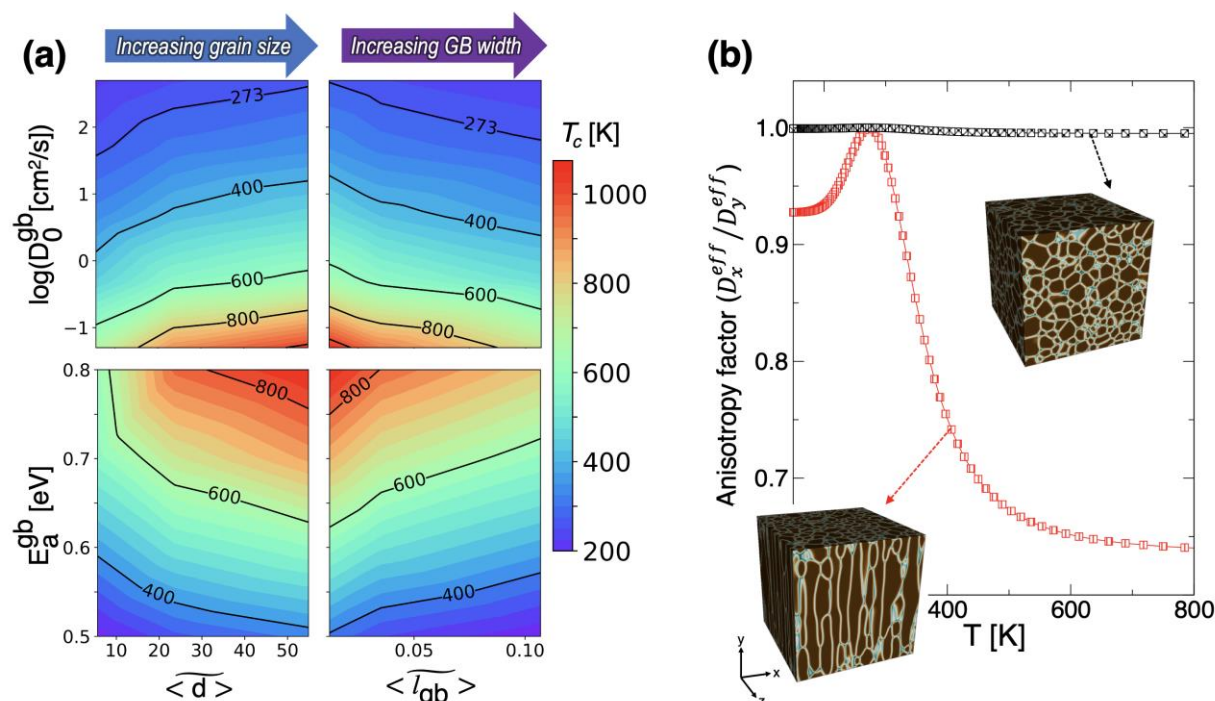


Figure 68. (a) Designability map of the critical temperature T_{crit} that determines the transition between bulk grain- and grain boundary-dominated ion conduction, based on engineering mesoscopic and atomistic microstructural features of polycrystalline LLZO. T_{crit} is shown as a function of varying atomistic grain boundary diffusive prefactor and activation energy (D_0^{gb} , E_a^{gb}), as well as mesoscale grain size and grain boundary width ($\langle d \rangle$, $\langle l_{gb} \rangle$). (b) Computed anisotropy factor (D_x^{eff}/D_y^{eff}) as a function of temperature for the two grain structures with different grain shapes.

Atomistic Simulations of LCO/LLZO Interfaces. Last quarter, the team created various LLZO|LCO interfaces to investigate interdiffusion across the interface through AIMD runs. This quarter, they report initial findings on interdiffusion behavior observed for LLZO (001) | LCO (100) interface. To understand the effect of lithium concentration at the interface, they ran simulations at two different interfacial lithium chemical potentials, representing the limits of full lithiation and full delithiation of the cathode. In both cases, the solid electrolyte shows evidence of significant restructuring. By tracking variation in the linear atomic densities along the direction normal to the interface cross-section, they can also gain insights into the interdiffusion of atomic species. Figure 69 shows variation of all the metal ions (lithium, lanthanum, zirconium, and cobalt) across the interface at the Li-rich limit. Both lithium and zirconium show evidence of migration toward the interface region from the bulk LLZO. Although the team cautions that the limited timescales prevent observation of equilibrium interface structures, they plan to conduct a careful analysis of variation in the local coordination of metal ions with oxygen within the interface region to look for evidence of precursors that can guide the next stage of model development for the interface region. Compared to the Li-poor interface, the Li-poor interface shows a more pronounced presence of lanthanum, cobalt, and zirconium ions at the interface, possibly because the initial surface has greater concentration of lanthanum and zirconium; however, these atomic species also appear to be overall less mobile. The team concludes that the Li-poor interface seems to be more stable overall than the Li-rich interface, which carries possible implications for understanding cycling behavior. They will continue to evaluate atomic density variation across other LLZO|LCO interfaces, while also evaluating the change in local coordination within the interface regions to gain further insight into interface evolution and impacts on transport.

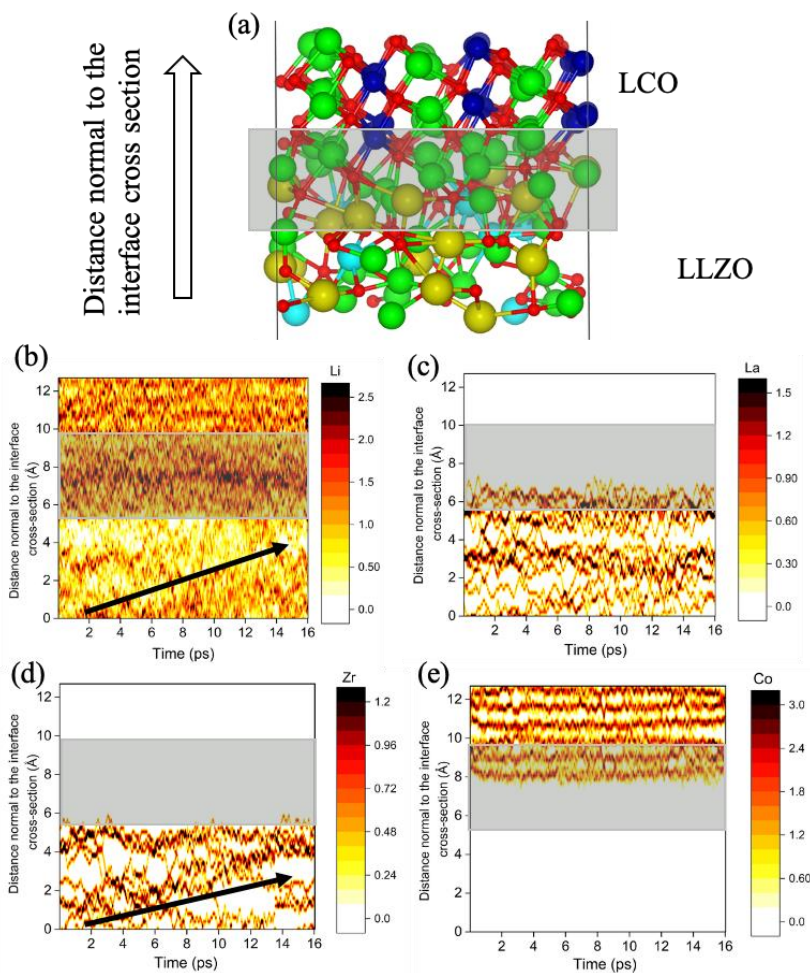


Figure 69. (a) Interfacial structure (Region 1: Li-rich) of LCO (100) / LLZO (001) from *ab initio* molecular dynamics (AIMD) simulations. The green, blue, yellow, cyan, and red spheres represent lithium, cobalt, lanthanum, zirconium, and oxygen in the LCO/LLZO structures, respectively. (b-e) Plots showing variation in linear atomic densities (along the direction normal to the interface cross-section) of lithium, lanthanum, zirconium, and cobalt, respectively, for the AIMD runs.

Modeling of Microstructural Effects on EIS. Traditionally, experimentally obtained EIS curves are fit to equivalent circuits with lumped resistors, capacitors, and complex impedances to characterize the bulk and interfacial impedances originating from key electrochemical processes such as ion transport and interfacial reactions. However, this limits the ability to directly connect information from lower-length scale simulations to macroscopic observables. Accordingly, last quarter, the team reported initiation of a physics-based model to understand microstructural impacts on EIS with an objective to inform microstructure design of solid electrolytes. This quarter, they extend the proof-of-concept model to polycrystalline microstructures, and to analyze the underlying heterogeneous electric field, the effects of grain size and GB width, and position-dependent ionic conductivity and permittivity on the shape of EIS curve. The model is being explored for further validation by the project’s German collaborators at DLR. One priority will be integration of electrical space-charge effects, which has been a focus of the German effort and will enable full chemo-electro-mechanical coupling of interfacial ion transport within EIS simulations.

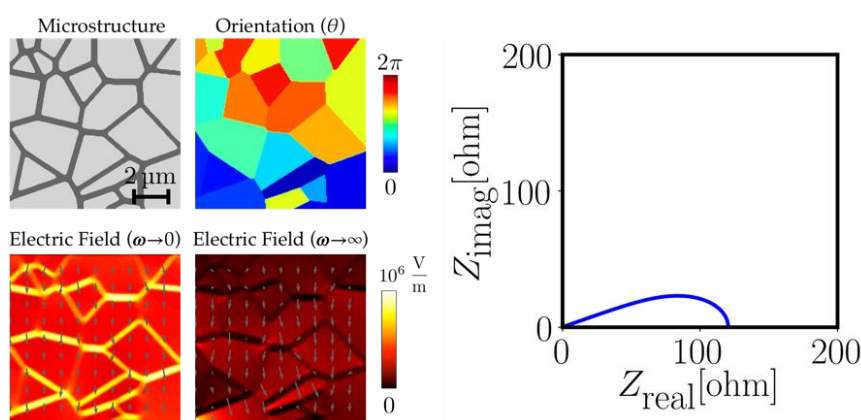


Figure 70. Demonstration of an electrochemical impedance spectroscopy of a model polycrystalline sample. Grain boundary width is proportional to the misorientation between the adjacent grains. A sinusoidally varying voltage, with a varying frequency (0 to 108 Hz), is applied on the top edge; the bottom edge remains electrically grounded. The grain boundaries perpendicular to the direction of the current show maximum electric field and contribute most to overall impedance at low frequencies, while the grains contribute most at high frequencies.

Patents/Publications/Presentations

Publication

- Heo, T. W., A. Grieder, B. Wang, S. A. Akhade, L. F. Wan, L-Q. Chen, N. Adelstein, and B. C. Wood. “Microstructural Impacts on the Ionic Conductivity of Garnet Solid Electrolytes: A Combined Atomistic-Mesoscale Approach.” Manuscript in preparation.

Presentations

- Chicheley, United Kingdom (scheduled for March 2020): “Paradigms of Structural, Chemical, and Dynamical Frustration in Superionic Conductors”; B. C. Wood. Invited talk – canceled due to COVID-19.
- Gordon Research Conference on Batteries, Ventura, California (February 2020): “Microstructural Effects on Electrochemical Impedance Spectroscopy”; A. Jana, T. W. Heo, M. Wood, J. Ye, L. Wan, and B. C. Wood.

Task 3.10 – First-Principles Modeling of Cluster-Based Solid Electrolytes (Puru Jena, Virginia Commonwealth University)

Project Objective. The objective of the project is to use cluster-ions, which are stable atomic clusters that mimic the chemistry of individual atoms, as the building blocks of new solid electrolytes and the corresponding battery system. The advantages of using cluster-ions to replace elemental ions is that the size, shape, and composition of the former can be tailored to achieve higher superionic conductivity, electrochemical stability, and charge transfer across the solid-solid interfaces than the conventional materials. More specifically, the goal is to develop superior solid electrolytes based on cluster-ions and to model these solid electrolytes and their interfaces with electrodes, especially with the Li-metal anode, for successful integration into high-performance SSBs for EVs. Compared to conventional solid electrolytes, the team will model and screen cluster-based solid electrolytes that have low activation energies, practical room-temperature ionic conductivities, wide electrochemical stability windows, and desired mechanical properties that, for example, can inhibit the Li-metal anode dendrite growth. They will provide a fundamental understanding of the ionic conduction mechanism in the newly developed, cluster-based solid electrolytes and identify means to further improve their property metrics via chemical and defect engineering. The team will model the interfacial properties, such as the structural, chemical, electrochemical, and ion/charge transfer properties, between the cluster-based solid electrolytes and electrodes at the atomic level, as well as find the interfacial coating materials with desired properties. Based on accumulated data from modeling, they will establish links between the basic parameters of the cluster-ions and the bulk/interface properties, which can directly guide experiments. Meanwhile, the team will work closely with experimentalists in the BMR Program to complement the project’s theoretical efforts and to guide them in focused development of the predicted cluster-based solid electrolytes and the interfaces.

Project Impact. The proposed project will open a new avenue for guiding experiments in the synthesis of SSBs equipped with cluster-based solid electrolytes and capable of operating over a wide temperature range. Modeling and understanding of the ionic conduction of cluster-based electrolytes and their interfacial properties with electrodes, especially with Li-metal anode, will enrich current battery science and also train the future work force in SSB development for next-generation EVs by supporting postdoctoral fellows.

Approach. This project will employ multi-scale theoretical methods and computational techniques.

Out-Year Goals. The out-year goals involve modeling development of new cluster-based solid electrolyte materials and database.

Collaborations. The team is working with Dr. J. Nanda of ORNL on antiperovskite-based SSEs.

Milestones

1. Structural studies of the designed cluster-based solid electrolyte materials with selected cluster-ions. (Q1, FY 2020; Completed, December 31, 2019)
2. Property characterizations of stable cluster-based solid electrolyte materials. (Q2, FY 2020; Completed, March 31, 2020)
3. Ionic conductivity characterization for cluster-based solid electrolyte materials and the ionic conduction mechanism. (Q3, FY 2020; In progress)
4. Complete development of new cluster-based solid electrolyte materials with a database. (Q4, FY 2020)

Progress Report

The milestone for this quarter was completed. The team has calculated the phonons and electronic structures of the newly developed cluster-based solid electrolyte materials, based on the low-energy structures obtained from the structural search last quarter. For each material, they have found the cell size that contains the right number of formula units to make the periodic structure lattice-dynamically stable. The reasons to study the phonons of each material are twofold. One, as mentioned, is to find the structure that is lattice-dynamically stable. The other is that, according to previous studies, certain atomic vibrational modes, especially those corresponding to motion of cluster-ions as near rigid bodies, are relevant to the ionic conductivity of the material. The team is looking for two major properties in the study of electronic structures. One is the bandgap of each material. Solid electrolytes should not be good electric conductors. The bandgap can be one measurement for electrochemical stability of the material, although it is common that the SEI formed between the electrolyte and electrode will determine the real value of the electrochemical stability window. The other property is the elemental composition of the electronic band structures. This can help to optimize properties of the solid electrolyte materials via composition engineering, which is planned in the second phase of the project.

There are several major findings. (1) In both the argyrodite and antiperovskite families according to their

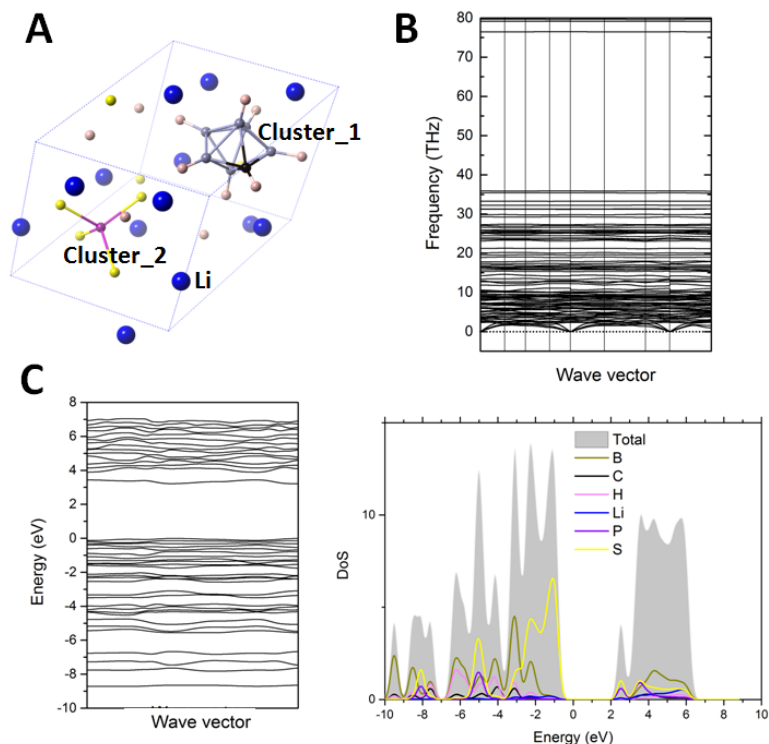


Figure 71. (a) The found unit cell of a cluster-based solid electrolyte material containing two types of cluster-ions with different compositions and shapes. (b) Calculated phonon spectrum of the material showing that the material is lattice-dynamically stable. (c) Calculated electronic band structure showing the bandgap and density of states showing the elemental contributions.

chemical compositions, some cluster-based solid electrolyte materials have large unit cells containing multiple formula units. (2) Cluster-ions containing more atoms and having fewer regular shapes will enable high population of low-energy phonon modes, which could result in high ionic conductivities. (3) Almost all cluster-based solid electrolytes show larger bandgaps compared to the halogen counter parts. (4) Sulfur is found to be the major contributor to the band edges of the materials, suggesting that the properties can be adjusted by replacing sulfur with the elements of the same group, including oxygen, selenium, and tellurium. (5) Rare cases that are electric conductors can serve as interfacial coating materials in the project's later studies. The team can also use composition engineering (for example, replacing sulfur by oxygen, selenium, or tellurium) to open the bandgaps. In demonstration, Figure 71 shows the calculated phonons and electronic structures of one cluster-based solid electrolyte material.

The phonon calculations are conducted using density functional perturbation theory, which avoids the use of large supercells. If imaginary frequencies are present for certain modes, the position in the reciprocal space can provide a hint on how to adjust the cell size in the lattice space to make sure the structure becomes lattice-dynamically stable. The phonon calculations are based on optimized structures with energy converged

to 10^{-8} eV and force converged to 10^{-4} eV/Å. To obtain reliable bandgaps, a meta-GGA functional (mBJ) implemented in VASP is used in the electronic structure calculations. These calculations are based on the optimized structures with dense k-grids, a cutoff energy of 550 eV, energy converged to 10^{-6} eV, and force converged to 10^{-3} eV/Å.

Patents/Publications/Presentations

- The project has no patents, publications, or presentations to report this quarter.

Task 3.11 – Predictive Engineering of Interfaces and Cathodes for High-Performance All-Solid-State Lithium-Sulfur Batteries (Badri Narayan, University of Louisville)

Project Objective. The primary goal of this project is to leverage data-driven methods and machine learning strategies to develop accurate multi-physics models for all-solid-state Li-S battery (ASLSB) materials that can capture electrochemical and transport phenomena over atomic to mesoscopic length/timescales; these models will be rigorously validated by synthesis and advanced characterization experiments. The team will leverage the predictive power of these models, alongside synthesis/characterization experiments and battery fabrication to address longstanding issues at the electrode/electrolyte interfaces in ASLSBs. The project’s proposed technology involves the following: (1) halide-doped solid sulfide electrolytes that can concurrently provide high Li^+ ion conductivity and suppress dendrite growth; (2) novel mesoporous cathode composed of interconnected carbon nano-cages co-infiltrated with sulfur and sulfide electrolyte, which hold potential to allow high sulfur loading and optimal ion/electron pathways; and (3) functionalization of sulfide electrolyte with ionic liquids to improve physical contact and minimize impedance at the cathode/electrolyte interface.

Project Impact. ASLSBs remain far from commercialization due to poor understanding of the fundamental electrochemical/chemical and transport processes that occur at the interfaces, especially at atomic to mesoscopic scales. Successful development of the proposed predictive models (at multiple scales) will bridge this knowledge gap and will advance fundamental understanding of reaction chemistry, kinetics, charge transfer, and dendrite growth at electrified solid-solid interfaces. This, in turn, would enable predictive design of effective strategies to mitigate interfacial problems in ASLSBs, including poor interfacial contact, interfacial impedance to Li^+ ion transport and poor electron/ion conduction within cathodes. Ultimately, the fundamental knowledge gained by this work will lead to development of high-performance ASLSBs that meet DOE targets of specific energy (350 Wh/kg @C/3), sulfur loading ($> 6 \text{ mg/cm}^2$), and high cycle life (1000).

Approach. The project brings together innovative solutions in multi-scale materials modeling, electrolyte synthesis, fabrication of cathode architecture, and electrolyte functionalization to overcome the issues at electrode/electrolyte interfaces in ASLSBs. The central idea is to employ a data-driven and machine-learning based approach to develop accurate multi-physics battery models at atomic-to-mesoscopic scales. This approach overcomes critical problems with existing model development methods by foregoing need for pre-defined functional forms, introducing deep-learning technique to describe reactivity, and employing optimization methods that do not require human intuition. Multi-scale simulations based on the newly developed models will provide insights into electrochemical phenomena at electrode/electrolyte interfaces.

Out-Year Goals. In Year 1, the goal is to optimize electrolyte composition and to develop accurate reactive atomic-scale interaction models of representative SSE system and ionic liquids.

Collaborations. The team collaborates with the groups under Dr. A. Ngo and Dr. L. A. Curtiss at ANL for quantum simulations of battery systems; they plan to collaborate with Dr. J. Nanda at ORNL for advanced spectroscopic *in situ* characterization of interfaces.

Milestones

1. Demonstrate scalable electrolyte synthesis with precise composition control. (Q1, FY 2020; Completed)
2. Computationally optimize electrolyte composition for high Li^+ conductivity (10^{-3} S/cm) and good electrochemical stability. (Q2, FY 2020; In progress)
3. Synthesize cathode architectures based on interconnected carbon nano-cages with co-infiltrated sulfur and SSE; obtain baseline for battery performance. (Q3, FY 2020; In progress)
4. Develop reactive models for electrolyte, and ionic liquid. (Q4, FY 2020; In progress)

Progress Report

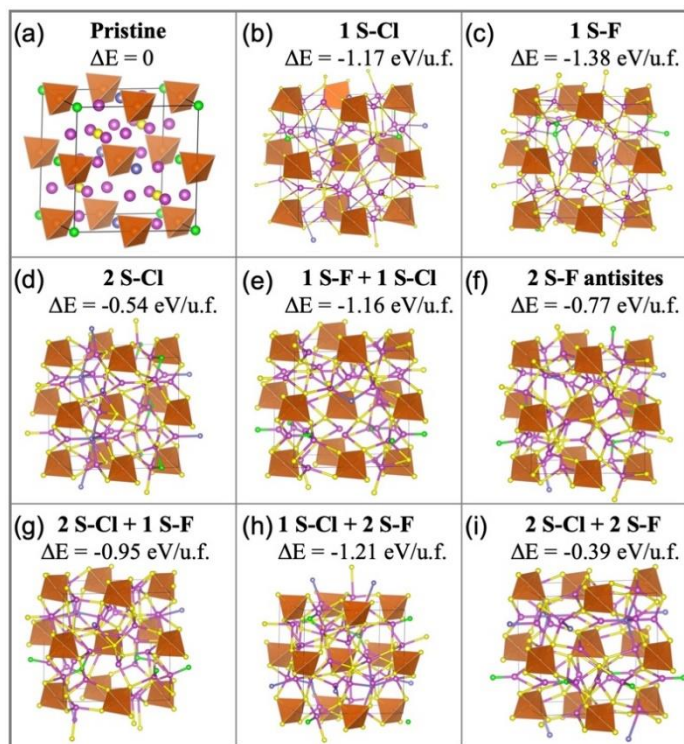


Figure 72. Energetics of sulfur-halogen site-disordering in lithium argyrodites $[\text{Li}_6\text{PS}_5\text{F}_k\text{X}_{1-k}]$ doped with two halogen species evaluated using density functional theory calculations. Using $\text{Li}_6\text{PS}_5\text{F}_{0.5}\text{Cl}_{0.5}$ as a representative example, selected configurations with different extent/type of site disordering between sulfur in $4c$ sites, and halogens (F/Cl) in $4a$ sites are shown, including (a) pristine fully ordered structure, (b-c) one antisite formed by swapping locations of nearest sulfur and chlorine [1 S-Cl (b)] and fluorine [1 S-F (c)], (d-f) two S/X antisites, (g-h) 3 S/X antisites, and (i) 4 antisites. In all panels, the final relaxed configuration is shown along with its cohesive energy relative to the fully ordered pristine structure (as shown in panel a). Quasi-rigid PS_4 tetrahedra are highlighted in orange, while lithium, sulfur, phosphorus, and chlorine atoms are depicted as purple, yellow, orange, green, and blue spheres, respectively.

ions occupying half of the $48h$ sites surrounding the $4c$ sites. On aliovalent substitution of sulfur, the halogens can occupy $4a$ and $4c$ sites, without impacting the sulfur belonging to PS_4 tetrahedra. Co-doping with two halogens opens up a wide range of possible configurations. Such site disordering over S and X sites can crucially impact stability and Li^+ ion conductivity of the SSE; yet, often, a fully ordered configuration (Figure 72a) in which all halogens occupy $4a$ sites is chosen for computational studies due to its simplicity. This quarter, the team performed DFT studies to determine the impact of introducing S-X anti-sites in the fully ordered structure (Figure 72). They first performed a Monte-Carlo based search guided by DFT to determine the most probable configuration of lithium atoms in the pristine cubic structure. Next, they introduced S-X anti-sites in this cubic structure by swapping sulfur (in $4c$ sites) with halogens (in $4a$ sites). On introduction of these anti-sites, the team finds that the structure undergoes slight distortions; that is, the sulfur and halogen atoms prefer to move away from their perfect crystal locations to form new Li-F and Li-Cl bonds. This, in turn, makes these site-disordered structures more energetically favorable than the fully ordered structure. Regardless of the number of anti-sites introduced, the site disordered structures are more thermodynamically stable than the fully ordered structure (for example, see Figure 72 for a representative example $\text{Li}_6\text{PS}_5\text{F}_{0.5}\text{Cl}_{0.5}$). The qualitative trends in

This quarter, the team made significant progress in understanding Li^+ ion diffusion in halide-doped sulfide electrolytes (SSE) using AIMD simulations and DFT calculations; liquid-phase synthesis of SSEs with optimized composition; and synthesis of carbon nanocages with co-infiltration of sulfur and SSE for cathode design.

Optimization of Electrolyte Composition to Achieve High Li^+ Ion Conduction

Aliovalent doping of lithium argyrodites SSE with multiple halogens provides a unique opportunity to concomitantly achieve enhanced Li^+ ion conduction, and a stable SEI (containing LiX) during battery operation. In particular, the presence of LiF in SEI has been found to limit formation of lithium dendrites, making fluorine a promising dopant for SSEs. Furthermore, co-doping SSEs with fluorine and Cl/Br/I ions could provide good electrochemical stability (via segregation of fluorine to Li-anode forming LiF) while enhancing Li^+ ion transport (as indicated by the *ab initio* simulations last quarter). Despite this promise, fluorine-containing SSEs have not been investigated until now.

DFT Assessment of Energetics of Structure of Halogen-Doped SSEs. Halogen-doped lithium argyrodites are structural derivatives of a parent sulfide Li_7PS_6 that possesses a cubic crystal (F-43m; space group: 216). The framework of this structure is composed of PS_4 tetrahedra centered at crystallographic $4b$ sites, with the remaining sulfur occupying sites $4a$ and $4c$ sites, and the lithium

energetics for S/disordering remain the same for other halogen co-dopants (that is, bromine and iodine) as well as for other compositions (dopant levels). In contrast, for SSEs doped with only one halogen, introducing multiple anti-sites is energetically up hill; this indicates that $S/X_{\text{disordering}}$ becomes more preferred with multiple halogen dopants.

AIMD Simulations of Li^+ Ion Conduction in Halogen-Doped SSEs. The particularly enhanced energetic preference for the S/X disordering in lithium argyrodites with multiple halogen species (as compared to single halogen cases) has a crucial impact on the Li^+ ion diffusivity (Figure 73).

This propensity of S/X disordering (between $4a$ and $4c$ sites) enables faster diffusion of Li^+ ions in the co-doped SSE as compared to the counterpart single halogen doped cases. For example, diffusivity of Li^+ in $\text{Li}_6\text{PS}_5\text{F}_{0.5}\text{Cl}_{0.5}$ ($4.17 \times 10^{-5} \text{ cm}^2/\text{s}$) is ~ 2.5 times higher than that in $\text{Li}_6\text{PS}_5\text{Cl}$ ($1.67 \times 10^{-5} \text{ cm}^2/\text{s}$), and ~ 4 times higher than that in $\text{Li}_6\text{PS}_5\text{F}$ ($1 \times 10^{-5} \text{ cm}^2/\text{s}$), as indicated by the AIMD simulations at 700 K (see Figure 73a). Such increase in lithium diffusivity is observed for any level of co-doping; however, the enhancement is most pronounced at equimolar dopant concentrations of the two halogens. To gain a fundamental understanding of this increased lithium diffusion in co-doped cases, the team plotted the density distribution of lithium ions within the supercell during the AIMD simulations (Figure 73b-d). These distribution plots provide a clear visual depiction of the sites that the lithium atoms prefer to occupy as they translate through the lattice with time.

In the single halogen doping cases, the lithium atoms remain largely restricted to cages composed of $48h$ sites surrounding a PS_4 tetrahedra; while in $\text{Li}_6\text{PS}_5\text{F}_{0.5}\text{Cl}_{0.5}$, the density distribution shows only a weak, cage-like structure. This clearly shows that in $\text{Li}_6\text{PS}_5\text{F}$ and $\text{Li}_6\text{PS}_5\text{Cl}$, the dominant pathway for Li-ion diffusion remains hopping between adjacent $48h$ sites confined within a cage (that is, intra-cage hopping). Such hopping, while frequent, does not contribute to macroscopic Li-ion conductivity, which requires translation of lithium ions through the lattice. On the other hand, in $\text{Li}_6\text{PS}_5\text{F}_{0.5}\text{Cl}_{0.5}$, the favorable S/X disordering energetics enable more lithium hopping from one cage to the other (that is, inter-cage hopping) allowing lithium ions to translate over large distances, which would provide much higher macroscopic Li-ion conductivity. This clearly demonstrates that co-doping is lucrative from the standpoint of improving Li-ion conduction. The team is leveraging their expertise with AIMD and DFT calculations to understand the impact of halogen ordering on (a) structure of lithium sub-lattice, (b) thermodynamic stability of the electrolyte against phase separation, and (c) evolution of the Li/electrolyte interface, and to continually build a large DFT training set of energies, structures, and charges in a wide variety of configurations (for developing ML-FFs) in F-containing SSEs co-doped with other halogens.

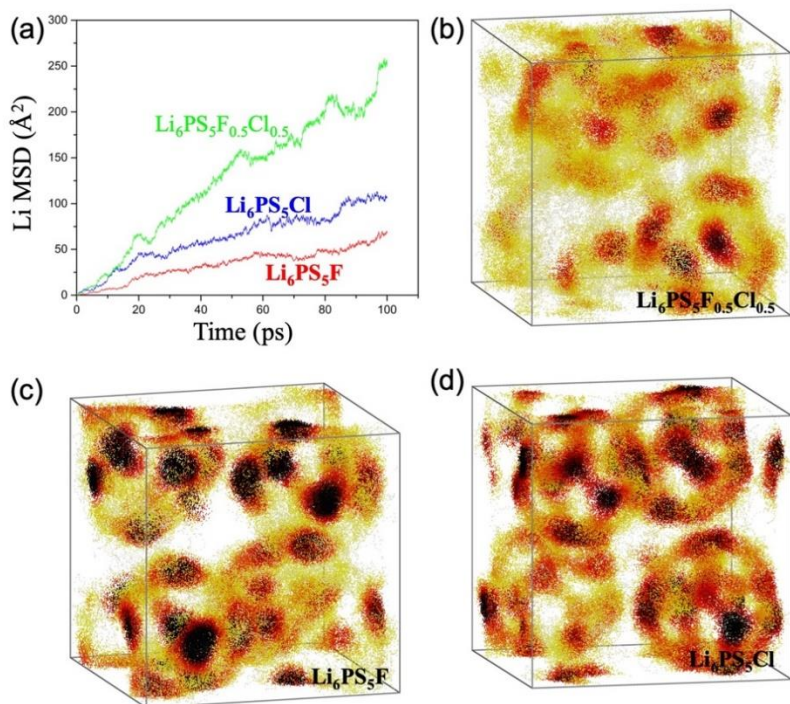


Figure 73. *Ab initio* molecular dynamics (AIMD) simulations to understand Li^+ ion transport in halogen-doped lithium argyrodites. (a) Mean-squared displacement of lithium atoms over 100 ps of AIMD simulations at 700 K in $\text{Li}_6\text{PS}_5\text{Cl}$, $\text{Li}_6\text{PS}_5\text{F}$, and $\text{Li}_6\text{PS}_5\text{F}_{0.5}\text{Cl}_{0.5}$ electrolytes. The spatial density distribution of lithium ions in the AIMD trajectory is shown for (b) $\text{Li}_6\text{PS}_5\text{F}_{0.5}\text{Cl}_{0.5}$, (c) $\text{Li}_6\text{PS}_5\text{F}$, and (d) $\text{Li}_6\text{PS}_5\text{Cl}$. Dark maroon colors represent the highest density value, followed by red and yellow colors.

Synthesis and Characterization of Sulfide Electrolytes Doped with Multiple Halogens. To validate the theory predictions on enhancement of Li-ion diffusion through doping with multiple halogen, the team employed their recently developed solvent-based synthesis method. They demonstrated this method last quarter for lithium argyrodites doped with single halogen; a manuscript on this work has been accepted for publication in *Journal of Power Sources*. This quarter, they extended this technique to introduce multiple halogens into Li_7PS_6 structure through a stoichiometric reaction between Li_2S , Li_3PS_4 , LiF , and other LiX ($\text{X} = \text{Cl}, \text{Br}, \text{I}$) in ethanol solvent. Figure 74a shows the XRD patterns of $\text{Li}_6\text{PS}_5\text{F}$ and $\text{Li}_6\text{PS}_5\text{F}\cdot\text{LiF}$ in comparison with Li_7PS_6 . Fluoride-doped argyrodites exhibit high crystalline while containing a small amount of LiF ($2\theta=38^\circ$), which may be due to the poor solubility of LiF in ethanol. $\text{Li}_6\text{PS}_5\text{F}$ shows a Li^+ ionic conductivity of 0.2 mS cm^{-1} at

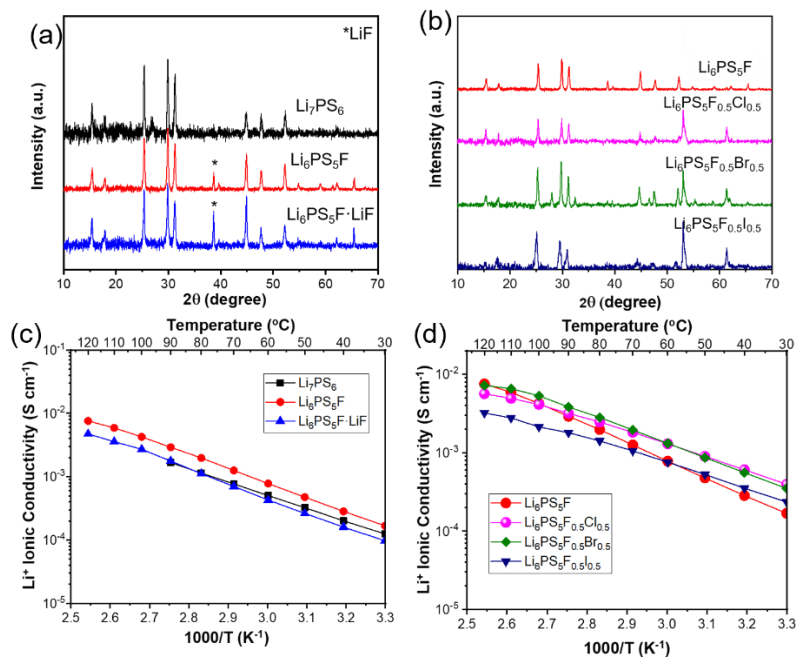


Figure 74. Synthesis and characterization of halogen-doped argyrodites. X-ray diffraction patterns of (a) F-doped lithium argyrodites and (b) F-Cl/Br/I co-doped lithium argyrodites. Arrhenius plots of (c) F-doped lithium argyrodites and (d) F-Cl/Br/I co-doped lithium argyrodites.

(Figure 74d). Similar to the AIMD simulations, the synthesized $\text{Li}_6\text{PS}_5\text{F}_{0.5}\text{Cl}_{0.5}$ exhibits the best conductivity of 0.4 mS/cm at room temperature (Figure 74d). Next, the team will study the electrochemical stability of F-doped and co-doped lithium argyrodites with lithium metal and investigate the SEI layer at interface.

Infiltrating SSE and Sulfur in Mesoporous Cathodes Made Up of Interconnected Carbon Nano-Cages (CNCs)

Mesoporous composite cathodes made up of nanocages (CNCs) encapsulating SSE and sulfur is lucrative to achieve large surface area $\sim 1000 \text{ m}^2/\text{g}$ and high sulfur loading ($> 6 \text{ mg/cm}^2$). The team synthesizes CNCs using their recently patented process involving thermolysis of sol-gel precursor consisting of nickel salt and carbon precursor, and templating on nickel nanoparticles; last quarter, they demonstrated precise control over the size and morphology of CNCs by varying precursor and reaction conditions. Citric acid and caffeine are used as carbon precursors for the synthesis of small ($\sim 3 \text{ nm}$) and large (20-100 nm) CNCs, respectively. The CNC powders were obtained by subsequent acid treatment and the dissolution of most of nickel. They also demonstrated impregnation of sulfur into CNCs using melt-injection at $\sim 120^\circ\text{C}$.

room temperature, higher than that of Li_7PS_6 (0.12 mS cm^{-1}). However, further increasing fluorine content results in a lower ionic conductivity for $\text{Li}_6\text{PS}_5\text{F}\cdot\text{LiF}$. Beside F-doping, the effect of co-doping with fluorine and Cl/Br/I ions on structure and conductivity of lithium argyrodites was studied. As shown in Figure 74c, all co-doped sulfide electrolytes exhibit high crystalline and high phase purity without the observation of LiF . However, a new peak at $2\theta=54^\circ$ becomes stronger, which could be related to the enhanced S/X site disordering observed in the first-principles calculation, but still needs further analysis. In comparison with $\text{Li}_6\text{PS}_5\text{F}$, the co-doped sulfide electrolytes show enhanced ionic conductivities as compared to single halogen counterparts, in excellent agreement with the team's theory predictions

This quarter, the team synthesized a large quantity (> 20 g) of CNCs (20-100 nm) by a batch process using caffeine as the carbon precursor to prepare for battery fabrication tests in Q3. More importantly, they achieved successful infiltration of both (a) sulfur via melt-injection method, and (b) sulfide electrolyte Li_7PS_6 (LPS) by soaking the CNCs in a solution of LPS dissolved in anhydrous alcohol inside a glove box (argon filled). Figure 75 shows an elemental map obtained from EDS in HAADF-STEM after infiltration of CNCs. Evidently, both sulfur and SSE (seen through the phosphorus map) have been successfully placed inside CNCs. Next, the team will extend this technique to prepare cathodes with optimized electrolyte compositions and to gain control over the morphology and distribution of the infiltrated sulfur and SSE.

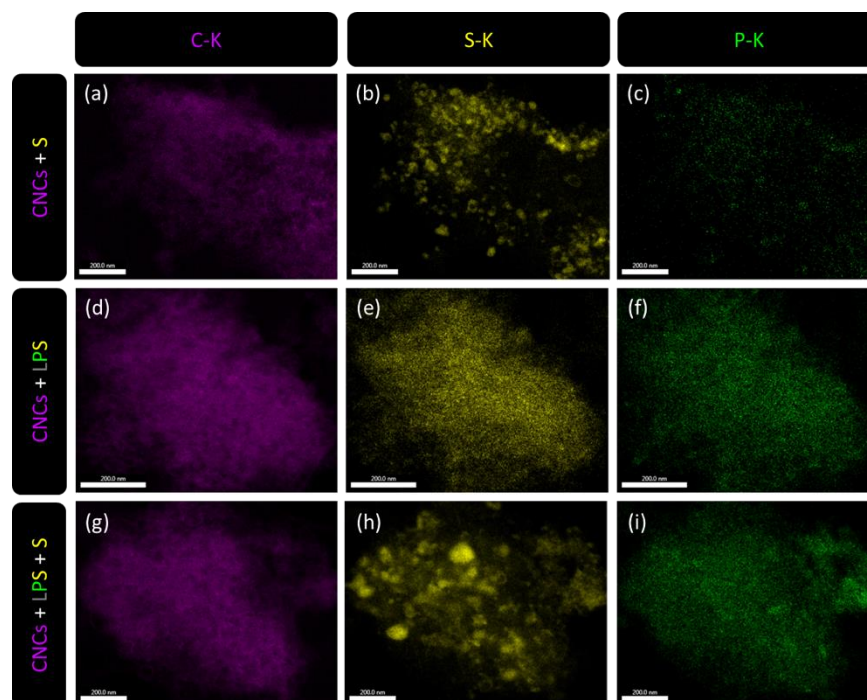


Figure 75. Fabrication of mesoporous composite cathodes with sulfur and sulfide electrolyte. Carbon, sulfur, and phosphorus elemental maps of large (20-100 nm) carbon nanocages impregnated with (a-c) sulfur, (d-f) LPS, and (g-i) sulfur followed by LPS.

Patents/Publications/Presentations

Publication

- Arnold, W., D. A. Buchberger, Y. Li, M. Sunkara, T. Druffel, and H. Wang. “Halide Doping Effect on Solvent-Synthesized Lithium Argyrodites $\text{Li}_6\text{PS}_5\text{X}$ (X= Cl, Br, I) Superionic Conductors.” *Journal of Power Sources* (2020). Accepted.

Task 3.12 – First-Principles Modeling and Design of Solid-State Interfaces for the Protection and Use of Lithium-Metal Anodes (Gerbrand Ceder, University of California Berkeley)

Project Objective. Determine the design principles that control the solid electrolyte / lithium electrode interfaces by determining the reaction products stemming from pairing solid electrolytes and lithium metal. A rigorous analysis based on computing electrolyte phase-diagrams closed and open to lithium. Li-ion transport properties in bulk electrolytes and interfacial products will be assessed through AIMD and NEB calculations. Simultaneously, a robust framework to identify factors controlling Li-dendrite propagation within solid electrolytes and interfacial products by accounting for irregularities, defects, and GBs, through a model that includes elements of fracture mechanics, thermodynamics, and electrochemistry.

Project Impact. The project will lead to understanding of the complex evolution of Li-metal / solid electrolyte interfaces during electrochemical cycling. The understanding of such a process is necessary to determine design principles to develop reliable ASSBs.

Approach. A HT computation method is used to screen suitable solid electrolyte with high electro-chemical stability and high ionic conductivity, by incorporating NEB and AIMD method. Meanwhile, DFT is used to calculate bulk elastic constants of involved material, and surface energies and interface de-cohesion energies of GBs; finally, continuum theorem (elastic-plastic-fracture mechanics) is used to assess the resilience of solid electrolytes and grain/particle boundaries toward lithium dendrite growth and propagation. FEM is used to couple several physical processes, including electro-chemical deposition, ionic diffusion, thermal expansion, and mechanical contacting.

Out-Year Goals. Obtain design criteria for solid electrolytes that can resist unstable lithium propagation by computing elastic properties surface energies, and decohesion energies. Adapt fracture mechanics models describing crack propagation to lithium dendrite propagation in different scenarios.

Collaborations. There are no collaborative activities this quarter.

Milestones

1. Determine materials design criteria based on developed failure models. (Q1, FY 2020; Completed)
2. Extend ionic conductor failure model to include effects of mixed ionic and electronic conduction. (Q2, FY 2020; Completed)
3. Adapt fracture models that describe crack propagation in materials to lithium dendrite propagation in perfect crystal with GBs. (Q3, FY 2020; On target)
4. Assess resistance to metal propagations and failure in candidate solid ionic conductor materials. (Q3, FY 2020; On target)

Progress Report

The Mix Ionic-Electronic Conductor Model to Include Effect of Electronic Conductivity of the SE

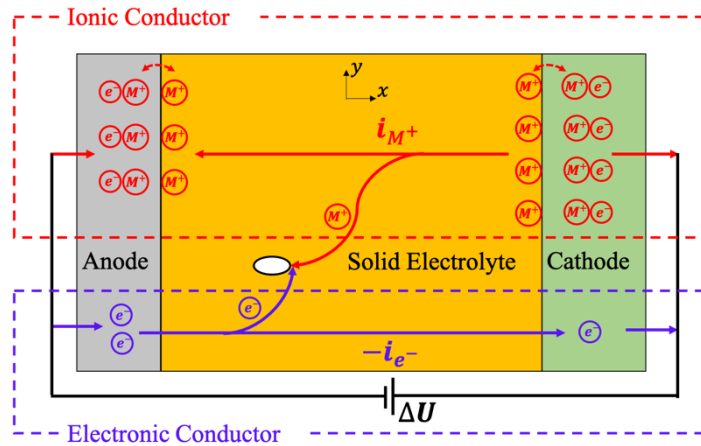


Figure 76. Schematic of the mix ionic-electronic conductor model for a full solid-state battery cell during charging process material.

When a solid electrolyte has ionic and electronic conductivities, both the conduction cation M^+ and electrons can migrate inside the solid electrolyte. During the charging process of the SSB cell shown in Figure 76, M^+ ions migrate like an “ionic conductor” from the cathode to the anode with partial current density i_{M^+} (red lines); meanwhile, electrons conduct as an “electronic conductor” from the anode to the cathode with partial current density i_{e^-} (blue lines). The “ionic conductor” and “electronic conductor” can be treated as an equivalent circuit that are connected in parallel under the same externally applied potential drop ΔU . Charge-transfer reactions (stripping at the cathode-SE interface, plating at the anode-SE interface, and metal deposition at the void-SE interface) can be described by the Butler-Volmer relation. Both the ionic (M^+) and the electronic conduction (e^-) in the solid electrolyte are assumed to follow Ohmic relation.

Effect of Electronic Conductivity of the Solid Electrolyte on the Lithium Penetration

The 1D solution shown in Figure 77 represents the ideal case when the structure and material are homogeneous, which can provide general trends for all potentials in the SSB cell. Under the galvanostatic condition with constant charging current, the electronic potential $\tilde{\mu}_{e^-}$ decreases from the anode to the cathode without potential drop when crossing the electrode / solid electrolyte interface. Contrarily, the ionic potential $\tilde{\mu}_{M^+}$ increases from the anode to the cathode, and with a potential drop when crossing the electrode / solid electrolyte interface. This drop at the interface provides overpotential needed for stripping and plating. The partial current densities i_{e^-} , i_{M^+} are proportional to the gradient of their potentials. The summation $\tilde{\mu}_{e^-} + \tilde{\mu}_{M^+}$ (green-dash line) in the solid electrolyte determines the overpotential for metal deposition in the solid electrolyte. The metal deposition will happen only when this value is positive, or say when this value is above the chemical potential of M in the metallic phase (black-dash line). Therefore, metal deposition will happen in voids with location within half of the solid electrolyte thickness in the symmetric cell.

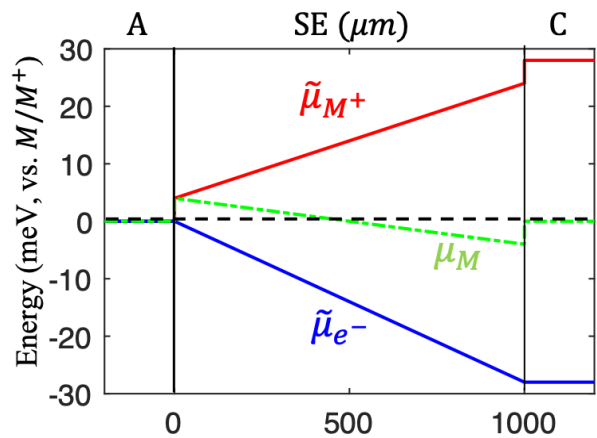


Figure 77. Potential distribution in the solid electrolyte in a symmetric cell.

Patents/Publications/Presentations

Publications

- Tu, Q., et al. “Modeling of Electro-Deposition and Mechanical Stability at Li Metal/Solid Electrolyte Interface during Plating in Solid-State Batteries.” Submitted to *Cell Reports Physical Science*.
- Barroso-Luque, L., Q. Tu, and G. Ceder. “An Analysis of Solid-State Electrodeposition-Induced Metal Plastic Flow and Predictions of Stress States in Solid Ionic Conductor Defects.” *Journal of the Electrochemical Society* 167, no. 2 (2020): 020534.

TASK 4 – METALLIC LITHIUM

Summary and Highlights

The use of a metallic lithium anode is required for advanced battery chemistries like Li-ion, Li-air, and Li-S to realize dramatic improvements in energy density, vehicle range, cost requirements, and safety. However, use of metallic lithium with liquid and solid polymer or ceramic electrolytes has so far been limited due to parasitic SEI reactions and dendrite formation that eventually short circuit the battery. Adding excess lithium to compensate for such losses negates the high-energy-density advantage of a Li-metal anode and leads to further concern for battery safety. For a long lifetime and safe anode, it is essential that no lithium capacity is lost either (1) to physical isolation by roughening, dendrites, or delamination processes, or (2) to chemical isolation from side reactions. The key risk, and current limitation, for this technology is the gradual loss of lithium over the cycle life of the battery.

BMR, Battery500, and other DOE programs are addressing this challenge with many innovative and diverse approaches. Key to all is the need for a much deeper analysis of the degradation processes and new strategies to maintain a dense, fully connected lithium and a dendrite-free electrolyte so that materials can be engineered to fulfill the target performance metrics for EV application, namely 1000 cycles and a 15-year lifetime, with adequate pulse power. Projecting the performance required in terms of just the lithium anode, this requires a high rate of lithium deposition and stripping reactions, specifically about 30 μm of lithium per cycle, with pulse rates up to 10 and 20 nm/s (15 mA/cm²) charge and discharge, respectively, with little or no excess lithium inventory. This is daunting in the total mass and rate of material transport that must be achieved without failures.

The efficient and safe use of metallic lithium for rechargeable batteries is then a great challenge, and one that has eluded R&D efforts for years. This project takes a broad look at this challenge for both SSBs and batteries continuing to use liquid electrolytes. Electrolytes reported here include nonflammable liquid solutions, gel type polymer-in-a-salt, composites of ceramic polymer phases, common and novel polymer electrolytes, and both oxide and sulfide ceramic electrolytes. In most studies, the electrolyte phases were modified by addition of plasticizers or interface coatings to improve transport, stability, and ease of manufacturing. Researchers are typically working toward cycling of full cells with relevant and balanced capacities for the lithium anode and cathode using measures of CE, interface resistance, and post-cycling observation of the disassembled cell components to assess stability of the Li-metal anode and chosen electrolyte.

Highlights. The highlights for this quarter are described below.

The PNNL group (Xu and Zhang) reports on several compositions of highly concentrated salt electrolytes, so-called solvent-in-a-salt and polymer-in-a-salt electrolytes. Their work is distinguished by an emphasis on using and testing non-flammable components and evaluating stability with lithium metal by measures of the CE and TEM observations of the SEI and lithium morphology on cycling. This quarter, a 1:1 PEO:LiFSI electrolyte was plasticized with an ionic liquid. The addition of the ionic liquid gave a gel-like electrolyte which, when contained in a porous polyimide separator membrane, was difficult to ignite and had good conductivity, near 1 mS/cm, above 50°C.

Work from ORNL (Chen and Dudney) highlights ceramic polymer composite electrolytes, most recently using a cross-linked polymer within a sintered ceramic skeleton, a structure designed to maximize the mechanical strength and Li-ionic transport conductivity. To date, the LATP-based ceramic is protected from reaction with the lithium by a thin excess polymer film at the interface. The added resistance of this polymer layer is reduced by adding a small amount of plasticizer. The work also reports an anomalous behavior that may be seen as an unexplained overcharge, which is believed to result from assembling full cells with a polymer electrolyte in coin cell hardware.

From ANL (Markovic and Curtis), the report showed the interface reaction of lithium with PEO as determined by X-ray photoelectron analysis before and after lithium deposition and heating to 100°C under vacuum. New features in the O1s, C1s, and Li1s spectra reveal evidence for lithium dissolution in the PEO and reaction forming organolithium (LiCR) and lithium alkoxide (LiOR) species.

Ye's group (LLNL) reports work to fabricate sintered garnet LLZO membranes, where various coatings have been applied to large batches of Ta-doped LLZO powder. The purpose of the coating is two-fold: to control the decomposition of Li_2CO_3 at the surface during sintering and to improve the interface of the sintered membrane with the Li-metal anode. This report highlights Al_2O_3 coatings applied by ALD onto LLTZO powder, using up to 5 cycles of the ALD process. Pellets of the coated LLTZO sintered at 1100°C were up to 96% dense. The interface of the LLZTO-Al with lithium metal was about 100 ohm cm^2 , but there was evidence of reaction with the lithium.

Nanda's group (ORNL) is investigating the synthesis and processing of lithium thiophosphate solid electrolyte membranes. In this report, results of solvent mediated synthesis were compared using five solvents. For each of the solvents, Raman spectroscopy reveals the $\text{P}_2\text{S}_6^{2-}$ anion; this was supported by XRD and XPS results for the dried materials. Variations of the final stoichiometry and conductivity depend largely on the thermal treatment and amount of excess Li_2S incorporated thiophosphate.

From Stanford, Cui's group reports on a simple, one-step process to lithiate a standard silicon slurry cathode cast onto copper foil. By adding a thin lithium foil between the silicon anode and the porous separator, on assembly of the full cell with a liquid electrolyte, the silicon becomes lithiated when allowed to rest for up to 4 hours before initial cycles. Disassembly of the cell reveals the larger silicon particles and SEI formed from the solvent decomposition.

Task 4.1 – Lithium Dendrite Prevention for Lithium Batteries (Wu Xu and Ji-Guang Zhang, Pacific Northwest National Laboratory)

Project Objective. The objective of this project is to enable lithium metal to be used as an effective anode in rechargeable Li-metal batteries with good stability and high safety. The investigation this fiscal year will focus on two aspects. First, develop nonflammable polymer electrolytes and investigate effects of various flame-retardant solvents and polymers on ionic conductivity, lithium CE, Li-anode morphology, flammability, and battery performances in terms of long-term cycling stability and rate capability at various temperatures. Second, establish correlation of morphologies of SEI layer and deposited lithium with electrolyte formulation, current density, and lithium deposition/stripping cycling.

Project Impact. Lithium metal is an ideal anode material for rechargeable batteries, but the application of Li-metal anode is hindered by lithium dendrites and low CE. Although much progress has been achieved in suppressing lithium dendrites and increasing lithium CE in liquid electrolytes, most of the liquid electrolytes are flammable and may pose a safety hazard in case of extreme conditions. Therefore, development of electrolytes with improved safety for advanced battery chemistry is imperative. An ideal electrolyte for Li-metal anode should not only suppress lithium dendrite growth and have high CE, but also be intrinsically nonflammable. This fiscal year, the team will develop low flammable or nonflammable hybrid polymeric composite electrolytes (NHPCEs) that have high lithium CE, suppress lithium dendrites, and are stable with high-voltage cathodes. The success of this project will increase safety of Li-metal and Li-ion batteries and accelerate market acceptance of EVs, especially for PEVs as required by the EV Everywhere Grand Challenge.

Approach. The approach will encompass several areas: (1) develop appropriate high-concentration phosphate liquid electrolytes (HCEs) that have high lithium CE over 98% and can suppress lithium dendrites, (2) add flame-retardant phosphate monomers into the HCEs and utilize radical polymerization to form crosslinked polymer gel electrolyte, and (3) investigate ionic conductivity, electrochemical window, flammability, lithium CE, and morphology; battery performance of HCEs and NHPCEs will also be investigated.

Out-Year Goals. The long-term goal of the proposed work is to enable Li-metal and Li-ion batteries with a specific energy of > 350 Wh/kg (in cell level), 1000 deep-discharge cycles, 15-year calendar life, and less than 20% capacity fade over a 10-year span to meet the goal of EV everywhere.

Collaborations. This project collaborates with C. Wang of PNNL on characterization by TEM/SEM; Dr. K. Xu and Dr. M. Ding of U. S. Army Research Laboratory (ARL) on solvent purification and DSC measurements; and Dr. B. Polzin at ANL on coated electrode sampling.

Milestones

1. Develop polymerization method to achieve nonflammable polymer electrolytes with lithium CE > 98%. (Q1, FY 2020; Completed, February 19, 2020)
2. Characterize morphologies of SEI layers and deposited lithium films at different current densities and deposition capacities. (Q2, FY 2020; Completed, March 31, 2020)
3. Investigate lithium CE, deposited lithium morphology, and flammability of hybrid polymer composite electrolytes. (Q3, FY 2020; In progress)
4. Achieve over 100 cycles for Li||NMC-622 batteries with nonflammable hybrid polymer composite electrolytes. Characterize compositions of SEI layers and deposited lithium films at different current densities and deposition capacities. (Q4, FY 2020)

Progress Report

This quarter, the morphologies of the electrochemically deposited lithium (EDLi) films on copper substrates in the electrolyte of 1.2 M LiPF₆/EC-EMC (3:7 by wt) with 5 wt% VC under different current densities and capacities, as well as the compositions of SEI layers formed on these EDLi films at various current densities, were studied in collaboration with Dr. C. Wang's team using SEM, cryo-TEM, EDS, and EELS.

For EDLi prepared at different current densities, a fixed lithium amount (0.167 mAh cm⁻²) was used. With the increase of deposition current density from 0.1 to 9 mA cm⁻², the nucleation overpotential increased from 95 to 948 mV, and the growth overpotential increased from ~ 85 to ~ 550 mV. As shown in Figure 78a-d, regardless of the current density variation, the EDLi exhibits whisker-like configuration with rough structure, indicating uncontrolled growth of lithium metal. The fine feature of EDLi varies as the current density changes. The number density of the whiskers decreases with increasing current density. In terms of chemical compositions, the EDLi and SEI layers at current densities from 0.1 to 5 mA cm⁻² are mainly comprised of oxygen and carbon, that is, Li₂O (Figure 78e), while at the high current density (9 mA cm⁻²), the EDLi and SEI consist of Li₂O and some LiF. The SEI formed at 0.1 mA cm⁻² has a monolithic amorphous structure, while the SEIs formed at 2 to 9 mA cm⁻² exhibit mosaic-like structures.

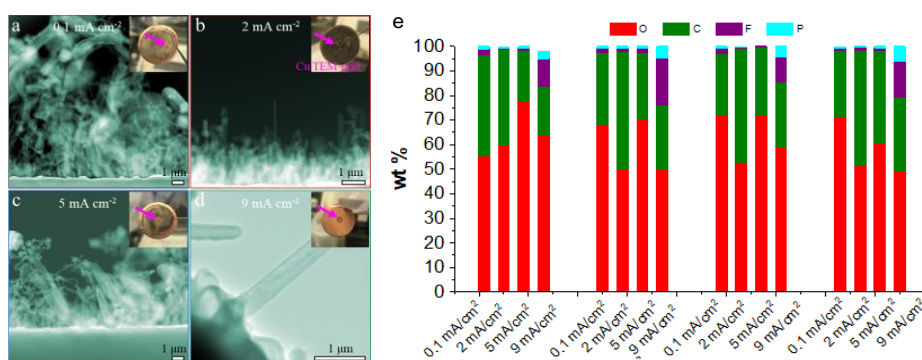


Figure 78. (a-d) Low magnification transmission electron microscopy images of electrochemically deposited lithium (EDLi) under current density of (a) 0.1 mA cm⁻², (b) 2 mA cm⁻², (c) 5 mA cm⁻², and (d) 9 mA cm⁻². Insets: Digital photos of deposited lithium. (e) Composition information acquired from EDLi interface between lithium and SEI, and SEI and the surface of SEI areas at different current densities.

When lithium is deposited under the different areal deposition capacities (1, 2, and 4 mAh cm⁻²) at the same current density of 0.1 mA cm⁻², the morphology of the EDLi slightly changes, from fine dendrites at 1 mAh cm⁻² to slightly larger size dendrites at 2 mAh cm⁻² and to some granular deposits at 4 mAh cm⁻² (Figure 79). The compositions of SEI and EDLi are under characterization.

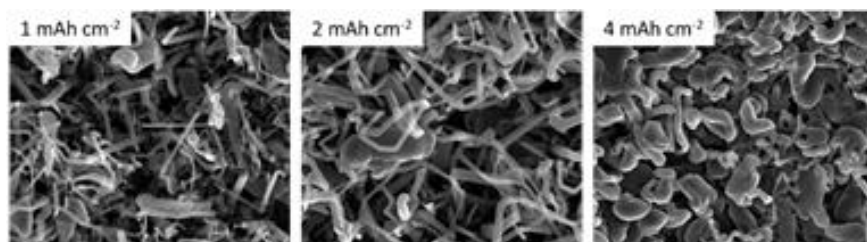


Figure 79. Scanning electron microscopy images of electrochemically deposited lithium under deposition capacity of 1, 2, and 4 mAh cm⁻² at a current density of 0.1 mA cm⁻².

In a separate effort, the oxidation stability and CE of polymer-in-salt electrolytes (PISEs) were further investigated. With the increase of salt concentration, the initial oxidation potential (defined as the voltage value when the current density is 0.3 μA cm⁻²) first shifts to a more positive potential and then decreases at highest concentration. The oxidation voltages of PISEs with EO/Li = 16, 2, and 1 are around 4.36 V, 4.52 V, and 4.48 V, respectively. The samples with the EO/Li ratio less than 4 all have higher oxidation voltage than those with higher EO/Li ratios. The CE of P(EO)₁LiFSI-0.4Pyr14FSI was tested with Li||Cu cell at 60°C. A CE of 99.3% is obtained when the current density is 0.1 mA cm⁻² and capacity is 0.2 mAh cm⁻², but the CE decreases to 69.2% when the current density increases to 0.5 mA cm⁻² and capacity is 1 mAh cm⁻², indicating that P(EO)₁LiFSI-0.4Pyr14FSI does not have good rate capability due to its high viscosity.

Patents/Publications/Presentations

Publication

- Peng, Z., X. Cao, P. Gao, H. Jia, X. Ren, S. Roy, Z. Li, Y. Zhu, W. Xie, D. Liu, Q. Li, D. Wang, W. Xu, and J-G. Zhang. “High-Power Lithium Metal Batteries Enabled by High-Concentration Acetonitrile-Based Electrolytes with Vinylene Carbonate Additive.” *Advanced Functional Materials* (2020). doi: 10.1002/202001285.

Task 4.2 – Composite Electrolytes to Stabilize Metallic Lithium Anodes (Nancy Dudney and X. Chelsea Chen, Oak Ridge National Laboratory)

Project Objective. The project has several objectives: (1) prepare novel polymer and ceramic electrolyte materials that can work together to achieve thin membranes that have the unique combination of electrochemical and mechanical properties required for practical manufacturing and to stabilize the metallic lithium anode for good power performance and long cycle life, (2) identify key features of the composite composition, architecture, and fabrication that optimize performance, and (3) fabricate thin electrolyte membranes to use with a thin metallic lithium anode that provides good power performance and long cycle life.

Project Impact. A stable lithium anode is critical to achieve high energy density with excellent safety, lifetime, and cycling efficiency. This study will identify key design strategies that should be used to prepare composite electrolytes to meet the challenging combination of physical, chemical, and manufacturing requirements to protect and stabilize the Li-metal anode for advanced batteries. By utilizing well characterized and controlled component phases, design rules developed for composite structures will be generally applicable toward substitution of alternative and improved solid electrolyte component phases as they become available. Success will enable DOE technical targets: 500-700 Wh/kg, 3000-5000 deep discharge cycles, and robust operation.

Approach. This project seeks to develop practical solid electrolytes to provide stable, long-lived protection for Li-metal anode. Current electrolytes have serious challenges when used alone; oxide ceramics are brittle, sulfide ceramics are air sensitive, polymers are too resistive and soft, and many electrolytes react with lithium. Composites provide a clear route to address these issues. While work continues to emphasize study of ceramic electrolyte / polymer electrolyte interfaces, this effort has expanded to address the following: (1) practical processing routes to fabricate full batteries using better composite electrolytes with a composite cathode and thin Li-metal anode, and (2) introduction of alternative polymer and ceramic phases to replace well-known model materials and develop improved composite electrolytes. In addition to solid-state devices, hybrid batteries are investigated using a fluid or gel catholyte within the porous cathode. Coatings have also been employed to stabilize electrode interfaces. These directions increase complexity of the studies, but are needed to improve cycling stability and rate performance and to advance practical implementation of the solid electrolyte and Li-anode technology.

Out-Year Goal. The goal is to use advanced manufacturing processes where the architecture of the composite membrane can be developed and tailored to maximize performance and cost-effective manufacturing.

Collaborations. Work is conducted by Dr. Y. Zhang and Dr. X. Chen. Ceramic electrolyte powders (LICGC™) are obtained from Ohara Corporation. ORNL internal collaborators include Dr. B. Armstrong and Dr. S. Kalnaus. For the single ion conducting (SIC) polymers, the team partnered with Prof. J. L. Schaefer at University of Notre Dame.

Milestones

1. Develop methods to minimize interconnected composite electrolytes' interfacial resistance with lithium by varying polymer chemistry. (Q1, FY 2020; Completed)
2. Fabricate interconnected ceramic network with different ceramic chemistry and particle size to increase strength of the composite. (Q2, FY 2020; Partially completed)
3. Investigate the trade-off between Li^+ transference number and ionic conductivity of the gel composite electrolytes, and optimize it. (Q3, FY 2020; Partially completed)

4. Fabricate full batteries using NMC cathode, composite electrolyte, and Li-metal anode. Identify cell failure mode. (Q4, FY 2020; Initiated)
5. Create chemical/physical bonding between polymer and interconnected ceramic network that leads to optimized interface to improve mechanical modulus and ionic conductivity. (Annual stretch milestone).

Progress Report

Progress was made on each of the milestones this quarter.

For Milestone 1, further improvement to reduce the interfacial resistances with both the lithium anode and ceramic electrolytes was sought through use of novel SIC polymers. This work is under review for journal publication. In principle, single ion conductors eliminate the concentration gradient due to mobile anions that is believed to accelerate lithium dendrite growth. The bulk conductivity of these SIC polymers, alone and as matrix for dispersed ceramic particle composites, was reported earlier (Q3, FY 2019). Formed by crosslinking poly(ethylene glycol) dimethacrylate (PEGDMA) polymer, different anions were covalently bound to the polymer and compared with similar dissolved anions. This included polymers with bound styrene sulfonate anion (SS⁻), bound styrene TFSI anion (STFSI⁻), and dissolved TFSI⁻ anions. Tests were recently completed with Li//Li symmetric cell cycling, Raman spectroscopy, and analysis of the Li-ion transference number to assess the stability with lithium metal, the relative Li⁺ mobility, and anion coordination. Because the membranes were thick, lithium plate/strip cycle tests were conducted at 70°C and at a DC current of only 50 μA/cm². Here, the lithium interface showed little degradation for > 100 cycles (> 100 hours), and the transference number for Li⁺ was ~ 0.90 for the PEGDMA-co-STFSI with and without both plasticizer and dispersed LATP particles. While not compelling candidates for SSLBs, these SIC polymer electrolytes are useful for comparison to other polymer and ceramic electrolytes to advance understanding of how anions coordinate with ceramic interfaces, thereby freeing Li⁺ ions for higher conductivity.

For Milestone 2, new composites of porous sintered LLZO filled with polymer electrolytes were prepared, but so far prove to be fragile. The team hopes to build on their promising thin composite membranes^[1] by prepared composites using the Li-stable LLZO in place of Ohara's glass ceramic powders. This activity will continue when a selection of LLZO powders promising uniform particle morphology and size is delivered from Argonne's Materials Engineering Research Facility.

Results to date pertaining to Milestone 3 utilize the Bruce Vincent method^[2] for approximating the transference number under Li//Li polarization. The team sees that there are few attempts to analyze the relaxation kinetics of the chronoamperometric step for these cells, yet results differ for various electrolytes and their laminates (see Figure 80). Detailed analysis and development of a model to describe the relaxation is under way. The team fabricated Li//Li symmetric cells with different layers of electrolyte, including polymer electrolyte (PE), CPE (70 wt% LiCGCTM in PE), CPE2 (30 wt% LiCGCTM in PE), commercial Ohara plate, LiPON thin film and sintered Ohara fabricated at ORNL. The electrolytes have the following thicknesses: PE = 120 μm, CPE = 130 μm, CPE2 = 70 μm, Ohara plate = 150 μm, sintered Ohara = 78 μm, and LiPON = 0.07 μm. The relaxation of each cell when a 10-mV bias is applied is shown in Figure 80. The drop in the current indicates the resistance of the cell, and the shape of the curve is related to the movement of ions in the electrolyte. The PEPE cell is the baseline for comparison. Compared with the PEPE cell, the sintered Ohara adds the least resistance, 88 Ohm, to the cell. With CPE2, a resistance of 230 Ohm is added to the cell.

A modeling effort is in progress to fully understand the transport behavior in these different electrolytes. The continuum scale model is being developed utilizing Nernst-Planck equations to describe movement of charge carriers in the electrolyte. While bulk of electrolyte follows electroneutrality, the charge balance may be violated in the double layer at the electrode surface. Therefore, for completeness, the distribution of potential due to charge carriers is described via Poisson equation. The resulting Poisson-Nernst-Planck (PNP) equations are expressed in the mass balance (time-dependent) form to capture the transient behavior on application of

potential difference to the electrolyte. As an example, the team shows evolution of cation concentration in Li//Li cell with PEO:LiTFSI polymer electrolyte after application of 10-mV potential difference in Figure 81. Small perturbations of the concentration in the vicinity of the electrodes are due to the double layer. With time, the system relaxes to steady state concentration profile; the corresponding decay in current is shown in the insert. Models are under development for the rest of the arrangements in Figure 80. The overall approach is to remove the diffusional term in PNP equations for the single ion conductor (Ohara LiCGC). The block corresponding to the composite electrolyte will be prescribed effective ionic conductivity calculated using a previously developed method.

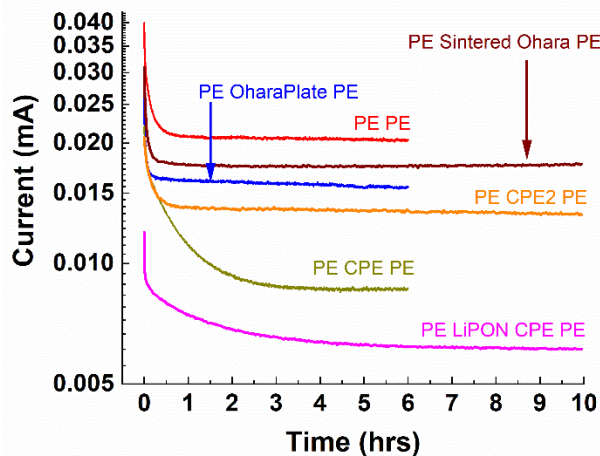


Figure 80. Relaxation behavior for different layers of electrolyte in Li//Li cell configuration under 10-mV DC bias.

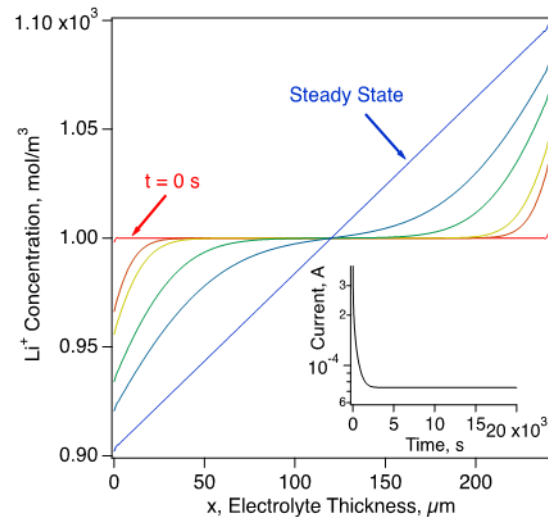


Figure 81. Simulated evolution of concentration of Li⁺ due to migration and diffusion in Li/PEPE/Li cell.

The team continued their detailed investigation of the composite electrolytes in full cells using dry LiFePO₄ (LFP) cathodes of 1.1mAh/cm² capacity, progressing toward Milestone 4. As their initial work with NMC polymer cathodes gave poor cycling, the team, as have others, attributed this to oxidation of the PE. Recent literature,^[3] however, provides convincing evidence that the primary PE decomposition occurs at 4.6 V for a variety of cathodes. The project's Li//LFP batteries are an important platform to study lithium stability leading into higher energy cells. Last quarter, the team reported that a large overcharge (> 1.1 mAh/cm²) capacity may relate to the overlap/alignment of the anode and cathode. This contrasts with the discharge capacity that is well behaved. An unexplained excess capacity on charge was also reported by G. Homann, et al.^[3]; however, the cycling results reveal a much larger and extended overcharge without failure. Continuing their work, the team observes the following: reproducibility of trends; cycling with a thinner polymer electrolyte; cycling of pouch cells; and FTIR of the aged PE. Figures 82 and 83 present results. The diameter of components is given in fractions of an inch, although the metal coin cell components provide larger contact areas. In Figure 82a, the charge capacity versus cycle number of three sets of Li (1/2) PE (5/8) LFP (1/2) is shown, where the team sees ~ 200% overcharge for three cells. The dots on the horizontal lines indicate the charge with cutoff controlled by the time for that cycle, and dots below the line are controlled by 3.7 V cutoff. Notably, the overcharge occurred earlier for the thinner electrolyte. In (b), two sets of tests are completed for a smaller area LFP and a consistent ~ 300% of overcharge is observed, even though the onset of overcharge occurred at a different cycle. In (c), for a smaller lithium, ~ 200% overcharge is shown with a thick electrolyte, while little overcharge is shown with a 65-μm electrolyte test. In (d), there is only one set of data for the Li (1/2) PE (1/2) LFP (1/2) cell, due to challenges in cell alignment with a small electrolyte layer. A Kapton washer is used to prevent unwanted electrical contact in the half-inch cell. Figure 82e shows that the discharge capacity for all types of cells is close to 1.1 mAh/cm², which is the theoretical capacity of the LFP cathode used in this study.

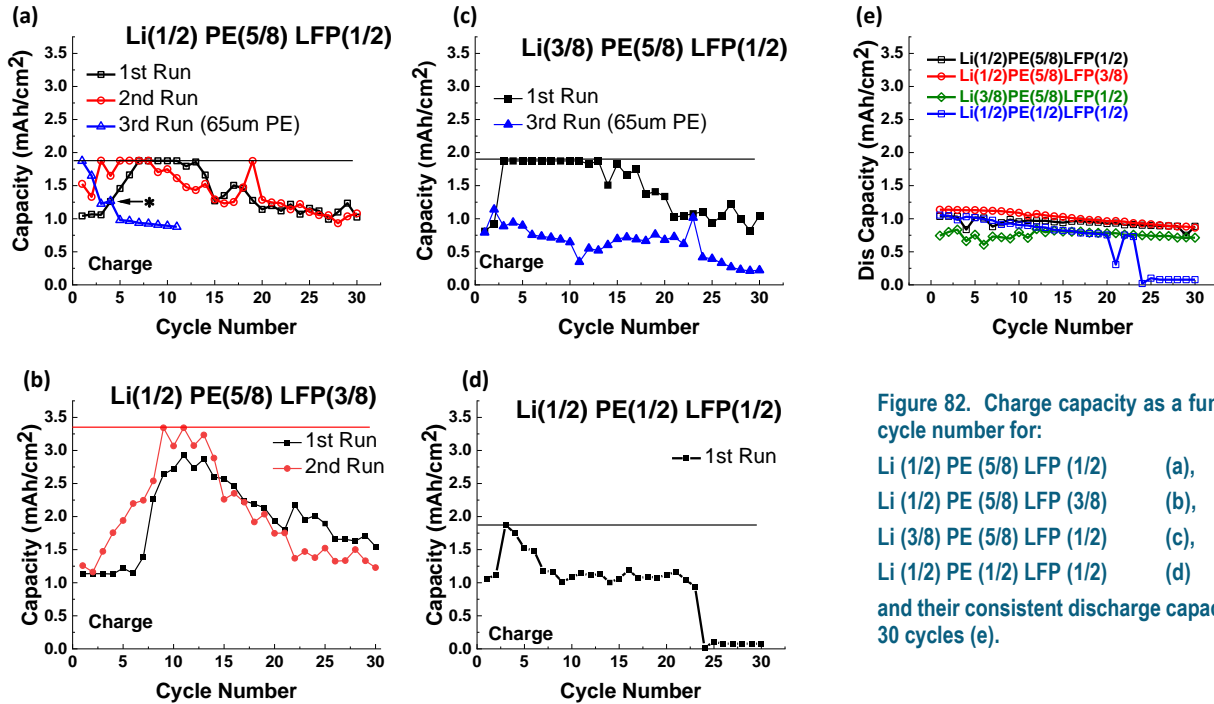


Figure 82. Charge capacity as a function of cycle number for:
 Li (1/2) PE (5/8) LFP (1/2) (a),
 Li (1/2) PE (5/8) LFP (3/8) (b),
 Li (3/8) PE (5/8) LFP (1/2) (c),
 Li (1/2) PE (1/2) LFP (1/2) (d)
 and their consistent discharge capacities for 30 cycles (e).

In reference [3], researchers concluded that formation of micro-dendrites at the Li/PE interface is the cause of the noisy voltage and apparent overcharge capacities. The team's observations suggest soft shorts may occur more frequently at electrode edges, but to account for the large and persistent overcharge requires more investigation. To test for reaction of the PE, it is harvested after cycling, and FTIR and SEM are used to examine changes in chemistry and morphology. As illustrated in Figure 83, IR spectroscopies of electrolyte indicate variations with cycle time and location. These changes require more study; however, for example, there are two peaks at 2800 cm⁻¹ (a broad peak and a narrow peak) that change in relative intensity after extensive cycling. In a previous study,^[4] the relative peak intensities at 2800 cm⁻¹ showed a similar trend when the [EO]/Li⁺ ratio decreased from 16:1 to 8:1. Based on this comparison, perhaps anion clustering occurs after extended cycling. Overall, variation in the PE indicated by FTIR seems far smaller than any reaction that could account for the integrated overcharge capacity.

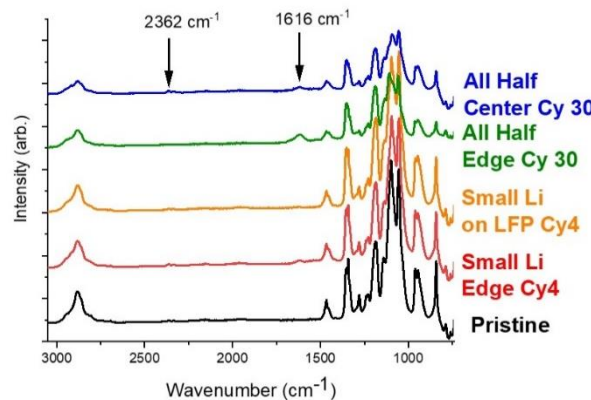


Figure 83. Infrared spectroscopy of polymer electrolyte (PE) from different regions (edge versus center) from Li (3/8) PE (5/8) LFP (1/2) after cycle 4 and cell Li (1/2) PE (1/2) LFP (1/2) after cycle 30.

References

- [1] Palmer, M. J., et al. "A Three-Dimensional Interconnected Polymer/Ceramic Composite as a Thin Film Solid Electrolyte." *Energy Storage Materials* 26 (2020): 242–249.
- [2] Balsara, N. P., and J. Newman. "Relationship between Steady-State Current in Symmetric Cells and Transference Number of Electrolytes Comprising Univalent and Multivalent Ions." *Journal of the Electrochemical Society* 162 (2015): A2720–22.
- [3] Homann, G., et al. "Poly(Ethylene Oxide)-Based Electrolyte for Solid-State-Lithium-Batteries with High Voltage Positive Electrodes: Evaluating the Role of Electrolyte Oxidation in Rapid Cell Failure." *Scientific Reports* 10 (2020): 2–10.
- [4] Wen, S. J., et al. "FTIR Characterization of PEO + LiN(CF₃SO₂)₂ Electrolytes." *Journal of Electroanalytical Chemistry* 408 (1996): 113–118.

Patents/Publications/Presentations

Publications

- Merrill, L. C., X. C. Chen, Y. Zhang, H. O. Ford, J. L. Schaefer, and N. Dudney. “Polymer-Ceramic Composite Electrolytes for Lithium Batteries: A Comparison between Single Ion Conducting Polymer Matrix and Its Counterpart.” Manuscript submitted.
- Y. Zhang, et al. “Poly(ethylene) Oxide Solid Polymer Electrolyte in Coin Cell Configuration: Insights on the Cell Assembling.” Manuscript in preparation.

Task 4.3 – Enabling Solid-State Batteries through Characterization and Modeling (Nenad M. Markovic and Larry A. Curtiss, Argonne National Laboratory)

Project Objective. The project objectives are multi-faceted, including development of a new mechanically and chemically stable and Li-ion conductive ($\geq 2 \times 10^{-4}$ S/cm at 298 K) crystalline/amorphous solid electrolyte for SSB. The anode and cathode are composed of lithium metal and a Li-based oxide, respectively, allowing operation at cathode potentials > 5 V (denoted as a S_{Li} - S_{EL} - S_C system).

Project Impact. Protective organic and inorganic compounds can enhance stability of the interface, improve Li-ion interfacial transport, minimize dendrite formation, and increase safety in Li-ion batteries.

Approach. The project proposes to develop and use interdisciplinary, atomic-/molecular-level insight obtained from integrating both experimental- and computational- based methodologies to define the landscape of parameters that control interfacial properties for a new generation of the Li-ion solid-solid battery systems. The strategy will involve transferring knowledge gained from well-characterized thin-film materials to real-world materials. This strategy forms a closed loop wherein the knowledge gained from model systems is used to design more complex, real-world materials, and vice versa. The work will focus on utilizing existing in-house synthesis and characterization methods to enable rapid transition from fundamental science to realistic cells.

Out-Year Goals. The out-year goals are to use and develop the physical and chemical synthesis methods for design of solid-solid interfaces with unique chemical/mechanical/conductivity properties. The proposed work will develop and exploit a variety of *ex situ* and *in situ* experimental optical and surface sensitive techniques and electrochemical methods to explore and explain bulk and interfacial properties of the selected materials. The results will serve to unravel many puzzling bulk and interfacial properties of S_{Li} - S_{EL} - S_C systems, including various types of ceramic and glass materials.

Collaborations. This project funds work at ANL and collaboration with J. Sakamoto at UM.

Milestones

1. Chemical stability, evaluation, and correlation with interfacial and bulk chemical reactivity for Li/PEO interfaces. (Q1, FY 2020; Completed)
2. Characterization of lithium / $Li_{0.33}La_{0.55}TiO_3$ (LLTO) interfaces: effect of crystallinity on surface and bulk reactivity and electrochemical stability. (Q2, FY 2020; Completed)
3. Characterization of LCO/electrolyte interfaces: effect of crystallinity and orientation on surface and bulk reactivity. (Q3, FY 2020)
4. Characterization of lithium interfaces with doped and undoped LLZO, with experimental and modeling study. (Q4, FY 2020)

Progress Report

Effect of LLTO(hkl) Orientation and Crystallinity on the LLTO/Li Interface: XAS and AIMD Studies.

LLTO is a perovskite solid electrolyte that crystallizes in a pseudo-perovskite structure with ordered lanthanum (A-site) vacancies along the c-axis in a tetragonal structure. Although LLTO exhibits orientation-dependent differences in bulk reactivity after short-term exposure to lithium thin films, long-term reaction (~ 3 days) with excess lithium eventually results in identical bulk reduction behavior regardless of orientation, indicating that the orientation-dependent differences observed are kinetic, rather than thermodynamic in origin. In contrast, *amorphous* LLTO thin films surprisingly exhibit no evidence of surface or bulk reactivity after the deposition of lithium thin films. This suggests that amorphous materials may represent a promising path toward realizing conductive solid electrolytes with reduced interfacial reactivity. The project's AIMD calculations for $\text{Li}/\text{La}_{0.55}\text{Li}_{0.33}\text{TiO}_3$ explored three different interfaces: Li/(001) LLTO, Li/(100) LLTO, and Li/amorphous LLTO. For the Li/(100) LLTO interface, considerable lithium exchange between the metallic lithium and lithium in LLTO was observed, with lithium ions hopping across the interface and along the Li-rich planes of LLTO. For the Li/(001) LLTO interface, there was no lithium exchange between lithium metal and LLTO at the simulation timescale. The AIMD results on amorphous LLTO indicate no redistribution of atomic species or lithium exchange in LLTO, suggesting that the reactivity of LLTO films toward lithium metal correlates with the feasibility of Li-ion exchange in LLTO.

Effect of LLTO(hkl) Orientation and Crystallinity on LLTO/Li Interface: Neutron Reflectivity Studies.

These studies of the interfaces between thin films of LLTO and metallic lithium aim to explore whether there exists a link between interfacial roughness and lithium diffusion, and if so, to determine whether this link depends on crystal orientation or crystallinity. An optimal tool for interfacial characterization is neutron reflectivity due to its sensitivity to interfacial reaction/roughening and/or variations in composition as a function of depth into the film. To conduct neutron reflectivity measurements, exceptionally smooth thin films are required. The team therefore used PLD to grow epitaxial LLTO thin films with different orientations and crystalline forms on NdGaO_3 , LSAO, SrTiO_3 , and silicon substrates. The film surfaces, as measured with AFM, showed ~ 2.5 nm roughness for the (001) oriented LLTO film, while the (100) film had roughness of ~ 0.5 nm (Figure 84).

The team started their neutron reflectivity study with bare LLTO films deposited with different crystal orientations and crystallinity at ambient conditions (Figure 85). To stabilize the desired LLTO crystallinity/orientation, different substrates are necessary, which means there could be differences in (strain induced) density as well as interface roughness. Measurements of bare LLTO also provide benchmarks for later experiments with lithium. This summer, during the project's NIST beamtime, the team will study LLTO films coated with or exposed to lithium, with different crystal orientations, crystallinity, and amounts of lithium deposited to determine the degree of lithium diffusion/intercalation into the LLTO layer. Due to the negative coherent scattering length of lithium, neutron reflectivity will be quite sensitive to changes in lithium distribution in the film, which ultimately will be measured as a function of temperature and electric field. Experiments on samples covered with lithium and under an electric field will require a more challenging sample environment due to their reactivity and sensitivity to air. These benchmark measurements of bare LLTO will also serve as a comparison for the LLTO and LiCoO_2 cathode bilayers, to help determine if and how the surface of the LLTO film roughens after the deposition of LiCoO_2 .

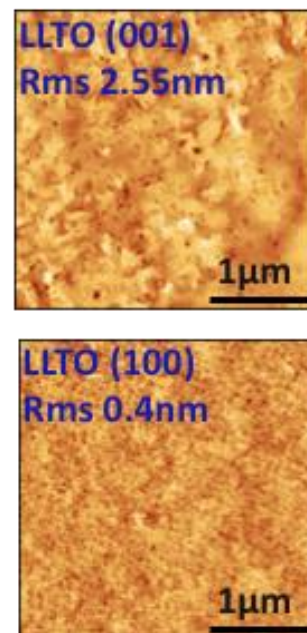


Figure 84. Atomic force microscopy roughness measurement on bare LLTO films in (100) and (001) orientations.

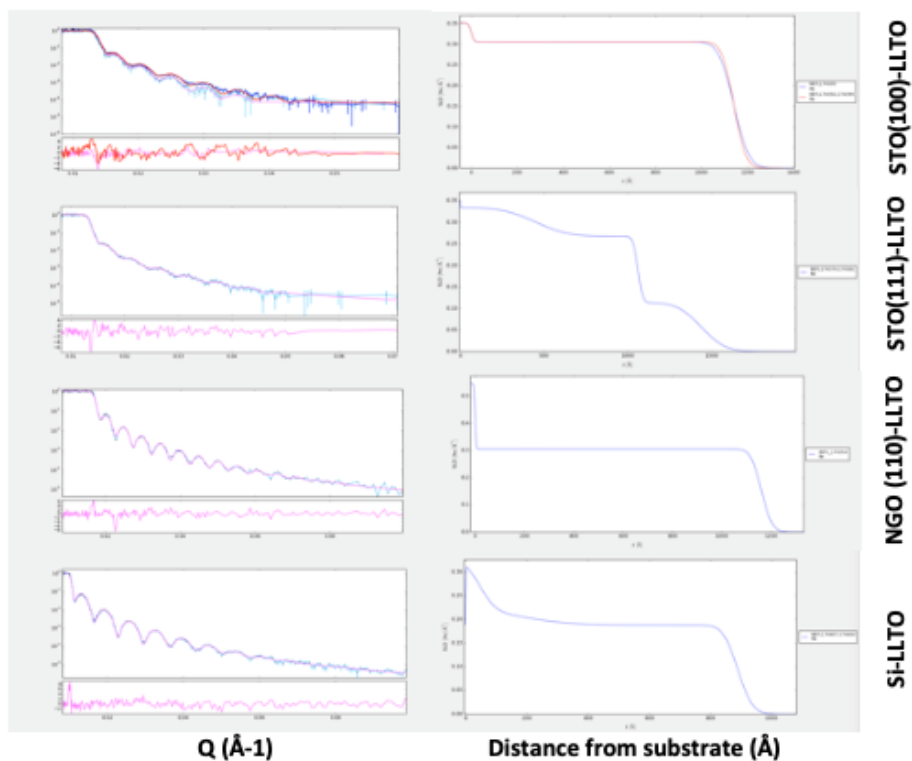


Figure 85. Neutron reflectometry of bare LLTO films with different crystal orientations and crystallinity.

Patents/Publications/Presentations

The project has no patents, publications, or presentations to report this quarter.

Task 4.4 – 3D Printing of All-Solid-State Lithium Batteries (Jianchao Ye, Lawrence Livermore National Laboratory)

Project Objective. This project has three objectives: (1) tuning microstructures of 3D-printed SSE separators, (2) determining material and processing compatibilities with cathode printing, and (3) 3D printing of sintering-free SSE separators.

Project Impact. All-solid-state lithium batteries are difficult to process due to the brittleness of ceramic materials, poor solid-solid contact, and electrolyte-electrode stability issues. As a result, the energy and power density and also cycling stability are far from satisfying. This project will address fabrication difficulties by using state-of-the-art 3D-printing techniques that can introduce 3D interfaces and architectures to enhance solid-solid contact and reduce charge transfer resistance. Success will benefit the DOE by establishing the best manufacturing methods for ASSBs to achieve VTO goals on the performance of beyond Li-ion batteries.

Approach. The project employs 3D-printing techniques to manufacture SSEs and related components for ASSBs. The team starts with direct ink writing (DIW) to develop ink recipes with desired rheological properties and explore post-sintering approaches to achieve high densification. In parallel with DIW 3D printing, the team also explores other 3D printing options, such as projection microstereolithography (PuSL), electrophoretic deposition (EPD), and projection-based two-photon polymerization. Both sintering and sintering-free approaches can gain benefit from 3D printing and therefore will be investigated.

Out-Year Goals. The team will determine particle sizes and morphologies as well as post-processing conditions that deliver good ionic conductivity and charge transfer properties of LLZTO separators. They will examine co-sintering of LLZTO/cathode and determine the effects of material, particle size, surface coating, and sintering conditions.

Collaborations. Microstructures, ionic conductivities, and mechanical properties will be provided to the LLNL simulation team, led by PI B. Wood, for establishing and validating phase-field modeling methods.

Milestones

1. ALD coating on LLZTO/electrode powders. (Q1, FY 2020; Completed)
2. Thermochemical stabilities of electrolyte-electrode-conductive additive mixtures. (Q2, FY 2020; In progress)
3. Down selection of electrolyte-electrode-conductive additive mixtures with good electronic and ionic conductivities. (Q3, FY 2020)
4. Evaluation of half-cell stability and failure mechanisms. (Q4, FY 2020)

Progress Report

The printed LLZTO films with high polymer /low ceramic contents tend to crack or warp during air-burning polymer removal. A two-step approach was developed to overcome this issue. First, the printed LLZTO / poly(ethylene glycol) diacrylate (PEGDA) film is pyrolyzed at 800-1100°C under argon flow. The inert environment may reduce the lithium loss and the residual carbon may act as binder, which keeps the film flat and crack-free even with large shrinkage. Then, the residual carbon is burnt off in dry air at relatively low temperatures to prevent short circuit.

XRD was taken to confirm the cubic phase and potential byproducts arising from different ink formulations and sintering conditions. Figure 86a shows results from raw and ball-milled LLZTO powders with PEGDA recipes. The raw LLZTO films after sintering at 900°C maintained the cubic phase with no detectable byproducts. By increasing sintering temperature to 1100°C, a tiny amount of $\text{La}_2\text{Zr}_2\text{O}_7$ byproduct was observed, probably due to the lithium loss. Those films with initial LLZTO particle size of $\sim 7 \mu\text{m}$ and volume fraction of 55% showed little shrinkage; therefore, the sintered product was highly porous. By replacing the raw powders with ball-milled LLZTO powders ($\sim 200 \text{ nm}$), a significant amount of $\text{La}_2\text{Zr}_2\text{O}_7$ phase and other related byproducts formed at or above 1000°C (Figure 86a). The thermal stability of printed films with ball-milled powders is poorer compared with hydraulic pressed pellets, which is likely due to the much higher surface area and lower solid content in ink recipes that promote the lithium loss at elevated temperatures. Increasing solid packing density in the printed green film may be the key to achieve better sintering results, while for ultraviolet (UV) curable recipes, it might be challenging. Understanding how the particle's initial morphological and chemical conditions affect sintering behaviors, including porosity and phase changes with temperature and time, would be useful for processing optimization. For that, *in situ* USAXS/WAXS studies on sintering of LLZTO were conducted and will be reported in another form.

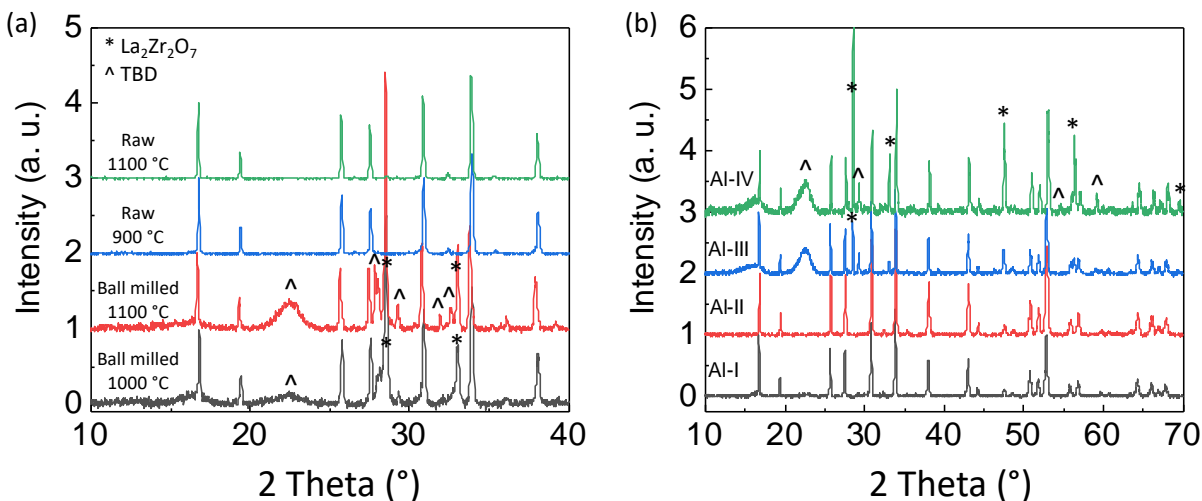


Figure 86. X-ray diffraction of sintered projection microstereolithography (PuSL) printed LLZTO films. (a) Bottom-up: LLZTO film with ball-milled powders, treated in argon at 1000°C (black) and 1100°C (red); LLZTO film with raw powders, treated at 900°C (blue) and 1100°C (green). (b) bottom-up: LLZTO-5LBO-1Al film treated in argon at 800°C (black), 900°C (red), 1000°C (blue), and 1100°C (green).

To avoid thermal decomposition at high temperature, additives were introduced in the ink formulation to accelerate densification. The team added 5 wt% Li_3BO_3 , which serves as sintering agent to facilitate densification, into LLZTO powders prior to ball milling. The obtained LLZTO-5LBO powders were further coated with 1 cycle of Al_2O_3 by ALD to improve the charge transfer property. The resulted LLZTO-5LBO-1Al powders were used in the PEGDA ink for PuSL printing and post thermal treatments. Figure 86b shows

XRD results after heat treatment at different temperatures from 800°C to 1100°C. Pure cubic LLZTO phase was obtained at 800°C and 900°C, while $\text{La}_2\text{Zr}_2\text{O}_7$ phase was formed at 1000°C and 1100°C. Although the addition of LBO and Al_2O_3 did not improve thermal stability, significant shrinkage was observed, even at temperatures lower than 900°C. The obtained films with no cracks and warpage allow the measurement of their electrochemical properties. Figure 87 shows an EIS plot of a LLZTO-5LBO-1Al film pyrolyzed at 900°C in argon and burnt at 700°C in dry air, in a lithium symmetrical cell setup. The bulk and interfacial resistances were extracted using an equivalent circuit model ($R_0+R_1/Q_1+R_2/Q_2$). An ionic conductivity of 7.6×10^{-5} S/cm and a charge transfer resistance of 314 ohm cm^2 were achieved, which met the original property goal.

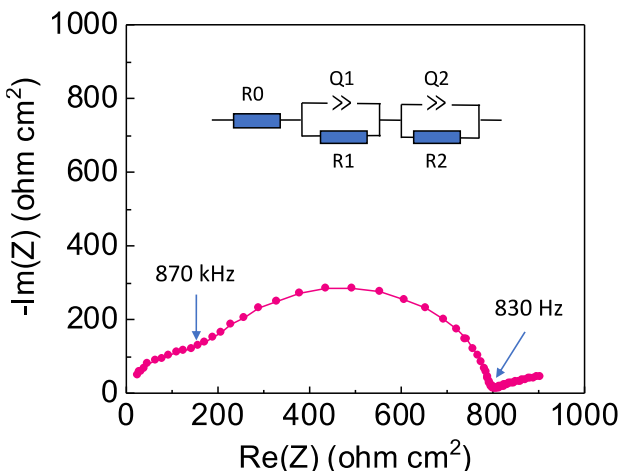


Figure 87. Electrochemical impedance spectroscopy of $\text{Li}|\text{LLZTO-5LBO-1Al}|\text{Li}$ symmetric cell at room temperature. The solid-state electrolyte separator was prepared by projection microstereolithography (PuSL) printing followed with 900°C argon pyrolysis and 700°C dry-air burning.

Efforts on thermal stability of cathode/LLZTO mixtures are in progress. Pellets of LLZTO/cathode mixtures with varying compositions have been prepared and will be subjected to sintering and characterization. Based on these results, selective LLZTO/cathode pairs will be used for film printing and post processing. Thermochemical and thermomechanical stabilities will be investigated in preparation for cell performance tests.

Patents/Publications/Presentations

Patent

- Ye, J., J. Roehling, and J. H. Yoo. "Systems and Methods for Laser Processing of Solid-State Batteries." U.S. Patent App. No. 16/783,910.

Publications

- Wood, M., X. Gao, R. Shi, J. Espitia, and J. Ye. "Reducing Sintering Temperature of Garnet Solid-State Electrolytes via High Energy Ball Milling." In preparation.
- Espitia, J., and J. Hammons, E. Ramos, M. Wood, M. Ceron, and J. Ye. "*In Situ* USAXS/WAXS Studies on Sintering of $\text{Li}_{6.4}\text{La}_3\text{Zr}_{1.4}\text{Ta}_{0.6}\text{O}_{12}$." In preparation.

Task 4.5 – Interfacial Studies on Lithium Thiophosphate Based Solid Electrolytes and Cathodes (Jagjit Nanda, Oak Ridge National Laboratory)

Project Objective. Capacity fading and the underlying interfacial side reactions between thiophosphate solid electrolytes and cathode active materials are not well understood. One of this project's key deliverables is to combine EIS measurements with complementary *in situ* and *ex situ* spectroscopy and microscopy to identify decomposition reaction products at the cathode/electrolyte interface. Ultimately, this work will enable a mechanistic understanding of factors that limit the rate performance and capacity loss of SSBs. The goal here is to combine the information from these techniques to provide a unified overview of the interfacial layer's composition, structure, and morphology. In this multi-year work, the team will investigate a number of solid electrolytes [Li_3PS_4 (LPS), $\text{Li}_{10}\text{GeP}_2\text{S}_{12}$ (LGPS), and $\text{Li}_{9.54}\text{Si}_{1.74}\text{P}_{1.44}\text{S}_{11.7}\text{Cl}_{0.3}$ (LSiPCl)] and cathode compositions belonging to different structural families [LiFePO_4 (olivine), FeS_2 (sulfide-based conversion cathode), and $\text{LiNi}_{0.6}\text{Mn}_{0.2}\text{Co}_{0.2}\text{O}_2$ (NMC-622, layered oxide)].

Project Impact. SSBs are poised to be the next-generation battery technology for meeting EV goals in terms of energy density, cycle life, and safety. Among other technical barriers, the success of this technology relies on design of stable electrode/electrolyte interfaces. Sulfide-based solid electrolytes have high ionic conductivity ($> 10^{-4}$ S/cm) and are mechanically soft, which simplifies processing compared to their oxide counterparts. Furthermore, sulfide solid electrolytes are comprised of earth abundant materials (for example, sulfur and phosphorus) and can be easily synthesized using scalable, low-temperature solution-based routes.

Approach. A low-temperature ($< 350^\circ\text{C}$) solution-based synthesis method will be used to synthesize the LPS family of solid electrolytes. The structure of these materials is characterized using XRD, Raman spectroscopy, and neutron scattering. Standard AC/DC electrochemical methods are used to characterize ionic conductivity, electrochemical stability, and CCD. The work scope includes using various *in situ* and *ex situ* electrochemical, microscopic, and spectroscopic tools for characterizing the structure, morphology, and kinetics of the interfacial reaction layer formed between thiophosphate solid electrolytes and cathodes.

Out-Year Goals. Develop thiophosphate solid electrolytes – sulfide cathode interfaces with low ASRs for ASSBs.

Collaborations. This project will collaborate with Profs. G. Ceder (UC Berkeley) and P. Jena (Virginia Commonwealth University) on modeling and synthesis guideline, as well as with Prof. S. Greenbaum on solid-state NMR to measure ion-diffusivity and local bonding.

Milestones

1. Identify synthesis, doping, and processing conditions to prepare Li_3PS_4 -based solid electrolytes with Li^+ conductivity exceeding 10^{-4} S/cm. (Q1, FY 2020; Completed, December 31, 2019)
2. Develop binder systems for Li_3PS_4 family of solid electrolytes for improving processability and stability at the Li-metal and cathode interfaces. (Q2, FY 2020; In progress)
3. Measure and compare the Li^+ diffusion coefficient for pristine Li_3PS_4 and substituted Li_3PS_4 solid electrolytes using solid-state NMR. (Q3, FY 2020)
4. Undertake *in situ* Raman and electron microscopy including cryo-TEM for characterizing Li_3PS_4 and cathode- Li_3PS_4 interfaces as part of determining the ASR. (Q4, FY 2020)

Progress Report

To improve processability of sulfide-based solid electrolytes, studies this quarter focused on development of $\text{Li}_3\text{PS}_4/\text{PEO}$ composites using a one-pot solvent-mediated synthesis route. Here, the Li_3PS_4 was synthesized *in situ* by blending Li_2S , P_2S_5 , and PEO (600 kDa) in acetonitrile followed by vacuum drying and thermal treatment steps. $\text{Li}_3\text{PS}_4/\text{PEO}$ composites with 0.2-56 wt% PEO were almost entirely amorphous even after annealing at temperatures up to 250°C as determined using XRD (results not shown). Cryo-TEM measurements in Figure 88a confirmed that the composites contained no nanocrystalline $\beta\text{-Li}_3\text{PS}_4$, but samples had small domains ($< 50\text{ nm}$) indexed to trace crystalline Li_2S ; see fast-Fourier transform (FFT) inset in Figure 88a.

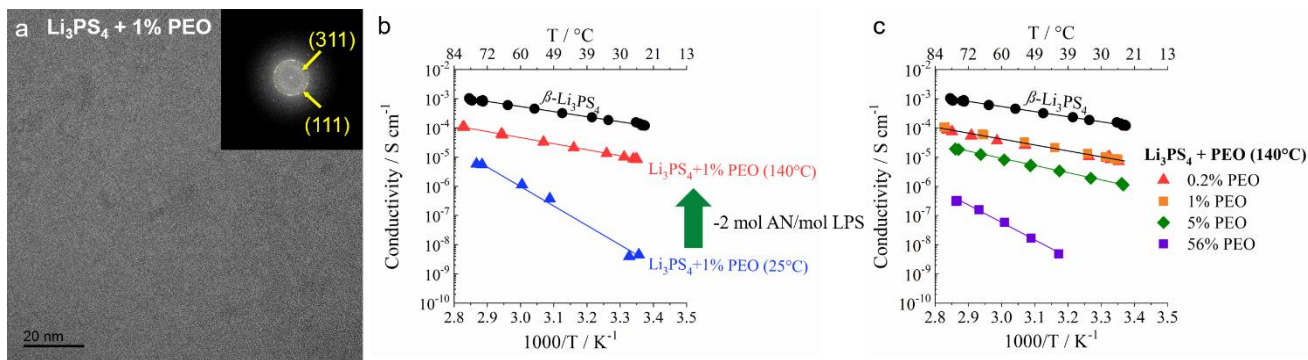


Figure 88. (a) Cryo – transmission electron microscopy image of a composite solid electrolyte containing amorphous $\text{Li}_3\text{PS}_4 + 1\text{ wt}\%$ PEO. (b-c) Li^+ conductivity measurements of $\beta\text{-Li}_3\text{PS}_4$ and $\text{Li}_3\text{PS}_4 + \text{PEO}$ composites showing (b) $\text{Li}_3\text{PS}_4 + 1\text{ wt}\%$ PEO dried at 25°C and 140°C and (c) $\text{Li}_3\text{PS}_4 + \text{PEO}$ composites containing 0.2-56 wt% PEO dried at 140°C .

The Li^+ conductivities of crystalline $\beta\text{-Li}_3\text{PS}_4$ (prepared through a similar solvent-mediated route, as reported in FY2019) and amorphous $\text{Li}_3\text{PS}_4 + \text{PEO}$ composites were evaluated in a blocking cell configuration using AC impedance spectroscopy. As shown in Figure 88b, the crystalline $\beta\text{-Li}_3\text{PS}_4$ exhibited high Li^+ conductivity (for example, $1.2 \times 10^{-4}\text{ S/cm}$ at room temperature) with an activation energy of 0.36 eV, values which are in good agreement with previous reports on the crystalline polymorph. In comparison, the ionic conductivity of the polymer/ceramic composites varied greatly depending on the thermal treatment. For instance, after drying under vacuum at 25°C , the conductivity of $\text{Li}_3\text{PS}_4 + 1\% \text{ PEO}$ was 5 orders of magnitude lower than that of $\beta\text{-Li}_3\text{PS}_4$ (for example, $4.5 \times 10^{-9}\text{ S/cm}$ at room temperature) due to the presence of coordinated AN. After heating to 140°C , the material evolved $\sim 2\text{ mol AN/mol Li}_3\text{PS}_4$ (corresponding to $\sim 30\text{ wt}\%$ loss), and the ionic conductivity increased 3 orders of magnitude at room temperature (that is, from 4.5×10^{-9} to $8.4 \times 10^{-6}\text{ S/cm}$). The higher conductivity coincided with a lower activation energy (1.37 versus 0.45 eV for samples dried at 25°C and 140°C , respectively), indicating the coordinated AN hindered Li^+ mobility and provided a less favorable energy landscape for long-range Li^+ migration. Raman spectroscopy and XPS measurements (results not shown) demonstrate that thermal annealing increased the amount of $\text{P}_2\text{S}_7^{4-}$ and PS_4^{3-} moieties, which promoted higher Li^+ conductivity.

Figure 88c shows the Li^+ conductivity of $\text{Li}_3\text{PS}_4 + \text{PEO}$ composites heated at 140°C as a function of polymer content. Samples with 0.2 and 1 wt% PEO exhibited identical conductivities and activation energies within experimental error. Increasing the PEO content from 1 to 5 wt% slightly decreased the conductivity (for example, $1.1 \times 10^{-6}\text{ S/cm}$ at room temperature) due to the insulating nature of PEO. As expected, higher PEO loading resulted in even lower conductivity, and the sample with 56 wt% PEO could only be measured at elevated temperature (for example, $4.8 \times 10^{-9}\text{ S/cm}$ at 42°C) due to its high resistance. Based on these findings, the polymer content in amorphous $\text{Li}_3\text{PS}_4 + \text{PEO}$ composites should be limited to ca. 1-5 wt% to ensure reasonable ionic conductivity, while providing enough binder to facilitate processing. Overall, the solvent-mediated synthesis approach developed here can be applied to a wide range of composite sulfide-based solid electrolytes where the material structure and electrochemical properties can be tuned by modifying key processing variables (for example, solvent, mixing protocol, binder content, and thermal post-treatment).

Patents/Publications/Presentations

Patents and Invention Disclosure

- Self, E. C., F. M. Delnick, and J. Nanda. “Amorphous Li_3PS_4 + Poly(ethylene Oxide): A New Class of Composite Electrolytes for Solid-State Batteries.” ORNL Internal Invention Disclosure No. 202004585.

Publication

- Self, E. C., Z. D. Hood, T. Brahmhatt, F. M. Delnick, H. M. Meyer III, G. Yang, J. L. M. Rupp, and J. Nanda. “A New Class of Amorphous Sulfide-Based Solid Electrolytes: Synthesis, Characterization, and Electrochemical Properties.” *ACS Energy Letters* (2020). Under review.

Task 4.6 – Prelithiation of Silicon Anode for High-Energy Lithium-Ion Batteries (Yi Cui, Stanford University)

Project Objective. Prelithiation of high-capacity electrode materials is an important means to enable those materials in high-energy batteries. This study pursues three main directions: (1) developing facile and practical methods to increase first-cycle CE of anodes, (2) synthesizing fully lithiated anode to pair with high-capacity Li-free cathode materials, and (3) prelithiation from the cathode side.

Project Impact. Prelithiation of high-capacity electrode materials will enable those materials in next-generation high-energy-density Li-ion batteries. This project's success will make high-energy-density Li-ion batteries for EVs.

Approach. Silicon electrode film will be prepared by coating the slurry of silicon nanoparticles, carbon black, and binder mixture on copper foil through a doctor-blading method. The silicon electrode film will be prelithiated by pressing a Li-metal foil on top of it and heating it in an argon glovebox for a certain time. Then, Li_xSi electrode film can be obtained by removing the redundant lithium foil through a peeling-off approach. The redundant lithium foil is reusable for the next prelithiation. The structure, morphology, and other properties can be analyzed by SEM, TEM, XPS, Raman spectroscopy, XRD, etc. In the first year, the team aims to fabricate Li_xSi freestanding electrode film and improve its air stability. In the second year, the team aims to improve the electrochemical stability in full cells.

Out-Year Goals. Materials containing a large quantity of lithium will be synthesized for pre-storing lithium ions inside batteries. Materials and process will be developed to be compatible with battery electrode and cell fabrication. First-cycle CE of anodes will be improved and optimized by prelithiation materials. Develop materials for prelithiation from the cathode side.

Collaborations. This project engages in collaboration with the following: BMR PIs; SLAC: Dr. M. Toney (*in situ* X-ray); and Stanford: Prof. Nix (mechanics).

Milestones

1. Demonstrate a new solvent-free dry method for anode prelithiation. (Q1, FY 2020; Completed)
2. Demonstrate control of prelithiation amount by adjusting contact duration between thick lithium foil and anode materials. (Q2, FY 2020; Completed)
3. Demonstrate synthesis of thin lithium foil with different thickness (5-20 μ) for use in dry prelithiation method. (Q3, FY 2020; In progress)
4. Demonstrate thin lithium foil with different thicknesses as dry prelithiation reagents for anode materials to pair with different-capacities cathode materials. (Q4, FY 2020)

Progress Report

Substantial improvements on energy density of Li-ion batteries require development of high-capacity electrodes. Alloy anodes with much higher capacity have been recognized as promising alternatives to graphites. However, the low initial Coulombic efficiency (ICE) accompanied with the alloying chemistry limits the full usage of the designed capacity in battery. Silicon, as an example of a typical alloy anode, has ICE as low as ~ 70%, indicating ~ 30% of the capacity will be lost after 1st cycle. Therefore, prelithiation as a strategy to compensate the irreversible capacity loss in the 1st cycle has become critically important for battery performance improvement.

In the last report, the team shows that prelithiation can be achieved through a novel one-step, heat-free, solvent-free approach by electrochemical shorting between silicon anode and a layer of thin lithium foil. Here, the team further develops this method and designs a series of lithium masks with different porosity to achieve controllable prelithiation.

A series of lithium masks with porosity varied from 50% to 80% has been designed and produced, as shown in Figure 89a. By controlling porosity in the lithium masks, the capacity in these prelithiation reagents can be tuned. The capacity stored in the lithium masks is first measured by stripping away all the lithium out of the masks; the stripping capacity, which corresponds to the capacity storage in lithium masks, is shown in Figure 89b as the 2nd Y-axis. The measured capacity in the series of lithium masks varies linearly with the porosity, whose range is around 1-2.5 mAh, which well matches the desired prelithiation amount for a full-cell battery with designed capacity of ~ 3-6 mAh. To further evaluate the effectiveness of this series of lithium masks in prelithiation, Li||Si half cells with different lithium masks inserted are assembled, and the 1st cycle voltage versus capacity curve is measured by a galvanostatic charge-discharge test. The ICE is calculated by dividing the charge capacity over the discharge capacity, and it is shown as the 1st Y-axis in Figure 89b. There is a clear trend that with lower porosity, corresponding to higher capacity stored in prelithiation reagent, a higher ICE is achieved in a controllable manner. In the condition of this experiment with silicon mass loading of ~ 1.5 mg, lithium masks with porosity of 70% or 80% match best, as they can improve the ICE of silicon anodes to around 100%. But when silicon mass loading goes higher or another anode material with lower ICE is used, the desired prelithiation amount will increase and also lithium masks with lower porosity will be needed. Thus, the wide range of capacity in the designed lithium masks with different porosity can satisfy the prelithiation need of a wide range of anode materials and enable their broad application.

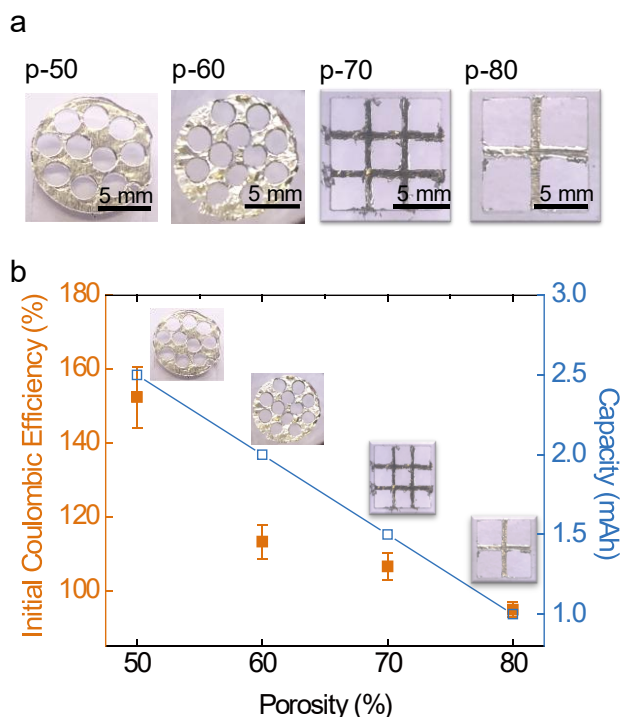


Figure 89. (a) Photographs of lithium masks reagent with varied porosity from 50% to 80%. (b) Initial Coulombic efficiency improvement after prelithiation with the series of lithium masks with different porosity and the corresponding capacity in lithium masks. (Silicon mass loading, ~ 1.5 mg)

Patents/Publications/Presentations

The project has no patents, publications, or presentations to report this quarter.

TASK 5 – SULFUR ELECTRODES

Summary

The collected work in this Task involves six projects that have focused on the following areas:

- Conducting focused fundamental research on the mechanism of “shuttle effect” inhibition for rechargeable Li-S batteries.
- Developing electrode and electrolyte systems that can mitigate the “shuttle effect” so the low self-discharge and long cycle life can be achieved.
- Synthesizing sulfur composite materials with an emphasis on polymer sulfur composite materials.
- Developing creative electrode-making processes to improve processability and aerial capacity; for example, polymeric sulfur composites may not be suitable for the traditional slurry casting process.
- Developing a novel S_xSe_y cathode material for rechargeable lithium batteries with high energy density and long life, as well as low cost and high safety.
- Delivering an electrochemically responsive self-formed hybrid LIC as a protective layer for Li-metal anodes, enabling Li-metal anodes to cycle with a high efficiency.
- Developing high-energy, low-cost Li-S batteries with long lifespan.

Highlights. The highlights for this quarter are reported below.

Task 5.1 led by Dr. Amine’s group at ANL continued their exploration of the SeS_x -HC system. Accordingly, they have tested the electrochemical performance of SeS_x -HC (10 wt% sulfur doping) under fast charging, lean electrolyte and high sulfur loading. They have demonstrated the combined influence of selenium doping and use of fluorinated ether electrolytes (hydrofluoroether, or HFE) in mitigating the sluggish reaction kinetics as well as the severe shuttle effect of Li-S batteries. Preliminary results of the system tested under high Se-S loading of 4.5 mg/cm^2 and electrolyte/Se-S (E/S) ratio of $10 \text{ }\mu\text{L/mg}$ after 100 cycles shows that the electrode could maintain a reversible areal capacity of greater than 3 mAh/cm^2 , indicating good feasibility of their selenium doping and use of HFE-based electrolytes.

Task 5.2 led by Dr. Liu’s group at PNNL continued their studies on carbon systems with different particle sizes of $> 70 \text{ }\mu\text{m}$ and $< 20 \text{ }\mu\text{m}$ under lean electrolyte conditions of $4 \text{ }\mu\text{L/mg}$ and high loading of 4 mg/cm^2 . In particular, they explored the change in *in situ* impedance during cycling of the electrodes with different particle sizes maintaining the same porosity of 45% and lean electrolyte $4\text{-}\mu\text{L/mg}$ conditions. The response was studied using a three-electrode system employing $Li_4Ti_5O_{12}$ as the third electrode. Results show that the electrode fabricated with $> 70\text{-}\mu\text{m}$ -sized particles of carbon showed better electrolyte infiltration and wetting behavior with diminished charge transfer resistances compared to the electrodes generated from $< 20\text{-}\mu\text{m}$ -sized particles of carbon.

Task 5.3 led by Dr. Cui’s group at Stanford demonstrated improvements in electrochemical performance achieved by using liquid sulfur in Li-S batteries. They have specifically chosen to use nickel foam and carbon-coated nickel foam to study the confinement and trapping of polysulfides formed on the surfaces of these systems and the resulting polarization and hysteresis response. They have accordingly shown that the nickel foam exhibits much better polysulfide trapping and chemisorption confinement response, displaying a capacity of 360 mAh/g and 300 mAh/g at 2C and 3C current rates, respectively, with a stable capacity of 500 mAh/g at the end of 100 cycles. On the other hand, the carbon-coated nickel exhibits a capacity of only 275 mAh/g and 110 mAh/g under similar current rates.

Task 5.4 led by Dr. Qu's group at UWM collaborated with Dr. Hu at BNL to synthesize new carbon structures containing metal-nitrogen containing anchors for sulfide and polysulfide species for $M = \text{Cu, Ni, Fe, Co}$. They designed ordered mesoporous carbons with metal/nitrogen containing species (GOMCs) as sulfur hosts with abundant porosity and high electrical conductivity. They conducted DFT calculations to show that Fe-N containing ordered mesoporous structures, Fe-N-GOMCs, exhibit the most favorable adsorption energies for Li_2S (-3.01 eV) compared to -0.3 eV for pure carbon and -0.54eV for nitrogen-doped carbon, suggesting the ability of nickel and iron dopants in carbon to effectively suppress active sulfur loss and consequent shuttling effect resulting in likely superior cycling stability.

Task 5.5 led by Dr. Liu's group at LBNL measured the ionic conductivities of amphiphilic HFE electrolyte additives exhibiting dual functionalities with a lithiophobic fluorocarbon moiety at one end and polar lithiophilic ethylene oxide moiety at the other. These additives significantly improve solubility of Li-ion salts in the fluorocarbon solvents such as 1,1,2,2-Tetrafluoroethyl 2,2,2-Trifluoroethyl Ether (TTE). The lithium salts follow a micelle solvation mechanism on dissolution in the HFE amphiphilic additives. They measured the ionic conductivity of 0.5 M LiTFSI electrolyte to be 10^{-4} - 10^{-3} S/cm with use of smaller HFE molecules of tetrafluoroethyl ethylene oxide (F_4EO_2) with a 1:1 dilution ratio of HFE with TTE, due to proper viscosity and larger micelle formation likely improving Li-ion transport and thus suggesting its use for battery applications.

Task 5.1 – Novel Chemistry: Lithium Selenium and Selenium Sulfur Couple (Khalil Amine, Argonne National Laboratory)

Project Objective. The project objective is to develop a novel S_xSe_y cathode material for rechargeable lithium batteries with high energy density and long life, as well as low cost and high safety.

Project Impact. Development of a new battery chemistry is promising to support the goal of PHEV and EV applications.

Approach. The dissolution of lithium polysulfides in nonaqueous electrolytes has been the major contribution to the low energy efficiency and short life of Li-S batteries. In addition, insulating characteristics of both end members during charge/discharge (sulfur and Li_2S) limit their rate capacity. To overcome this problem, sulfur or Li_2S is generally impregnated in a carbon-conducting matrix for better electronic conductivity. However, this makes it difficult to increase the loading density of practical electrodes. It is proposed to solve these barriers using the following approaches: (1) partially replace sulfur with selenium, (2) nano-confine the S_xSe_y in a nanoporous conductive matrix, and (3) explore advanced electrolytes with suppressed shuttle effect.

Out-Year Goals. This new cathode will be optimized with the following goals:

- A cell with nominal voltage of 2 V and energy density of 600 Wh/kg.
- A battery capable of operating for 500 cycles with low capacity fade.

Collaborations. This project engages in collaboration with the following: Dr. Y. Ren and Dr. C. Sun of APS at ANL, Dr. L. A. Curtiss at ANL, and Prof. A. X. Sun at Western University, Canada.

Milestones

1. Synthesize new carbon materials to prepare SeS_x /carbon composites with high sulfur loading in the composite. (Q1, FY 2020; Completed)
2. Optimize cathode structures to increase SeS_x areal loading, and improve battery performance. (Q2, FY 2020; Completed)
3. Gain interface understanding on the cycled SeS_x cathode using TOF-SIMS and XPS. (Q3, FY 2020)
4. Gain interface understanding on the cycled lithium metal using TOF-SIMS and XPS. (Q4, FY 2020)

Progress Report

This quarter, the team further tested the electrochemical performance of $\text{SeS}_x\text{-HC}$ (10 wt% selenium doping) composite under fast charging, lean electrolytes and high sulfur loading conditions to demonstrate the concept of using selenium doping and fluorinated ether electrolytes to overcome the sluggish reaction kinetics and severe shuttle effect of Li-S batteries.

Figure 90 shows the rate capability test of $\text{SeS}_x\text{-C}$ with 10 wt% selenium doping in HFE electrolytes with a 1.2 mg cm^{-2} Se-S loading. At a relatively low rate of 0.5C, the electrode can deliver an average capacity of $\sim 1000 \text{ mAh g}^{-1}$. As the charge/discharge rates were successively increased from 0.5C to 0.75C, 1C, 1.5C, 2C, 2.5C, 3C, to 3.7C, the reversible capacities decreased accordingly. At a high rate of 3.73C (ca. 15 minutes of charge/discharge), the electrode can still maintain a reversible capacity of $\sim 500 \text{ mAh g}^{-1}$, demonstrating superior rate capability. This was due to the addition of selenium, which significantly improves electronic transport during charge/discharge. Moreover, when charge/discharge rates are decreased back to 0.5C, capacities can be almost 100% recovered, demonstrating excellent structural and lithiation/delithiation stability.

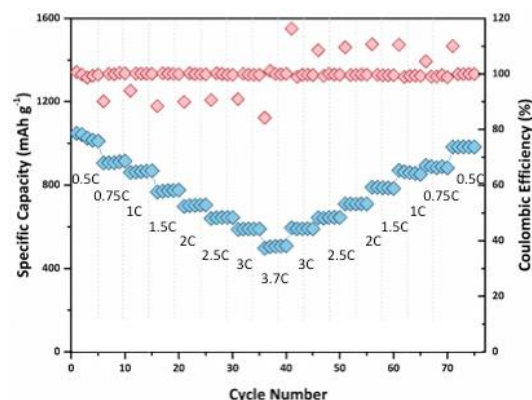


Figure 90. Rate performance of $\text{SeS}_x\text{-C}$ with 10 wt% selenium doping in HFE electrolytes with a 1.2 mg cm^{-2} Se-S loading.

Figure 91 compares the charge/discharge curves of $\text{SeS}_x\text{-C}$ with 10 wt% selenium doping with a 2.5 mg cm^{-2} Se-S loading in DME and HFE electrolyte under different electrolyte/Se-S (E/S) ratio. Decreasing the E/S ratio has been found critical and necessary to achieve higher energy density of pouch cells.

However, it would also significantly reduce utilization of active material due to decreased reaction kinetics. In the case of conventional DME-based electrolytes (Figure 91a), increase of the E/S ratio from 10 to 15 did not increase specific capacity, but induced a more severe shuttle effect, which may be caused by more dissolution of polysulfides/polyselenides in the electrolytes. Decrease of the E/S ratio from 10 to 5 also aggravated the shuttle effect. This is because of the significantly decreased discharge specific capacity under low E/S ratio. As a comparison, in the case of HFE-based electrolytes, the cell did not show any visible shuttle effect at different E/S ratios. The E/S ratio of this study in high loading Se-S electrodes was set at $10 \mu\text{L mg}^{-1}$ due to a trade-off between specific capacity and E/S ratio.

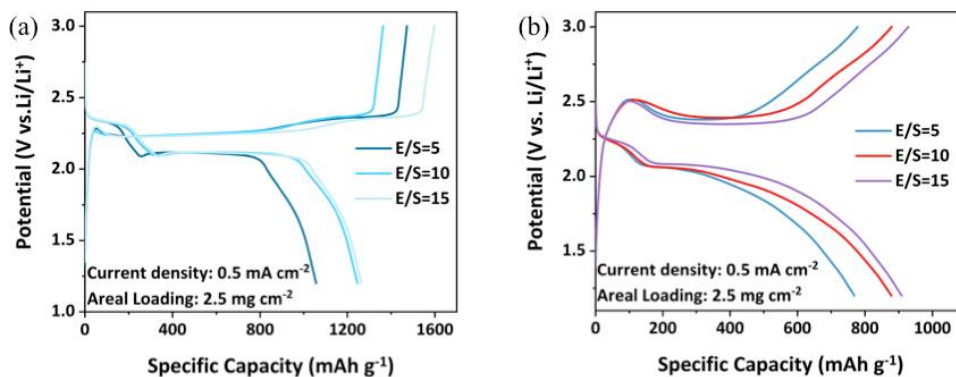


Figure 91. Charge/discharge curves of $\text{SeS}_x\text{-C}$ with 10 wt% selenium doping in (a) DME and (b) HFE electrolytes with a 2.5 mg cm^{-2} Se-S loading under different electrolytes/Se-S ratio ($\mu\text{L mg}^{-1}$).

To demonstrate feasibility of the team's concept in high Se-S loading, they fabricated a $\text{SeS}_x\text{-C}$ with 10 wt% selenium doping laminate with a high Se-S loading of 4.5 mg cm^{-2} . Figure 92a shows its cycle performance with an E/S ratio of $10 \mu\text{L mg}^{-1}$ at 0.8 mA cm^{-2} (ca. 0.1C). As shown, under a high Se-S loading, the electrode

can still deliver a high areal capacity of 5.5 mAh cm^{-2} , corresponding to a specific capacity of $\sim 1200 \text{ mAh g}^{-1}$. During 100 cycles of charge/discharge, the electrode could well maintain a high reversible areal capacity of $> 3 \text{ mAh cm}^{-2}$. The capacity retention of the 100th cycle is $\sim 80\%$ of the 2nd cycle, demonstrating excellent cycle stability. Moreover, the cell also demonstrated an extremely low shuttle effect as the CE during cycling was all close to 100%. Figure 92b shows its charge/discharge curves during cycling, which exhibited minimal voltage polarization during cycling.

In a brief summary, selenium doping and fluorinated electrolytes have remarkably improved reaction kinetics and suppress the shuttle effect for high Se-S loading. More fundamental understanding is needed to explore the underlying mechanism, which will be reported next quarter.

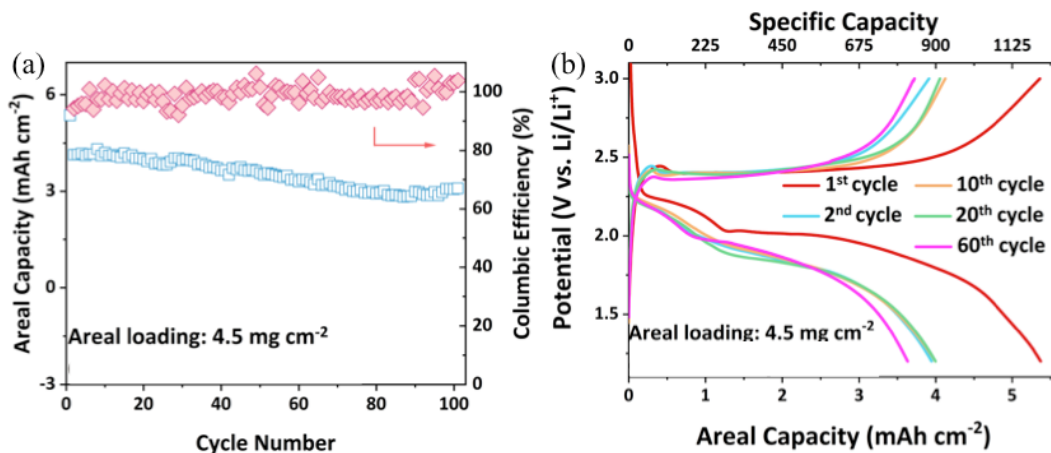


Figure 92. (a) Cycling performance and (b) charge/discharge curves of SeS_x-C with 10 wt% selenium doping in HFE electrolytes with a high Se-S loading of 4.5 mg cm^{-2} at 0.8 mA cm^{-2} and E/S ratio of $10 \text{ } \mu\text{L mg}^{-1}$.

Patents/Publications/Presentations

Patents

- Xu, G. L., and K. Amine. “Non-Flammable Electrolytes.” U. S. Patent Application. Filed.
- “Selenium-Doped Sulfur Cathodes for Rechargeable Batteries.” U. S. Patent US10601077B2. Granted.

Publication

- Amine, K., et al. “Revisiting the Role of Conductivity and Polarity of Host Materials for Long-Life Lithium-Sulfur Battery.” *Advanced Energy Materials* (2020): 1903934.

Task 5.2 – Development of High-Energy Lithium-Sulfur Batteries (Dongping Lu and Jun Liu, Pacific Northwest National Laboratory)

Project Objective. The project objective is to develop high-energy, low-cost Li-S batteries with long lifespan. All proposed work will employ thick sulfur cathode (≥ 2 mAh/cm² of sulfur) at a relevant scale for practical applications. The diffusion process of soluble polysulfide out of thick cathode will be revisited to investigate cell failure mechanism at different cycling. The fundamental reaction mechanism of polysulfide under the electrical field will be explored by applying advanced characterization techniques to accelerate development of Li-S battery technology.

Project Impact. The theoretical specific energy of Li-S batteries is ~ 2300 Wh/kg, which is almost three times higher than that of state-of-the-art Li-ion batteries. The proposed work will design novel approaches to enable Li-S battery technology and accelerate market acceptance of long-range EVs required by the EV Everywhere Grand Challenge.

Approach. The project proposes to (1) identify and address key issues of applying high-energy sulfur cathodes including materials, binders, electrode architectures, and functional electrode additives, (2) advance the mechanism study of sulfur cathode and electrolyte by using *in situ* / *ex situ* techniques and custom-designed hybrid cell setup, and (3) verify effectiveness of the new approaches with coin/pouch cells by using high-loading electrodes (> 4 mg/cm²), limited lithium ($< 200\%$ lithium excess), and lean electrolyte (E/S < 4 μ L/mg).

Out-Year Goals. This project has the following out-year goals:

- Fabricate Li-S pouch cells with thick electrodes to understand sulfur chemistry/electrochemistry in environments similar to real application.
- Leverage the Li-metal protection project funded by the DOE and PNNL advanced characterization facilities to accelerate development of Li-S battery technology.
- Develop Li-S batteries with a specific energy of 400 Wh/kg at cell level, 1000 deep-discharge cycles, improved abuse tolerance, and less than 20% capacity fade over a 10-year period to accelerate commercialization of EVs.

Collaborations. This project engages in collaboration with the following: Dr. X-Q. Yang (BNL), Dr. D. Qu (University of Wisconsin at Madison), Dr. G. Zhang (University of Alabama), and Dr. J. Tao (PNNL).

Milestones

1. Synthesis of IKB with controlled secondary particles from 5 to 100 μ m for high-loading sulfur electrodes (> 4 mg S/cm²). (Q1, FY 2020; Completed)
2. Realize sulfur utilization rate > 1200 mAh/g in dense sulfur electrodes (S > 4 mg/cm², porosity $\leq 50\%$) at an E/S ≤ 4 μ L/mg through electrode architecture control. (Q2, FY 2020; Completed)
3. Demonstrate > 80 cycles (80% capacity retention) in dense sulfur electrodes at E/S ≤ 4 μ L/mg through the hybrid electrode design. (Q3, FY 2020; In progress)
4. Complete evaluation of high-loading sulfur electrodes at E/S ≤ 3 μ L/mg and transfer sufficient materials to Battery500 for high-energy pouch cell demonstration. (Q4, FY 2020; In progress)

Progress Report

To extend cycle life of Li-S batteries at a very lean electrolyte condition, it is essential to conserve the limited electrolyte to support cycling rather than filling the large electrode pores. Rationalizing the electrode structure to a low porosity is necessary for that purpose. The S/C composites with controlled particle size were synthesized last quarter and used as example materials to investigate correlations of material property and electrode performance this quarter. Study of the dense electrodes indicates particle size has an especially important impact on cell performance. It was observed that at the same level of electrode porosity, the electrodes using $> 70\text{-}\mu\text{m}$ particles show much better performance compared to those using the $< 20\text{-}\mu\text{m}$ particles in terms of electrochemical polarization, reversible capacity, and cycling stability. For electrodes prepared by different electrode processing methods, reversible capacities of $> 1000\text{ mAh/g}$ at 0.1C and $> 1200\text{ mAh/g}$ at 0.05C were achieved with electrode porosities as low as 45%.

To understand how particle size affects cell performance, sulfur cathodes comprised of small and large particles were prepared and studied by *in situ* EIS. To decouple the interferences of lithium metal while acquiring EIS spectra, a three-electrode cell configuration was used, where a tiny strip of LTO ($\text{Li}_4\text{Ti}_5\text{O}_{12}$) electrode was wrapped with polypropylene separator and placed in between the sulfur working electrode and Li-metal counter electrode. Figure 93 shows the first discharge curves of the dense (45%) and high loading (4 mg/cm^2) electrodes at lean electrolyte conditions ($4\text{ }\mu\text{L/mg}$ sulfur). EIS spectra were acquired during the discharging of the cell in an interval of 7000 seconds. The dense electrode using large particles shows two typical discharge plateaus, which are comparable with highly porous sulfur cathodes. Conversely, in the dense electrode comprised of small particles, only one discharging plateau with increased polarization was observed. Those distinct electrochemical behaviors were ascribed to the varied electrolyte infiltration and subsequent sulfur reaction processes in different electrode architectures built on different size particles.

Given the same materials and electrolyte, the EIS before cell cycling is an indicator of electrode wetting with electrolyte. Compared with the small particle electrode, the large particle electrode shows much smaller resistances for both the bulk and the overall charge-transfer (R_{ct}). This suggests better electrolyte infiltration/distribution among the large particle electrode. On discharging, the overall R_{ct} of the large particle electrode decreased gradually from Phase I to Phase III. This is due to the generation of soluble polysulfides that lead to enhanced reaction kinetics. An increase of R_{ct} was observed only at the end of Phase IV and was greatly enhanced during Phase V, which is due to formation of solid Li_2S_2 and Li_2S , as well as their deposition on the carbon surface. However, for the small particle electrode, the overall resistance increased significantly at the end of Phase II to a value comparable to the R_{ct} in phase V of the large particle electrode. This means reactions of the small particle electrode were prematurely terminated by the end of Phase II, explaining well its limited discharge capacity and large polarization. Despite the same levels of electrode mass loading and overall porosity, the pore structures and their distribution inside the electrodes were varied by using different particle sizes, leading to different electrode tortuosity. Therefore, electrolyte diffusion, polysulfide solubility, and sulfur reaction pathways are altered and result in different electrochemical performance. Detailed characterization of the electrodes with different particles, before and after cycling, is in progress to correlate cell performance to material properties.

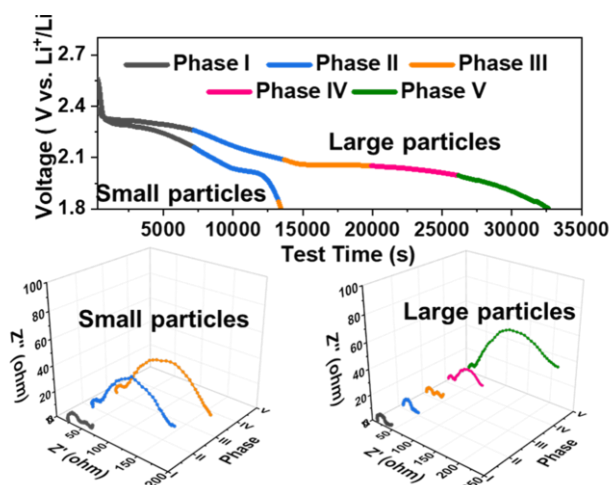


Figure 93. First discharging profiles and *in situ* electrochemical impedance spectroscopy of electrodes with $< 20\text{-}\mu\text{m}$ and $> 70\text{-}\mu\text{m}$ particles (Electrode: 45% porosity, 4 mg S/cm^2 , and $E/S = 4\text{ }\mu\text{L/mg S}$, $I = 0.1\text{C}$, room temperature, and electrolyte: $1\text{ M LiTFSI/DOL/DME} + 0.3\text{ M LiNO}_3$).

Patents/Publications/Presentations

Publication

- Shi, L., and S. Bak, Z. Shadik, C. Wang, C. Niu, P. Northrup, H. Lee, A. Baranovskiy, J. Qin, S. Feng, X. Ren, D. Liu, X. Yang, F. Gao, D. Lu, J. Xiao, and J. Liu. “High-Energy Lithium-Sulfur Pouch Cells: Nanoscale Reaction Heterogeneity and Mitigation Strategies.” *Proceedings of the National Academy of Sciences of the United States of America*. Under review.

Presentation

- TMS 2020 Annual Meeting & Exhibition, San Diego, California (February 23–27, 2020): “Sulfide Based Solid Electrolyte for Lithium-Sulfur Batteries”; D. Lu, Z. Yu, J. Xiao, and J. Liu.

Task 5.3 – Nanostructured Design of Sulfur Cathodes for High-Energy Lithium-Sulfur Batteries (Yi Cui, Stanford University)

Project Objective. The charge capacity limitations of conventional TM oxide cathodes are overcome by designing optimized nano-architected sulfur cathodes. This study aims to enable sulfur cathodes with high capacity and long cycle life by developing sulfur cathodes from the perspective of nanostructured materials design, which will be used to combine with Li-metal anodes to generate high-energy Li-S batteries. Novel sulfur nanostructures as well as multi-functional coatings will be designed and fabricated to overcome issues related to volume expansion, polysulfide dissolution, and the insulating nature of sulfur.

Project Impact. The capacity and cycling stability of sulfur cathode will be dramatically increased. This project's success will make Li-S batteries to power EVs and decrease the high cost of batteries.

Approach. The approach involves three main parts:

- Advanced nanostructured sulfur cathodes design and synthesis, including (1) engineer empty space into sulfur cathode to solve problem of electrode volume expansion, (2) develop novel sulfur nanostructures with multi-functional coatings for confinement of S/Li polysulfides to address issues of active materials loss and low conductivity, (3) develop/discover optimal nanostructured materials that can capture the polysulfide dissolved in the electrolyte, (4) develop space-efficiently-packed nanostructured sulfur cathode to increase volumetric energy density and rate capability, and (5) identify interaction mechanism between sulfur species and different types of oxides/sulfides, and find optimal material to improve capacity and cycling of sulfur cathode.
- Structure and property characterization, including *ex situ* SEM, XPS analysis, and *in operando* XRD and optical microscopy.
- Electrochemical testing including coin cells and pouch cells as well as a set of electrochemical techniques.

Out-Year Goals. The cycle life, capacity retention, and capacity loading of sulfur cathodes will be greatly improved (200 cycles with 80% capacity retention, > 0.3 mAh/cm² capacity loading) by optimizing material design, synthesis, and electrode assembly.

Collaborations. This project collaborates with the following: BMR PIs; SLAC: Dr. M. Toney (*in situ* X-ray); and Stanford: Prof. Nix (mechanics) and Prof. Bao (materials).

Milestones

1. Understanding the mechanism of liquid sulfur on the surface of 3D materials. (Q1 FY 2020; Completed)
2. Demonstrate improvement by utilizing liquid sulfur in Li-S batteries. (Q2, FY2020; Completed)
3. Develop high sulfur loading cathode based on understanding of liquid sulfur. (Q3, FY 2020; In progress)
4. Enable Li-S batteries with high sulfur loading, low E/S ratio, and fast kinetics. (Q4, FY 2020)

Progress Report

In the last report, the team discussed understanding the mechanism of liquid sulfur on the surface of 3D materials. This quarter, they demonstrate improvement by utilizing liquid sulfur in Li-S batteries.

The team chose nickel foam and carbon-coated nickel foam as the 3D porous architecture to reveal the sulfur growth behavior and distinguish battery performance. Nickel foam can be employed as a template for the growth of graphene on its surface by chemical vapor deposition (CVD), thus enabling the comparison between 3D nickel foam and graphene-coated nickel (G/Ni) foam. Compared to the pristine nickel foam, wrinkled graphene layers adhered to the surface of nickel foam can be clearly observed after CVD growth (Figure 94A/E). To obtain a more complete understanding of the reaction mechanism and to analyze the morphology change of sulfur on the 3D nickel foam and G/Ni framework, the transparent cell was used to monitor sulfur evolution in real time under battery operation. Figure 94B-D presents optical images of a nickel foam electrode at initial, charged, and discharged states. Initially, the nickel foam was immersed in the polysulfides (Figure 94B), and sulfur droplets were observed and grew large during the charging process. Two droplets touching each other merged together and became a larger one (Figure 94C). The sulfur droplets were gradually dissolved into the electrolyte, and completely disappeared at the end of the discharge process (Figure 94D). The sulfur dissolution and reformation can be well controlled and repeated during tens of charge/discharge cycles. In contrast, the irregular sulfur crystals grew slowly and randomly distributed on the surface of G/Ni foam, as displayed in Figure 94F-G. The sulfur crystals slowly dissolved into the electrolytes during discharge and finally disappeared on discharging to 1.5 V (Figure 94H). Notably, the liquid sulfur droplets grow faster than sulfur crystals at the constant voltage charging process, in which at the same charging time the nickel foam electrode produces more nuclei and faster growth of sulfur (Figure 94I-L) than that of G/Ni foam (Figure 94M-P), indicating the faster kinetics of liquid sulfur beneficial for fast charging.

The electrochemical properties of nickel and G/Ni foams were measured in coin cells to verify whether the liquid or solid state of sulfur affects battery performance. Figure 94Q shows the rate performance of the cells at various current rates between 1.5 and 2.8 V. The 3D nickel foam electrode demonstrates good rate performance with capacities of around 360 and 300 mAh g⁻¹ at 2C and 3C, respectively, whereas the cell with the G/Ni foam electrode only maintains capacities of 275 and 110 mAh g⁻¹. The corresponding charge-discharge profiles at 0.2C, 1C, and 3C for nickel and G/Ni foam electrodes are compared in Figure 94R. It can be clearly seen that the voltage hysteresis between charge/discharge is much smaller for nickel foam compared to that of the G/Ni foam electrode, which shows large polarization. Moreover, the cell with the nickel foam electrode retains two distinct discharge voltage plateaus even at 3C, while there is almost no discharge plateau for the G/Ni foam electrode at the same current density (Figure 94R). Meanwhile, nickel foam also shows outstanding cycling stability and retains a capacity of 500 mAh g⁻¹ over 100 cycles with CE of ~ 99% (Figure 94S). The slight capacity increase in the first few cycles is possibly due to gradual wetting of some previously inaccessible areas in the nickel foam electrode. Conversely, the battery with the G/Ni foam electrode exhibits rapid capacity decay on cycling, with a capacity retention of only 50% due to weak polysulfide adsorption on the carbon surface, leading to inevitable polysulfide dissolution into the electrolyte. The impressively improved cycle performance and rate capability of the nickel foam-based electrode as compared to that of the G/Ni electrodes arise from the chemisorption of polysulfides by the nickel framework, and the accelerated kinetics between liquid sulfur and liquid polysulfides on the surface of the nickel electrode.

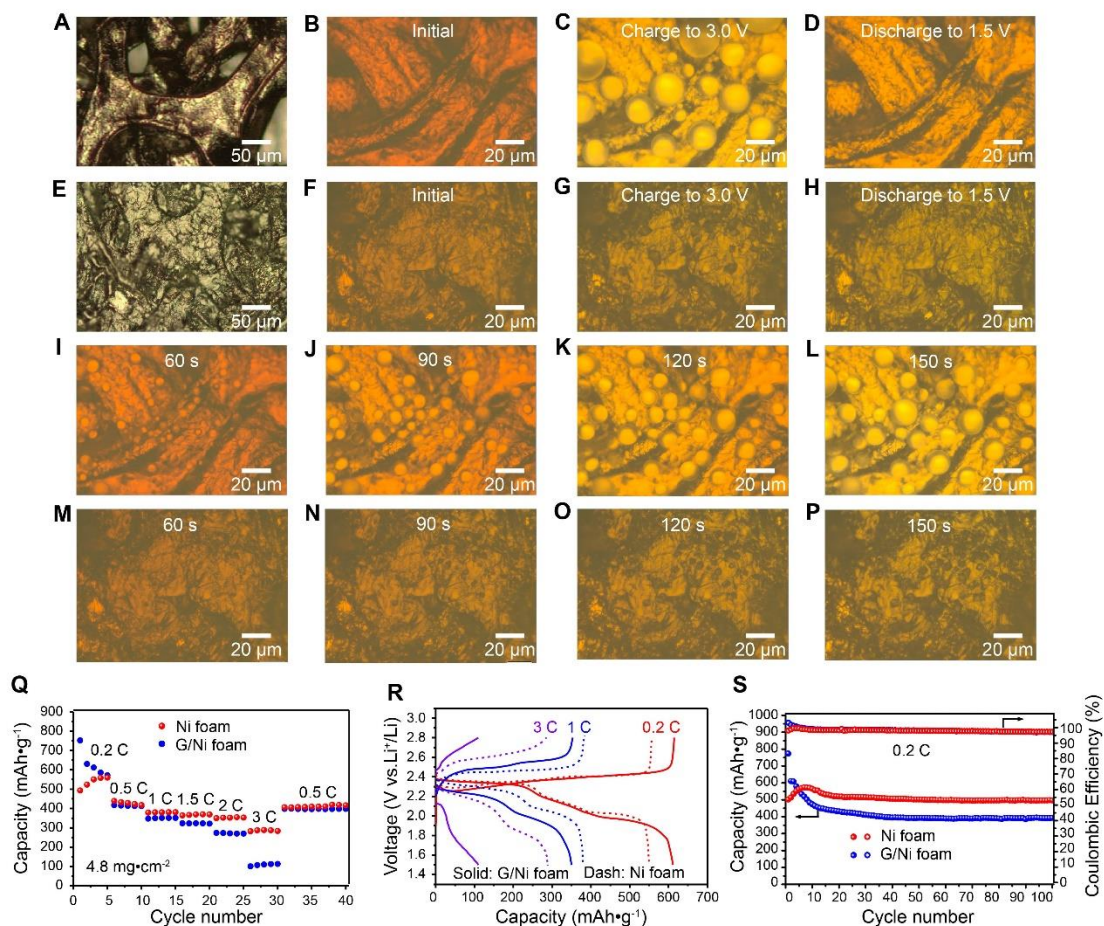


Figure 94. *In situ* optical observation and electrochemical performance of the nickel foam and graphene-coated nickel (G/Ni) foam electrodes in lithium polysulfide electrolyte. Optical images of (A) nickel foam, (E) G/Ni foam. Optical images of nickel foam in lithium polysulfide electrolyte: (B) at initial state, (C) after charging to 3.0 V, and (D) discharging to 1.5 V. Optical images of G/Ni foam in lithium polysulfide electrolyte: (F) at initial state, (G) after charging to 3.0 V, and (H) discharging to 1.5 V. Snapshots of the constant voltage charging process for nickel foam electrode at: (I) 60 s, (J) 90 s, (K) 120 s, and (L) 150 s. Snapshots of the constant voltage charging process for G/Ni foam electrode at: (M) 60 s, (N) 90 s, (O) 120 s, and (P) 150 s. (Q) Rate performance of the nickel foam and G/Ni foam electrodes at different current densities. (R) Charge/discharge voltage profiles of the nickel foam (dash line) and G/Ni foam (solid line) electrodes at 0.2C, 1C, and 3C. (S) Cycling performance and Coulombic efficiency of the nickel foam and G/Ni foam electrodes at 0.2 C for 100 cycles.

Patents/Publications/Presentations

The project has no patents, publications, or presentations to report this quarter.

Task 5.4 – Investigation of Sulfur Reaction Mechanisms (Enyuan Hu, Brookhaven National Laboratory; Deyang Qu, University of Wisconsin at Milwaukee)

Project Objective. The primary objectives are as follows:

- To continue conducting focused fundamental research on the mechanism of “shuttle effect” inhibition for rechargeable Li-S batteries.
- To continue developing the polymeric sulfur electrode, adequate anode, and corresponding electrolyte to achieve high-energy-density, long-cycle Li-S batteries.
- To carry out spatially resolved XRF image and S-K edge XAS [including X-ray absorption near edge structure (XANES) and X-ray absorption fine structure (XAFS)] studies of polymeric sulfur compounds.
- To investigate the alternative anode materials so they will not react with dissolved polysulfide ions.
- To continue developing and optimizing creative electrode-making processes to improve processability and aerial capacity, for example, dry process and thick electrode.

Project Impact. Further understanding of the mechanisms of all reactions in a Li-S cell will lead to mitigation of the “shuttle effect.” The project results will thus guide development of sulfur cathode and Li-S designs with significant increase of energy density and of cycle life and with reduction of cost. This will greatly accelerate deployment of EVs and reduce carbon emission associated with fossil fuel consumption.

Approach. This project will use not only *in situ* electrochemical high-performance liquid chromatography (HPLC)/MS, XPS and TXM, but also synchrotron-based *in situ* X-ray diagnostic tools such as XRD and XAS to study sulfur electrodes. The team will continue to develop thicker sulfur electrode with high areal capacity using dry process.

One-Year Goals. The major goal this fiscal year is to extend successful investigation of dissolved polysulfides to the polysulfides in the solid phase. This includes the following actions: (1) synthesize cross-linked polymerized sulfur compounds, (2) explore additives that can rapidly catalyze polysulfide radicals, (3) continue exploring alternative anode materials, and (4) develop *in situ* synchrotronic method to investigate sulfur and polysulfide in the solid phase.

Collaborations. The PI works closely with beamline scientists at synchrotron facilities to develop novel Li-S characterization tools. The PI and co-PI collaborate closely with top scientists at ANL, LBNL, and PNNL, as well as U. S. industrial collaborators at GM, Duracell, Clarios, etc. The PI and co-PI also collaborate with scientists in China, Japan, and South Korea. These collaborations will be strengthened and expanded to give this project a vision on both today’s state-of-the-art technology and tomorrow’s technology in development, with feedback from the material designer and synthesizers upstream and from industrial end users downstream.

Milestones

1. Test the newly synthesized polymeric sulfur compounds. Conduct spatially resolved XRF image and S-K edge XAS (including XANES and XAFS) studies of polymeric sulfur compounds. (Q1, FY 2020; Completed)
2. Survey alternative anode materials and determine their interaction with dissolved polysulfide ions. Continue synthesis and testing of polymeric sulfur compounds, and optimize electrode-making processes. (Q2, FY 2020; Completed)

- Investigate radical disproportionation catalyst, and test alternative electrolytes in which the solubility of polysulfide ions is lower than ether-based electrolyte. (Q3, FY 2020; In progress)
- Complete initial design of the full cell consisting of polymeric sulfur compounds, alternative anode, and adequate additive in either coin-cell or pouch-cell format. (Q4, FY 2020; In progress)

Progress Report

This quarter, the second milestone was completed progress was made on other milestones. The BNL and University of Wisconsin teams have been working to together to synthesize new polymer compounds, sulfur-containing composites with inorganic anchors, to optimize electrode-making processes.

Synthesis of Sulfur-Containing Materials with Inorganic Anchors. The overall performances of Li-S batteries are highly dependent on the structure and surface feature of carbon scaffolds as well as the architecture of sulfur cathodes. A series of semi-graphitic ordered mesoporous carbons with metal/nitrogen doping (Me-N-GOMCs; Me = Fe, Co, Ni, and Cu) was designed as sulfur hosts with abundant porosity and high electrical conductivity. It was revealed that the carbon capability of anchoring polysulfides can be remarkably enhanced through the synergistic effect of iron and nitrogen doping.

DFT calculations were performed to reveal the corresponding adsorption energies and sites of Me-N-GOMCs toward sulfides. Compared with other samples, Fe-N-GOMC showed the most favorable surface tightly adhered to Li_2S , implying its strongest binding ability with LiPSs. The adsorption energies of Li_2S on the surfaces of iron, cobalt, nickel, and Cu-N-GOMC are -3.01 , -2.80 , -2.15 , and -1.48 eV, respectively. These values are much higher than those on the pure carbon (-0.3 eV) or nitrogen-doped carbon (-0.54 eV) reported in the literature. The theoretical results reveal that iron and nitrogen dopants can work synergistically to boost the anchoring ability of carbon materials toward sulfides, thus more effectively suppressing the active sulfur loss and shuttle effect and eventually resulting in superior cycling stability.

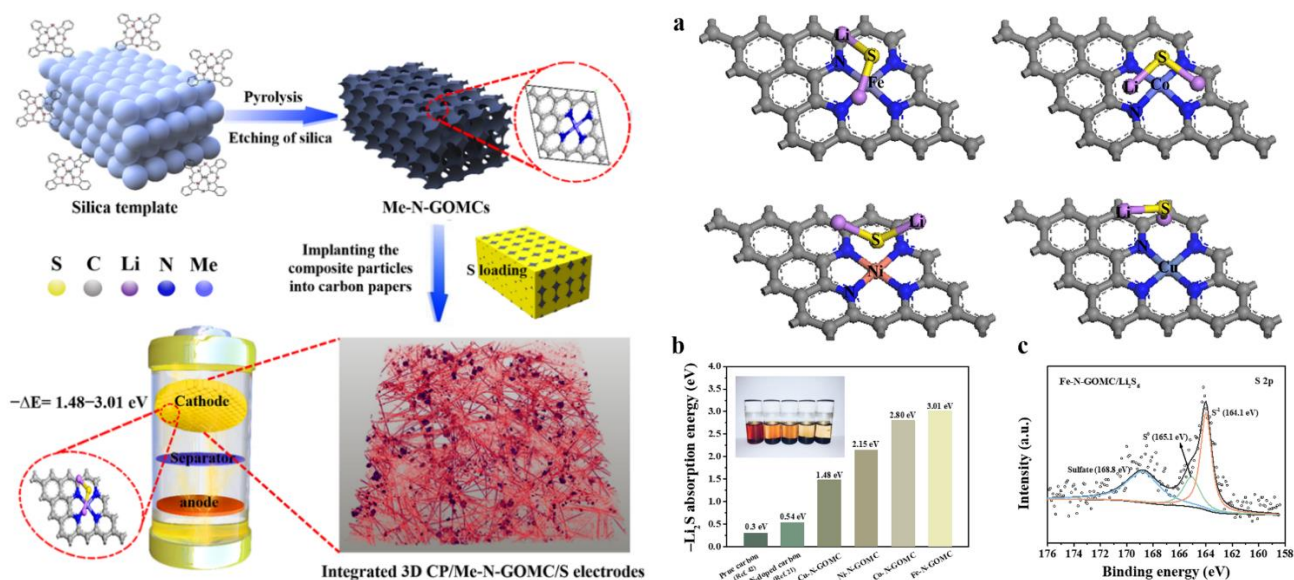


Figure 95. (left): Schematic representation of the synthesis process for the semi-graphitic ordered mesoporous carbons with metal and nitrogen anchor to lock sulfur within; sulfide anchoring mechanism on Me-N-GOMCs. (right): (a) optimized geometries of most stable Li_2S on Fe/Co/Ni/Cu and nickel double-doped carbon framework surfaces, (b) corresponding adsorption energies on different surfaces of framework and visual adsorption tests of Li_2S_6 in DME by the various powders (inset, left to right: control, Ni-N-GOMC, Cu-N-GOMC, Co-N-GOMC, and Fe-N-GOMC), and (c) S 2p X-ray photoelectron spectra of Fe-N-GOMC/ Li_2S_6 .

Patents/Publications/Presentations

The project has no patents, publications, or presentations to report this quarter.

Task 5.5 – New Electrolytes for Lithium-Sulfur Battery (Gao Liu, Lawrence Berkeley National Laboratory)

Project Objective. The project objective is to develop new electrolytes, additives, and electrode compositions for Li-S battery with high ion-conductivity, stable toward polysulfide and promoting the polysulfide affiliation with the electrode substrate to prevent polysulfide dissolution.

Project Impact. This work will address the high cost and low energy density of Li-ion rechargeable batteries. The emerging Li-S batteries could feature both high energy density and low cost. This project enables applications of the low-cost, abundant sulfur element as a major chemical component for electrical energy storage. This project will develop new approaches for electrolytes and electrode compositions of Li-S rechargeable batteries.

Approach. This project aims to develop new electrolytes and additives for Li-S battery. The properties of the ideal electrolyte for sulfur electrode would be high ion conductivity, stable towards polysulfide, and promoting the polysulfide affiliation with the electrode substrate to prevent polysulfide dissolution. The project is designed to first understand the electrode substrate interaction with the polysulfides in different electrolytes. This will lead to better understandings of the polysulfide nucleation and precipitation mechanisms in common electrolytes. The second stage of the project will focus on chemically modifying the structures of the solvent and salt electrolyte molecules to increase electrolyte stability and ionic conductivity and to prevent polysulfide dissolution and promote polysulfides precipitation.

Out-Year Goals. The team will also investigate the contribution of Li-metal electrodes to overall Li-S battery performance and will develop methods to stabilize Li-metal surface.

Collaborations. This project collaborates with Dr. J. Guo and Dr. W. Yang (ALS/LBNL), Prof. A. Minor (National Center for Electron Microscopy at LBNL/UC Berkeley), Dr. L-W. Wang (LBNL), and Prof. P. B. Balbuena, TAMU.

Milestones

1. Use the synchrotron analyses in studying new electrolytes. (Q1, FY 2020; Completed)
2. Measure and optimize compositions of the new electrolyte for conductivities, Li-ion transference numbers, and amount of polysulfide dissolution. (Q2, FY 2020; Completed)
3. Study cycling properties of lithium metal under new electrolytes. (Q3, FY 2020)
4. Select two electrolyte compositions to test in Li-S battery. (Q4, FY 2020)

Progress Report

A new class of amphiphilic electrolyte additive based on HFEs has been synthesized. The HFE amphiphilic additives in combination with lithium salt (for example, LiTFSI) and fluorocarbon solvents (for example, TTE) form micelle structures. These HFE amphiphilic additives have special structure design: a lithiophilic head [ethyleneoxide (EO) moiety) attached to a lithiophobic tail (hydrofluorocarbons). The lithium salts follow a micelle solvation mechanism on dissolution in the HFE amphiphilic additives. The dissociated Li^+ ions readily coordinate with EO moiety to induce self-assembly of the amphiphilic HFE additive into micelle structures. The ionic conductivities of 0.5 M LiTFSI electrolyte as a function of chain lengths of HFE molecules and solvent dilution ratio were studied and reported in Table 5. All electrolyte formulations were prepared in the glovebox. Conductivity measurement was performed by using a conductivity meter (Seven2Go™ pro, METTLER TOLEDO). About 5 ml of electrolyte was used for each measurement to allow the probe tip to be fully submerged in the solution for a high accuracy measurement. The probe tip was cleaned by rinsing with the dilution solvent TTE and dried by Kimwipe between measurements.

Prior to the conductivity measurement, the solubility of lithium salts (LiTFSI and LiFSI) in the amphiphilic HFE additives was tested. The maximum solubility reaches 4.0 M for both salts in F_4EO_2 solvent; however, the solutions are too viscous as a battery electrolyte at the concentration. Therefore, the highly concentrated solutions are diluted with TTE solvent. Table 5 lists the measured ionic conductivities of 0.5 M LiTFSI in HFE additive and TTE electrolyte solutions. The conductivity of formulated electrolytes is 10^{-4} - 10^{-3} S/cm. Higher ionic conductivity is achieved with the smaller HFE molecule F_4EO_2 . The larger micelle complexes are formed with smaller HFE additive molecules. The larger micelles may reduce overall ion diffusion path and facilitate ion conduction. Another observation is that higher ionic conductivity is favored by the 1:1 dilution ratio of HFE additive versus TTE. Considering ionic conductivity and proper viscosity, 0.5 M concentration of lithium salt is selected for further study in Li-S cells.

In summary, the conductivity of electrolytes with varying chain lengths and dilution ratios has been investigated. Results show HFE amphiphilic additive based electrolyte has an acceptable ionic conductivity (10^{-4} - 10^{-3} S/cm) for battery application.

Table 5. Room-temperature (25°C) ionic conductivity (σ) of 0.5 M LiTFSI electrolyte with various HFE amphiphilic additives (F_4EO_2 and F_8EO_4) and TTE dilution.

HFE : TTE by volume	σ (mS/cm)	
	F_4EO_2	F_8EO_4
1:1	3.2	0.61
1:5	1.05	0.35

Patents/Publications/Presentations

The project has no patents, publications, or presentations to report this quarter.

TASK 6 – AIR ELECTRODES / ELECTROLYTES

Summary and Highlights

High-density energy storage systems are critical for EVs required by the EV Everywhere Grand Challenge. Conventional Li-ion batteries still cannot fully satisfy the ever-increasing needs because of their limited energy density, high cost, and safety concerns. As an alternative, the rechargeable lithium-oxygen (Li-O₂) battery has potential to be used for long-range EVs. The practical energy density of a Li-O₂ battery is expected to be ~ 800 Wh kg⁻¹. The advantages of Li-O₂ batteries come from their open structure; that is, they can absorb the active cathode material (oxygen) from the surrounding environment instead of carrying it within the batteries. However, the open structure of Li-O₂ batteries also leads to several disadvantages. The energy density of Li-O₂ batteries will be much lower if oxygen must be provided by an onboard container. Although significant progress has been made in recent years on fundamental properties of Li-O₂ batteries, research in this field is still in an early stage, with many barriers to be overcome before practical applications. These barriers include:

- Instability of electrolytes—The superoxide species generated during discharge or O₂ reduction process is highly reactive with electrolyte and other components in the battery. Electrolyte decomposition during charge or O₂ evolution process is also significant due to high over-potentials.
- Instability of air electrode (dominated by carbonaceous materials) and other battery components (such as separators and binders) during charge/discharge processes in an O-rich environment.
- Corrosion of Li-metal anode in an electrolyte saturated with oxygen.
- Low energy efficiency associated with large over-potential and poor cyclability of Li-O₂ batteries.
- Low power rate capability due to electrode blocking by the reaction products.
- Absence of a low-cost, high-efficiency oxygen supply system (such as oxygen selective membrane).

The main goal of this Task is to provide a better understanding on the fundamental reaction mechanisms of Li-O₂ batteries and identify the required components (especially electrolytes and electrodes) for stable operation of Li-O₂ batteries. This task will investigate several new approaches to improve stability of Li-metal anode in Li-O₂ batteries:

- Li-metal anodes will be protected using two approaches: (1) *in situ* formation of a stable SEI layer before Li-O₂ cell operation through various electrolyte formulations and treatment protocols, and (2) *ex situ* formation of stable inorganic/polymeric hybrid electrolyte layers through dip-coating or tape-casting method to coat the inorganic/polymeric hybrid electrolyte layer on Li-metal surface.
- A joint theoretical/experimental approach for design and discovery of new cathode and electrolyte materials will act synergistically to reduce charge overpotentials and increase cycle life. Synthesis methods, in combination with design principles developed from computations, will be used to make new cathode architectures. Computational studies will be used to help understand decomposition mechanisms of electrolytes and how to design electrolytes with improved stability.
- A new cathode will be developed based on high-efficiency catalyst such as 2D TMDs. These cathode materials will be combined with new electrolyte blends and additives that work in synergy to reduce charge potentials and increase stability of the Li-air system.

State-of-the-art characterization techniques and computational methodologies will be used to understand charge and discharge chemistries. Success of this Task will establish a solid foundation for further development of Li-O₂ batteries toward practical applications for long-range EVs. The fundamental understanding and breakthrough in Li-O₂ batteries may also provide insight on improving performance of Li-S batteries and other energy storage systems based on chemical conversion process.

Highlights. The Task highlights for this quarter are as follows:

- The ANL Group (Amine, Curtiss, and Lu) reported on a biomass-derived activated carbon with high specific surface area synthesized by an activator-assisted pyrolysis route for use in a Li-O₂ battery. The oxygen electrode combined with soluble catalyst was found to have greatly improved overall performance mainly due to the synergetic effect of the novel designed oxygen electrode capable of mediating the soluble catalyst to trigger the oxygen reduction and oxygen evolution processes.
- The PNNL (Zhang and Xu) group systematically investigated factors that affect performance of electrolytes used for Li-air and Li-O₂ batteries. They found that performance strongly depends on not only the electrochemical stability of the electrolyte, but also on their oxygen solubility, viscosity, volatility, and the stability against singlet oxygen (¹O₂).
- The Argonne/UIC Group (Curtis/Ngo/Salehi-Khojin) demonstrated a new bifunctional additive InBr₃ that can simultaneously improve energy efficiency of the battery and enable long-term performance in a dry air atmosphere. Although Li-air cells with InBr₃ additive have a slightly higher overvoltage (1.0 V) as compared with those using InI₃ additive (0.7 V) reported before, InBr₃ additives enable a Li-O₂ cell with a long cycle life of ~ 600 cycles.

Task 6.1 – Rechargeable Lithium-Air Batteries (Ji-Guang Zhang and Wu Xu, Pacific Northwest National Laboratory)

Project Objective. The objective of this project is to develop rechargeable Li-O₂ batteries with long-term cycling stability through in-depth research on more stable electrolytes and highly efficient catalysts for air electrodes, protection of Li-metal anodes, and deeper understanding on the oxygen reduction reaction (ORR) and oxygen evolution reaction (OER) mechanisms behind the electrochemical performance of Li-O₂ cells. In FY 2020, the team will further investigate the stability of electrodes and electrolytes to build more stable Li-O₂ batteries with long-term cycling capability.

Project Impact. The objective of this project is to develop rechargeable Li-O₂ batteries with long-term cycling stability through in-depth research on more stable electrolytes and highly efficient catalysts for air electrodes and protection of Li-metal anodes. This fiscal year, the team will further investigate stability of electrodes and electrolytes to build more stable Li-O₂ batteries with long-term cycling capability.

Approach. Develop highly stable electrolytes, including localized high concentration electrolytes (LHCEs) and optimize their compositions to prevent the irreversible parasitic reactions at the electrodes (cathode and anode). The electrochemical test of Li||Li symmetric cell containing above stable electrolyte will be first measured comparatively with typical ether (TEGDME) based electrolyte to evaluate the stability of the electrolyte itself and the SEI layer. Then, the stability of proposed electrolytes at the cathode side with reactive oxygen species during ORR/OER will be further characterized in the Li-O₂ cells. In addition, with comparative measurements for physical properties of electrolytes, the team will find the key parameters of suitable electrolyte in Li-O₂ batteries.

Out-Year-Goals. The long-term goal of the proposed work is to enable rechargeable Li-air batteries with a specific energy of 800 Wh/kg at cell level, 1000 deep-discharge cycles, improved abuse tolerance, and less than 20% capacity fade over a 10-year period to accelerate commercialization of long-range EVs.

Collaborations. This project collaborates with C. Wang of PNNL on characterization of cycled air electrodes by TEM/SEM, and with Dr. P. Gao of PNNL on computational calculations and simulations.

Milestones

1. Develop stable electrolyte to minimize parasitic reactions at the electrodes. (Q1, FY 2020; Completed, December 31, 2019)
2. Protect anodes to prevent the lithium dendrite and LiOH formation. (Q2, FY 2020; Completed, March 31, 2020)
3. Develop stable additives (solid or soluble) or methods for sustainable catalytic effect. (Q3, FY 2020)
4. Complete evaluation of cycling performance of Li-O₂ batteries with optimized cell components and conditions. (Q4, FY 2020)

Progress Report

This quarter, the LHCEs were further studied for rechargeable Li-O₂ battery applications. The effects of diluent in LHCEs on the electrochemical performance of Li-O₂ batteries have been systematically investigated. Three diluents, Tris(2,2,2-trifluoroethyl)orthoformate (TFEO), TTE, and 1H,1H,5H-Octafluoropentyl 1,1,2,2-tetrafluoroethyl ether (OTE), were investigated in LiTf/G4 electrolytes using a diluted concentration electrolyte (DCE, 1M LiTf/G4) as the baseline. Li||Li symmetric and Li-O₂ cell tests demonstrate the excellent stability of OTE-LHCE over TFEO-LHCE, TTE-LHCE, and DCE in Li-O₂ batteries. Li-O₂ cells with OTE-LHCE and an air electrode composed of carbon paper without any catalyst can be cycled stably for 73 cycles under the capacity limited protocol of 1.0 mAh cm⁻² at a current density of 0.2 mA cm⁻², while the cells with DCE, TFEO-LHCE, and TTE-LHCE can only run for 25, 6, and 17 cycles, respectively under the same testing conditions (Figure 96a-b). Although DCE has a lower viscosity and volatility than LHCEs investigated in this work, other more important factors, such as stability of Li-metal anode in the electrolyte may lead to the early failure of Li-O₂ battery using DCE electrolyte. As shown in Figure 96c, all of Li-metal anodes removed from the cycled Li-O₂ batteries using LHCEs still exhibit well-maintained morphology after cycling, while the Li-metal anode removed from the cycled Li-O₂ battery using DCE showed severe pulverization after cycling. The electrochemical performance of Li-O₂ batteries using different LHCEs also largely depends on diluent types. Thus, various physical and electrochemical properties of the electrolytes mentioned above (including their stability with lithium anodes and singlet oxygen (¹O₂), fluidity/viscosity, conductivity, O₂ solubility, and volatility) have been investigated to understand the key electrolyte parameters required for high performance Li-O₂ batteries. The results are summarized in Figure 96d. Among these parameters, the activation energy of the diluents reacting with ¹O₂ largely determined the electrochemical stabilities of the electrolytes in Li-O₂ batteries (Figure 96e). As a result, LHCE containing the diluent (OTE) with the highest activation energy against ¹O₂ demonstrates the best chemical and electrochemical stabilities and lead to the best long-term cycling stability of Li-O₂ batteries, as shown in Figure 96c.

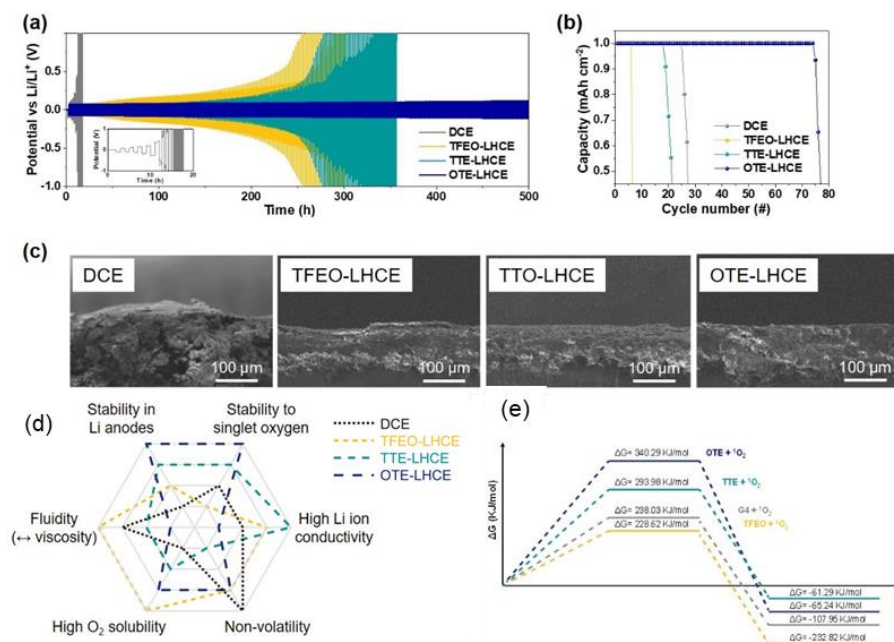


Figure 96. (a) Voltage profiles of Li||Li symmetric cells cycling in different electrolytes at a current density of 1.0 mA cm⁻² under a capacity limited protocol of 1.0 mAh cm⁻². (b) Cycle life of Li-O₂ battery using different electrolytes with repeated discharge and charge cycles at 0.2 mA cm⁻² (200 mA g⁻¹) and capacity cutoff at 1.0 mAh cm⁻² (1000 mA g⁻¹). (c) Cross-sectional scanning electron microscopy images of Li-metal anodes in cycled Li-O₂ battery cells with DCE, TFEO-LHCE, TTE-LHCE, and OTE-LHCE after 10th cycle at a current density of 0.2 mA cm⁻² with a capacity limited protocol of 1.0 mAh cm⁻². (d) The radar chart for the properties of the electrolytes in this study. (e) Density functional theory calculation data about parasitic reaction energies of G4 solvent and three diluents with singlet oxygen.

Patents/Publications/Presentations

Publication

- Kwak, W-J., H-S. Lim, P. Gao, R. Feng, S. Chae, L. Zhong, J. Read, M. H. Engelhard, W. Xu, and J-G. Zhang. “Effects of Fluorinated Diluents in Localized High-Concentration Electrolytes for Lithium-Oxygen Batteries.” Submitted for publication.

Task 6.2 – Lithium-Air Batteries

(Khalil Amine, Larry A. Curtiss, and Jun Lu; Argonne National Laboratory)

Project Objective. This project will develop new cathode materials and electrolytes for Li-air batteries for long cycle life, high capacity, and high efficiency. The goal is to obtain critical insight that will provide information on the charge and discharge processes in Li-air batteries to enable new advances to be made in their performance. This will be done using state-of-the-art characterization techniques combined with state-of-the-art computational methodologies to understand and design new materials and electrolytes for Li-air batteries.

Project Impact. The instability of current nonaqueous electrolytes and degradation of cathode materials limits performance of Li-air batteries. The project impact will be to develop new electrolytes and cathode materials that are stable and can increase energy density of electrical energy storage systems based on lithium.

Approach. The project is using a joint theoretical/experimental approach for design and discovery of new cathode and electrolyte materials that act synergistically to reduce charge overpotentials and increase cycle life. Synthesis methods, in combination with design principles developed from computations, are used to make new cathode architectures. Computational studies are used to help understand decomposition mechanisms of electrolytes and how to design electrolytes with improved stability. The new cathodes and electrolytes are tested in Li-O₂ cells. Characterization, along with theory, is used to understand the performance of materials used in the cell and to make improved materials.

Out-Year Goals. The out-year goals are to find catalysts that promote discharge product morphologies that reduce charge potentials and find electrolytes for long cycle life through testing and design.

Collaborations. This project engages in collaboration with Prof. K. C. Lau (UC at Norridge), Prof. F. Wu (Beijing Institute of Technology), Dr. D. Zhai (China), and R. Shahbazian-Yassar (UIC).

Milestones

1. Investigation of effect of salt modification on discharge product and charge overpotentials. (Q1, FY 2020; Completed)
2. Development of electrolyte blends for improving the OER and protecting Li-anode for longer cycle life. (Q2, FY 2020; Completed)
3. Investigation of new alloys for templating LiO₂ discharge products with low charge potentials. (Q3, FY 2020)
4. Development of novel electrocatalysts for low charge potentials in synergy with new electrolyte blends. (Q4, FY 2020)

Progress Report

The practical applications of Li–O₂ batteries are hindered by their poor cycle life, high over-charge potential, and low energy efficiency. Numerous studies are focused on how to improve the electrochemical reaction kinetics by designing good ORR and OER catalyst systems. Thus, an oxygen electrode combined with soluble catalyst is designed, and an ultrahigh areal specific capacity of 7.95 mAh/cm² and a long cycling life up to 1000 cycles with suppressed polarization (about 0.46 V) are achieved. The greatly improved overall performance is mainly due to the synergetic effect of the novel designed oxygen electrode capable of mediating the soluble catalyst to trigger the ORR and OER processes.

In this report, the team prepared a biomass-derived activated carbon (ACs) with high specific surface area (1033 m²/g) and decent porosity (0.52 cm³/g) through an activator-assisted pyrolysis route. As shown in Figure 97: (1) hierarchically pores (0.52 μm) are coherently distributed on ACs, which can promote the exposure of ORR and OER active sites; (2) the presence of macropores not only provides transport channels for oxygen diffusion, but also supplies uniform and slithery wetting channels for electrolyte and soluble catalyst LiI to infiltrate the oxygen electrode; (3) more importantly, macropores can accommodate more discharge products without causing blockages and provide multiple three-phase regions for discharge product deposition.

As shown in Figure 98a, compared with Cs (pyrolytic carbon materials without activation), ACs can deliver higher capacity due to its optimized structure. After combining ACs with soluble catalyst LiI, areal specific capacity is significantly increased up to 7.95 mAh/cm² (among the highest values reported for Li–O₂ batteries), and the overpotential between discharge and charge process is also effectively reduced.

It should be noted that in this study, water is present in the quantities of impurities. The addition of a small amount of water to aprotic Li–O₂ battery does not affect the formation of Li₂O₂ as the dominant product. When LiI and water are coexisting, the formation mechanism of the discharge product will undergo complicated changes, and LiOH would be formed as the main discharge product. As shown in Figure 98b, the positively shifted E_{pc} peak is corresponding to the discharge plateau of 2.7 V, and E_{pa1} and E_{pa2} peaks are attributed to I⁻/I₃⁻ and I₃⁻/I₂ redox couples, and LiOH will be chemically oxidized by I₃⁻ to form O₂ and H₂O. The overall reaction should be: 4 Li⁺ + O₂ + 4e⁻ + 2H₂O ⇌ 4 LiOH. Based on the optimization of oxygen electrode combined with soluble catalyst, the Li–O₂ battery can exhibit a large discharge capacity and ultralong cycle life, and can withstand the influence of impurity moisture in the air.

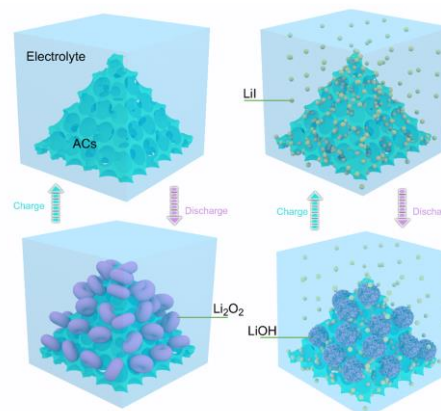


Figure 97. Schematic illustration of the charge and discharge processes with or without the LiI in Li–O₂ batteries using ACs electrodes.

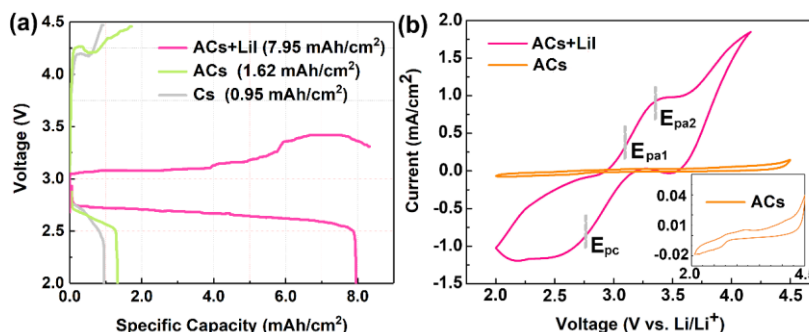


Figure 98. The initial discharge–charge voltage profiles of LiI/1M LiTFSI/TEGDME||Cs–O₂ cell, LiI/1M LiTFSI/TEGDME||ACs–O₂ cell, and LiI/1M LiTFSI/TEGDME+0.5M LiI||ACs–O₂ cell at a current density of 0.02 mA/cm² (a), the CV curves of LiI/1M LiTFSI/TEGDME||ACs–O₂ cell and LiI/1M LiTFSI/TEGDME + 0.5M LiI||ACs–O₂ cell within a voltage window of 2.0~4.5 V at a scanning rate of 1 mV/s [inset: enlarged cyclic voltammetry curve of biomass-derived activated carbons] (b).

Patents/Publications/Presentations

Patent

- Zeng, X., J. Lu, K. Amine, and Y. Guo. “Cathode for Earth Air Batteries.” IN-19-153.

Publications

- Wang, M., Y. Yao, X. Bi, T. Zhao, G. Zhang, F. Wu, K. Amine, and J. Lu. “Optimization of Oxygen Electrode Combined with Soluble Catalyst to Enhance the Performance of Lithium–Oxygen Battery.” *Energy Storage Materials* 28 (2020): 73–81.
- Bi, X., K. Amine, and J. Lu. “The Importance of Anode Protection towards Lithium Oxygen Batteries.” *Journal of Materials Chemistry A* 8 (2020): 3563–3573.

Task 6.3 – Lithium Oxygen Battery Design and Predictions (Larry A. Curtiss/Anh Ngo, Argonne National Laboratory; Amin Salehi-Khojin, University of Illinois at Chicago)

Project Objective. The objective of this work is to develop new materials for Li-O₂ batteries that give longer cycle life and improved efficiencies in an air environment. New electrolyte blends and additives will be investigated that can reduce clogging and at the same time promote the cathode functionality needed to reduce charge overpotentials. New cathode and anode materials will be investigated that can work in conjunction with the electrolytes to improve cycle life in the presence of air components.

Project Impact. Li-air batteries are considered as a potential alternative to Li-ion batteries for transportation applications due to their high theoretical specific energy. The major issues with the existing Li-O₂ systems include degradation of the anode electrode, reactions with air components, clogging of the cathode, and electrolyte instability. Thus, this project is using a comprehensive approach to improve cycle life and efficiency through development of new materials for electrodes, anodes, and electrolytes that work in synergy.

Approach. The experimental strategy is to use cathode materials based on 2D transition metal dichalcogenides (TMDs) that the team has found to be among the best oxygen reduction and evolution catalysts. These cathode materials will be combined with new electrolyte blends and additives that work in synergy to reduce charge potentials and increase stability of the Li-air system. DFT and AIMD simulations are used to gain insight at the electronic structure level of theory of the electrolyte structure and function both in the bulk and at interfaces with the cathode, anode, and discharge product. Classical MD is used to obtain understanding at longer length and time scales of processes occurring in the electrolyte and growth mechanisms of discharge products. The team will also utilize a HT screening strategy based on experiment and theory to develop a large database of properties and outcomes of electrolyte combinations that can be analyzed using machine learning to predict electrolytes and additives that will have the best performance.

Out-Year Goals. The out-year goals are to find electrolytes that give high capacities and long cycle life in an air atmosphere using HT screening.

Collaborations. This project engages in collaboration with R. Assary and J. G. Wen of ANL, B. Narayanan of University of Louisville, Tao Li of Northern Illinois University, and F. Khalili-Araghi and R. Klie of UIC.

Milestones

1. Investigate various salt combinations for Li-O₂ electrolytes for both lithium anode protection and low charge potentials for the performance of Li-O₂ batteries with use of computations to provide understanding. (Q1, FY 2020; Completed)
2. Investigate bromine-based redox mediators (RMs) by experiment and theory for comparison with iodine-based redox mediators with MoS₂ cathode materials. (Q2, FY 2020; Completed)
3. Develop method for screening of additive and electrolytes by experiment and theory to develop a database of properties and performance data for optimizing Li-O₂ batteries by machine learning. (Q3, FY 2020; Initiated)
4. Investigate electrolytes and cathodes that can greatly increase Li-O₂ coin cell capacities compared to current capacities through optimization of ORRs. (Q4, FY 2020; Initiated)

Progress Report

Li-O₂ batteries are considered as an advanced energy storage system that could provide a much higher specific energy than Li-ion batteries for electrical transportation. However, there are major issues with the existing Li-O₂ systems including degradation of the anode electrode, poor volumetric energy density, electrolyte instability and high charge overpotential. The team is focused on finding a combination of electrolytes, additives, and cathode catalysts to enable a Li-O₂ battery that can operate in an air atmosphere with a low charge potential while maintaining a long cycle life. During the past quarter, they have finished a study comparing two bifunctional additives, with one of the functions being that of RMs to reduce the charge potential and the other function being to provide anode protection. Previously, the team reported on an additive based on InI₃, which was found to give a low charge potential and a cycle life of about 200 cycles. This quarter, the team reports

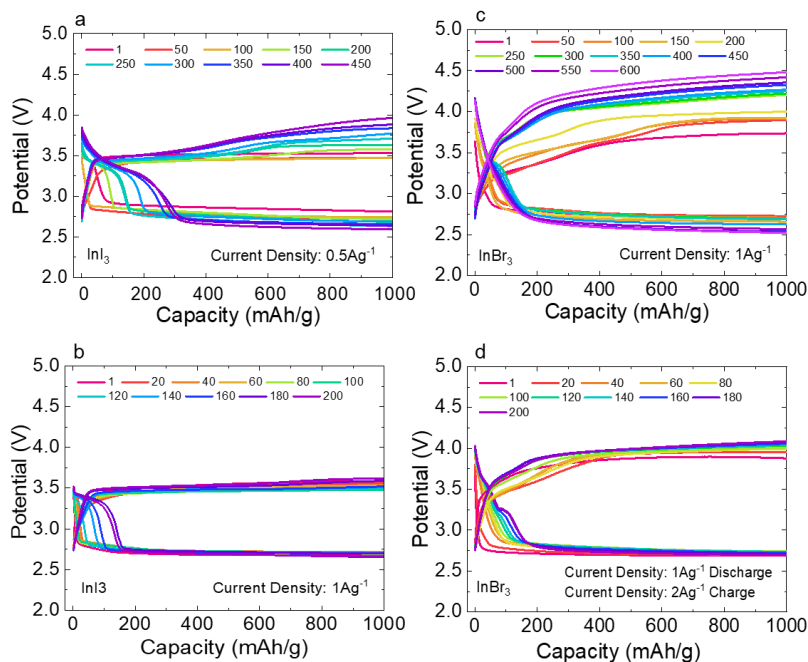


Figure 99. Discharge/Charge voltage profile. (a) 25mM InI₃ and current density of 0.5Ag⁻¹. (b) 25mM InI₃ and current density of 1Ag⁻¹. (c) 25mM InBr₃ and current density of 1Ag⁻¹. (d) 25mM InBr₃ and current densities of 1Ag⁻¹ discharging and 2Ag⁻¹

on results using the bromide equivalent, that is, InBr₃. Results for the InI₃ additive are given in Figure 99a-b for comparison with the new work on InBr₃ (Figure 99c-d).

The battery with InBr₃ as the additive was run with the same cathode and electrolyte as the InI₃. The cell configuration was based on a molybdenum disulfide cathode in a hybrid electrolyte of 10% ionic liquid (EMIM BF₄) and 90% DMSO and 0.1 M LiTFSI. The additive was 0.025 M InI₃. This composition enabled operation of the battery in a dry air environment with a capacity of 1000 mAh/g at a rate of 1 A/g up to 600 cycles. The team obtained a polarization gap of ~ 1.0 for ~ 200 cycles (Figure 99c) and then the charge potential increased for the rest of the cycles. A battery with a higher charge rate of 2 A/g runs for ~ 200 cycles with a charge potential

of ~ 4 V (Figure 99d). Also, the capacity loss of both batteries is less than 10% after more than 200 cycles. Different characterization techniques have been used to show the discharge product, and all of them verify the presence of Li₂O₂, including Raman spectroscopy.

These results indicate that InBr₃ is not as good a redox mediator as the InI₃, as the gap in the latter case is ~ 0.7 V (Figure 99b) compared to ~ 1 V for InBr₃ (Figure 99c) for the same discharge/charge current densities of 1 A/g. However, the InBr₃ additive enables a Li-O₂ cell with long life of ~ 600 cycles before failure, at which point the charge potential has increased to ~ 4.4 V. In addition, the InBr₃ system can handle a higher current density, as shown in Figure 99d.

The experimental and computational results on the InBr₃ additive system have revealed that while Br₃⁻ from InBr₃ is the source of the redox mediator, that is, LiBr at the cathode, the In³⁺ reacts on the lithium anode side to form a protective layer on the surface. The protective layer enables the long cycle life as well as the operation in a dry atmosphere. In summary, this study has demonstrated a new bifunctional additive similar to InI₃ that can simultaneously improve energy efficiency of the battery and enable long-term performance in a dry air atmosphere.

Patents/Publications/Presentations

Patent

- Salehi-Khojin, A., A. Ahmadiparidari, L. A. Curtiss, and F. Khalili-Araghi. “Lowering Charge Potentials with Negligible Capacity Loss in High Rate Lithium Oxygen Batteries.” Patent disclosure submitted.

Publications

- Hemmat, Z., J. Cavin, A. Ahmadiparidari, A. Ruckel, S. Rastegar, S. N. Misal, L. Majidi, K. Kumar, S. Wang, J. Guo, R. Dawood, F. Lagunas, P. Parajuli, A. T. Ngo, L. A. Curtiss, S. B. Cho, J. Cabana, R. F. Klie, R. Mishra, and A. Salehi-Khojin. “Quasi-Binary Transition Metal Dichalcogenide Alloys: Thermodynamic Stability Prediction, Scalable Synthesis, and Application.” *Advanced Materials* (2020) 1907041.
- Ahmadiparidari, A., S. Fuladi, L. Majidi, S. Plunkett, E. Sarnello, Z. Hemmat, S. Rastegar, S. N. Misal, P. C. Redfern, J. Wen, T. Li, A. T. Ngo, F. Khalili-Araghi, L. A. Curtiss, and A. Salehi-Khojin. “Lowering Charge Potentials with Negligible Capacity Loss in High Rate Lithium Oxygen Batteries.” Submitted.
- Rastegar, S., Z. Hemmat, C. Zhang, S. Plunkett, J. G. Wen, N. Dandu, T. Rojas, L. Majidi, S. N. Misal, A. T. Ngo, L. A. Curtiss, and A. Salehi-Khojin. “A Lithium-Oxygen Battery that Operates in Dry Air with a Bifunctional InX_3 (X = Br, I) Electrolyte Additive.” Submitted.
- Zhang, C., N. Dandu, S. Rastegar, S. N. Misal, Z. Hemmat, A. T. Ngo, L. A. Curtiss, and A. Salehi-Khojin. “A Comparative Study of Redox Mediators for Improved Performance of Li-Oxygen Batteries.” Submitted.

TASK 7 – SODIUM-ION BATTERIES

Summary

During FY 2019, the BMR added new projects, including several in the area of Na-ion batteries. Four of these projects are continuously funded into FY 2020. Progress on these four projects is described in this report. The Na-ion battery will require investigations to identify optimal electrode materials, electrolytes, separators, and binders to reach full potential. The BMR program will therefore have a limited effort directed toward identifying Na-ion battery materials that have potential value for vehicle applications. More detailed information on this BMR Task will be provided in upcoming reports.

Highlights. The highlights for this quarter are as follows:

- The BNL group (Yang and Hu) used synchrotron-based XRD and x-PDF analysis to study the structural evolution of a sodium cathode NaCrSSe during cycling. They found a reversible phase transition of O'3 to O1 and a reversible shortening of the S/Se-S/Se bonds due to anion redox reaction.
- The ANL group (Johnson and Amine) synthesized a series of Pb-based multi-metallic nanocomposite anode materials using a mechanochemical reaction method where the simultaneous nano-scale pulverization and reductive metal alloying are achieved in the reaction vessel. They found that effective metal alloying can significantly improve the electrochemical properties of the Pb-based nanocomposite anodes in both Li- and Na-ion cells.
- The LBNL team (Doeff) synthesized a third member of the lepidocrocite titanate series $Cs_xTi_{2-x/4}O_4$ and ion-exchanged it with Na^+ using a new faster method. The thermal properties of the two other previously synthesized materials were studied to determine the best drying temperature.
- The PNNL group (Zhang) developed a non-flammable electrolyte, NaFSI:TEP:TTE (1:1.5:2 in molar), for Na-ion batteries that can enable Na||HC cells to retain 96.7% capacity after 400 cycles.

Task 7.1 – Exploratory Studies of Novel Sodium-Ion Battery Systems (Xiao-Qing Yang and Enyuan Hu, Brookhaven National Laboratory)

Project Objective. The objective of this project is to develop new advanced *in situ* material characterization techniques and apply these techniques to explore the potentials, challenges, and feasibility of new rechargeable battery systems beyond the Li-ion batteries, namely, the Na-ion battery systems for EVs, such as PHEV and BEV. To meet the challenges of powering PHEVs and BEVs, new rechargeable battery systems with high energy and power density, low cost, good abuse tolerance, and long calendar and cycle life need to be developed. This project will use the synchrotron-based *in situ* X-ray diagnostic tools, combined with TEM and STEM imaging techniques developed at BNL, to evaluate the new materials and redox couples to obtain fundamental understanding of the reaction mechanisms of these materials aiming for improvement of and guidance for new material and new technology development regarding Na-ion battery systems.

Project Impact. In the VTO MYPP, the goals for battery were described: “Specifically, lower-cost, abuse-tolerant batteries with higher energy density, higher power, better low-temperature operation, and longer lifetimes are needed for the development of the next-generation of HEVs, PHEVs, and EVs.” The knowledge learned from diagnostic studies and collaborations with U. S. industries through this project will help U. S. research institutions and industries to develop new materials and processes for a new generation of rechargeable battery systems, namely, Na-ion battery system, in their efforts to reach these VTO goals.

Approach. This project will use the synchrotron-based *in situ* X-ray diagnostic tools developed at BNL to evaluate the new materials and redox couples to enable a fundamental understanding of the mechanisms governing performance of these materials and provide guidance for new material and new technology development regarding Na-ion battery systems.

Out-Year Goals. Complete the synchrotron-based *ex situ* XRD, PDF, XAS, and XRF studies of novel anion redox-based cathode materials $\text{NaTi}_{1/3}\text{Cr}_{2/3}\text{S}_2$ and NaCrSeS at different SOCs.

Collaborations. The BNL team has been closely working with top scientists on new material synthesis at ANL, LBNL, and PNNL and with U. S. industrial collaborators at General Motors and Johnson Controls, as well as with international collaborators.

Milestones

1. Complete chromium, titanium, and sulfur K-edge XAS (including XANES and EXAFS) studies of $\text{NaTi}_{1/3}\text{Cr}_{2/3}\text{S}_2$ cathode material at different SOCs. (Q1, FY 2020; Completed)
2. Complete synchrotron-based *ex situ* XRD and PDF analysis of novel anion redox-based cathode material NaCrSeS at different SOCs. (Q2, FY 2020; Completed)
3. Complete the chromium and selenium K-edge XAS study and analysis of NaCrSeS cathode material at different SOCs. (Q3, FY 2020; In progress)
4. Complete the sulfur K-edge XANES and EXAFS studies of NaCrSeS cathode material at different SOCs. (Q4, FY 2020; In progress)

Progress Report

This quarter, the second milestone was completed. BNL has focused on synchrotron-based XRD and PDF studies for NaCrSeS cathode material at different SOCs. Figure 100a-b shows the *ex situ* XRD and PDF data of pristine, charged, and discharged samples. Figure 100a (XRD) indicates that the O'3 phase of the pristine material is changed to the O1 phase at charged state and back to the O'3 phase at the discharged state. In Figure 100b (PDF), the intensity of G(r) peaks of charged and discharged samples is significantly reduced from that of the pristine sample, especially at the larger atomic pair distance ($> 50 \text{ \AA}$), indicating that the charged and discharged samples have poorer crystallinity than the pristine sample. Figure 100c-d shows the fitted PDF patterns for pristine and charged samples, respectively. Contribution from major atomic pairs are also shown. The structure models are obtained from DFT calculation. In Figure 100c, the first peak at 2.52 \AA is related to the Cr-S/Se atomic pair, and the second peak at around 2.92 \AA is related to the Na-S/Se atomic pair. The broad and strong peak at 3.60 \AA is attributed to the Cr-Cr (3.64 \AA), S-S (3.60 \AA), and Se-Se (3.60 \AA) atomic pairs. After charging, the first and third peaks shift to lower positions of 2.44 and 3.36 \AA , respectively, indicating the shortening of Cr-S/Se, Cr-Cr, S-S, and Se-Se atomic pairs. More importantly, the peak related to the Na-S/Se correlation at 2.92 \AA has essentially disappeared, indicating that the sodium ions are fully extracted from the structure, which is consistent with the initial charge capacity of NaCrSSe.

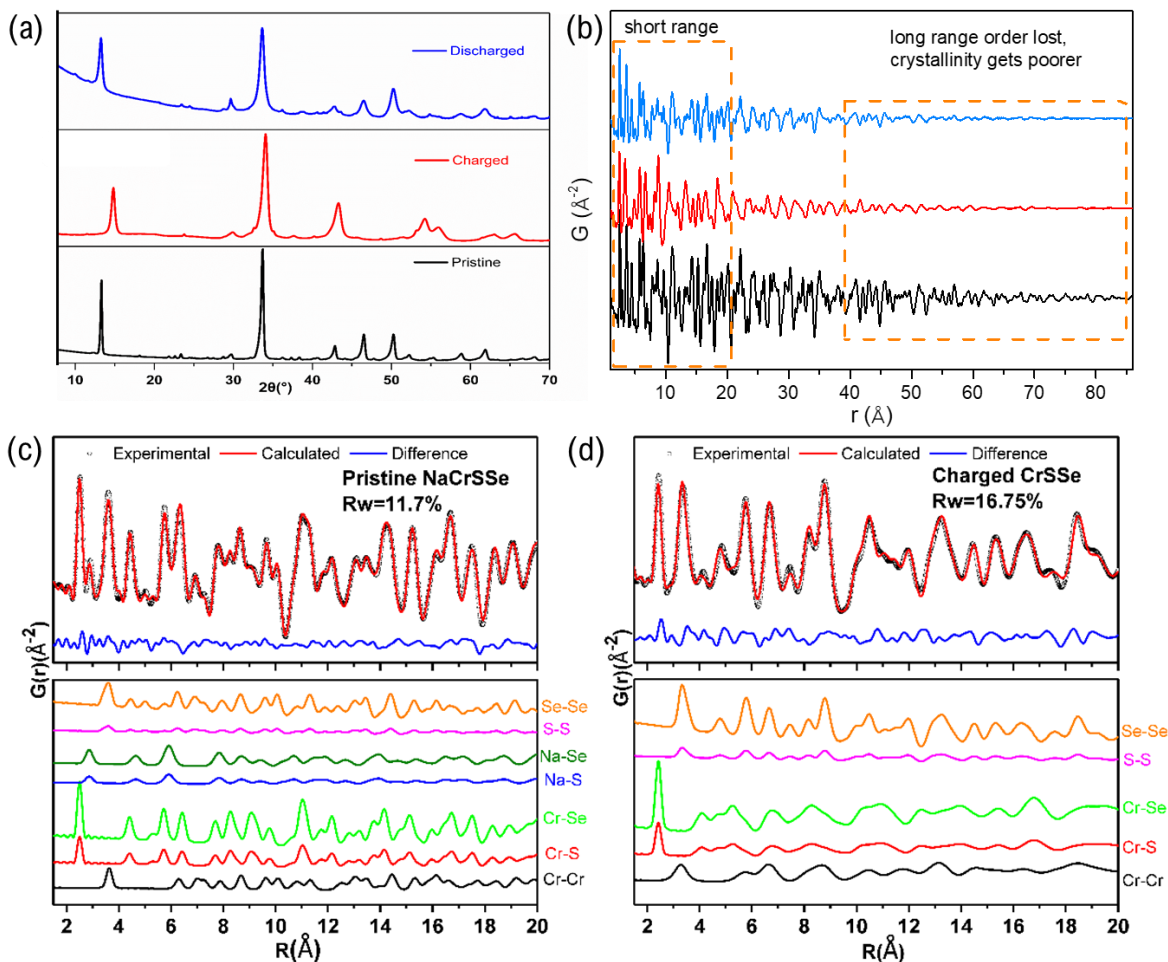


Figure 100. (a) *Ex situ* X-ray diffraction data and (b) *ex situ* pair distribution function (PDF) data of pristine, charged, and discharged NaCrSSe. (c) PDF data of pristine sample and (d) PDF data of charged sample fitted using density functional theory calculated structural models. In both (c) and (d), contributions from major atomic pairs are also shown in the lower panels.

Patents/Publications/Presentations

The project has no patents, publications, or presentations to report this quarter.

Task 7.2 – Development of a High-Energy Sodium-Ion Battery with Long Life (Chris Johnson and Khalil Amine, Argonne National Laboratory)

Project Objective. The project objective is to develop a high-energy Na-ion battery with long life. Moreover, the battery chemistry should utilize low-cost materials. The energy density target is 200 Wh/kg and/or 500 Wh/L, wherein the anode and cathode capacity targets are 600 mAhg⁻¹ and 200 mAhg⁻¹, respectively.

Project Impact. A Na-ion battery on par with the energy density of a Li-ion battery can have a high impact in the transportation sector with the assumption that the cost is significantly below \$85/kWh and the battery pack provides a 300-mile range. The consumer is not concerned about the battery chemistry employed if these metrics can be met. Development of these battery chemistries will situate the United States in a strong position as relates to new low-cost energy storage systems beyond lithium ion.

Approach. In a team approach, the Na-ion battery group will create a versatile Na-ion battery chemistry with beneficial advantages such as low cost, safety, recycling, and sustainability of materials used. The team will work synergistically so that the final design is the culmination of advances in phosphorus carbon composites mated with optimized lead or other highly dense metalloids, such as tin and/or antimony and derivatives thereof, for the recyclable anode. Synthesis and optimization of such blended composite anodes will be conducted in parallel to diagnostic characterization of structures, phase formation, and cycling stability. Cathode work will begin at the end of the first year and will involve gradient cathodes consisting of Fe-Mn compositions, as well as intergrowths of layer stacking sequenced oxides. If resources allow, the team also will attempt to stabilize cathode surfaces using ALD methods, particularly for the benefit of staving off dissolution of manganese and iron/electrolyte reactivity. Electrolytes will be partly procured from Dr. H. Li at PNNL.

Out-Year Goals. The state-of-the-art Na-ion battery in the literature has now been surpassed by this team, but performance is still too low for commercialization. Thus, the goal is to move forward and continually invent the most superior Na-ion battery chemistry that can compete worldwide through work output from this project.

Collaborations. Researchers from PNNL who are developing electrolytes for Na-ion batteries will provide this project with formulations to test with the various electrode combinations investigated at ANL. The team also exchanges commercial samples with Dr. J. Barker of Faradion Ltd. in the United Kingdom.

Milestones

1. Investigate reaction mechanism of P- and Pb-based anode. (Q1, FY 2020; Completed)
2. Synthesize high-performance layered oxide cathodes using continuous stirred tank reactor (CSTR) method. (Q2, FY 2020; In progress)
3. Optimize the interface of P- and Pb-based anode for long cycle life and high initial CE. (Q3, FY 2020; In progress)
4. Develop composition-gradient oxide cathodes. (Q4, FY 2020; In progress)

Progress Report

Previous reports have described the synthesis and electrochemistry of Pb-O-C nanocomposite anode materials prepared by high-energy-ball-milling (HEBM) in an inert atmosphere. Of the various synthesis parameters tested, such as milling time, the choice of lead oxide starting materials, and carbon content, the Pb-O-C nanocomposite synthesized via 6h of HEBM with 30% carbon black has shown the most promising electrochemical properties. To explore further improvement, a series of Pb-M-O-C nanocomposite materials was synthesized with an additional element M (Sn, Sb, Fe, Mn, or Ni) and tested in both sodium and lithium cells using carbonate-based electrolytes.

Anode powder samples were prepared by HEBM of PbO, carbon black, and a source of the additional element, M. The starting materials for the additional element M were Sn, SnO, Sb, Fe₂O₃, Mn₂O₃, and NiO. The synthesis conditions were determined from previous studies that showed nanoscale pulverization and carbothermal reduction of the PbO starting material. Figure 101 shows the XRD patterns of the Pb_{1-x}M_x-O-C nanocomposite samples where x = 0.3 and 0.5. All samples clearly exhibit strong peaks indexed to metallic lead structure, suggesting that the additional materials react well with PbO forming a Pb-based metallic alloy as the major phase. The broad hump at 28° is attributed to the PbO minor phase that is formed as a result of surface oxidation of the metallic lead nanoparticles on air-exposure. A careful examination of the XRD patterns for the iron, manganese, or nickel added samples further reveals a trace amount of unreacted impurity phases such as Fe₂O₃, Mn₂O₃, or NiO, respectively. In contrast, the tin or antimony addition does not form an apparent impurity phase up to 30% addition. The additional peaks corresponding to metallic tin or antimony structure are only observed for the 50% tin or antimony added samples.

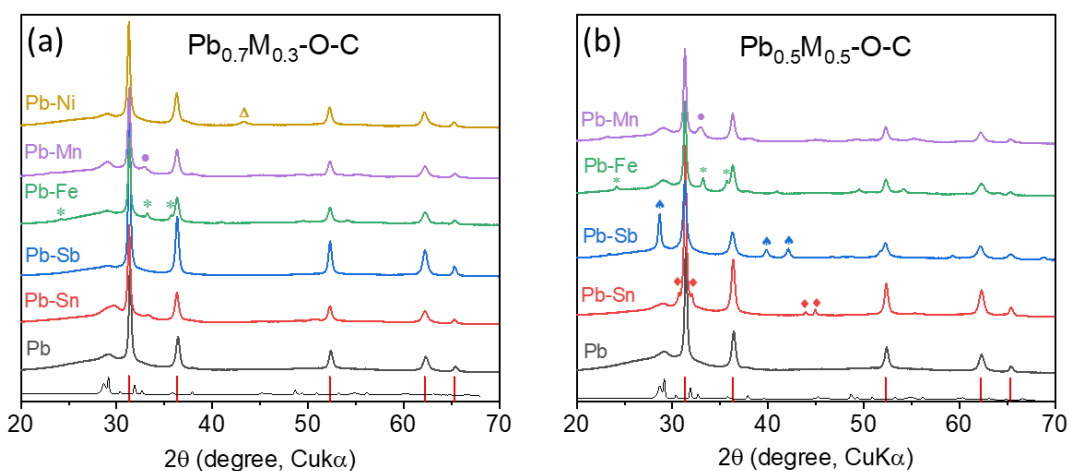


Figure 101. X-ray diffraction patterns for the (a) Pb_{0.7}M_{0.3}-O-C and (b) Pb_{0.5}M_{0.5}-O-C nanocomposite materials prepared by high energy ball mill of PbO, carbon, and the additional elements, M (Sn, Sb, Fe, Mn, or Ni). The marked impurity phases are Sn (♦), Sb (♠), Fe₂O₃ (*), Mn₂O₃ (•), and NiO (Δ).

Figure 102 compares the initial specific capacity of the Pb_{1-x}M_x-O-C nanocomposite anodes cycled in sodium and lithium half-cells. While the addition of iron, manganese, or nickel does not have a beneficial effect on the electrochemical performance of sodium cells, the Pb_{1-x}Sn_x-O-C and Pb_{1-x}Sb_x-O-C anodes show an improvement in the specific capacity, first cycle efficiency, and cycle stability. The advantage of the additional elements is more significant when the electrodes are tested in lithium cells. For instance, the specific discharge capacity of Pb_{0.7}Sn_{0.3}-O-C is ~ 100 mAh/g higher than that of the Pb-O-C baseline, and the Pb_{0.7}Sb_{0.3}-O-C anode shows a significantly improved CE and cycle stability. The highest specific capacity of ~ 800 mAh/g is achieved by 50% antimony addition and is attributed to the synergistic effect of the coexistence of both Pb_{1-y}Sb_y and antimony phases, as shown in Figure 101b. The marginal performance improvements in sodium cells, which

contrast with the significant effects of the M addition in lithium cells, corroborate the team’s previous observations that suggest the improvement of interface kinetics is of critical importance for the high energy Pb-O-C nanocomposite anode for Na-ion batteries (see Q4, FY 2019 report).

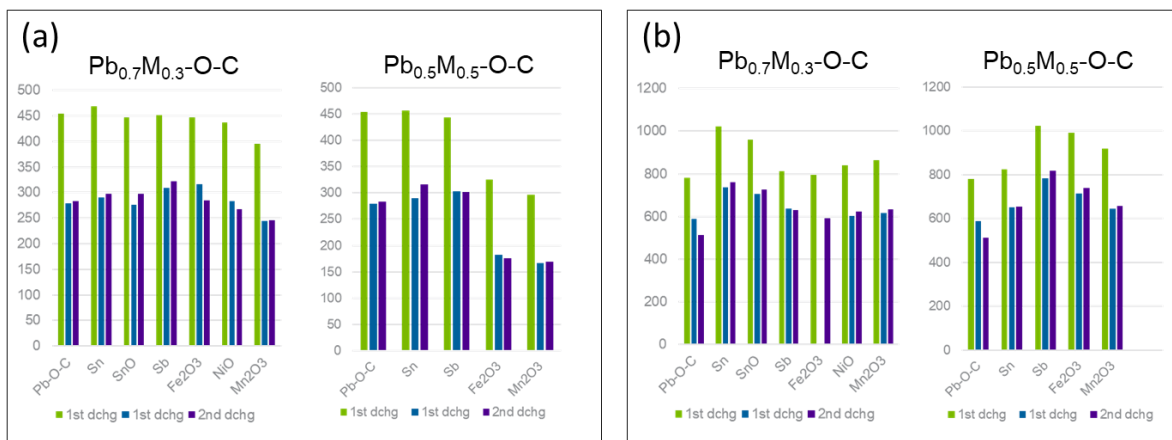


Figure 102. The initial specific capacity of the $Pb_{1-x}M_x-O-C$ nanocomposite anodes tested in (a) sodium and (b) lithium half-cells (voltage = 0.005 – 2.0 V versus sodium, and 0.005 – 3.0 V versus lithium; current density = 100 mAh/g; electrolytes = 1 M $NaPF_6$ in EC/DEC with 2% FEC for sodium cells, and 1.2 M $LiPF_6$ in EC/EMC with 10% FEC for lithium cells).

Patents/Publications/Presentations

Patent

- Xu, G-L., X. Liu, and K. Amine. “Electroactive Materials for Secondary Batteries.” IN-19-0160, U. S. Patent application. Filed.

Publication

- Xiong, B-Q., X. Zhou, G-L. Xu, Y. Liu, L. Zhu, Y. Hu, S-Y. Shen, Y-H. Hong, S-C. Wan, X-C. Liu, X. Liu, S. Chen, L. Huang, S-G. Sun, K. Amine, and F-S. Ke. “Boosting Superior Lithium Storage Performance of Alloy-Based Anode Materials via Ultraconformal Sb Coating-Derived Favorable Solid-Electrolyte Interphase.” *Advanced Energy Materials* 10 (2020): 1903186.

Presentation

- Center for Electrochemistry Workshop, UT, Austin, Texas (February 22–23, 2020): “Na-Ion Batteries: The Best Option for Beyond Li-Ion Batteries?”; C. S. Johnson.

Task 7.3 – High-Capacity, Low-Voltage Titanate Anodes for Sodium-Ion Batteries (Marca Doeff, Lawrence Berkeley National Laboratory)

Project Objective. The objectives are to understand differences in the sodium intercalation mechanism of various sodium titanate anodes through an array of synthetic, electrochemical, and structural characterization techniques, and to overcome practical impediments to their use, such as the high first-cycle Coulombic inefficiencies that are currently observed. The ultimate goal is to produce a 200-250 mAh/g anode that cycles reversibly.

Project Impact. Although several suitable cathode materials for Na-ion batteries exist, there are few suitable anode materials due to low potential instabilities. Therefore, sodium titanate variations will be synthesized through different routes to develop materials with various morphologies and dopants. Decreasing the first-cycle inefficiencies and improving cycling performance will allow enabling technology for a practical high-energy Na-ion battery.

Approach. Candidate stepped layered titanates will be synthesized by appropriate routes (hydrothermal, solid-state routes, etc.). Materials will then be characterized electrochemically and physically. Structure-function relationships will be built to correlate the effect of changing structure (for example, step size) on electrochemical properties.

Out-Year Goals. A series of synchrotron characterization techniques will be used to further develop sodium titanate anode materials with stable cycling while delivering high capacities.

Collaborations. TXM is done in collaboration with Dr. Y. Liu (SSRL). Synchrotron hard, sXAS, and X-ray Raman efforts are in collaboration with Dr. D. Nordlund and Dr. D. Sokaras (SSRL). Electrolyte design is done in collaboration with Dr. K. Xu (ARL).

Milestones

1. Conduct SEI studies. (Q1, FY 2020; In progress, pending beam time at SSRL)
2. Synthesize lepidocrocite titanates. (Q2, FY 2020; In progress)
3. Select best electrolyte solution. (Q3, FY 2020)
4. *Go/No-Go Decision:* On sodium nonatitanate, stop if problems are not solved. (Q4, FY 2020)

Progress Report

This quarter, a third composition of the $\text{Cs}_x\text{Ti}_{2-x/4}\text{O}_4$ series (that is, $\text{Na}_{0.67}\text{Ti}_{1.8325}\text{O}_4$) has been synthesized to enable a systematic comparison with the two compositions studied last quarter. Detailed electrochemical characterizations are planned and are expected to be finished next quarter. In addition, the team carried out a range of physical characterization on $\text{Na}_x\text{Ti}_{2-x/4}\text{O}_4$. Temperature-dependent XRD data (Figure 103) reveal that the $\text{Na}_x\text{Ti}_{2-x/4}\text{O}_4$ phase is stable up to 125°C ; further increasing the temperature to 150°C results in shifting of the (020) peak to its higher angle side, suggesting the removal of water. A weight loss of 8 wt% due to water removal at $\sim 138^\circ\text{C}$ is calculated from thermogravimetric analysis. This dehydrated $\text{Na}_x\text{Ti}_{2-x/4}\text{O}_4$ phase further decomposes into a new phase at temperatures above 200°C (Figure 103).

To further optimize the synthesis procedure of $\text{Na}_x\text{Ti}_{2-x/4}\text{O}_4$, a new solid-state ion-exchange (SSIE) method was employed aside from the aqueous ion-exchange one used last quarter, as inspired by a recent work [*Inorganic Chemistry* 59, no. 6 (2020): 4024–4029], given its merits of shorter reaction time and solvent (water)-free. Successful ion-exchange is confirmed by the gradual disappearance of the diffraction peaks belonging to NaCl along with the appearance of the diffraction peaks belonging to CsCl in the XRD patterns of the ion-exchanged products (Figure 104), according to the following chemical reaction: $\text{Cs}_x\text{Ti}_{2-x/4}\text{O}_4 + x \text{NaCl} \rightarrow \text{Na}_x\text{Ti}_{2-x/4}\text{O}_4 + x \text{CsCl}$. The team plans ICP optical emission spectrometry to obtain quantitative information of such solid-state ion-exchange reactions.

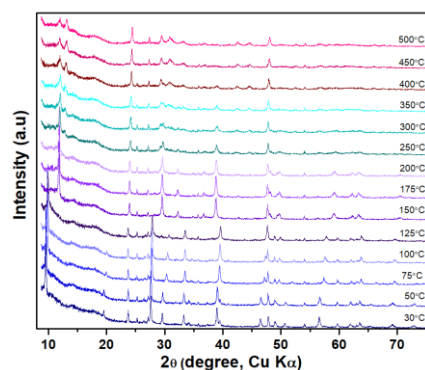


Figure 103. Temperature-dependent powder X-ray diffraction data of $\text{Na}_x\text{Ti}_{2-x/4}\text{O}_4$.

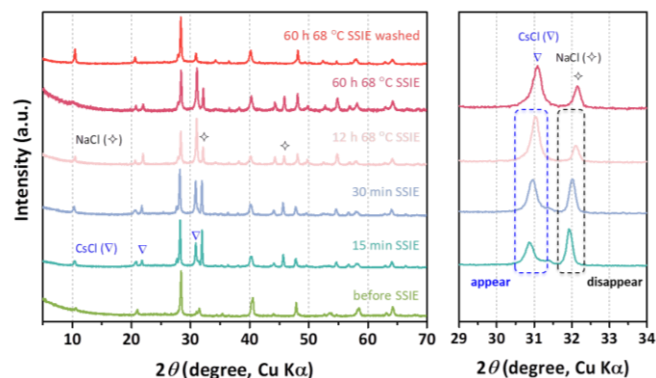


Figure 104. Powder X-ray diffraction patterns of the products after the solid-state reactions of $\text{Cs}_x\text{Ti}_{2-x/4}\text{O}_4$ with NaCl.

Work next quarter will include three parts: (1) electrochemical characterization of the three $\text{Na}_x\text{Ti}_{2-x/4}\text{O}_4$ phases, (2) understanding of SEI, using surface-sensitive synchrotron radiation techniques including s-XAS and XPS, and (3) further improving electrochemical properties of lepidocrocite electrodes via carbon additive and electrolyte optimization.

Patents/Publications/Presentations

The project has no patents, publications, or presentations to report this quarter.

Task 7.4 – Electrolytes and Interfaces for Stable High-Energy Sodium-Ion Batteries (Ji-Guang Zhang, Pacific Northwest National Laboratory)

Project Objective. This project will develop innovative electrolytes and enable fundamental understanding on the interface between electrode and electrolyte for stable operation of high-energy Na-ion batteries. The proposed research will enhance the achievable capacities of both anode and cathode for Na-ion battery and improve the stability of electrodes/electrolyte interface, establish correlation (electrolyte design rule) between electrochemical performances of Na-ion batteries and the electrolyte/interface properties, and enable long cycle life and safe operation of high-energy Na-ion batteries.

Project Impact. Success of this project will provide a solid understanding on the electrolyte/electrode interphase of Na-ion batteries and significantly improve their energy density, cycle life, and safety. It will also accelerate the practical application of Na-ion batteries in both EV and stationary energy storage.

Approach. This project will optimize the electrolyte components and concentrations to develop innovative electrolytes and additives with improved electrochemical and physical properties. *In situ* and *ex situ* spectroscopy methods will be used to unravel the origin of the SEI at the dynamic interface, providing guidance for the electrolyte and interface design and enabling high capacity and long life of Na-ion batteries.

Out-Year Goals. This project will select the electrolyte compounds and identify the formation of interfacial SEI layer on hard carbon and CEI layer on layer oxide cathode and its effect on the electrode materials. It will also provide guidance to electrolyte optimization and improve CE of sodium deposition/stripping to be more than 99%.

Collaborations. This project will collaborate with ANL and LBNL and other leading scientists in the field of cathode and anode materials for Na-ion batteries. It will also collaborate with Dr. C. Wang and Dr. M. Engelhard of PNNL for TEM and XPS characterization.

Milestones

1. Optimize electrolyte composition: Na-based LHCE will be developed to improve cycling stability. (Q1, FY 2020; Completed)
2. Develop electrolyte additives to improve stability of SEI on anode and of CEI layer on cathode. (Q2, FY 2020; Completed)
3. Develop compatible polymer separator (or polymer electrolyte) to stabilize long-term cycling and provide a stable/adequate interphase. (Q3, FY 2020; In progress)
4. Apply the new electrolytes and additives in Na-ion batteries to improve CE to more than 99%. (Q4, FY 2020; In progress)

Progress Report

This quarter's milestone has been accomplished. Electrolyte additive is studied in both carbonate electrolyte and localized high concentration phosphate electrolyte. $\text{Na} \parallel \text{NaCu}_{1/9}\text{Ni}_{2/9}\text{Fe}_{1/3}\text{Mn}_{1/3}\text{O}_2$ (Na-CNFM) cells were used to evaluate electrolyte additive effect on cathode performance (Na-CNFM weight ratio in cathode: 93.5%, mass loading: 13-16 mg cm^{-2}). All cells were cycled at 0.1 C for the first 3 cycles and 0.2 C for the later cycling (1 C = 100 mAh g^{-1}). $\text{Na} \parallel$ hard carbon (HC) cells were used to evaluate electrolyte additive effect on HC anode performance. (HC electrode:HC:PVDF: CB = 90:5:5, mass loading: 2-3 mg cm^{-2}). All the cells were cycled at 0.1 C, 0.2 C, 0.5 C, 1 C, and 2 C for rate test (5 cycles each) and 0.2 C for the later cycling (1 C = 300 mAh g^{-1}).

In carbonate electrolyte, 1 M NaClO_4 in EC:PC:DMC (1:1:1 in vol.) (named as E1) was the baseline electrolyte. 2 wt% VC additive was added into baseline electrolyte, which showed significant improvement on the cathode performance. Capacity retention after 100 cycles was improved from 33.1% (39.4 mAh g^{-1}) to 85.7% (105.7 mAh g^{-1}), as shown in Figure 105a. The initial CE was increased from 74% of baseline electrolyte to 96% of electrolyte with 2 wt% VC additive. The long-cycling CE was also increased to 99.6-99.7% compared with 97-99% in baseline electrolyte (Figure 105b). However, 2 wt% VC additive did not show any improvement on HC anode.

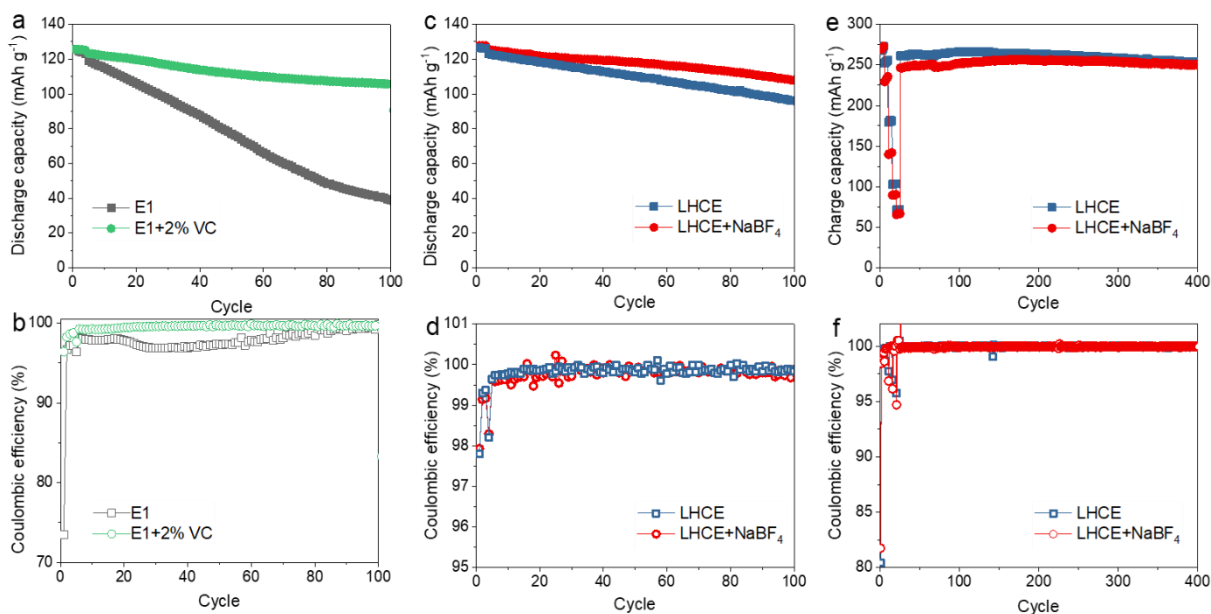


Figure 105. Electrolyte additive effect on cathode and hard carbon electrochemical performance. (a) Cycling stability and (b) Coulombic efficiency (CE) of $\text{Na} \parallel \text{NaCu}_{1/9}\text{Ni}_{2/9}\text{Fe}_{1/3}\text{Mn}_{1/3}\text{O}_2$ cells in carbonate electrolyte with/without VC additive. (c) Cycling stability and (d) CE of $\text{Na} \parallel \text{NaCu}_{1/9}\text{Ni}_{2/9}\text{Fe}_{1/3}\text{Mn}_{1/3}\text{O}_2$ cells in phosphate electrolyte with/without NaBF_4 additive. (e) Cycling stability and (f) CE of $\text{Na} \parallel$ hard carbon cells in phosphate electrolyte with/without NaBF_4 additive.

In nonflammable phosphate electrolyte, $\text{NaFSI}:\text{TEP}:\text{TTE}$ (1:1.5:2 in molar) was the baseline LHCE. Based on the team's experience that 1M NaBF_4 in TEGDME was quite stable for HC and Na-metal anode, NaBF_4 salt additive was added into baseline electrolyte to form advanced electrolyte $\text{NaFSI}:\text{NaBF}_4:\text{TEP}:\text{TEGDME}:\text{TTE}$ (0.95:0.05:1.3:0.2:2 in molar). $\text{NaFSI}:\text{TEP}:\text{TEGDME}:\text{TTE}$ (1:1.3:0.2:2 in molar) was also prepared to evaluate TEGDME effect, which showed no improvement for cathode performance. Thus, NaBF_4 was the only effective additive component for the improvement of cathode performance. Capacity retention after 100 cycles was improved from 78.11% (96 mAh g^{-1}) for LHCE to 86.10% (107.8 mAh g^{-1}) for LHCE+ NaBF_4 (Figure 105c). The CE for both LHCE and LHCE+ NaBF_4 was stable around 99.8-99.9% (Figure 105d). For HC anode, the capacity retention after 400 cycles was 96.67% (252.3 mAh g^{-1}) for LHCE and 101.38% (249.7 mAh g^{-1}) for

LHCE+NaBF₄ (Figure 105e). The CE for both LHCE and LHCE+NaBF₄ was higher than 99.9% (Figure 105f). In summary, NaBF₄ salt was a beneficial electrolyte additive, promoting electrochemical performance improvement for both cathode and hard carbon anode.

Patents/Publications/Presentations

Publication

- Le, P. M., T. D. Vo, H. Pan, Y. Jin, Y. He, X. Cao, H. V. Nguyen, M. H. Engelhard, C-M. Wang, J. Xiao, and J-G. Zhang. “Excellent Cycling Stability of Sodium Anode Enabled by a Stable Solid Electrolyte Interphase Formed in Ether-Based Electrolytes.” *Advanced Functional Materials*. Accepted.

Innovation Center for Battery500

(Jun Liu, Pacific Northwest National Laboratory; Yi Cui, Stanford University)

Project Objective. The project aims to develop commercially viable lithium battery technologies with a cell-level specific energy of 500 Wh/kg through innovative electrode and cell designs that enable the extraction of the maximum capacity from advanced electrode materials. In addition to achieving high specific energy, the project aims to be able to achieve 1,000 cycles for the developed technologies.

Project Impact. The Battery500 Consortium will develop next-generation lithium battery technologies that will significantly increase energy density, improve cycle life, and reduce cost. This will greatly accelerate deployment of EVs and reduce carbon emission associated with fossil fuel consumption. The consortium will utilize first-class expertise and capabilities in battery research in the United States and develop an integrated and multi-disciplinary approach to accelerate development and deployment of advanced electrode materials in commercially viable high-energy batteries. The advances made in this consortium will also benefit the improvement of current Li-ion battery technologies.

Approach. This project will utilize an assortment of national resources located at the national laboratory level and university level. The lithium anode combined with a compatible electrolyte system and two cathodes—one high-Ni $\text{LiNi}_x\text{Mn}_y\text{Co}_z\text{O}_2$ and another sulfur—will be studied and developed to reach high-energy density. The project focus is to design novel electrode and cell architectures to meet the 500 Wh/kg goal. The consortium will work closely with R&D companies, battery/materials manufacturers, and end users/OEMs to ensure that the developed technologies are aligned with industry needs and can be transitioned to production.

Out-Year Goals. This project aims for the following out-year goals. (1) Fabricate and test a pouch cell capable of 350 Wh/kg and 350 cycles. (2) Fabricate and test a pouch cell capable of 400 Wh/kg and 100 cycles.

Collaborations. Collaboration among consortium team members will be well coordinated by the leadership team, which includes the keystone project leads and co-leads along with PIs at all member institutions. Collaboration with the community outside of this consortium and with industry will be facilitated by the executive committee, the advisory board, and the industry committee.

Milestones

1. Deliver pouch-cell design and pouch-cell parameters for over 400 Wh/kg pouch cells. (Q1, FY 2020; Completed)
2. Develop new 3D anode structures; test and validate such using coin-cell standard protocols. (Q2, FY 2020; Completed)
3. Fabricate and test 350 Wh/kg Li-S pouch cells with over 50 stable cycles. (Q3, FY 2020; In progress)
4. Fabricate and test a pouch cell capable of 400 Wh/kg and 100 cycles. (Q4, FY 2020; In progress)

Progress Report

Keystone Project 1: Materials and Interfaces

The goal of Keystone 1 is to provide the materials and chemistry support for Keystone projects 2 and 3. This quarter, the different behaviors of first-cycle loss between NMC-811 and LCO were elaborated and niobium oxide cathode coating was identified to be effective (Binghamton); anode-to-cathode crossover was suggested as a contributor to failure in Li-metal batteries (UT Austin); and a series of fluorinated ether electrolytes was designed and synthesized to simultaneously obtain both high ion conductivity, high transference number, and high-voltage stability (Stanford).

Previously, Binghamton University reported that the slow in-diffusion of lithium ions at high lithiation levels is the main contributor to the first-cycle capacity loss for NMC-811 cathode. Even when only 10 mAh/g lithium was extracted, the insertion was severely limited at 21°C, as shown in Figure 106 (left). This quarter, the researchers compare NMC-811 with LCO (Figure 106, right), when both were charged to remove 120 mAh/g. The first-cycle loss for the LCO is much less, and is not much impacted by raising the temperature to 45°C. In contrast, much of the first-cycle loss of the NMC-811 can be eliminated at 45°C, again indicating kinetic limitations. However, this required small increase of temperature suggests that lattice substitution should be able to have the same effect.

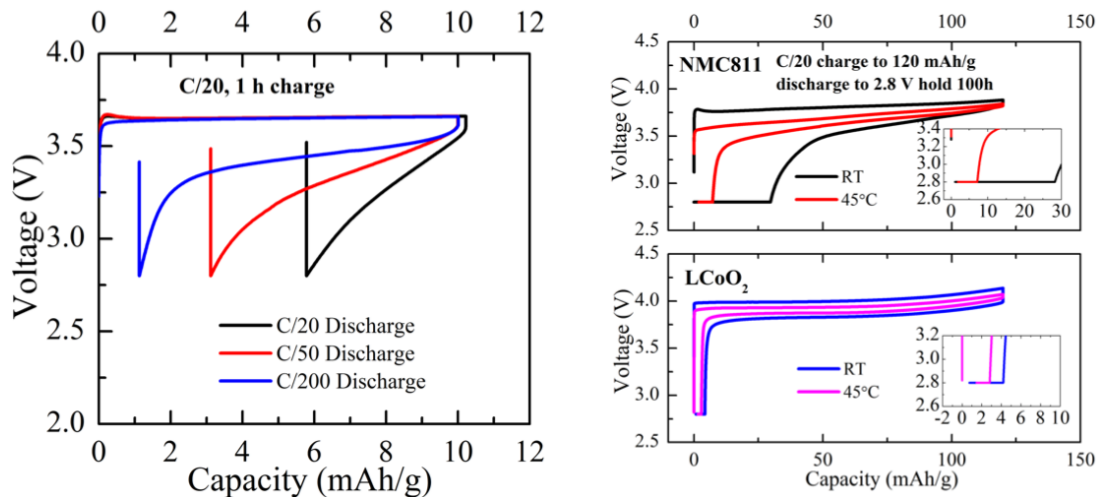


Figure 106. (left) First-cycle of ECOPRO NMC-811 versus lithium with 1 hour charge at C/20 and then discharged to 2.8 V with different current rates: C/20, C/50, and C/200. (right) Comparison of NMC-811 with LCO charged to 120 mAh/g lithium removal.

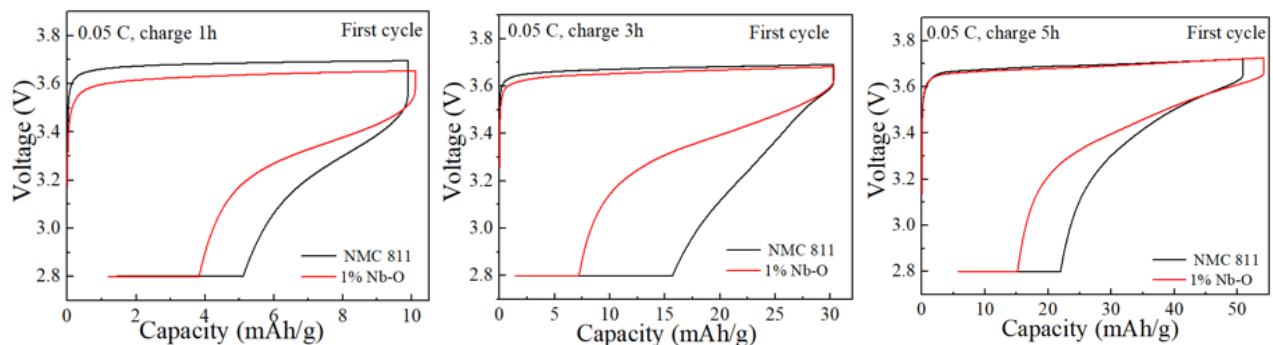


Figure 107. Reduction of first loss of NMC-811 by a niobium treatment for three charge levels.

A second approach the researchers have found to reduce the first-cycle loss is surface coating (and partial substitution) of the NMC-811. Figure 107 shows that for each of three low charging levels, the first-cycle loss is less for the Nb-treated NMC-811. They conclude that modification of the NMC to make it more like LCO is a viable method to mitigate the first-cycle loss; this might be accomplished by substitution. The optimum coating/substitution must now be found.

The UT Austin team assembled coin cells by pairing ultrahigh-nickel $\text{LiNi}_{0.9}\text{Mn}_{0.05}\text{Co}_{0.05}\text{O}_2$ (NMC-900505) cathode with graphite anode as well as with Li-metal anode. Three-electrode EIS was performed periodically during cycling to track changes in cathode impedance, with an aim to understand whether decomposition species from the Li-metal anode would crossover and affect the cathode. Figure 108 shows the EIS data after 1, 20, and 100 cycles. As can be seen, cathode impedance for the cell paired with Li-metal anode is remarkably higher than that for the cell paired with graphite anode, even after just one cycle; this was confirmed with duplicate cells. However, cathode impedance growth on extended cycling appears comparable between the two cell types. The data suggest that anode-to-cathode crossover in NMC | Li-metal cells occurs predominantly during formation cycles. In the first cycle, pristine lithium reacts particularly aggressively to form SEI and other soluble decomposition products. In addition, the cathode has not yet formed its own protective SEI and may be more vulnerable to the attack or deposition of these crossover products. The finding suggests anode-to-cathode crossover as another contributor to failure in Li-metal batteries.

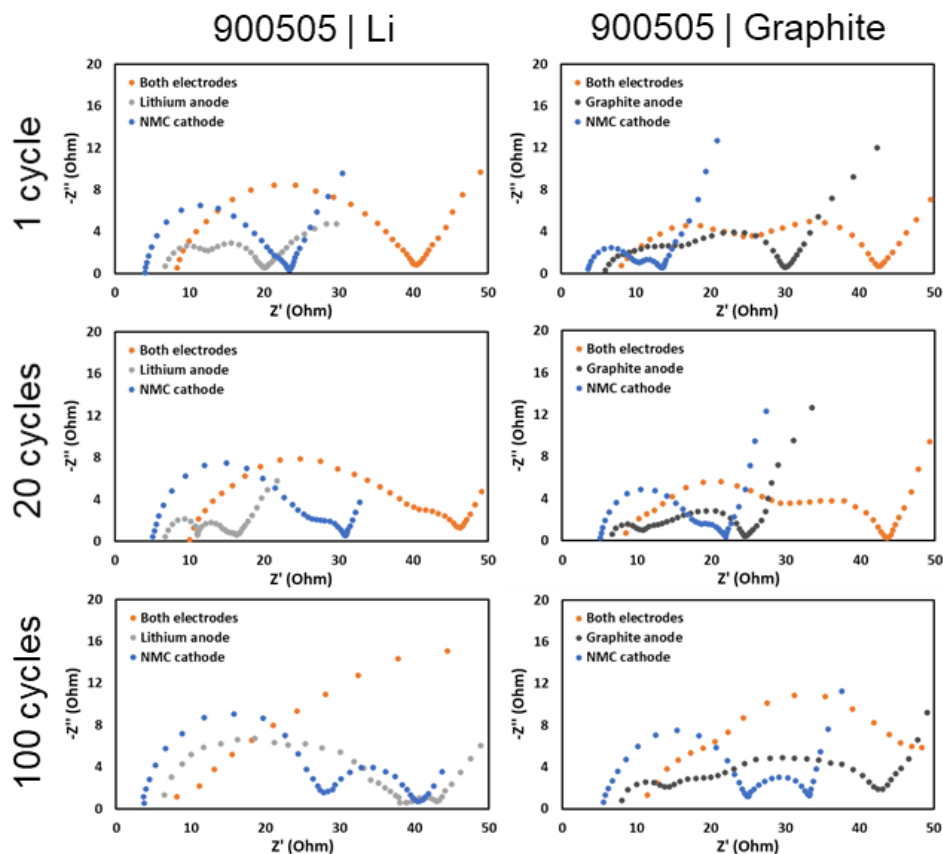


Figure 108. Nyquist plots showing the electrode-level and whole-cell impedances for NMC-900505 cathodes cycled with Li-metal (left) and graphite (right) anodes as a function of cycle number.

The Stanford team developed a novel method to synthesize a new class of fluorinated ether electrolytes (Figure 109) with combined high ionic conductivity and high oxidative stability in a single molecule. Structure–property relationship was obtained through varying the length and type of the ether group, as well as the length of the fluorinated segment. They show that the molecules (although in liquid state at room

temperature with low molecular weight) actually have glass transitions rather than the melting transitions of typical ethers. For compound in this class with different structures, the ionic conductivity is higher for those with longer ether groups combined with a shorter fluorinated segment. It is demonstrated that ion conductivities as high as 2.7×10^{-4} S/cm can be obtained, which is remarkably close to the typical ethers such as tetraglyme; however, the lithium transference numbers are higher than that (Figure 110a-d). In addition to high ionic conductivity, these compounds also have high oxidative stabilities up to 5.6 V, which is at least 1.4 V greater than tetraglyme or a tetraglyme:TTE mixture, as shown in Figure 110e. These results demonstrate the great advantages of these compounds with a combination of high ionic conductivity and high oxidative stability originated from the covalently attached ether segment and fluorinated segment, respectively.

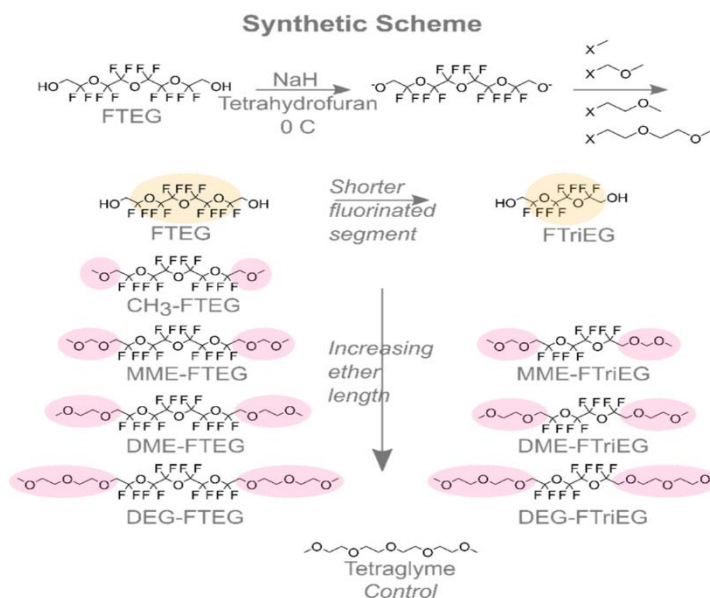


Figure 109. Covalently attaching an ether to the hydrofluoroether allows for both high ionic conductivity and oxidative stability (the team's approach). Synthesis of fluorinated ethers through deprotonation of fluorinated tetraethylene glycol (FTEG) and fluorinated triethylene glycol (FTriEG) and subsequent addition of varying alkoxy halides.

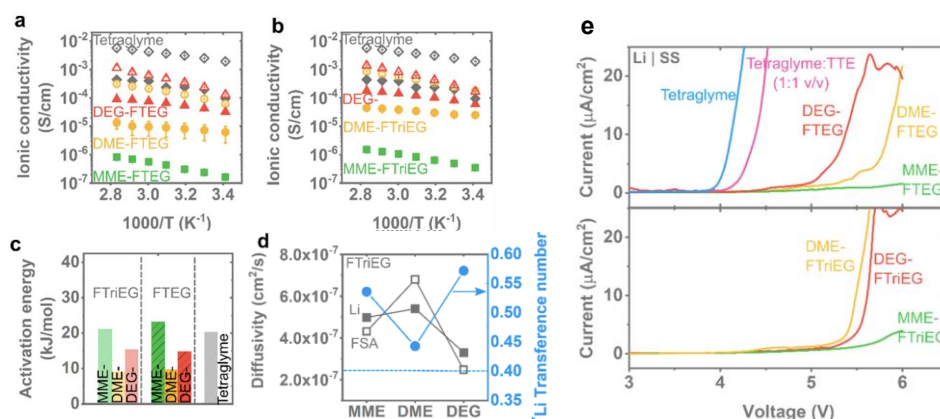


Figure 110. Ionic transport and conductivity. Ionic conductivity as a function of LiFSA salt content (closed symbol: 0.1 M; open symbol: 1 M) for (a) FTEG compounds and (b) FTriEG compounds with tetraglyme as the control in both. (c) Activation energy obtained from Arrhenius fits of conductivity versus temperature for 0.1 M LiFSA salt concentration. (d) ${}^7\text{Li}$ cation and FSA (${}^{19}\text{F}$) anion diffusivities and lithium transference number obtained through pulsed field gradient nuclear magnetic resonance for 0.1 M LiFSA in FTriEG compounds. (e) Linear sweep voltammetry of Li | stainless-steel cells with different electrolytes to measure their oxidative stability.

Highlights of Keystone Project 1

The highlights for this quarter are as follows:

- The different behaviors of first-cycle loss between NMC-811 and LCO were elaborated, and niobium oxide cathode coating was identified to be effective (Binghamton University and UCSD).
- Anode-to-cathode crossover was suggested as a contributor to failure in Li-metal batteries (UT Austin).
- A series of fluorinated ether electrolytes was designed and synthesized to simultaneously obtain high ion conductivity, high transference number, and high-voltage stability (Stanford).

Keystone Project 2: Electrode Architecture

The goal of Keystone 2 is to design, model, fabricate, and characterize the effect of electrode architecture on electrode and cell performance in support of reaching the project goal of 500 Wh/kg cell specific energy. Included in this Keystone are architecture design of thick cathodes (UCSD), Li-metal electrode architectures (PNNL, UCSD, and Stanford), inorganic (UT Austin) and polymer (Stanford) electrolytes, and electrode performance modeling (UW). Highlighted this quarter are recent advancements at multiple institutions in understanding the importance of Li-metal architecture and developing approaches to address the failure mechanisms.

Sulfur/polyacrylonitrile (SPAN) is a promising cathode due to no known polysulfide dissolution in carbonate electrolytes arising from the physical confinement of the small molecular sulfur in the conductive polymer network, which provides a high specific capacity of $> 600 \text{ mAh g}^{-1}$. However, there remain significant challenges to make this a practical and high-energy cathode material, including rapid capacity fading and conflict electrolyte requirements for anode and cathode.

This quarter, Meng's group at UCSD studied high fidelity and quantitative dependence of lithium nucleation, growth, dissolution, morphology, and cell performance on stack pressure (using SPAN). Figure 111a shows the first-cycle CE of Li-Cu cells as a function of applied stack pressure under current densities up to 2 mA/cm^2 , using an advanced ether-based electrolyte. At 0 psi, CE decreased from 92.5% at 1 mA/cm^2 to 85.5% at 2 mA/cm^2 . When slightly increasing the stack pressure to 5 psi, the CE at 2 mA/cm^2 significantly increased to 92%; CE also increased from 87% to 92.5% at 1.5 mA/cm^2 . A gradual increment of CE at three current densities was observed when gradually increasing stack pressure to 20 psi. At 20 psi, CE was boosted to 97.5%, 96.5%, and 96% at 1, 1.5, and 2 mA/cm^2 , respectively. On further increasing the stack pressure from 20 psi to 50 psi, the CE remains almost unchanged. For the electrochemical performance testing, pressure was set as the on-set value. The team then chose two representative pressures (0 and critical pressure) to study the deposited lithium morphology using cryo-FIB-SEM. A high current density of 2 mA/cm^2 was applied for the morphological study. At 0 psi, highly porous and whisker-like lithium deposits were formed, even using advanced ether-based

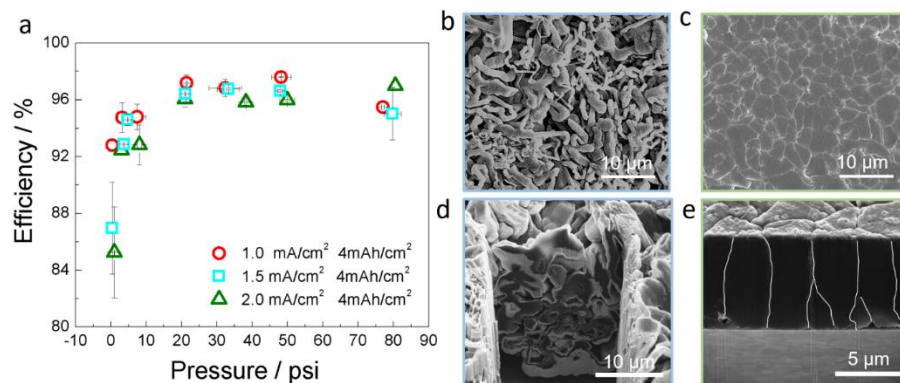


Figure 111. (a) Coulombic efficiency as a function of stacking pressure under various current densities. (b/d) Top view and cross-section view of deposited lithium morphology formed under no pressure. (c/e) Top view and cross-section view of deposited lithium morphology formed under critical pressure. The lithium in (b-e) was deposited at 2 mA/cm^2 for 1 hour.

electrolyte, as shown in Figure 111b (top view) and 111d (cross-section). This type of morphology is highly similar to the one formed in commercial carbonate electrolyte using coin cells with internal stack pressure of ~ 30 psi. When applying a critical pressure, the lithium deposits become highly close-packed (Figure 111c). The cross-section morphology (Figure 111e) shows that the lithium deposits form a perfect columnar structure with large granular diameter of ~ 4 μm , near-theoretical thickness of ~ 10 μm , and minimum electrode-level porosity, indicating that pressure plays an important role in tuning lithium deposition morphology. Meng's group predicted in the past that the columnar lithium deposits may help to improve CE of lithium metal by mitigating the isolated metallic lithium formation. This study corroborates that the columnar lithium deposits can be achieved by optimizing stack pressure, in combination with ether-based electrolytes.

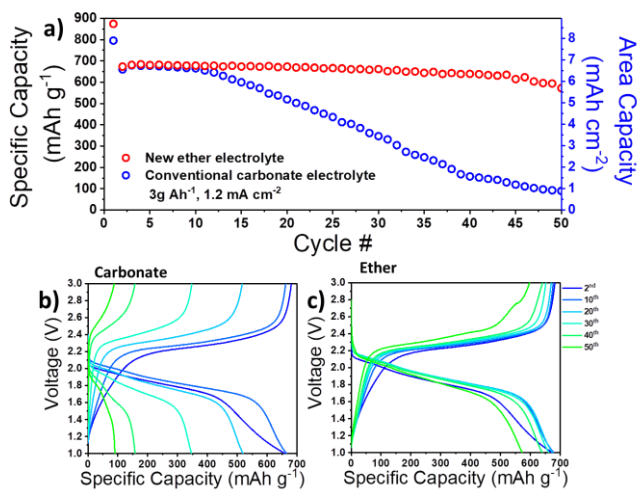


Figure 112. Comparison of cycling performance of sulfur/polyacrylonitrile (SPAN) electrodes in different electrolytes. (a-c) Thick SPAN electrode with areal capacity loading of 6 mAh cm⁻², at 1.2 mA cm⁻² (C/5). (b) Voltage profiles of thick SPAN electrode in conventional carbonate electrolyte. (c) Voltage profiles of thick SPAN electrode in novel ether electrolyte. The amount of electrolyte is 3g Ah⁻¹.

The Liu group at UCSD discovered a novel ether electrolyte, which is compatible with both lithium metal and SPAN. To achieve a Li||SPAN pouch cell with energy density of > 300 Wh kg⁻¹, the areal capacity of the SPAN electrode should be larger than 6 mAh cm⁻². By increasing the areal mass loading of SPAN material to 10 mg cm⁻², the reversible capacity of SPAN electrode reaches 6.7 mAh cm⁻² (Figure 112a). In comparison, the Li||SPAN cells were cycled using 1 M LiPF₆ in EC/EMC (vol. ratio 1:1) at C/5 between 1.0 and 3.0 V. As a further advancement from last quarter, the cells were tested under lean electrolyte condition. The amount of electrolyte in each cell is only 3 g Ah⁻¹. The Li||SPAN cell with high SPAN loading showed fast degradation in carbonate electrolyte (Figure 112b). After 50 cycles, the capacity of the Li||SPAN cell degraded from 6.60 mAh cm⁻² to 0.91 mAh cm⁻², only 13.8% of its original capacity. As a comparison, the Li||SPAN cell using the novel ether electrolyte showed much better capacity retention with little capacity decay, which maintained a high capacity of 5.68 mAh cm⁻² (Figure 112c). This performance forms the foundation for realizing a > 300 Wh/kg Li||SPAN cell in a pouch cell.

The Subramanian group at UW successfully developed a 2D moving boundary model to study the 2D nature of transport in the electrolyte and the resulting 2D deposition profile on the lithium anode. The key inputs to this model are applied current density, design parameters, transport parameters for the liquid phase, and exchange current density on the anode. The model provides the 2D distribution of the concentration, anode potential, deposition profile, and rate of deposition as the outputs. This 2D model and pressure aware model can be used to study how charging rate, anode length, separator length and thickness, and cycling influence the deposition profile on the anode. As a comparison to the 1D model developed previously, the voltage obtained using the 1D and 2D models for 10 cycles at charging rates of 1C and C/3 are shown in Figure 113. Voltage trends observed by the 2D model do not seem to be captured by the 1D model. This can be attributed to the fact that, unlike the 2D model, the 1D model cannot capture 2D transport, and the resulting distribution in concentration and liquid phase potential along the x direction. This further highlights the importance of using the 2D model to study performance of Li-metal anode.

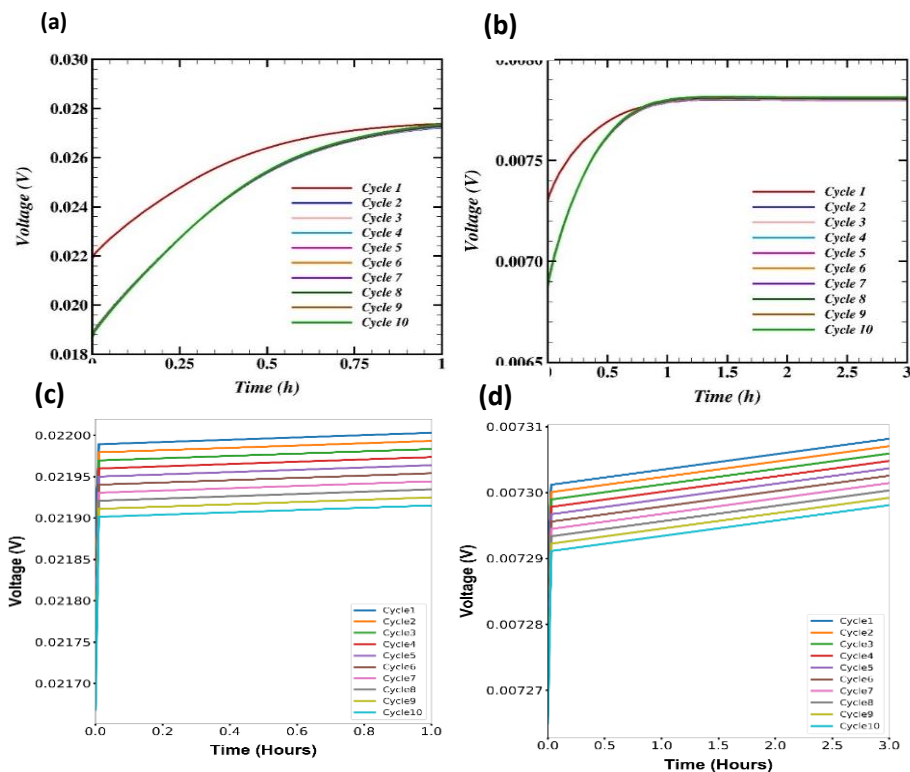


Figure 113. Voltage versus time for 10 cycles: (a) 2D model 1C rate, (b) 2D model C/3 rate, (c) 1D model 1C rate, and (d) 1D model C/3 rate.

The Yang group at UW revealed previously that both surface coating and doping on NMC-811 can reduce polarization and improve cycling performance. However, a long activation period is needed for the coated cathode because the low-conductivity coating layer reduces the electron-transfer rate between particles. This quarter, they tried to resolve this issue using direct coating on cathodes without disrupting the inter-particle electronic/ionic pathways. Figure 114a shows the initial charge–discharge curves of the pristine and LATP($\text{Li}_{1.3}\text{Al}_{0.3}\text{Ti}_{1.7}(\text{PO}_4)_3$)-coated Al-NMC-811 (Al-doped NMC-811) electrodes. The Al-NMC-811 cathode exhibits an initial reversible capacity of 222.2 mAh g^{-1} with CE of 89.7% at 0.1 C between 2.8 V and 4.4 V, similar to those of LATP-coated Al-NMC-811 electrode (223.2 mAh g^{-1} , 89.5%). After the formation cycles, both Al-NMC-811 and LATP-coated Al-NMC-811 cathodes deliver similar discharge capacities and CE at 0.33 C (Figure 114c). Figure 114b displays the charge–discharge curves of both electrodes at the 50th cycle. The two curves are almost overlapped, indicating the two electrodes show similar reversible capacity and polarization. These results demonstrate that direct LATP coating on Al-NMC-811 electrodes will not affect their electrochemical performance. These batteries are still cycling; the team will report the results next quarter.

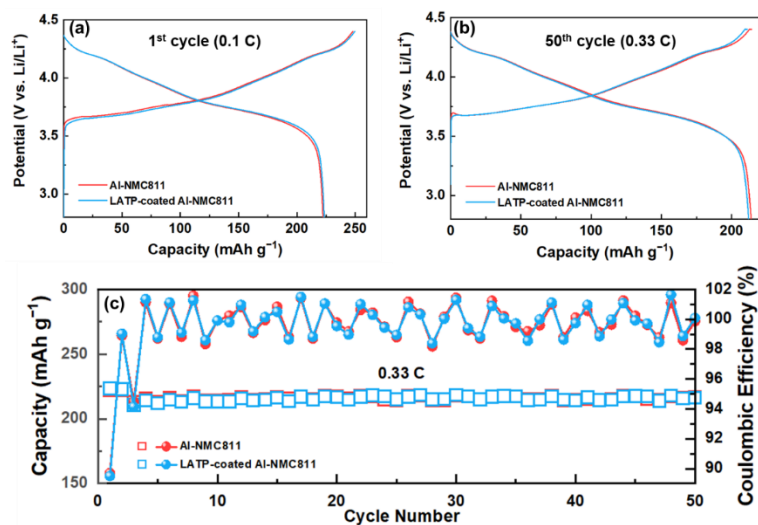


Figure 114. (a) Initial and (b) 50th charge–discharge curves of pristine and LAMP-coated Al-NMC-811 electrodes. (c) Cycling performance of pristine and LAMP-coated Al-NMC-811 electrodes.

Highlights of Keystone Project 2

The highlights for this quarter are as follows:

- Significant advancement in understanding the quantitative dependence of lithium nucleation, growth, dissolution, morphology, and cell performance on stack pressure using SPAN cathode (UCSD).
- Novel ether-base electrolyte discovered for improving cycle life of Li||SPAN cells (UCSD).
- 2D moving boundary model is developed to study 2D nature of transport in the electrolyte and the resulting 2D deposition profile on the lithium anode (UW).
- LAMP-coated high-Ni cathode show promising electrochemical performance (UW).

Keystone Project 3: Cell Fabrication, Testing, and Diagnosis

Directing the morphology of Li-metal deposits during electrodeposition is crucial to development of safe, high-energy-density batteries with robust cycle life. Toward this end, mechanistic insight into correlation among various electrolyte components or cycling conditions and different lithium morphologies is imperative. Recently, the team has used a standard carbonate-based electrolyte while systematically adding water

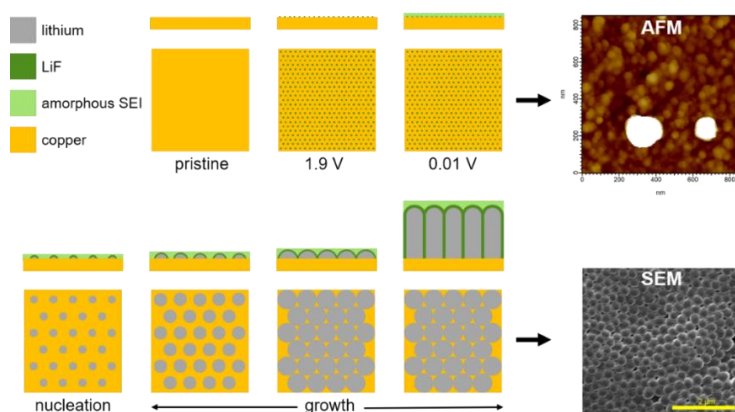


Figure 115. Proposed mechanism and corresponding data for initial nucleation and growth of Li-metal deposits in electrolyte that contains HF.

(ppm levels) in Li||Cu cells to study the links between electrolyte composition, initial SEI formation, and morphology of electroplated lithium metal using electrochemical characterization, X-ray scattering, XPS, and electron microscopy techniques. Under certain conditions (for example, electrolyte with 100 ppm added HF and an applied constant current of 0.5 mA/cm^2) this system yields electrodeposited lithium metal with a highly monodisperse columnar morphology. Systematic experimental investigation of the HF reduction process, nanostructure of the initial SEI, and crystallographic texture of electrodeposited lithium metal enable insights to be drawn concerning the underlying mechanisms of columnar lithium formation, as illustrated in Figure 115. The columnar morphology arises from an SEI layer comprising crystalline LiF deposits, formed through preferential reduction of HF, embedded in an amorphous matrix of solvent reduction products. This interphase structure contains fast Li-ion diffusion pathways that lead to a high nucleation density and uniform growth of Li-metal deposits. This mechanistic understanding will help to inform future electrolyte additive design and rational cycling protocols for Li-metal batteries. The current phase includes investigating the combined effects of an additive that promotes columnar growth and applied external pressure. The team hypothesizes that the two variables will synergistically combine to result in an “anode-free” Li-metal cell with large, uniform Li-metal deposits with preferred texture and enhanced CE due to a decrease in both “dead” lithium and SEI formation during cycling.

In other work, efforts to understand signatures from reduced lithium inventory were refined. Figure 116 includes the incremental capacity (IC) variations in a Li | LiFSI/DME-TFEO | NMC-811 cell over 350 cycles. The analysis provides insight into the transitions from H1, to M, to H2, to H3 phases in NMC-811. These transitions index the capacity – lattice structure correspondence. In Figure 116, the IC peak near 3.7 V is dominant. The sharp rise in IC implies a distinct phase transition from H1 to monoclinic (M) phase. A secondary IC peak is also observed, of which the origin is not yet clear (see Area ①). Over cycle aging, the distinct H1-M transition IC peak retreated from Cycle 50 to 350, and the primary IC peak gradually disappeared, survived with the secondary peak. This retreat is, however, not the result of increasing polarization, but due to the shortage of lithium supplies, as shown in Area ②. In Area ③, the IC peak marked by the H2-H3 transition drastically reduced/disappeared after 150 cycles. The congruent disappearance of the H1-M primary peak and the H2-H3 peak seems to suggest that these two might be related; yet, with limited data, it is difficult to confirm. This observation by ICA allows us to correlate cell performance with NMC cathode materials characterization and understanding. The methods developed will continue to be further integrated with both Keystone 1 and 3 to enhance efforts for materials development and full-cell cycling analysis and optimization.

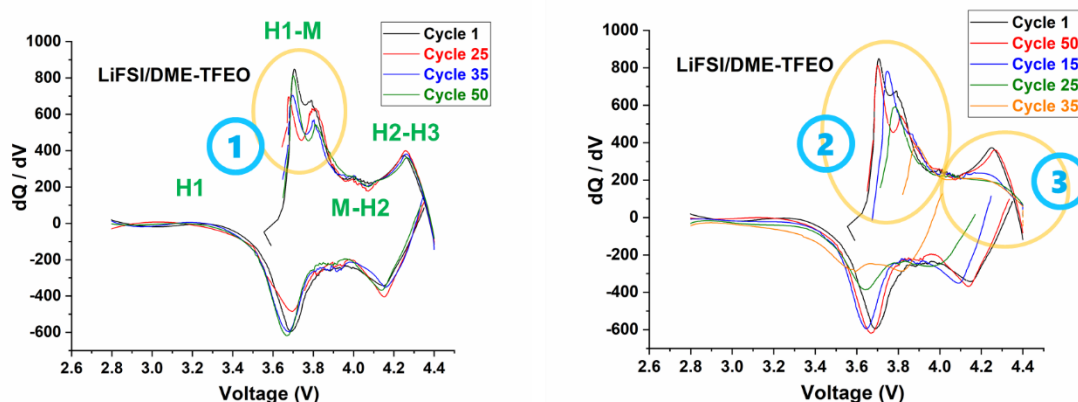


Figure 116. Incremental capacity analysis (dQ/dV) of Li||NMC-811 performance and capacity fading with a LiFSI/DME-TFEO diluted high-concentration electrolyte-containing cell. Incremental capacity variations associated with phase transitions (H1-M-H2-H3) are identified and quantified.

The team also focused on further refining the computational modeling of cells. A 2D moving boundary model was successfully developed to study the 2D nature of transport in the electrolyte and the resulting 2D deposition profile on the anode. The key inputs to this model are applied current density, design parameters, transport parameters for the liquid phase, and exchange current density on the anode. The model provides the

2D distribution of the concentration, anode potential, deposition profile, and rate of deposition as the outputs. This 2D model and pressure aware model can be used to study how charging rate, anode length, separator length and thickness, and cycling influence the deposition profile on the anode.

Highlights of Keystone Project 3

The highlights for this quarter are as follows:

- Characterization of initial stages of electrolyte decomposition and lithium nucleation provides insight into new possible strategies to improve cycle life and cell performance (SLAC).
- Incremental capacity analysis aids in identifying cycling implications from loss of lithium inventory (INL).
- A pressure aware model has been developed that can be used to study how charging rate and design parameters influence the deposition profile on the anode (UW/UT).

Patents/Publications/Presentations

Patent

- Liaw, B., Y. Zhang, and Q. Wang. “Electrochemical Analytic Diagnosis for Battery Cell Qualification.” Provisional patent application, no. 62/961,096, January 14, 2020.

Publications

- Zhang, Y., Q. Wang, B. Liaw, S. C. Nagpure, E. J. Dufek, and C. C. Dickerson. “A Quantitative Failure Analysis on Capacity Fade in Rechargeable Lithium Metal Cells.” *Journal of the Electrochemical Society* 167 (2019): 090502. doi:10.1149/1945-7111/ab6cf4. Publication Date (Web): January 7, 2020.
- Raj, A., C. C. Dickerson, S. C. Nagpure, S. Kim, C. Niu, J. Xiao, B. Liaw, and E. J. Dufek. “Communication—Pressure Evolution in Constrained Rechargeable Lithium-Metal Pouch Cells.” *Journal of the Electrochemical Society* 167 (2020): 020511. doi: 10.1149/1945-7111/ab6439. Publication Date (Web): January 2, 2020.
- Boyle, D. T., X. Kong, A. Pei, P. E. Rudnicki, F. Shi, W. Huang, Z. Bao, J. Qin, and Y. Cui. “Transient Voltammetry with Ultramicroelectrodes Reveals the Electron Transfer Kinetics of Lithium Metal Anodes.” *ACS Energy Letters* 5.3 (2020): 701–709. Publication Date (Web): February 3, 2020.
- Cui, Y., J. Wan, Y. Ye, K. Liu, L-Y. Chou, and Y. Cui. “A Fireproof, Lightweight, Polymer–Polymer Solid-State Electrolyte for Safe Lithium Batteries.” *Nano Letters* 20.3 (2020): 1686–1692. Publication Date (Web): February 5, 2020.
- Wu, D. S., G. Zhou, E. Mao, Y. Sun, B. Liu, L. Wang, J. Wang, F. Shi, and Y. Cui. “A Novel Battery Scheme: Coupling Nanostructured Phosphorus Anodes with Lithium Sulfide Cathodes.” *Nano Research* (2020): 1–6. Publication Date (Web): March 2, 2020.
- Huang, W., H. Wang, D. T. Boyle, Y. Li, and Y. Cui. “Resolving Nanoscopic and Mesoscopic Heterogeneity of Fluorinated Species in Battery Solid-Electrolyte Interphases by Cryogenic Electron Microscopy.” *ACS Energy Letters* (2020). Publication Date (Web): March 16, 2020.
- Yue, X-Y., J. Bao, S-Y. Yang, R-J. Luo, Q-C. Wang, X-J. Wu, Z. Shadike, X-Q. Yang, and Y-N. Zhou. “Petaloid-Shaped ZnO Coated Carbon Felt as a Controllable Host to Construct Hierarchical Li Composite Anode.” *Nano Energy*. doi: 10.1016/j.nanoen.2020.104614. Publication Date (Web): February 13, 2020.

- Yin, L., Z. Li, G. S. Mattei, J. Zheng, W. Zhao, F. Omenya, C. Fang, W. Li, J. Li, Q. Xie, E. M. Erickson, J.-G. (Jason) Zhang, M. S. Whittingham, Y. S. Meng, A. Manthiram, and P. G. Khalifah. “Thermodynamics of Anti-Site Defects in Layered NMC Cathodes: Systematic Insights from High-Precision Powder Diffraction Studies.” *Chemistry of Materials* 32 (2020): 1002–1010. doi: 10.1021/acs.chemmater.9b03646. [ACS “Editor’s Choice” manuscript; January 30, 2020]
- Liu, H., Z. Li, A. Grenier, G. Kamm, L. Yin, G. S. Mattei, M. R. Cosby, P. G. Khalifah, P. J. Chupas, and K. W. Chapman. “Best Practices for *Operando* Depth-Resolving Battery Experiments.” *Journal of Applied Crystallography* 53 (2020): 133–9. doi: 10.1107/S1600576719016315. Publication Date (Web): February 2020.

Presentations

- Battery India, Bengaluru, India (January 10–12, 2020): “Battery Technologies for India”; A. Manthiram. Invited keynote.
- Battery India, Bengaluru, India (January 10–12, 2020): “Lithium Battery Chemistry”; A. Manthiram. Invited tutorial.
- Gordon Research Conference, Ventura, California (February 16–21, 2020): “Understanding the Limits and Failure Mechanisms of Layered Oxide Cathodes”; A. Manthiram. Invited.
- Workshop on Emerging Technologies and Trends in Electric Mobility, Kolkata, India (March 2, 2020): “Battery Technologies for Electric Mobility”; A. Manthiram. Invited.
- India Smart Grid Forum, New Delhi, India (March 3, 2020): “Energy Storage: Battery Technologies for Grid Storage and E-Mobility”; A. Manthiram. Invited short course.
- India Smart Grid Forum, New Delhi, India (March 4–5, 2019): “Battery Technologies for Grid Storage and E-Mobility”; A. Manthiram. Invited plenary.
- Lithium Metal Electrode Characterization and Modeling Workshop, University of California San Diego, La Jolla, California (February 13, 2020): “Lithium Metal Electrode—Stability, Reversibility, and Durability”; B. Liaw.
- Battery Innovation Summit, NAATBatt Annual Meeting, Pasadena, California (February 12, 2020): “From Battery Failure Analysis to Life Prediction”; B. Liaw.
- Materials Science and Engineering Department Seminar, University of Michigan, Ann Arbor, Michigan (January 2020): “Solid State Batteries – From Interfaces to High Energy Density”; J. Yang. Invited.
- International Conference on Nanoscience and Nanotechnology 2020 (ICONN 2020), Brisbane, Australia, (February 9–13, 2020): “Nanomaterials Design for Energy and Environment”; Y. Cui. Plenary – online talk due to COVID-19.
- University of Illinois at Urbana Champaign (UIUC) Materials Science Seminar, Urbana, Illinois (February 17, 2020): “Materials and Interface Design for Batteries”; Y. Cui. Invited.
- Rice University (February 20, 2020): “Nanomaterials Design for Energy and Environment”; Y. Cui. Invited.
- Rockwell Lectureship, University of Houston, Houston, Texas (February 21, 2020): “Nanomaterials Design for Energy and Environment”; Y. Cui.
- NAATBatt Annual Meeting, Pasadena, California (February 11, 2020): “Trends for the Future of High Energy Density Battery Technology”; M. S. Whittingham, Chief Scientific Officer. Internet.
- Applied Materials, Santa Clara, California (February 28, 2020): “The Origins of the Lithium Battery and Future Chemistry and Materials Challenges”; M. S. Whittingham.
- International Coalition for Energy Storage and Innovation Conference (ICESI), Sydney, Australia (March 2, 2020): “The Origins of the Lithium Battery and Future Challenges”; M. S. Whittingham. Online plenary lecture.

- Battery Materials Supply Chain, Toronto, Canada (March 2, 2020): “The Li-Ion Battery and its Global Impact”; M. S. Whittingham. Keynote lecture.
- Prisker School of Molecular Engineering Colloquium, University of Chicago, Chicago, Illinois (February 25, 2020): “X-Rays Show Operating Principles of Energy Storage Materials”; M. Toney. Invited.
- Chemical Engineering Colloquium, University of Colorado, Boulder, Colorado (January 23, 2020): “X-Rays Show Operating Principles of Energy Storage Materials”; M. Toney. Invited.
- Gordon Research Conference on Electrochemistry, Ventura, California (January 6, 2020): “Probing and Understanding the Electrochemical Interfaces and Interphases by Combining Advanced Characterization with Computation Modeling”; Y. S. Meng. Invited.